Journal of Pharmaceutical Analysis

EDITORIAL BOARD

Contents lists available at ScienceDirect

Journal of Pharmaceutical Analysis

journal homepage: www.elsevier.com/locate/jpa

Preface for special issue on new analytical techniques and methods in drug metabolism and pharmacokinetics

Analytical technologies and approaches for drug metabolism and pharmacokinetics (DMPK) research in the pharmaceutical industry and academic research institutes have evolved rapidly over the past decade. On one hand, the discovery and development of small molecule drug candidates requires earlier and better understanding of their absorption, distribution, metabolism and excretion (ADME) in human as well as their interactions with metabolizing enzymes, transporters and drug targets, such as receptors and DNA. On the other hand, several new drug modalities and deliver systems, such as peptide and protein therapeutics, antibody-drug conjugates (ADC) and nano drug delivery systems, have been introduced into the drug pipeline. Their bioanalysis and ADME investigation in vitro and in vivo represent great challenges, and as such, demand suitable analytical technologies and strategies that may be totally different from those routinely used for DMPK studies of small molecules. This special issue of the Journal of Pharmaceutical Analysis focuses on analytical technologies and methods recently developed for improving the efficiency and quality of ADME studies in support of traditional drug discovery programs or for investigating the metabolism and disposition of new drug modalities and delivery systems.

In this special issue, we are pleased to feature three comprehensive review articles on state-of-the-art bioanalytical technologies. Shou gives an overview on high-throughput in vitro ADME screening as an essential part of lead optimization for synthetic molecules, which has been recently "industrialized" through the development of cutting-edge analytical technology, software and automation. Zhu et al. summarize current LC-MS-based strategies for characterization and quantification of ADC and discuss the challenges and opportunities in this rapidly evolving field. Wang et al. evaluate newly developed techniques for bioanalysis of nano drug delivery systems in animals and human, which is far more complicated than the monitoring of small molecular drugs in plasma in terms of structure, composition and aggregation state, whereby almost all of the conventional LC/MS methods are inadequate.

We also feature six research articles in the areas of development and application of new analytical techniques and methods in support of DMPK research. Sauter et al. present an ultra-sensitive bioanalytical method of the therapeutic peptide exenatide for accurate pharmacokinetic assessment using UPLC-MS/MS. Yao et al. provide results of evaluating and applying a new software-aided analytical workflow for targeted and untargeted detection and structural characterization of cyclic peptide metabolites in vitro by LC/HRMS. Ma et al. report a novel method to evaluate DNA binding efficiency of the DNA alkylator pyrrolobenzodiazepine in

tumors of mouse models following IV administration of its ADC conjugate. Zhang et al. discuss a selective and sensitive bioluminescence assay for rapidly evaluating CES1 activity in vivo and its application to investigating the effects of orally administered TCMs on CES1 activity in rats. Ge et al. developed an ultra-sensitive and easy-to-use assay for sensing human UGT1A1 activities in biological systems, which provided a practical approach for exploring the biological roles of UGT1A1 in living systems and characterization the modulatory effects of small molecules on this key conjugative enzyme. Sharma et al. established a convenient testing scheme for rapidly screening all human CYPs for activity towards any given candidate substrate using a cocktail enzyme bag strategy.

Altogether, this special issue is a collection of research topics on cutting-edge technologies for studying biotransformation, pharmacokinetics and interactions with metabolizing enzymes and targeted molecules of a verity of drug modalities. We thank all of the authors for their contributions, and hope the readers find their articles as compelling as we did.

Dr. Guangbo Ge received his Ph. D degree in biochemical engineering in 2009 from Dalian Institute of Chemical Physics, Chinese Academy of Sciences (CAS). After eight-year working at Dalian Institute of Chemical Physics, Dr. Ge joined Shanghai University of Traditional Chinese Medicine as a professor and the vice dean of Institute of Interdisciplinary Integrative Medicine Research in 2017. His research interests are focused on drug metabolism and drug-drug interactions. His group has developed more than ten novel optical substrates for sensing the real activities of target drug-metabolizing enzyme (DME) in living systems, and most of them have been successfully used for high-throughput screening of DME inhibitors/modulators. Now he is the co-author of more than 180 papers and five books, and his publications have been cited more than 3500 times, with an H-index of 34.

Dr. Mingshe Zhu is an independent consultant in drug metabolism, drug development and LC/MS technology. Dr. Zhu previously worked at Bristol-Myers Squibb for 20 years, where he supported drug discovery and development DMPK programs, including global approvals for ABILIFY (Aripiprazole) and FORXIGA (Dapagliflozin). His team and collaborators at BMS developed several innovative LC/MS technologies and workflows for drug metabolite profiling and identifications, including mass defect filter, background subtraction and multiple ion monitoring. Dr. Zhu has co-authored over 100 research publications and co-edited two books, Drug Metabolism in Drug Design and Development and Mass Spectrometry in Drug Metabolism and Disposition.

Guangbo Ge[*]

Institute of Interdisciplinary Integrative Medicine Research, Shanghai University of Traditional Chinese Medicine, Shanghai, 201203, China

Mingshe Zhu

MassDefect Technologies, Princeton, NJ, 08540, USA

[*] Corresponding author.

E-mail address: geguangbo@dicp.ac.cn (G. Ge).

Review paper

Current status and future directions of high-throughput ADME screening in drug discovery

Wilson Z. Shou

Bristol-Myers Squibb, PO Box 4000, Princeton, NJ, 08540, USA

ARTICLE INFO

ABSTRACT

During the last decade high-throughput in vitro absorption, distribution, metabolism and excretion (HT-ADME) screening has become an essential part of any drug discovery effort of synthetic molecules. The conduct of HT-ADME screening has been "industrialized" due to the extensive development of software and automation tools in cell culture, assay incubation, sample analysis and data analysis. The HT-ADME assay portfolio continues to expand in emerging areas such as drug-transporter interactions, early soft spot identification, and ADME screening of peptide drug candidates. Additionally, thanks to the very large and high-quality HT-ADME data sets available in many biopharma companies, in silico prediction of ADME properties using machine learning has also gained much momentum in recent years. In this review, we discuss the current state-of-the-art practices in HT-ADME screening including assay portfolio, assay automation, sample analysis, data processing, and prediction model building. In addition, we also offer perspectives in future development of this exciting field.

1. Introduction

High-throughput in vitro ADME (absorption, distribution, metabolism and excretion) screening (HT-ADME) has been widely adopted as an essential part of lead optimization for synthetic molecules (small molecules and more recently peptides) since around the year 2000 [1—3]. HT-ADME screening usually consists of in vitro assay suites that assess compound properties (or liabilities) such as metabolism [4,5], permeability [6—8], drug-drug-interactions [9—11], physicochemical properties [12,13] and also toxicities [14,15]. Several key technologies, including automated liquid handling [16], high speed liquid chromatography—tandem mass spectrometry (LC-MS/MS) for sample analysis [17,18], and software and automation tools [19—21], have together enabled these in vitro assays to be performed in high-density plate format (96, 384 or even 1536-well plates [22]) with the throughput and capacity required for early phases of drug discovery. It has been proven with industry-wide data that addressing ADME properties early in the discovery process helps significantly reduce attrition rates of drug candidates due to pharmacokinetic properties later in development [23]. There have been a number of comprehensive reviews covering the history

and common practices of HT-ADME screening and sample analysis [17,24—28].

Due to its critical role in drug discovery, the last decade (2010—2019) saw a number of significant developments in HT-ADME screening. First of all, the conduct of ADME screening has been "industrialized" through the development of software and automation that has facilitated assay incubation, sample analysis, data review and reporting. While in vitro ADME screening used to be conducted almost exclusively at big pharmaceutical companies, these mostly off-the-shelf tools have really "industrialized" ADME screening, empowering labs of different sizes, operating models (centralized, distributed, outsourced, etc.) and geographic locations to perform these screening assays with high efficiency. Secondly, cutting edge liquid handling and analysis technologies continued to be incorporated into ADME screening to further improve speed, quality and cost-effectiveness. Thirdly, the ADME screening assay portfolio continued to expand, especially in areas such as drug-transporter interactions, early soft spot identification, and ADME screening of peptide drug candidates. And lastly, the data generated by ADME screening assays have been widely used to develop in silico models with machine learning approaches to predict ADME properties. In this review we cover the recent developments and the state-of-the-art in these aforementioned areas; in addition we also offer a perspective on emerging sciences and technologies for next decade in the field of ADME screening.

2. The "industrialization" of ADME screening

At the time of its inception in the late 1990's, in vitro ADME screening was almost exclusively performed at large pharmaceutical companies, where the significant size of the discovery portfolio ensured enough assay demand, therefore justifying the substantial investment required in infrastructure and expertise development [24,29–31]. There were no existing commercially-available solutions to HT-ADME automation and sample analysis at the time; therefore, many companies developed their own customized solutions. The assay automation of that era tended to be stand-alone, workstation-based, with limited integration of various components [29,32]. Similarly, various custom solutions were developed for automated LC-MS/MS method development, sample analysis and data review [33–36]. While these highly innovative solutions laid the foundation for the field of HT-ADME screening as we know today, they required a high level of expertise in automation and bioanalysis to develop and maintain. The proprietary nature of these solutions also prevented them from being used in any other companies. As a result, HT-ADME screening was very much a "luxury" enjoyed by drug discovery organizations in only a handful of the largest pharmaceutical companies at the time.

From 2010 to 2019, with the importance of ADME screening in drug discovery well understood, and also thanks to the maturation of the underlying technologies, vendors started to commercialize products based on these previously proprietary tools specifically designed for HT-ADME screening.

2.1. Assay automation

In assay automation, multiple vendors including Tecan, Hamilton, PerkinElmer and many others, now offer complete, off-the-shelf solutions for ADME screening assays [4,16,37]. These solutions are typically based on a core platform of liquid handling, with additional accessories such as plate stores, shakers, incubators, filtration devices, centrifuges and sealers to perform tasks necessary for various HT-ADME assays. Several other vendors, including HighRes Biosolutions [38] and Agilent [39], offer fully integrated automation systems consisting of all of the aforementioned components, as well as one (or more) robotic arm(s) and corresponding software schedulers, for fully automated, truly walk-away assay operation. Multiple plates and multiple assays can be scheduled and conducted on the same system, thus realizing the most operation efficiency.

2.2. LC-MS/MS bioanalysis

LC-MS/MS with step or ballistic gradient LC, coupled with selected reaction monitoring (SRM) on triple-quadrupole mass spectrometers, has been the method of choice for HT-ADME sample analysis [40]. As pointed out by our previous review, the key challenges there are the large number of compounds requiring MS/MS optimization, the large sample number requiring analysis, and the large amount of data to process and review [17]. To address the requirement of SRM MS/MS conditions, automated optimization through flow injection analysis (FIA) is usually the solution [41]. To speed up the LC-MS/MS sample analysis, several approaches have been developed. The first is multiplexed LC-MS/MS, where multiple independent LC systems (channels) are connected through a switching valve to a single mass spectrometer; staggered injections are then made in synchronization with the switching valve, so that at any given time only the elution window from a single channel goes into the mass spectrometer. Either a 2x (for a 2-channel system) or a 4x (for a 4-channel system) speed improvement is possible with the multiplexing approach [13,42]. Another commonly used approach is direct online solid phase extraction – mass spectrometry (online SPE-MS), often also called "trap and elute", where small SPE cartridges packed with quite large particles (~50 μm) are used to perform essentially a desalting step for the sample first, and the analytes are then eluted with 100% organic solvent directly into the mass spectrometer [9,43,44]. The online SPE-MS approach offers a higher speed (5–10 s/sample) than the multiplexed LC-MS approach (30–60 s/sample), but obviously affords less chromatographic separation. Therefore, online SPE-MS is typically used for probe-based assays (i.e., Cytochrome P450 inhibition), where a single analyte and its stable isotopically labeled internal standard are analyzed for a large number of samples. On the other hand, multiplexed LC-MS/MS is commonly used in assays where many different compounds, all with different physico-chemical properties, need to be analyzed from a single assay batch (i.e., from metabolic stability or permeability assays).

Recently, similar to automation solutions, several vendors now offer complete hardware and software packages for the LC-MS/MS sample analysis of HT-ADME assay samples using these aforementioned approaches. For example, Thermo offers the QuickQuan™ package where MS/MS optimization, method generation and sample analysis can be fully automated on their triple-quadrupole instruments [5,45,46]. Optionally, QuickQuan can be further integrated with the Thermo multiplexed frontend LC system (Aria) to achieve an analysis time as fast as 15 s/sample with gradient elution, which is desirable for the large number of samples encountered in HT-ADME screening [42,47].

Another vendor, Sciex, offers a highly integrated solution for HT-ADME analysis named DiscoveryQuant™. Originally based on a proprietary solution developed at Pfizer [48], DiscoveryQuant™ underwent multiple iterations of development as a collaboration project between Sciex and multiple partners in the biopharma industry, and has now evolved into the most widely adopted software tool for HT-ADME bioanalysis [21,49,50]. The automated SRM MS/MS optimization routine in DiscoveryQuant™ has two unique and very useful features. First, it uses only a single loop injection (~1 min) with nested MS(/MS) scans to perform optimization of precursor ion, product ion, de-clustering voltage and collision energy, which has greatly simplified the optimization process and increased the optimization speed. Secondly, DiscoveryQuant™ has a powerful database feature where all optimized conditions from one instrument can be uploaded to a centralized database that allows sharing among many different Sciex instruments across the hall, or even across the globe, as illustrated in Fig. 1. A closely-related product, LeadScape™, not only incorporates all DiscoveryQuant™ features, but also controls the Apricot Designs Dual Arm (ADDA) [51] or LeadScape-1 (LS-1) [52] multiplexed auto-sampler for high-speed online-SPE or gradient LC separation in front of Sciex mass spectrometers. The online SPE-MS approach can achieve an analysis speed as fast as 5 s/sample, whereas the gradient LC mode can have a speed of approximately 15 s on the ADDA/LS-1 platform. Once the data are acquired, DiscoveryQuant™/LeadScape™ also has a data review module to perform automatic peak integration. Additional data review tools, including MultiQuant™ by Sciex and Gubbs Mass Spec Utility (GMSU) by Gubbs Inc, have also been widely used to process LC-MS/MS data from HT-ADME samples.

Taken together, these off-the-shelf and scalable solutions greatly enabled HT-ADME workflows in labs in biopharmaceutical companies of various sizes [9,43,53–55], in contract research organizations (CRO's) [56] and in academic research centers [57,58]. Therefore, HT-ADME screening has evolved from a workflow done by only a few large pharmaceutical companies in the 2000's to a standard practice anywhere where drug discovery research is conducted during the last decade.
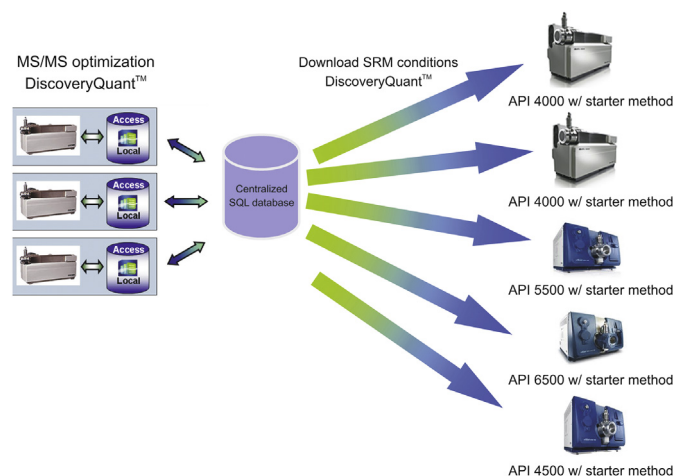
Fig. 1. Centralized SRM database allows sharing of MS/MS conditions across multiple sites and instrument platforms using DiscoveryQuant™. SRM: selected reaction monitoring. Instrument pictures are used with permission from Sciex.

3. Cutting-edge technologies in HT-ADME screening

In parallel to the industrialization of routine HT-ADME screening, novel and cutting-edge technologies have also continued to be tested and implemented in the field during the last decade thanks to the innovative culture of the existing HT-ADME community of practitioners. In this section, we review some of the technologies that have been adopted or are currently being evaluated in the HT-ADME screening laboratory.

3.1. Liquid handling

Liquid handling of sub-μL volumes has become a truly enabling technology for all screening communities (lead discovery, HT-ADME, etc.) in drug discovery. Low volume dispensing is critical in limiting the percentage of organic solvent (0.5% or lower) in the assay mixture, and the ability to accurately and reproducibly dispense nanoliter volumes can pave the way to assay miniaturization by reducing total incubation volume (and therefore reagent consumption). There are many technologies capable of nanoliter dispensing, with two enjoying the most success to date.

The mosquito® line of liquid handlers by SPT Labtech uses disposable, miniaturized positive displacement pipette tips to accurately transfer volumes as low as 25−50 nL. Since it uses a positive displacement approach for pipetting, a mosquito® liquid handler can easily transfer different liquid types, without resorting to re-calibration based on viscosity. Successful applications of mosquito® liquid handlers for low volume dispensing in HT-ADME assays have been reported [59].

Another highly successful nanoliter transfer approach uses sound waves to acoustically separate nanoliter-sized droplets from liquid meniscus in the source plate and eject them to the destination plate. Highly accurate, reproducible and rapid transfer of liquid volumes as low as 2.5 nL can be achieved in only several minutes for a 384-well plate [60]. First adopted in the high-throughput screening [61] and compound management [62] environment, acoustic transfer technologies have now been applied extensively in HT-ADME screening assays, especially those requiring serial dilutions for IC_{50} determination [25]. One caveat of the acoustic transfer approach is the need for calibration for each liquid type since different sound energy levels need to be applied for liquids with different properties (surface tension, viscosity, etc.). Two vendors currently offer acoustic dispensers: Echo by Labcyte®, and

ATS® by EDC Biosystems. A comparison of the two low-volume transfer approaches is presented in Table 1.

3.2. High-throughput sample analysis approaches

Sample analysis is another area where emerging technologies have been continuously evaluated and implemented. As mentioned previously, LC-MS/MS is still the workhorse in HT-ADME bioanalysis. However, it has been very difficult to break the 1 s/sample barrier for any chromatography and autosampler-based systems, despite the development of online SPE [44,63] and multiplexed LC systems [46]. To achieve even higher throughput, direct MS analysis from samples deposited onto solid support using various ionization methods has been attempted. These ionization methods include matrix assisted laser desorption ionization (MALDI) [64], laser diode thermal desorption (LDTD) [65], direct analysis in real time (DART) [66], coated blade spray [67], and dip-and-go inductive nanoelectrospray [68] amongst others. As pointed out in a previous review [17], although many of these ionization methods can achieve (or potentially achieve) a very high speed of analysis (several samples per second), they require an additional liquid handling step to transfer liquid assay samples into a solid support, which adds cost and complexity in automation. This disadvantage can be mitigated by using the aforementioned nanoliter transfer technologies for sample transfer [69], with several examples of HT-ADME applications reported in the literature [70]. Another disadvantage of these direct ionization approaches is the moderate to severe ionization suppression effect observed [71] (since there is no chromatographic separation), and the resulting generally lower data quality when compared to LC-MS-based approach.

A very innovative approach combining acoustic ejection and direct ionization for high-throughput mass spectrometry (HTMS) analysis has been recently developed by a group from AstraZeneca [72,73]. Dubbed acoustic mist ionization mass spectrometry, this approach uses a modified Echo acoustic dispenser to eject a "mist" of picoliter-sized droplets through a heated transfer tube directly into the mass spectrometer. Ionization is accomplished by a high voltage applied to the well top. The direct, contactless and high-speed (<1s/sample) features of this technology make it a highly attractive HTMS option for various screening areas and the group has published several papers describing its use in lead discovery. The biggest challenge of the acoustic mist ionization methodology is its data quality. This is due to (1) the difficulty in maintaining reproducibility in the mist generation (since regular acoustic dispensers operate by ejecting discrete, well-controlled nL droplets); and (2) the suppression effect exerted by the sample matrix. As a result, a CV of ~30% has been reported for repeated analysis, which is considered somewhat to be high for ADME applications.

A more recent development in direct acoustic mass spectrometry has made significant progress in addressing these challenges. Developed by Sciex, their acoustic ejection mass spectrometer (AEMS) uses a simple yet elegant interface called open port

Table 1
Comparison of the two low-volume liquid handlers.

Parameters	Positive displacement	Acoustic transfer
Transfer range	25 nL to 1.2 μL	2.5 nL to 5 μL
Sample contact	Contact	Contactless
Transfer speed	Minutes per 384-well plate	Minutes per 384-well plate
Consumables	Special tips	Special plates
Sample type	Any liquids	Aqueous, DMSO
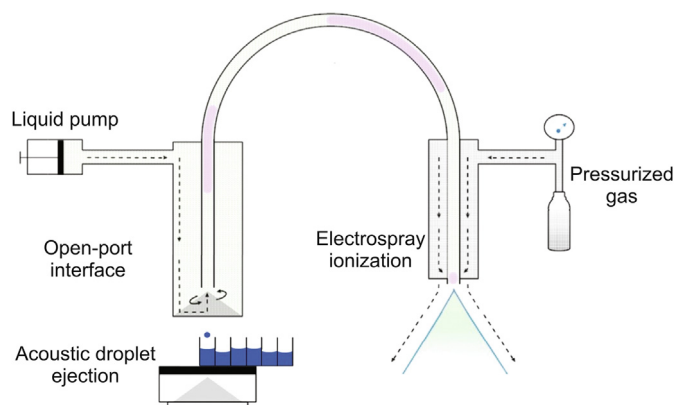
Fig. 2. Schematic of the acoustic ejection mass spectrometer (AEMS) system. Reprinted with permission from Refs. [76], Copyright (2020) American Chemical Society.

interface (OPI) to capture the droplets and transport them with a stream of carrier solvent (typically methanol) into a conventional electrospray ionization source [74–76]. Fig. 2 shows the schematic of an AEMS system [76]. AEMS with OPI enjoys the similar sub-second/sample speed and direct analysis features to those of the AMI-MS approach. In addition, it has been demonstrated that AEMS can generate highly reproducible results from assay samples thanks to the low variability of acoustic ejection of nL-sized droplets and, more importantly, the mitigation of ionization suppression by the significant dilution (~1000x) of the droplets by the carrier solvent. As a result, a typical CV of 3%–5% without the use of internal standards has been reported using AEMS for HTS and HT-ADME assay samples [74]. Obviously, the dilution effect does negatively affect the detection limit of the analytes. However, the low nM lower limit of quantitation (LLOQ) typically reported with AEMS should be sufficient to meet the requirements of most in vitro assays. Therefore, with its balance of high speed and high data quality, AEMS is poised to become the detection method of choice for label-free, biochemical or cell-based assays including those used in HT-ADME screening. A comparison of the several high-throughput MS-based readout methods for HT-ADME assays is presented in Table 2.

3.3. High resolution mass spectrometry

In addition to the speed increase on the triple-quadrupole MS platform mentioned above, another emerging trend in HT-ADME bioanalysis is the use of high-resolution accurate mass (HRAM) capability of time-of-flight or Orbitrap mass spectrometers for sample analysis. Quantitative sample analysis of HT-ADME samples has been demonstrated with HRAM, typically by using the sample pooling approach to reduce sample numbers and take full advantage of the high resolving power of the mass spectrometer [77]. More importantly, a number of quantitative/qualitative workflows have been introduced to perform metabolic soft spot analysis

concurrently with metabolic stability sample analysis [78,79].

4. Expansion of HT-ADME screening assay portfolio

4.1. Transporter assays

The assay portfolio of in vitro HT-ADME screening has continued to expand during the last decade and here we highlight some of the recently deployed assays in the field. Drug-drug-interactions and toxicity due to transporter involvement have been increasingly recognized as an important potential liability of drug candidates. As a result, inhibition assays for hepatobiliary and renal transporters (in addition to the existing intestinal transporters) have become an integral part of the drug-drug interaction (DDI) portfolio of many HT-ADME screening labs [10,11]. Some of the most commonly studied transporters in HT-ADME include hepatobiliary transporters such as organic anion-transporting polypeptide 1B1 (OATP1B1), organic anion-transporting polypeptide 1B3 (OATP1B3), sodium (Na^+) taurocholate cotransporting polypeptide (NTCP), bile salt export pump (BSEP) [80], renal transporters such as organic anion transporter 1 (OAT1), organic anion transporter 3 (OAT3), organic cation transporter 1 (OCT1), organic cation transporter 2 (OCT2), multidrug and toxin extrusion protein 1 transporter (MATE1), multidrug and toxin extrusion protein 2K transporter (MATE2K) [10], and intestinal transporters such as P-glycoprotein (P-gp) and breast cancer resistance protein (BCRP) [81]. Most of the transporter screening assays are conducted in inhibition mode by assessing the potential of a drug candidate to act as a "perpetrator" by inhibiting the activity of a given transporter. If necessary, substrate assays can be used to assess whether a drug candidate is likely to become a "victim" of a transporter-mediated DDI [82].

4.2. HT-ADME assays for peptide drug candidates

Another growing area in HT-ADME screening is the characterization of peptide drug candidates. Since its inception, HT-ADME has been mostly used to assess the properties and liabilities of small molecule drug candidates. Recently, peptides have emerged as an attractive drug modality since they can combine target affinities similar to those of biologics with physicochemical properties closer to those of small molecules. Most peptide drugs are dosed by injection due to their poor proteolytic stability, low membrane permeability and low oral bioavailability [83]. A number of synthetic strategies [84–86] have been attempted to address these challenges for orally-dosed peptide drug candidates and, correspondingly, new or modified HT-ADME assays have been developed to facilitate the lead optimization in oral peptide drug discovery. For example, permeability assays such as colon adenocarcinoma cell line (Caco-2) or parallel artificial membrane permeability assay (PAMPA) have both been used to assess the permeability of peptides [84,87]. However, due to the non-specific binding typically exhibited by peptides and the generally very low permeability values, they tend to generate null results in these

Table 2
Comparison of high-throughput MS analysis approaches. SPE: solid phase extraction; LDI: laser desorption ionization; AMI: acoustic mist ionization; AE: acoustic ejection.

Parameters	LC-MS/MS	SPE-MS/MS	LDI-MS	AMI-MS	AE-MS
Speed per well	60s	10 s	1 s	1 s	1 s
In situ sample clean up	Yes	Yes	No	No	Yes
Data variability	Low	Low	High	High	Low
Sample format	96/384	96/384	96/384	384	384/1536
Sample volume	>40 μL	>40 μL	<1 μL	<1 μL	<1 μL
Direct analysis	Yes	Yes	No	Yes	Yes

assays. Therefore, assay conditions have been modified to address these challenges. Also, additional assays such as chromatography-based experimental polar surface area (EPSA) have been developed specifically to assess the permeability of peptides [88].

4.3. High-throughput soft spot identification assays

The in vitro metabolic soft spot assay is another recent addition to the HT-ADME assay portfolio [89]. Unlike most HT-ADME assays with numbers as end points (IC_{50}, permeability values, percent bound, etc.), the metabolic soft spot assay provides structural information about the sites of metabolism (SOM), or "soft spots" of discovery compounds. Historically a very low throughput assay conducted only for a handful of lead compounds, metabolic soft spot assays have recently become quite common in HT-ADME. This is due to technological developments in two areas: first, the availability of high-performance, high-resolution mass spectrometers with generic data acquisition methods [90,91]; and, second, the development of software tools to perform automated structural elucidation in batch mode [92,93]. Equipped with the SOM information from the soft spot assay, discovery projects can now address metabolic instability synthetically for both small molecules and peptides in a more targeted way than before.

5. Future perspective

Thanks to the evolving sciences and enabling technologies, we anticipate more exciting developments in the field of HT-ADME in next decade. From an assay portfolio standpoint, emerging areas of ADME sciences will inevitably find their way into HT-ADME screening. Examples of these include new, more physiologically relevant in vitro microphysiological systems (MPS) such as 3D tissue cultures and organ(s)-on-a-chip [94−98], for better in vitro in vivo translation (IVIVT). Another trend in ADME is the use of endogenous probes (essentially biomarkers) for transporter DDI studies in vivo, which has the potential advantages of reducing pill burden and obtaining transporter DDI information from a regular phase I study [99−104]. Once the endogenous probes are validated, it is foreseeable that the corresponding in vitro HT assays can be implemented in a screening mode as well. Yet another example is HT-ADME screening of new drug modalities. In addition to small molecules and peptides, the field is poised to enter early ADME screening of new modalities including protein degraders [105−107], antisense oligonucleotides (ASO's) [108−110], antibody drug conjugates (ADC's) [111−114] and biologics [115−117]. Although the ADME science of these modalities is still currently developing, we expect more and more HT-ADME format assays will become online to support discovery efforts along with the evolving science.

With the long history of HT-ADME operation in many companies and the resulting wealth of ADME data that can be "mined", developing in silico models to predict ADME properties has long been recognized as the logical next step for HT-ADME screening [118,119]. While many ADME predictive models reported in the literature use a training set of only several hundred compounds, a large pharmaceutical company's HT-ADME dataset could contain assay results from several hundred thousand compounds. These datasets can serve as the ideal training sets for model development due to its large size, and also the fact that they are a much better representation of the chemical space occupied by the compound collection of the particular company. Computational chemistry approaches aimed at developing quantitative structure-activity relationship (QSAR) models have long been applied to ADME

properties [120,121]. More recently, various machine learning (ML) methods have been applied to develop models for clearance, permeability and DDI potentials [122−126]. With the recent rapid development in machine learning methodologies, and the large size of the HT-ADME datasets available to use as training sets, it is expected that even better predictive ADME models can be developed in the future to guide efforts such as hit triaging from lead discovery screens and in the design-make-test cycles of lead optimization in drug discovery [127].

Conflicts of interest

The author declares that there are no conflicts of interest.

Acknowledgments

Appendix A. Supplementary data

Supplementary data to this article can be found online at https://doi.org/10.1016/j.jpha.2020.05.004.

References

[1] A.P. Li, Screening for human ADME/Tox drug properties in drug discovery, Drug Discov. Today 6 (2001) 357−366.
[2] E.H. Kerns, Editorial: high throughput in vitro ADME/tox profiling for drug discovery, Curr. Drug Metabol. 9 (2008) 845−846.
[3] T.J. Carlson, M.B. Fisher, Recent advances in high throughput screening for ADME properties, Comb. Chem. High Throughput Screen. 11 (2008) 258−264.
[4] R. Xu, M. Manuel, J. Cramlett, et al., A high throughput metabolic stability screening workflow with automated assessment of data quality in pharmaceutical industry, J. Chromatogr. A 1217 (2010) 1616−1625.
[5] K. Kieltyka, J. Zhang, S. Li, et al., A high-throughput bioanalytical platform using automated infusion for tandem mass spectrometric method optimization and its application in a metabolic stability screen, Rapid Commun. Mass Spectrom. 23 (2009) 1579−1591.
[6] X. Cai, A. Walker, C. Cheng, et al., Approach to improve compound recovery in a high-throughput Caco-2 permeability assay supported by liquid chromatography−tandem mass spectrometry, J. Pharm. Sci. 101 (2012) 2755−2762.
[7] X. Cai, S. Madari, A. Walker, et al., Addition of optimized bovine serum albumin level in a high-throughput Caco-2 assay enabled accurate permeability assessment for lipophilic compounds, SLAS Discov. 24 (2019) 738−744.
[8] S. Skolnik, X. Lin, J. Wang, et al., Towards prediction of in vivo intestinal absorption using a 96-well Caco-2 assay, J. Pharm. Sci. 99 (2010) 3246−3265.
[9] X. Wu, J. Wang, L. Tan, et al., In vitro ADME profiling using high-throughput rapidfire mass spectrometry: cytochrome P450 inhibition and metabolic stability assays, J. Biomol. Screen 17 (2012) 761−772.
[10] M. Vath, L. Gallagher, W. Shou, et al., Development of an LC−MS/MS method for high throughput quantification of metformin uptake in transporter inhibition assays, J. Chromatogr. B 967 (2014) 211−218.
[11] A.D. Wagner, L. Elkin, K. Mosure, et al., Development of a high-throughput mass spectrometry based analytical method to support an in vitro OATP1B1 inhibition screening assay, Rapid Commun. Mass Spectrom. 30 (2016) 1787−1796.
[12] J. Alsenz, M. Kansy, High throughput solubility measurement in drug discovery and development, Adv. Drug Deliv. Rev. 59 (2007) 546−567.
[13] J. Zhang, W.Z. Shou, M. Vath, et al., An integrated bioanalytical platform for supporting high-throughput serum protein binding screening, Rapid Commun. Mass Spectrom. 24 (2010) 3593−3601.
[14] G.Y. Di Veroli, M.R. Davies, H. Zhang, et al., High-throughput screening of drug-binding dynamics to HERG improves early drug safety assessment, Am. J. Physiol. Heart Circ. Physiol. 304 (2012) H104−H117.
[15] X. Su, E.W.K. Young, H.A.S. Underkofler, et al., Microfluidic cell culture and its application in high-throughput drug screening: cardiotoxicity assay for hERG channels, J. Biomol. Screen 16 (2010) 101−111.
[16] A. Soikkeli, C. Sempio, A.M. Kaukonen, et al., Feasibility evaluation of 3 automated cellular drug screening assays on a robotic workstation, J. Biomol.

Screen 15 (2009) 30—41.

[17] W.Z. Shou, J. Zhang, Recent development in high-throughput bioanalytical support for in vitro ADMET profiling, Expet Opin. Drug Metabol. Toxicol. 6 (2010) 321—336.

[18] V.P. Miller, SPE—MS analysis of absorption, distribution, metabolism and excretion assays: a tool to increase throughput and steamline workflow, Bioanalysis 4 (2012) 1111—1121.

[19] W.Z. Shou, J. Zhang, Recent development in software and automation tools for high-throughput discovery bioanalysis, Bioanalysis 4 (2012) 1097—1109.

[20] B. Larson, P. Banks, H. Sherman, et al., Automation of cell-based drug absorption assays in 96-well format using permeable support systems, J. Lab. Autom. 17 (2012) 222—232.

[21] J. Janiszewski, N. Levitt, Enabling software for high-throughput bioanalysis, in: W.Z. Shou, N. Weng (Eds.), Eliminating Bottlenecks for Efficient Bioanalysis: Practices and Applications in Drug Discovery and Development, Future Science Ltd., London, 2014, pp. 34—50.

[22] L. Heinle, V. Peterkin, S.M. de Morais, et al., A high throughput, 384-well, semi-automated, hepatocyte intrinsic clearance assay for screening new molecular entities in drug discovery, Comb. Chem. High Throughput Screen. 18 (2015) 442—452.

[23] M.J. Waring, J. Arrowsmith, A.R. Leach, et al., An analysis of the attrition of drug candidates from four major pharmaceutical companies, Nat. Rev. Drug Discov. 14 (2015) 475—486.

[24] J. Wang, L. Urban, D. Bojanic, Maximising use of in vitro ADMET tools to predict in vivo bioavailability and safety, Expet Opin. Drug Metabol. Toxicol. 3 (2007) 641—665.

[25] H. Wan, A.G. Holmén, High throughput screening of physicochemical properties and in vitro ADME profiling in drug discovery, Comb. Chem. High Throughput Screen. 12 (2009) 315—329.

[26] J. Wang, S. Skolnik, Recent advances in physicochemical and ADMET profiling in drug discovery, Chem. Biodivers. 6 (2009) 1887—1899.

[27] J. Zhang, W.Z. Shou, Mass spectrometry for quantitative in vitro ADME assays, in: W.A. Korfmacher (Ed.), Mass Spectrometry for Drug Discovery and Drug Development, John Wiley & Sons, Inc., New York, 2013, pp. 97—113.

[28] M.A.M. Fitzgerald, Strategies for high-throughput sample analysis, in: W.Z. Shou, N. Weng (Eds.), Eliminating Bottlenecks for Efficient Bioanalysis: Practices and Applications in Drug Discovery and Development, Future Science Ltd., London, 2014, pp. 18—33.

[29] E.H. Kerns, L. Di, Automation in pharmaceutical profiling, J. Lab. Autom. 10 (2005) 114—123.

[30] E.H. Kerns, L. Di, Utility of mass spectrometry for pharmaceutical profiling applications, Curr. Drug Metabol. 7 (2006) 457—466.

[31] D.B. Kassel, Applications of high-throughput ADME in drug discovery, Curr. Opin. Chem. Biol. 8 (2004) 339—345.

[32] K.M. Jenkins, R. Angeles, M.T. Quintos, et al., Automated high throughput ADME assays for metabolic stability and cytochrome P450 inhibition profiling of combinatorial libraries, J. Pharmaceut. Biomed. Anal. 34 (2004) 989—1004.

[33] J.S. Janiszewski, K.J. Rogers, K.M. Whalen, et al., A high-capacity LC/MS system for the bioanalysis of samples generated from plate-based metabolic screening, Anal. Chem. 73 (2001) 1495—1501.

[34] R. Xu, C. Nemes, K.M. Jenkins, et al., Application of parallel liquid chromatography/mass spectrometry for high throughput microsomal stability screening of compound libraries, J. Am. Soc. Mass Spectrom. 13 (2002) 155—165.

[35] S. Briem, B. Pettersson, E. Skoglund, Description and validation of a four-channel staggered LC-MS/MS systems for high-throughput in vitro screens, Anal. Chem. 77 (2005) 1905—1910.

[36] E.H. Kerns, T. Kleintop, D. Little, et al., Integrated high capacity solid phase extraction-MS/MS system for pharmaceutical profiling in drug discovery, J. Pharmaceut. Biomed. Anal. 34 (2004) 1—9.

[37] K.A. Youdim, R. Lyons, L. Payne, et al., An automated, high-throughput, 384 well Cytochrome P450 cocktail IC50 assay using a rapid resolution LC—MS/MS end-point, J. Pharmaceut. Biomed. Anal. 48 (2008) 92—99.

[38] G. Dutton, Life sciences labs need cobots, not robots, Genet. Eng. Biotechnol. News 38 (2018) 8—9.

[39] S. Mukadam, S. Tay, D. Tran, et al., Evaluation of time-dependent Cytochrome P450 inhibition in a high-throughput, automated assay: introducing a novel area under the curve shift approach, Drug Metabol. Lett. 6 (2012) 43—53.

[40] M.J. Berna, B.L. Ackermann, A.T. Murphy, High-throughput chromatographic approaches to liquid chromatographic/tandem mass spectrometric bioanalysis to support drug discovery and development, Anal. Chim. Acta 509 (2004) 1—9.

[41] K. Kieltyka, J. Zhang, S. Li, et al., A high-throughput bioanalytical platform using automated infusion for tandem mass spectrometric method optimization and its application in a metabolic stability screen, Rapid Commun. Mass Spectrom. 23 (2009) 1579—1591.

[42] J. Zhang, M. Vath, C. Ferraro, et al., A high-speed liquid chromatography/tandem mass spectrometry platform using multiplexed multiple-injection chromatography controlled by single software and its application in discovery ADME screening, Rapid Commun. Mass Spectrom. 27 (2013) 731—737.

[43] A.H. Luippold, T. Arnold, W. Jörg, et al., Application of a rapid and integrated

analysis system (RIAS) as a high-throughput processing tool for in vitro ADME samples by liquid chromatography/tandem mass spectrometry, J. Biomol. Screen 16 (2011) 370—377.

[44] A.H. Luippold, T. Arnold, W. Jörg, et al., An integrated platform for fully automated high-throughput LC—MS/MS analysis of in vitro metabolic stability assay samples, Int. J. Mass Spectrom. 296 (2010) 1—9.

[45] J. Smalley, B. Xin, T.V. Olah, Increasing high-throughput Discovery bioanalysis using automated selected reaction monitoring compound optimization, ultra-high-pressure liquid chromatography, and single-step sample preparation workflows, Rapid Commun. Mass Spectrom. 23 (2009) 3457—3464.

[46] J. Zhang, W.Z. Shou, M. Vath, et al., Integrated bioanalytical platform for supporting a high throughput serum protein binding screen, Rapid Commun. Mass Spectrom. 24 (2010) 3593—3601.

[47] K. Murphy, P.K. Bennett, N. Duczak, High-throughput quantitation of large molecules using multiplexed chromatography and high-resolution/accurate mass LC—MS, Bioanalysis 4 (2012) 1013—1024.

[48] K.M. Whalen, K.J. Rogers, M.J. Cole, et al., AutoScan: an automated workstation for rapid determination of mass and tandem mass spectrometry conditions for quantitative bioanalytical mass spectrometry, Rapid Commun. Mass Spectrom. 14 (2000) 2074—2079.

[49] K. Whalen, J. Gobey, J. Janiszewski, A centralized approach to tandem mass spectrometry method development for high-throughput ADME screening, Rapid Commun. Mass Spectrom. 20 (2006) 1497—1503.

[50] A. Amaral, C. Saran, J. Amin, et al., A comparison of LC-MS/MS and a fully integrated autosampler/solid-phase extraction system for the analysis of protein binding samples, J. Biomol. Screen 21 (2016) 620—625.

[51] J. Janiszewski, R. Schneider, B. Kapinos, et al., Development of a high-speed, multiplexed sample-delivery instrument for LC—MS/MS bioanalysis, Bioanalysis 4 (2012) 1039—1056.

[52] B. Kapinos, J. Liu, M. Piotrowski, et al., Development of a high-performance, enterprise-level, multimode LC—MS/MS autosampler for drug discovery, Bioanalysis 9 (2017) 1643—1654.

[53] P. Ballard, P. Brassil, K.H. Bui, et al., The right compound in the right assay at the right time: an integrated discovery DMPK strategy, Drug Metab. Rev. 44 (2012) 224—252.

[54] X. Lu, Development of an Excel-based laboratory information management system for improving workflow efficiencies in early ADME screening, Bioanalysis 8 (2016) 99—110.

[55] H. Wang, M. Zrada, K. Anderson, et al., Understanding and reducing the experimental variability of in vitro plasma protein binding measurements, J. Pharm. Sci. 103 (2014) 3302—3309.

[56] G.T. Clark, HT-ADME in a contract research organization laboratory: can you ensure bioanalytical quality in a highly automated environment? Bioanalysis 7 (2015) 403—406.

[57] E.C. Padilha, J. Wang, E. Kerns, et al., Application of in vitro drug metabolism studies in chemical structure optimization for the treatment of fibrodysplasia ossificans progressiva (FOP), Front. Pharmacol. 10 (2019) 234.

[58] S.J. Gardell, G.P. Roth, D.P. Kelly, Cardiovascular drug discovery in the academic setting: building infrastructure, harnessing strengths, and seeking synergies, J. Cardiovasc. Transl. Res. 3 (2010) 431—437.

[59] Integrated nanoliter dispensing aids drug discovery. https://www.tecan.com/hubfs/Tecan_Journal/201401/20_21_Integrated_nanoliter_dispensing_aids_drug_discovery_012014.pdf, 2014.

[60] R. Ellson, M. Mutz, B. Browning, et al., Transfer of low nanoliter volumes between microplates using focused acoustics—automation considerations, J. Lab. Autom. 8 (2003) 29—34.

[61] R.J. Grant, K. Roberts, C. Pointon, et al., Achieving accurate compound concentration in cell-based screening: validation of acoustic droplet ejection technology, J. Biomol. Screen 14 (2009) 452—459.

[62] D. Griffith, R. Northwood, P. Owen, et al., Implementation and development of an automated, ultra-high-capacity, acoustic, flexible dispensing platform for assay-ready plate delivery, J. Lab. Autom. 17 (2012) 348—358.

[63] A.H. Luippold, T. Arnold, W. Joerg, et al., A novel and integrated platform for fully automated high-throughput LC/MS/MS analysis of in vitro ADME samples, in: Proceedings of the 57th ASMS Conference on Mass Spectrometry and Allied Topics, Philadelphia, United States, 2009.

[64] M. Winter, R. Ries, C. Kleiner, et al., Automated MALDI target preparation concept: providing ultra-high-throughput mass spectrometry—based screening for drug discovery, SLAS Technol. 24 (2018) 209—221.

[65] A. Dion-Fortier, A. Gravel, C. Guérette, et al., Signal enhancement in laser diode thermal desorption-triple quadrupole mass spectrometry analysis using microwell surface coatings, J. Mass Spectrom. 54 (2019) 167—177.

[66] S. Yu, E. Crawford, J. Tice, et al., Bioanalysis without sample cleanup or chromatography: the evaluation and initial implementation of direct analysis in real time ionization mass spectrometry for the quantification of drugs in biological matrixes, Anal. Chem. 81 (2009) 193—202.

[67] A. Kasperkiewicz, G.A. Gómez-Ríos, D. Hein, et al., Breaching the 10 second barrier of total analysis time for complex matrices via automated coated blade spray, Anal. Chem. 91 (2019) 13039—13046.

[68] Z. Wei, Z. Xie, R. Kuvelkar, et al., High-throughput bioassays using "dip-and-go" multiplexed electrospray mass spectrometry, Angew. Chem. 58 (2019) 17594—17598.

[69] C. Haslam, J. Hellicar, A. Dunn, et al., The evolution of MALDI-TOF mass spectrometry toward ultra-high-throughput screening: 1536-well format and beyond, J. Biomol. Screen 21 (2015) 176–186.

[70] Z. Haarhoff, A. Wagner, P. Picard, et al., Coupling laser diode thermal desorption with acoustic sample deposition to improve throughput of mass spectrometry−based screening, J. Biomol. Screen 21 (2015) 165–175.

[71] J. Chandler, C. Haslam, N. Hardy, et al., A systematic investigation of the best buffers for use in screening by maldi−mass spectrometry, SLAS Discov. 22 (2016) 1262–1269.

[72] I. Sinclair, R. Stearns, S. Pringle, et al., Novel acoustic loading of a mass spectrometer: toward next-generation high-throughput ms screening, J. Lab. Autom. 21 (2015) 19–26.

[73] I. Sinclair, M. Bachman, D. Addison, et al., Acoustic mist ionization platform for direct and contactless ultrahigh-throughput mass spectrometry analysis of liquid samples, Anal. Chem. 91 (2019) 3790–3794.

[74] H. Zhang, C. Liu, W. Hua, et al., Acoustic ejection mass spectrometry for high-throughput analysis, bioRxiv (2020) 2020, 01.28.923938.

[75] H. Zhang, Acoustic dispensing-mass spectrometry: the next high throughput bioanalytical platform for early drug discovery, Bioanalysis 9 (2017) 1619–1621.

[76] K.J. DiRico, W. Hua, C. Liu, et al., Ultra-high-throughput acoustic droplet ejection-open port interface-mass spectrometry for parallel medicinal chemistry, ACS Med. Chem. Lett. (2020), https://doi.org/10.1021/acsmedchemlett.0c00066.

[77] J. Zhang, J. Maloney, D.M. Drexler, et al., Cassette incubation followed by bioanalysis using high-resolution MS for in vitro ADME screening assays, Bioanalysis 4 (2012) 581–593.

[78] G. Backfisch, B. Reder-Hilz, J. Hoeckels-Messemer, et al., High-throughput quantitative and qualitative analysis of microsomal incubations by cocktail analysis with an ultraperformance liquid chromatography-quadrupole time-of-flight mass spectrometer system, Bioanalysis 7 (2014) 671–683.

[79] M.F. Grubb, W.G. Humphreys, J.L. Josephs, A semi-automated method for the integrated evaluation of half-life and metabolic soft spots of discovery compounds, Bioanalysis 4 (2012) 1747–1761.

[80] H. Tang, D.R. Shen, Y.-H. Han, et al., Development of novel, 384-well high-throughput assay panels for human drug transporters: drug interaction and safety assessment in support of discovery research, J. Biomol. Screen 18 (2013) 1072–1083.

[81] A.D. Wagner, J.M. Kolb, C.C. Özbal, et al., Ultrafast mass spectrometry based bioanalytical method for digoxin supporting an in vitro P-glycoprotein (P-gp) inhibition screen, Rapid Commun. Mass Spectrom. 25 (2011) 1231–1240.

[82] K.L.R. Brouwer, D. Keppler, K.A. Hoffmaster, et al., In vitro methods to support transporter evaluation in drug discovery and development, Clin. Pharmacol. Ther. 94 (2013) 95–112.

[83] L. Di, Strategic approaches to optimizing peptide ADME properties, AAPS J. 17 (2015) 134–143.

[84] A.C. Rand, S.S.F. Leung, H. Eng, et al., Optimizing PK properties of cyclic peptides: the effect of side chain substitutions on permeability and clearance, Med. Chem. Commun. 3 (2012) 1282–1289.

[85] M. Werle, A. Bernkop-Schnürch, Strategies to improve plasma half life time of peptide and protein drugs, Amino Acids 30 (2006) 351–367.

[86] J. Chatterjee, B. Laufer, H. Kessler, Synthesis of N-methylated cyclic peptides, Nat. Protoc. 7 (2012) 432–444.

[87] R. Ano, Y. Kimura, M. Shima, et al., Relationships between structure and high-throughput screening permeability of peptide derivatives and related compounds with artificial membranes: application to prediction of Caco-2 cell permeability, Bioorg. Med. Chem. 12 (2004) 257–264.

[88] G.H. Goetz, L. Philippe, M.J. Shapiro, EPSA: a novel supercritical fluid chromatography technique enabling the design of permeable cyclic peptides, ACS Med. Chem. Lett. 5 (2014) 1167–1172.

[89] A.A. Paiva, C. Klakouski, S. Li, et al., Development, optimization and implementation of a centralized metabolic soft spot assay, Bioanalysis 9 (2017) 541–552.

[90] R.J. Mortishire-Smith, H. Zhang, K.P. Bateman, High-resolution mass spectrometry and drug metabolite identification, in: M.S. Lee, M. Zhu (Eds.), Mass Spectrometry in Drug Metabolism and Disposition, John Wiley & Sons, Inc., New York, 2011, pp. 407–448.

[91] X. Zhu, Y. Chen, R. Subramanian, Comparison of information-dependent acquisition, SWATH, and MSA techniques in metabolite identification study employing ultrahigh-performance liquid chromatography−quadrupole time-of-flight mass spectrometry, Anal. Chem. 86 (2014) 1202–1209.

[92] A. Paiva, W.Z. Shou, Recent developments in software tools for high-throughput in vitro ADME support with high-resolution MS, Bioanalysis 8 (2016) 1723–1733.

[93] M. Ahlqvist, C. Leandersson, M.A. Hayes, et al., Software-aided structural elucidation in drug discovery, Rapid Commun. Mass Spectrom. 29 (2015) 2083–2089.

[94] S. Fowler, W.L.K. Chen, D.B. Duignan, et al., Microphysiological systems for ADME-related applications: current status and recommendations for system development and characterization, Lab Chip 20 (2020) 446–467.

[95] K. Fabre, B. Berridge, W.R. Proctor, et al., Introduction to a manuscript series on the characterization and use of microphysiological systems (MPS) in pharmaceutical safety and ADME applications, Lab Chip 20 (2020) 1049–1057.

[96] L. Docci, N. Parrott, S. Krähenbühl, et al., Application of new cellular and microphysiological systems to drug metabolism optimization and their positioning respective to in silico tools, SLAS Discov. 24 (2019) 523–536.

[97] F. An, Y. Qu, Y. Luo, et al., A laminated microfluidic device for comprehensive preclinical testing in the drug ADME process, Sci. Rep. 6 (2016) 25022.

[98] S. Ishida, Organs-on-a-chip: current applications and consideration points for in vitro ADME-Tox studies, Drug Metabol. Pharmacokinet. 33 (2018) 49–54.

[99] A.D. Rodrigues, K.S. Taskar, H. Kusuhara, et al., Endogenous probes for drug transporters: balancing vision with reality, Clin. Pharmacol. Ther. 103 (2018) 434–448.

[100] X. Chu, M. Liao, H. Shen, et al., Clinical probes and endogenous biomarkers as substrates for transporter drug-drug interaction evaluation: perspectives from the international transporter consortium, Clin. Pharmacol. Ther. 104 (2018) 836–864.

[101] A. King-Ahmad, S. Clemens, R. Ramanathan, et al., A fully automated and validated human plasma LC−MS/MS assay for endogenous OATP biomarkers coproporphyrin-I and coproporphyrin-III, Bioanalysis 10 (2018) 691–701.

[102] L. Luo, J. Kay, J. Zhang, et al., LC−MS/MS assay for N1-methylnicotinamide in humans, an endogenous probe for renal transporters, Bioanalysis 10 (2018) 673–689.

[103] S. Barnett, K. Ogungbenro, K. Ménochet, et al., Comprehensive evaluation of the utility of 20 endogenous molecules as biomarkers of OATP1B inhibition compared with rosuvastatin and coproporphyrin I, J. Pharmacol. Exp. Therapeut. 368 (2019) 125–135.

[104] D. Rodrigues, A. Rowland, From endogenous compounds as biomarkers to plasma-derived nanovesicles as liquid biopsy; has the golden age of translational pharmacokinetics-absorption, distribution, metabolism, excretion-drug−drug interaction science finally arrived? Clin. Pharmacol. Ther. 105 (2019) 1407–1420.

[105] M. Toure, C.M. Crews, Small-molecule PROTACS: new approaches to protein degradation, Angew. Chem. 55 (2016) 1966–1973.

[106] S.D. Edmondson, B. Yang, C. Fallan, Proteolysis targeting chimeras (PROTACs) in 'beyond rule-of-five' chemical space: recent progress and future challenges, Bioorg. Med. Chem. Lett 29 (2019) 1555–1564.

[107] C. Cantrill, P. Chaturvedi, C. Rynn, et al., Fundamental aspects of DMPK optimization of targeted protein degraders, Drug Discov. Today (2020), https://doi.org/10.1016/j.drudis.2020.03.012.

[108] R.S. Geary, Antisense oligonucleotide pharmacokinetics and metabolism, Expet Opin. Drug Metabol. Toxicol. 5 (2009) 381–391.

[109] F. Kazmi, P. Yerino, C. McCoy, et al., An assessment of the in vitro inhibition of Cytochrome P450 enzymes, UDP-glucuronosyltransferases, and transporters by phosphodiester- or phosphorothioate-linked oligonucleotides, Drug Metab. Dispos. 46 (2018) 1066–1074.

[110] D. Ramsden, J.-T. Wu, B. Zerler, et al., In vitro drug-drug interaction evaluation of GalNAc conjugated sirnas against CYP450 enzymes and transporters, Drug Metab. Dispos. 47 (2019) 1183–1194.

[111] E. Kraynov, A.V. Kamath, M. Walles, et al., Current approaches for absorption, distribution, metabolism, and excretion characterization of antibody-drug conjugates: an industry white paper, Drug Metab. Dispos. 44 (2016) 617–623.

[112] L.N. Tumey, S. Han, ADME considerations for the development of biopharmaceutical conjugates using cleavable linkers, Curr. Top. Med. Chem. 17 (2017) 3444–3462.

[113] K.R. Durbin, M.S. Nottoli, N.D. Catron, et al., High-Throughput, multispecies, parallelized plasma stability assay for the determination and characterization of antibody−drug conjugate aggregation and drug release, ACS Omega 2 (2017) 4207–4215.

[114] A. Fourie-O'Donohue, P.Y. Chu, J. dela Cruz Chuh, et al., Improved translation of stability for conjugated antibodies using an in vitro whole blood assay, mAbs 12 (2020) 1715705.

[115] T. Prueksaritanont, C. Tang, ADME of biologics—what have we learned from small molecules? AAPS J. 14 (2012) 410–419.

[116] A. Datta-Mannan, Mechanisms influencing the pharmacokinetics and disposition of monoclonal antibodies and peptides, Drug Metab. Dispos. 47 (2019) 1100–1110.

[117] J. Tibbitts, D. Canter, R. Graff, et al., Key factors influencing ADME properties of therapeutic proteins: a need for ADME characterization in drug discovery and development, mAbs 8 (2016) 229–245.

[118] C.E.C.A. Hop, M.J. Cole, R.E. Davidson, et al., High throughput ADME screening: practical considerations, impact on the portfolio and enabler of in silico adme models, Curr. Drug Metabol. 9 (2008) 847–853.

[119] L.L.G. Ferreira, A.D. Andricopulo, ADMET modeling approaches in drug discovery, Drug Discov. Today 24 (2019) 1157–1165.

[120] Z.D. Arkadiusz, A. Tomasz, G. Jorge, Computational methods in developing quantitative structure-activity relationships (QSAR): a Review, Comb. Chem. High Throughput Screen. 9 (2006) 213–228.

[121] K. Mahmud Tareq Hassan, Predictions of the ADMET properties of candidate drug molecules utilizing different QSAR/QSPR modelling approaches, Curr. Drug Metabol. 11 (2010) 285–295.

[122] V.G. Maltarollo, J.C. Gertrudes, P.R. Oliveira, et al., Applying machine learning techniques for ADME-Tox prediction: a review, Expet Opin. Drug Metabol. Toxicol. 11 (2015) 259–271.

[123] S. Wang, H. Sun, H. Liu, et al., ADMET evaluation in drug discovery. 16. predicting hERG blockers by combining multiple pharmacophores and

machine learning approaches, Mol. Pharm. 13 (2016) 2855—2866.

[124] J. Wenzel, H. Matter, F. Schmidt, Predictive multitask deep neural network models for ADME-Tox properties: learning from large data sets, J. Chem. Inf. Model. 59 (2019) 1253—1268.

[125] T.P. Stratton, A.L. Perryman, C. Vilchèze, et al., Addressing the metabolic stability of antituberculars through machine learning, ACS Med. Chem. Lett. 8 (2017) 1099—1104.

[126] M. Yang, J. Chen, L. Xu, et al., A novel adaptive ensemble classification framework for ADME prediction, RSC Adv. 8 (2018) 11661—11683.

[127] D.V.S. Green, Using machine learning to inform decisions in drug discovery: an industry perspective, in: E.O. Pyzer-Knapp, T. Laino (Eds.), Machine Learning in Chemistry: Data-Driven Algorithms, Learning Systems, and Predictions, American Chemical Society, Washington DC, 2019, pp. 81—101.

Review paper

Current LC-MS-based strategies for characterization and quantification of antibody-drug conjugates

Xiaoyu Zhu [a, b], Shihan Huo [a, b], Chao Xue [b, c], Bo An [d], Jun Qu [a, b, *]

[a] Department of Pharmaceutical Sciences, School of Pharmacy & Pharmaceutical Sciences, University at Buffalo, State University of New York, Buffalo, NY, 14214, USA
[b] New York State Center of Excellence in Bioinformatics & Life Sciences, Buffalo, NY, 14203, USA
[c] Department of Chemical and Biological Engineering, School of Engineering and Applied Science, University at Buffalo, State University of New York, Buffalo, NY, 14260, USA
[d] Exploratory Biomarker, In-vitro/In-vivo Translation, R&D Research, GlaxoSmithKline Pharmaceuticals, 1250 South Collegeville Rd, Collegeville, PA, 19426, USA

ARTICLE INFO

ABSTRACT

The past few years have witnessed enormous progresses in the development of antibody-drug conjugates (ADCs). Consequently, comprehensive analysis of ADCs in biological systems is critical in supporting discovery, development and evaluation of these agents. Liquid chromatography-mass spectrometry (LC-MS) has emerged as a promising and versatile tool for ADC analysis across a wide range of scenarios, owing to its multiplexing ability, rapid method development, as well as the capability of analyzing a variety of targets ranging from small-molecule payloads to the intact protein with a high, molecular resolution. However, despite this tremendous potential, challenges persist due to the high complexity in both the ADC molecules and the related biological systems. This review summarizes the up-to-date LC-MS-based strategies in ADC analysis and discusses the challenges and opportunities in this rapidly-evolving field.

1. Introduction

Antibody-drug conjugates (ADCs) constitute one of the most promising types of targeted cancer therapeutics. Typically, an ADC molecule includes an antibody targeting a tumor cell surface antigen, coupled with a number of potent cytotoxic payloads, via covalent conjugation (i.e., a linker). To date, eight ADCs that have been approved by U.S. Food and Drug Administration (FDA) include gemtuzumab ozogamicin (Mylotarg, Pfizer, Inc.), brentuximab vedotin (Adcetris, Seattle Genetics, Inc.), ado-trastuzumab emtansine (Kadcyla, Genentech, Inc.), inotuzumab ozogamicin (Besponsa, Pfizer, Inc.), polatuzumab vedotin-piiq (Polivy, Genentech, Inc.), enfortumab vedotin-ejfv (Padcev, Seattle Genetics, Inc.), trastuzumab deruxtecan (Enhertu, Daiichi Sankyo, Inc.) and sacituzumab govitecan (Trodelvy, Immunomedics, Inc.) and more than 100 in active clinical trials [1].

Though antibodies in ADCs rarely have antitumor activities by themselves, their specificity to target antigens often makes them useful delivery vehicles of payloads targeting tumor cells [2]. The toxic payloads used in most approved and clinical-stage ADCs are microtubule disruptors (e.g., maytansinoid and dolastatin analogs) or DNA-damaging agents (e.g., duocarmycins, pyrrolobenzodiazepines, and calicheamicins). The conjugating linkers in ADCs are generally classified into cleavable and non-cleavable ones, which behave quite differently in a biological system, and produce distinct in vivo forms of released toxin. Specifically, cleavable linkers (e.g., valine-citrulline dipeptide, hydrazine, and disulfide bridge) could be sensitive to cancer cell-specific intracellular properties, such as expression of certain protease, pH, and glutathione, and thus carrying the potential to achieve selective release of payloads [3]. By comparison, non-cleavable linkers contain no specific release mechanism and rely on intracellular proteolytic degradation following ADC internalization [3]. From an analytical perspective, while ADCs with cleavable linkers release free payload in a biological system, those with non-cleavable linkers usually release active payload-linker-amino acid moieties that are produced after

the complete degradation of ADCs [3]; consequently, different analytes should be targeted.

Due to the high complexity of ADCs, analysis of these compounds is uniquely challenging, especially in a biological system. For instance, both the small-molecule payloads and the protein portion need to be analyzed. In addition, drug-to-antibody ratio (DAR) is an important parameter describing the number of payloads conjugated to the antibody since the DAR species could dynamically change in vivo, which brings additional challenges for bioanalysis. Compared to other traditional methods, liquid chromatography–mass spectrometry (LC-MS) has the unique capability in ADC analysis, since it can broadly analyze small molecules, intact proteins, digested proteins, as well as specific domain of proteins with the molecule-level resolution. Therefore, LC-MS represents a highly versatile and valuable tool and has played an indispensable role in ADC characterization, both quantitatively and qualitatively.

In the initial development stage, especially for linker and payload discovery, LC-MS is highly valuable in providing structure-activity relationship information [4]. LC-MS has also been widely employed in characterization of the physicochemical properties of ADCs, which have profound effects on the safety and efficacy profile [5]. For in vivo analysis, typically quantification in plasma, including enzyme-linked immunosorbent assay (ELISA), LC-MS, or a combination of the two methods are often employed. In general, ELISA is more commonly used in quantification of ADCs in plasma but is often matrix- and species-dependent. Moreover, the method development for ELISA is often time consuming and costly, which is impractical in the early phase of ADCs development. Another challenge for ELISA is that it cannot differentiate DAR species of ADCs. By comparison, LC-MS is often matrix- and species-independent, and method development is much faster, therefore providing a promising alternative to ELISA for ADC quantification [6,7]. Additionally, owing to the molecular-resolution of LC-MS, it is capable of determining DAR in biological samples directly and therefore is very helpful in characterizing DAR species [4].

Moreover, the therapeutic window is narrow for most of the current ADCs due to off-target toxicity [8]. It is critical to perform a comprehensive in vivo analysis of ADCs to understand the effects of various species produced by ADC (*e.g.,* via biotransformation) on toxicity [9]. One paradigm is that measurement of tissue distribution of ADC-derived species at the off-target sites would be highly valuable for identifying perpetrators of toxic side effects. Radio-labeling approach has been used in previous studies to investigate ADC tissue distribution, which suffered from low accuracy and specificity owing to issues associated with radiolabeling [10,11]. By comparison, LC-MS-based method could be a promising solution to quantification of ADCs in tissue because of its high specificity and matrix independency [12].

With the ever-increasing interests in ADCs, a deeper understanding of the molecular characteristics and in vivo behaviors, as well as the connection between the two is urgently needed and appears to be a good fit for LC-MS. That being said, further technical improvements are essential for overcoming current hurdles and warranting reliable and practical investigation.

2. Analysis of the large-molecule portion

With the capability of protein analysis at peptide, subunit and intact levels, LC-MS can provide comprehensive protein characterization, both qualitatively and quantitatively. In this section, we review LC-MS analysis on whole ADC and protein levels, including conjugation site analysis, biotransformation characterization, localization of post-translational modification (PTM), and antibody structural integrity confirmation.

2.1. Qualitative characterization

Extensive characterization of ADC products is often required by FDA, such as DAR analysis, drug-load-distribution (DLD) assessment, conjugation sites characterization, and PTM evaluation. LC-MS-based techniques are one of the most important tools for these assays, and particularly useful for characterization of the protein component of ADCs. Depending on the purpose of analysis, LC-MS can analyze proteins at bottom-up (*i.e.,* peptide mapping), middle-down (*i.e.,* subunit analysis) or top-down (*i.e.,* intact protein) levels. These different levels of protein analysis are also often performed in parallel to provide orthogonal and more comprehensive information [13]. Reversed-phase liquid chromatography (RPLC) is the most commonly used for separation because of high efficiency and robustness, and high-resolution MS such as Orbitrap, Quadrupole-Time-of-Flight (Q-TOF), and Fourier Transform Ion Cyclotron Resonance (FTICR) are routinely used for detection because their high resolving power benefits identification of biotransformation/PTM as well as differentiation of DAR species [14–16]. Typically, a 17,500 resolution could be sufficient for DAR characterization, and it has been reported that a resolution limited around 35,000 could be beneficial to DAR characterization when using Orbitrap [17]. Here we review the use of LC-MS with peptide mapping as well as the intact/subunit approaches for in-depth ADC characterization.

2.1.1. Peptide mapping for analysis of conjugation site and PTMs

Due to the high heterogeneity of ADCs, the analysis of antibody vehicle is often challenging. Moreover, PTMs such as glycosylation, phosphorylation, deamidation and methylation further compound this problem. Peptide mapping or bottom-up LC-MS represents a powerful tool for characterization of the sequence and PTMs of proteins with high specificity and reproducibility, and thereby has been extensively used in quality control [18]. The protein molecules are regularly prepared with or without protein purification depending on the complexity of sample, followed by denaturation, reduction, alkylation and enzyme digestion to produce relatively short, completely proteolyzed peptides. The digest is then analyzed on RPLC-High-Resolution-MS and a data processing tool (usually including a searching engine) to obtain detailed information on protein primary sequence and modifications.

With the ability to elucidate site-specific information, peptide mapping is the most frequently used tool for conjugation site identification and characterization. One study has utilized peptide mapping analysis on a UPLC-MS for confirmation of T-DM1 primary sequence and evaluation of site of conjugation/occupancy [19]. The work identified 82 conjugated lysine sites accounting for nearly 90% of available lysine residues and achieved much improved site coverage compared with several previous studies which had identified 38–44 conjugation sites [19–21]. A group employed peptide mapping with UPLC-Q-TOF to determine the stability of 26 conjugation sites of T-DM1 and compared the degradation rates at each site to provide guidance for quality control [22]. Another group developed a new procedure with enhanced depth-of-analysis, including improved reduction, immune-globulin degrading enzyme of *Streptococcus pyogenes* (IdeS) digestion protocol and the use of UPLC-TOF to identify payload positional isomers at cysteine residues of brentuximab vedotin [23].

However, one concern is that the conjugation of the payload often results in a significant increase in hydrophobicity of the conjugated peptides derived from ADCs and thus the LC separation of such conjugated peptides may be difficult [24,25]. A number of studies attempting to address these challenges have been reported. For example, capillary zone electrophoresis (CZE)/MS peptide mapping has been used as an orthogonal tool to help the separation

of large hydrophobic peptides, hydrophilic di-/tri-peptides and glycopeptides from ADCs [26]. Another work adopted micro-pillar array columns in LC-nano-electrospray ionization (ESI)-Q-TOF for ado-trastuzumab emtansine (T-DM1) characterization, which offers highly efficient separations even for hydrophobic segments, and achieved a high sequence coverage of peptide mapping [27].

Identification and quantification of PTMs are imperative owing to its potential of altering protein functions such as deactivating proteins and leading to a decreased efficacy. LC-MS-based peptide mapping is the gold standard to evaluate PTMs of therapeutic antibodies owing to the ability of accurate site localization. Though no study has yet used peptide mapping for evaluation of PTMs in ADCs, many studies on therapeutic antibodies have been reported [28–30]. While the technique is proved to be very useful and widely practiced, some issues remain. Proper protocols in the database searching process are important for minimizing the false positive of the PTM annotation [29]. Additionally, multiple-step sample preparation may introduce artificial modifications [13]. The optimization of sample preparation protocols, especially the digestion step, has been conducted in attempt to address this problem [18,31,32]. Analysis on intact/subunit levels was also performed for evaluation of PTMs as well as other forms of biotransformation. Though these approaches may not be able to provide the exact location of PTMs, the reduced sample preparation step could decrease artificial modifications and improve throughput. Moreover, such methods can preserve information of the functional relationship of multiple PTMs and identify different proteoforms [33,34].

2.1.2. Intact/subunit analysis

Characterization of ADC at intact/subunit levels is an important component for LC-MS-based ADC analysis. Table 1 summarizes the analytical conditions of intact/subunit level LC-MS-based ADC analysis [17,24,25,35–48].

2.1.2.1. Biotransformation characterization. ADC in vivo biotransformations such as payload deconjugation, protein mass adduct/loss and payload metabolism often occur due to the nature of the in vivo environment, and the instability and complexity of the conjugation sites or linkers [35,49]. Such biotransformations could potentially decrease efficacy and increase off-target toxicity. Even though some new engineering technologies (*e.g.*, cystine engineering, non-natural amino acid engineering, enzyme-mediated conjugation, peptide tags engineering, new heterobifunctional reagent) have been utilized in a site-specific manner to produce more homogenous and stable ADCs, in vivo biotransformations could very well persist [35,36]. Therefore, the analytical method to characterize ADC biotransformations is particularly important in helping guide the engineering efforts of ADCs as well as elucidate the paths of ADC metabolism/catabolism [16].

In this regard, intact and subunit LC-MS is the method of choice due to its ability to provide high-level sequence and structure information in a high-throughput manner [50]. While intact analysis measures the intact ADCs (*e.g.,* $\geq$ 150 kDa) either under native or denaturing conditions, subunit analysis measures fragments (20–50 kDa) produced by reduction or enzyme digestion such as papain, IdeS and carboxypeptidase B digestion [51]. In plasma, affinity capture using specific capture agents is often employed for in vivo biotransformation analysis [35]. Previously, several subunit LC-MS studies surveyed biotransformations of Fab-conjugated ADCs using affinity capturing, but the developed technical procedures are often not applicable to Fc-conjugated ADCs [37]. More recently, an improved affinity capture LC-MS assay has been developed for analysis of biotransformation and conjugation sites in a variety of antibody types [35], which, according to the authors,

could identify small-size modifications such as hydrolysis with enhanced sensitivity and resolution. The authors have applied this method to evaluate in vivo biotransformation of HC-Fc conjugated ADCs and discovered catabolites from deacetylation of conjugated tubulysin. Although LC-MS analysis of intact proteins or large protein fragments usually carries significantly lower sensitivity and limited site-specific information, this problem could be partially alleviated with the recent development with high-resolution MS. For example, one group has studied the catabolites of T-DM1 at intact level and found Orbitrap showed superior results compared with Q-TOF MS [38]. They have identified three types of biotransformation involving cysteine and glutathione adduct formation, loss of maytansinol and hydrolysis at the linker-drug sites.

It is often found that combined multi-level analysis is beneficial since it provides complementary information. For example, a study has shown that middle-level analysis combined with intact and native MS provided broader insights into the conjugation heterogeneities and DAR analysis of ADCs [36]. In the same way, intact and subunit LC-MSs are also frequently used for DAR and DLD analysis, which is to be discussed in the "DAR characterization" section.

2.1.2.2. Characterization of antibody assembly. One recent development in the field is the ADC with a bi-specific antibody. Generally, poor internalization rate has been a prominent issue for ADCs; the bi-specific ADCs emerged to enhance the internalization and trafficking to the lysosome by either targeting a fast internalizing receptor and tumor cell surface specific target using the two arms respectively, or targeting two different epitopes of the same antigen. Examples of bi-specific ADCs currently on clinical trials are MEDI4276 and ZW49 [52,53]. Given that ADCs containing bi-specific antibody represent a future trend, and that evaluating structural integrity of bi-specific antibody is important in ensuring safety and efficacy, here we review the utilization of LC-MS in assessment of the structural heterogeneity of bi-specific antibodies. Although all three components of ADCs (*i.e.,* the antibody, payload and linker) are critical for structural integrity, this section will mainly discuss bi-specific antibody assembly, and payload conjugation will be discussed in detail in a later section [54,55]. Despite emerging strategies to promote correct chain pairing, undesirable antibody assembly persists, which must be characterized [56]. Intact-level LC-MS analysis is a promising technique in this regard, for instance, characterization of the assembly of heavy and light chains [57]. The correctly assembled antibodies can be separated from byproducts such as hole-hole dimer, hole half-antibody and hole half-antibody fragments by different chromatographic techniques including KappaSelect affinity chromatography, Lambda-FabSelect affinity chromatography, hydrophobic interaction chromatography (HIC) and RPLC [58].

Additionally, the use of high-resolution MS can differentiate the correctly assembled antibodies from its byproducts by mass shift, thus achieving unambiguous identification [59]. Schachner et al. [59] described an LC-MS method using Exactive Plus Extended Mass Range Orbitrap, which had identified low levels of mis-paired anti-interleukin (IL)-4/IL-13 bispecific immunoglobulin G (IgG). Due to the different masses of anti-IL-4 light chain and anti-IL-13 light chain, the mass analyzer readily distinguishes the correctly assembled form with the 2x IL-4 L form and 2x IL-13 L form. Additionally, Woods et al. [60] utilized an advanced ESI-Q-TOF MS and intact level analysis to evaluate the heterodimeric purity of a prototype asymmetric antibody containing two different heavy chains and two identical light chains. Moreover, Gomes et al. [61] employed Q-TOF MS to characterize heterogeneity of in-house produced antibody.

However, when the two different light chains show similar properties (*e.g.,* molecular weight and/or polarity), discrimination

Table 1
Recent applications of intact/subunit LC-MS to ADC analysis.

ADC	Subject	Condition	Intact/Subunit	LC	Column	Mobile phase	MS	Ref.
Trastuzumab-vc-MMAE	In vitro DAR characterization	Denature	Subunit	RPLC	C4 (100 mm × 2.1 mm i.d., 3.5 μm, 450 Å)	A: 0.1% FA in water; B: 0.1% FA in ACN	Q-TOF	[17]
					C4 (150 mm × 1 mm i.d., 5 μm, 300 Å)	A: 0.1% FA in water; B: 0.1% FA in ACN	Orbitrap	
Site-specific ADC	Conjugation site and glycosylation site identification	Denature	Subunit	RPLC	PS/DVB (100 mm × 1 mm i.d., 4 μm, 1500 Å)	A: 0.1% FA in water; B: 0.1% FA in ACN	Orbitrap	[24]
Lys-conjugated ADC, site-specific ADC	In vitro DAR characterization	Denature	Intact	Organic SEC	Ethylene bridged hybrid-based particle, diol bonding (150 mm × 4.6 mm i.d., 1.7 μm,200 Å)	30% ACN, 70% water with 0.05% TFA	Q-TOF	[25]
Cys-conjugated ADC		Native	Intact	SEC		20 mM−40 mM ammonium acetate in water		
Cys-conjugated ADC, site-specific ADC	In vitro DAR characterization	Denature	Subunit	RPLC	C4 (100 mm × 2.1 mm i.d., 1.7 μm, 300 Å); Diphenyl (100 mm × 2.1 mm, 1.8 μm, 300 Å)	Consisting of TFA, water, isopropanol, ACN		
Site-specific ADC	Biotransformation characterization	Denature	Subunit	RPLC	C4 (50 mm × 2.1 mm i.d., 1.8 μm, 300 Å)	A: 0.1% FA in water; B: 0.1% FA in ACN	Q-TOF	[35]
Site-specific ADC	In vivo DAR characterization	Denature	Subunit	RPLC	PS/DVB (150 mm × 2.1 mm i.d., 8 μm, 1000 Å)	A: 0.1% TFA in water B: 0.08% TFA in ACN	Q-TOF	[36]
		Native	Intact	SEC	Ethylene bridged hybrid-based particle, diol bonding (150 mm × 2.1 mm i.d., 1.7 μm, 200 Å)	A: 0.1% FA/0.025%TFA in water B: 0.1% FA/0.025%TFA in ACN	Q-TOF or Orbitrap	
Site-specific ADC	In vivo DAR characterization and catabolite characterization	Denature	Subunit	RPLC	PS/DVB (50 mm × 500 μm i.d.)	A: 0.1% FA in water; B: 0.1% FA in ACN	Q-TOF	[37]
Trastuzumab emtansine	Biotransformation characterization	Denature	Intact or subunit	RPLC	PS/DVB (5 cm × 500 μm i.d.), PS/DVB (25 cm × 200 μm i.d.)	A: 0.1% FA in water; B: 0.1% FA in ACN	Orbitrap	[38]
Cysteine-conjugated ADC, site-specific ADC, lysine-conjugated ADC	In vivo DAR characterization	Denature	Intact or subunit	RPLC	PS/DVB (50 mm × 0.3 mm i.d., 5 μm, 4000 Å)	A: 0.1% FA in water; B: 0.1% FA in ACN	Q-TOF	[39]
THIOMAB-vc-MMAE	In vivo DAR characterization	Denature	Intact	RPLC	PS/DVB (50 mm × 0.3 mm i.d., 5 μm, 4000 Å)	A: 0.1% FA in water; B: 0.1% FA in ACN	Q-TOF	[40]
Brentuximab Vedotin	In vitro DAR characterization, positional isomer characterization	Native	Intact	HIC × SEC	HIC: PA (100 mm × 4.6 mm i.d., 5 μm, 1000 Å); SEC: Silica-based particle, hydrophilic bonding (50 mm × 4.6 mm, 2.7 μm, 300 Å)	HIC: 2.5 M of ammonium acetate and 0.1 M phosphate buffer (pH 7.0); 0.1 M phosphate buffer (pH 7.0); SEC: 100 mM ammonium acetate	IM × MS	[41]
Trastuzamab Entansine, cysteine-conjugated ADC	In vitro DAR characterization	Native	Intact	SEC	Ethylene bridged hybrid-based particle, diol bonding (150 mm × 2.1 mm i.d., 1.7 μm, 200 Å)	50 mM ammonium acetate in water	Q-TOF	[42]
Trastuzumab-DSEA-fluorophore	In vitro DAR characterization	Denature	Subunit	RPLC	PS/DVB (150 mm × 2.1 mm i.d., 8 μm, 1000 Å)	A: 0.05% TFA in water; B: 0.05% TFA in ACN	Q-TOF	[43]
Trastuzumab-mc-MMAF, Trastuzumab-vc-MMAE	In vitro DAR characterization	Denature	Subunit	RPLC	Phenyl (5 mm × 2.1 mm i.d., 20 μm, 1000 Å)	Water; ACN; 1% FA	Q-TOF	[44]
		Native	Intact	SEC	Ethylene bridged hybrid-based particle, diol bonding (150 mm × 4.6 mm i.d., 1.7 μm, 200 Å)	10 mM ammonium acetate in water (pH 6.9)		
		Denature	Intact	RPLC			TOF	[45]

Lysine-conjugated ADCs, dual-payload ADC, site-specific ADC	In vitro DAR characterization	Denature	Intact	SEC	PS/DVB (100 mm × 3.0 mm i.d., 4 µm, 1500 Å)	20% ACN, 80% water with 0.1% FA	TOF	[46]
Cantuzumab-SPDB-DM4	In vitro DAR characterization	Denature	Intact	RPLC	Diol-bonded silica (30 cm × 4.6 µm i.d., 4 mm, 250 Å)	50% aqueous ACN containing 0.02% TFA and 1% FA	Q-TOF	[47]
Site-specific ADC	In vivo DAR characterization	Denature	Intact	RPLC	C4 (100 mm × 0.3 mm i.d., 1.7 µm, 300 Å)	A: 0.1% FA in water; B: 0.1% FA in ACN	Q-TOF	[48]
Trastuzumab Emtansine	Quantification in biological samples	Denature	Intact		C4 (50 mm × 2.1 mm i.d., 1.7 µm, 300Å)	A: 0.1% FA in water; B: 0.1% FA in ACN		

PS/DVB: Polystyrene Divinylbenzene, FA: formic acid, ACN: acetonitrile, TFA: trifluoroacetic acid, PA: Polyamide.

of swapped dimeric products from the correctly assembled ones would be difficult using intact analysis. In such events, partial digestion and analysis of subunits become helpful. For example, Wang et al. [62] incubated a bispecific antibody product with the enzyme GingisKHAN, which specifically cuts between the K and T residues above the hinge region. In the digest, the two Fabs generated from the swapped light chains were clearly different from these from the correctly assembled antibody, which can be specifically analyzed by LC-MS.

2.2. DAR characterization

In most cases, payloads are conjugated to the ε-NH$_2$ of surface-exposed lysine residues or the sulfhydryl group of interchain cysteine residues of the antibody, or specifically conjugated to engineered cysteine resides (THIOMAB) to form an ADC with well-defined DAR [3]. For the first two types of ADCs, since over 70 lysine residues and about 8 cysteine residues are available in an antibody molecule, linkages of cytotoxins result in a heterogeneous mixture of ADCs in the final product, with a wide distribution of DAR [63–65]. Because various DAR species could carry different efficacy and safety, the DAR value is a critical parameter for ADCs. In practice, weighted average DAR has become a key attribute to ADCs quality control, which is routinely measured in ADC products to validate homogeneity [57,66]. Furthermore, although ADCs are designed to remain stable until internalized, non-specific deconjugation occurs after ADCs administration, resulting in altered DAR in vivo [39,40]. Therefore, monitoring DAR changes after drug administration is important in determining ADC stability and assessing therapeutic effects. While DAR measurement is typically conducted at the protein level, average DAR, especially for in vivo systems, could also be alternatively calculated by separated quantification of conjugated payloads and total antibody [57,67,68]. In this section, we only focus on DAR measurement at intact protein/subunit level, and bottom-up strategy will be discussed in the "Conjugated payload in biological sample" section.

Traditional analytical techniques available for DAR characterization include ultraviolet/visible (UV/Vis) spectroscopy, absorbance spectroscopy coupled with chromatographic techniques including hydrophobic HIC, CE, capillary isoelectric focusing (cIEF), ion exchange chromatography (IEC), and RPLC [5,40,69–77]. More recently, LC-MS and other MS-based approaches, which provide far more accurate and detailed characterization of DAR, have been devised. These include intact/subunit LC-MS, matrix-assisted laser desorption/ionization (MALDI)-TOF-MS, CE-MS, ion mobility (IM)-MS et al. [17,57]. Selection of method should be based on the considerations of conjugation chemistry, characteristics of the linker and payload, and sample matrix. Given that several publications have discussed this topic in detail [2,4,57], here the focus is on the application and future trends of LC-MS-based technologies in DAR measurement.

LC-MS is a powerful tool for DAR measurement because of its molecular-level resolution and the compatibility with various matrices [78]. Moreover, compared with the widely-used HIC-UV/Vis, LC-MS consumes significantly less sample for DAR measurement, while delivers comparable or better analytical performance than other methods [17]. That being said, several important issues are worth noting. Firstly, the composition and pH of mobile phase should be adjusted for ADCs with acid-labile linkers such as hydrazone in order to maintain linker-drug integrity during analysis [3,25]. Secondly, ESI source parameters must be carefully optimized to minimize in-source dissociation of ADCs, and therefore maintain minimal analytical artifacts and sufficient sensitivity [4,25]. A general procedure of LC-MS-based DAR measurement at intact protein/subunit level involves deconvoluting the mass spectra to a series of "zero-

charge" masses, and then obtaining DAR distribution or computing average DAR by integrating and weighting the spectral peak area or peak intensities [2]. Though widely practiced, one potential concern is that different states of payload conjugation or other modifications could change MS response, resulting in biased DAR [79]. Moreover, ionization of co-eluted DAR species might interfere with each other [2]. To address these concerns, one study suggested using an orthogonal approach to validate LC-MS-obtained DAR [17].

2.2.1. In vitro DAR characterization for product quality control

As mentioned above, the majority of ADCs are either Cys- or Lys-linked. Deglycosylation is commonly performed in sample preparation to reduce spectra complexity. For Cys-conjugated ADCs, conventional RPLC-MS-based DAR analysis using intact ADCs is not suitable, since the harsh, acidic mobile phase used in conventional RPLC-MS dissociates Cys-conjugated ADCs where the heavy and light chains may not be covalently bound [2]. Native MS is preferred for intact analysis of Cys-conjugated ADC because of its non-denaturing condition [80–82]. Size exclusion chromatography (SEC)-native MS using non-denaturing and MS-compatible mobile phase conditions enables direct DAR measurement of intact Cys-conjugated ADCs [25,42,83]. However, SEC could not resolve each DAR species, and the differentiation among various DAR species relies on high-resolution mass analyzers. Instead, HIC can resolve DAR species but involves the use of nonvolatile salts that are not compatible with ESI-MS. Although traditionally HIC is not preferred for MS analysis, it favors Cys-conjugated ADC analysis owing to its non-denaturing feature. More recently, efforts have been directed toward online coupling of HIC with native MS [41,84,85]. Nonetheless, despite potentials of native MS in DAR measurement of Cys-conjugated ADCs, native MS requires instruments to have extended mass range, and often demands strong expertise and laborious procedure, especially for complex samples [80,86]. Alternatively, reduction with dithiothreitol (DTT) or tris(2-carboxyethyl)phosphine (TCEP) is performed followed by RPLC-MS-based DAR measurement from the dissociated light and heavy chains, and RPLC is capable of separating chains with various payloads [2]. In addition, partial-digestion with IdeS followed by a reduction step generating various ~25 kDa fragments, along with the non-conjugated Fc/2 fragment as internal reference, improves DAR measurement accuracy and provides supplementary structural information of ADCs such as C-terminal lysine truncation, pyroglutamylation, oxidation and degradation products [43,44].

Unlike Cys-linked ADCs, Lys-linked ADCs remain intact under the denaturing conditions of RPLC-MS, where the average DAR could be directly calculated from deconvoluted spectra [2,45]. A study comparing DAR obtained by LC-ESI-MS and a reference method (UV/Vis) for a Lys-conjugated ADC product (huC242-SPDB-DM4) suggested LC-MS produced an average DAR comparable to that by UV/Vis; the study also found it is important to use a full charge envelope for deconvolution of mass spectra [46]. Nonetheless, the interpretation of the mass spectra of Lys-conjugated ADCs is often challenging due to their high heterogeneity and high charge states under denaturing conditions (thus narrowly-spaced MS peaks). Therefore, C-terminal lysine removal to reduce charge-heterogeneity during sample preparation are recommended to reduce the spectral complexity [57]. Compared with RPLC-MS, SEC-native MS shifts the charge envelope to a higher mass window, which could improve mass spectrum quality for Lys-conjugated ADCs [42].

2.2.2. In vivo DAR characterization

The in vivo dynamic change of the average DAR reflects ADC stability after drug administration. Measurement of DAR in biological samples is highly challenging owing to problems associated with sensitivity and the complex biological matrices. Towards this end, a highly efficient and selective immunoaffinity enrichment of ADCs must be performed prior to intact LC-MS-based in vivo DAR measurement [37,39,40]. Though such strategy has been adopted in plenty of work of DAR measurement in plasma, it suffers from low sensitivity rooting from the intrinsic low MS response for intact analysis. Alternatively, reduced or limitedly-digested samples can be used to enhance sensitivity for in vivo DAR determination, as shown in a number of reports [47,87–89]. Furthermore, the intact analysis in vivo requires a highly specific and efficient capturing reagent, which may not be available in many cases. Finally, immunoaffinity enrichment does not work well in tissues, limiting the method only applicable to plasma analysis [90]. One new approach to determining in vivo DAR is to separately quantify conjugated payload and total antibody, currently applicable to ADCs containing cleavable linkers [67,68,91–94]. Compared with intact DAR measurement, this method has much higher sensitivity favored by peptide-level protein quantification. Examples are described in the "conjugated payload in biological sample" part.

In order to further take the advantage of the superior ability of LC-MS in DAR measurement, a number of new techniques are under development at the moment. For example, to obtain improved separation, DAR measurement using 2-dimensional LC (2D-LC) such as HIC × RPLC and HIC × SEC was described [41,76,85]. Furthermore, IM technique that provides a new, orthogonal dimension for separation of ADC samples has attracted considerable interest [41,82]. IM-MS separates gas-phase ions based on their differential mobility against a buffer gas [95]. By providing a third dimension of separation, IM-MS could help to achieve unambiguous identification of DAR species and allow more accurate DAR measurement [41].

2.3. Quantitative analysis in biological samples for pharmacokinetic investigation

Pharmacokinetic investigation of ADC in vivo is complicated by nature. For instance, it is still under debate as to which ADC forms in plasma are the most representative of the exposure-response relationship, and consequently, efficacy and safety [96]. A position paper on ADCs bioanalysis has recommended that the following components should be measured at an early drug development stage for evaluation purpose: conjugated forms (conjugated antibody or antibody-conjugated drug), the total antibody, and unconjugated drug [66]. Correspondingly, sample preparation procedure is often quite complicated in order to achieve comprehensive ADC bioanalysis and fit-for-purpose protocols should be developed based on the desired target analytes as well as nature of the sample. The general sample preparation strategies for LC-MS-based ADC bioanalysis are summarized in Fig. 1. For LC-MS based quantification methods, peptide-level quantification of the antibody part is at the main stage, while intact ADC quantification is picking up albeit slowly. Here both the peptide- and intact-level quantification methods are reviewed. Analysis of unconjugated drugs and metabolites entities is discussed in a latter section.

2.3.1. Protein quantification using peptide-level (bottom-up) approach

2.3.1.1. Total antibody.
After drug administration, due to the change of DAR in vivo, the calibration curve prepared using the drug as the reference may not exactly represent the analytes in the study samples over the time course of PK measurement. Total antibody quantification targets all antibody forms regardless of the presence of conjugated drug, which is considered to be the most useful in characterization of antibody-related PK behavior of the ADCs [2,97]. Quantitative strategy for total antibody of ADCs is usually the same
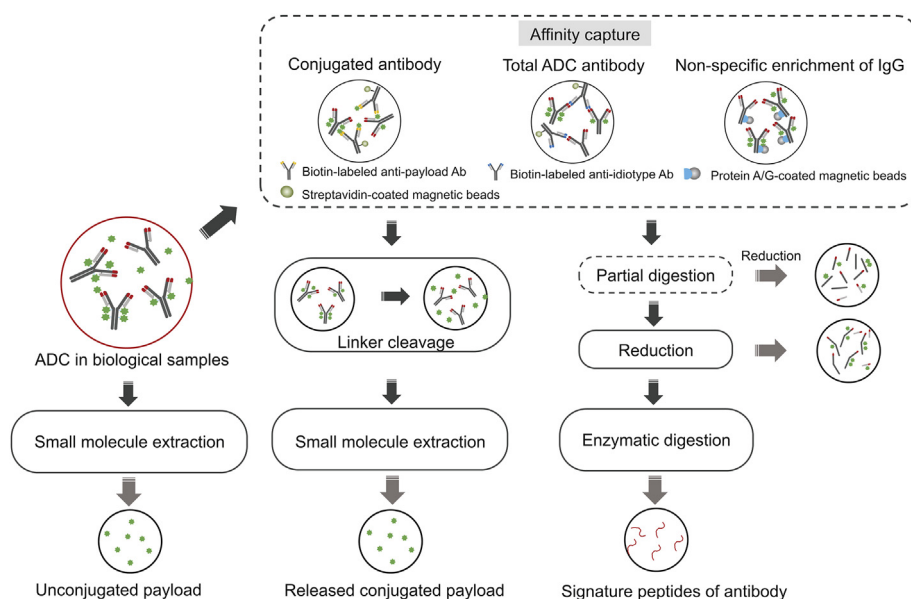
Fig. 1. Summarized schematic for the general sample preparation procedure for LC-MS-based ADC bioanalysis.
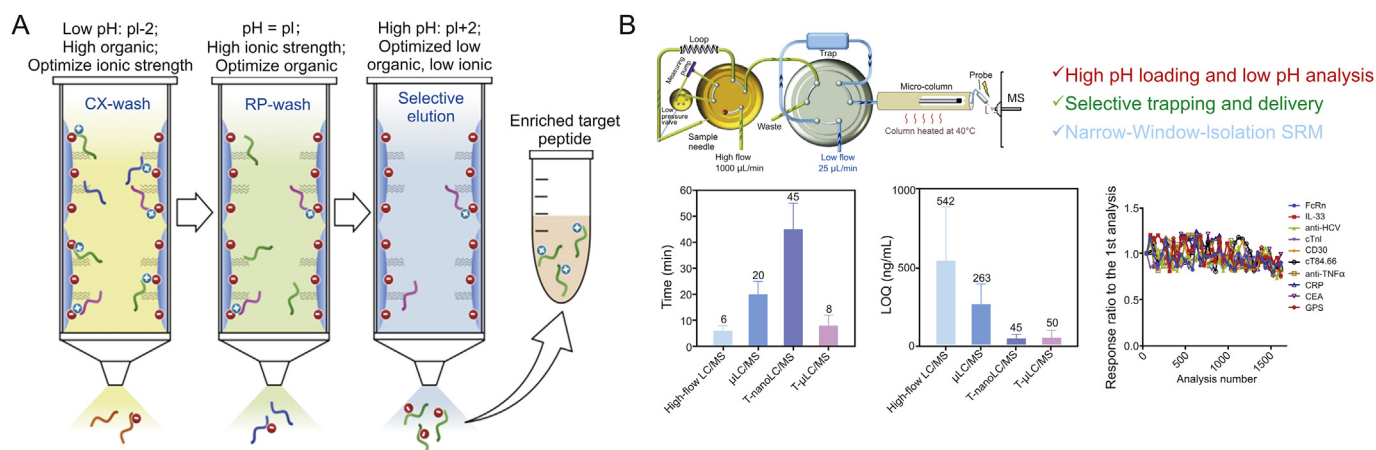
Fig. 2. Examples for non-immunoaffinity methods to improving sensitivity for LC-MS-based quantification of antibodies from plasma or tissue homogenates. The detailed procedures can be found in the corresponding publications. (A) General workflow of a selective antibody free, peptide-level CX-RP enrichment, to improve sensitivity for LC-MS quantification. Adapted with permission from Ref. [107]. Copyright (2020) American Chemical Society. (B) A trapping-micro-LC-MS workflow for quantitative analysis of mAb with high sensitivity, exceptional robustness and high throughput. Reprinted with permission from Ref. [108]. Copyright (2020) American Chemical Society.

as these for general antibodies, where bottom-up LC-MS strategy is a widely used quantitative method [78,93,97—99]. Many factors such as LC conditions, sample preparation and charge states all affect the sensitivity for protein quantification [100]. To achieve desired sensitivity, affinity capture is typically incorporated. For instance, antibodies are isolated from the matrix by capture reagents such as anti-idiotype (anti-ID) antibody or protein A/G [94]. The isolated antibodies are denatured/reduced, alkylated and then proteolyzed. Based on several generally-accepted criteria, usually signature peptides (SP) from complementarity-determining region (CDR) will be selected and monitored by LC-MS [12,50,93,101]. One issue with the anti-ID antibody enrichment is that only the ADC species with at least one unbound variable region could be captured by anti-ID antibody. Therefore, binding to soluble target compromises anti-ID antibody capture efficiency [94]. Furthermore, protein-level enrichment only works well in plasma but not tissues [90]. Use of protein G/A also has further limitation because of their indiscriminately binding of endogenous IgG. One alternative is to develop a sensitive LC-MS strategy without protein-level

enrichment. For instance, we described an immuno-enrichment-free procedure affording highly sensitive LC-MS-based quantification of antibodies directly from plasma or tissue homogenates, which includes the following technical advances: i) A high-throughput on-the-fly orthogonal array optimization (OAO) strategy [6,102,103], which utilizes a systematic experimental design to develop the optimal LC/SRM-MS conditions for multiple SP candidates in matrix, enabling experimental identification of the optimal SP in a high-throughput and accurate manner. Moreover, synthesis of potential SP candidates is not necessary for the SP selection in this method, which is time/cost effective. ii) A surfactant-aided precipitation/on-pellet-digestion (SOD) sample preparation procedure. The method enables high and reproducible peptide recovery regardless of the matrix (e.g., tissues or plasma), thus achieving accurate and sensitive antibody quantification with good robustness [104,105]. Surfactant treatment followed by precipitation achieves high and reproducible protein/peptide recovery from various matrices, because surfactant allows not only a high protein extraction efficiency but also extensive denaturation of proteins,
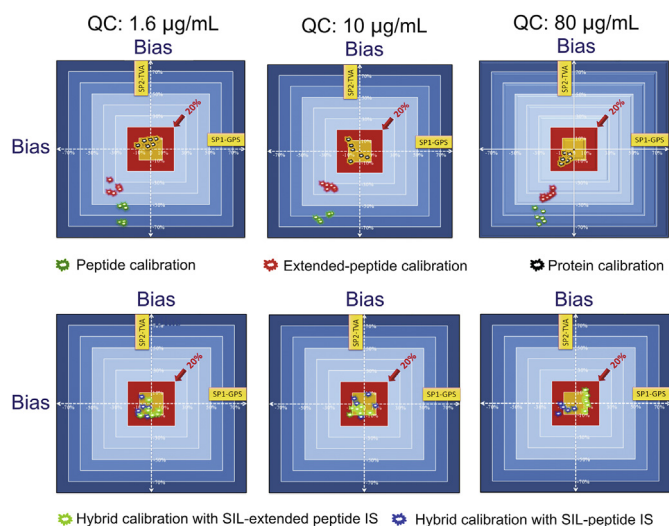
Fig. 3. Two-dimensional representations of the quantitative accuracy by peptide-, extended-peptide-, and protein-level calibration approaches and the "hybrid" calibration approaches, indicating the profound effects of calibration approaches on the accuracy for LC–MS targeted quantification of therapeutic protein. Reprinted with permission from Ref. [7]. Copyright (2020) American Chemical Society.

rendering them more accessible to digestive enzymes. Moreover, it was found that surfactant greatly facilitates the removal of detrimental matrix components such as lipids and fatty acids [106]. iii) An antibody-free multiple-mechanism peptide-level enrichment via strategic regulation of pH, and ionic and solvent strengths (Fig. 2A). The retention of a target peptide on SPE cartridge via cation exchange (CX) and reversed phase (RP) mechanisms is relied on ionic and hydrophobic interactions, respectively; both are profoundly regulated by pH. Thus a highly specific method was developed to enrich SP by a series of selective wash and elution steps using buffers with strategically controlled pH, ionic strength and organic solvent composition. This method eliminates a majority of non-target peptides and matrix components, improving sensitivity and robustness significantly [107]. Moreover, unlike protein-level enrichment methods, this peptide-level strategy works well in tissues. iv) A trapping-micro-LC-MS method (Fig. 2B) [108]. The system enables selective trapping and delivery of the SP while specifically removing matrix peptides to a large extent. Meanwhile, the target peak is concentrated prior to the micro-flow LC/MS, coupled with narrow window isolation (NWI)-SRM, which further boosts the sensitivity. This method achieves high sensitivity comparable to nano-LC/MS while maintaining the comparable throughput to high-flow-LC/MS and excellent robustness. v) Hybrid calibration strategy with full-length protein calibrator and stable isotope labeled (SIL) peptide or extended peptide internal standard (IS) to enable highly accurate quantification of antibodies in a cost-effective manner (Fig. 3) [7]. It is worth noting that severe negative bias is almost inevitable when synthesized peptides or extended peptides are used as the calibrator [7].

2.3.1.2. Conjugated antibody. Conjugated antibody refers to antibody forms with at least one conjugated payload. Though the correlation between levels of conjugated antibody and efficacy or toxicity of an ADC has not yet been fully established, considerable interests have been directed to measurement of the conjugated antibody, which is recognized as one of the important active species of ADCs. For conjugated antibody quantification, ligand-binding assay (LBA) using an anti-payload antibody is widely practiced, while a 'hybrid' assay combining immunoaffinity

enrichment and LC-MS analysis also serves as an alternative [64,93,94]. In such hybrid assays format, the sample enriched by immunocapture with anti-payload antibody is digested and then the antibody is quantified with bottom-up LC-MS approach [94]. It should be noticed that peptides-linker-drug moieties might be generated after tryptic digestion of ADCs [2]. These species are often highly heterogenous in the digest, which should not be selected as the signature peptide for antibody quantification, especially for these ADCs with non-cleavable linkers. Another important issue worth noting is that during the early drug development stage, anti-payload reagents may not be available, which poses a challenge for both LBA and LC-MS-based hybrid assays format.

2.3.2. Protein quantification at intact level

As discussed earlier, advancement of high-resolution MS instruments greatly facilitated LC-MS based intact quantification [109]. Compared with bottom-up quantification, intact quantification, if properly carried out, can preserve the whole protein information instead of using an SP which could only partially represent the original target. For ADC quantification, LC-MS-based intact quantification is able to provide DAR information.

For intact quantification, major challenges remain such as the low sensitivity, requirement of highly specific and effective capturing reagents, as well as a high-resolution MS suitable for large, intact protein analysis (*e.g.,* proper pressure and ion optic settings). Moreover, the spectra are usually hard to interpret in a quantitative manner, owing to the many charge states and isotopes forms, which further compounds the sensitivity problem [48]. The large molecule weight of antibody often results in low ionization efficacy and therefore low sensitivity for intact analysis. ADCs exhibit even lower sensitivity than that of a naked antibody because of the signal distribution into different DAR species. Therefore, the success heavily relies on the immunocapture process, which must provide a high recovery and effective removal of interference from biological matrix. For accurate quantification, internal standard (IS) is often indispensable [110]. However, not only the antibody IS is costly, other issues also exist. For example, one group has tried intact quantification on T-DM1, where the IS co-eluted with the target caused a much more complex spectra that was hard to deconvolute [48]. As a comparison, the authors further applied narrow-window XIC extraction and deconvolution method for quantification without IS and achieved acceptable quantitative performance within the concentration ranging from 5 to 100 μg/mL. Consequently, though intact-level quantification has been applied for antibodies, quantification of intact ADCs is still in its infancy, rooting from various technical challenges.

3. Analysis of payload

Payload related analytes include residual payloads and associated compounds in the drug product, as well as unconjugated payloads, conjugated payloads, and payload-related metabolites in biological samples after drug dosing [5,12,111]. Because of its unique advantages in specificity and sensitivity, LC-MS plays a pivotal role in payload analysis. For example, the high-sensitivity feature of LC-MS, which enables quantification of unconjugated payload that presents at a very low concentration in vivo making it highly valuable [112]. Also, LC coupled to high-resolution MS is commonly used in identification of payload-related metabolites.

3.1. Unconjugated payload

During ADC production, incomplete removal of unconjugated payload or payload-linker may pose a risk for toxicity due to the

extreme potency of the payload toxin [112]. Therefore, measurement of residual unconjugated payload and related compounds is designated as a CQA for ADC products, which must be routinely monitored [113]. In an in vivo system, unconjugated payloads refer to the payload forms deconjugated in plasma or target tissues postdosing [12]. Plasma level of unconjugated payload closely correlates with off-target toxicities [47]. Intra-tissue distribution of unconjugated payload is also of great importance in understanding efficacy and toxicity of ADCs [114]. In this regard, mass spectrometry imaging (MSI) has been proved to be valuable by visualizing spatial distribution of unconjugated payload [115].

The forms of unconjugated payload from cleavable and noncleavable linkers are often different owing to the disparate release mechanisms. Specifically, deconjugation of an ADC with cleavable linkers releases the free cytotoxin, while an ADC with non-cleavable linker mainly produces more complicated formats such as amino acid-linker-payload moieties after near-complete degradation of the antibody [3]. It should be noted that catabolism of ADCs with non-cleavable linkers might produce free cytotoxins as well, which is also characterized in pharmacokinetics studies [116].

ADCs with cleavable linkers primarily release free cytotoxin; consequently, LC-MS-based analysis of unconjugated payload from these agents usually employs the same strategy as that for quantification of the cytotoxin. Due to the high hydrophobicity of typical cytotoxins, liquid-liquid extraction (LLE) and solid-phase extraction (SPE) are often carried out for extraction. Additionally, deconjugation of payload should be minimized during sample preparation to avoid positive bias. For example, to avoid deconjugation, the pH should be adjusted for acid-labile linkers such as hydrazone linker; adding protease inhibitors is preferred considering various proteases present in the sample may cleave enzyme-cleavable linkers, and sample extraction in an ice-water bath is recommend to minimize deconjugation [12,117]. A specific consideration for maytansinoid payloads is that the reactive thiol groups could undergo disulfide exchange with other thiol-containing molecules in the matrix, e.g., forming dimers after release [38,117,118]. Therefore, reduction and derivation of thiol are usually necessary before LC-MS analysis of this type of payloads.

For ADCs with non-cleavable linkers, several payload-containing forms could be produced, which should be quantified together. For example, in the PK and toxicokinetic (TK) studies of Kadcyla (ado-trastuzumab-mcc-emtansine), DM1, Lys-mcc-DM1 and mcc-DM1 are monitored [116,119]. LC-MS analysis of those species could be achieved in one run with satisfying resolution using a typical reversed-phase chromatography [118].

3.2. Conjugated payload in biological sample

The level of conjugated payload is generally considered as a valuable indicator related to ADC efficacy and toxicity [119]. As mentioned previously, LC-MS based quantitative analysis of conjugated ADCs is usually coupled with immunoaffinity pull-down [57,68,91,97]. For ADCs with cleavable linkers, conjugated payload is quantified after isolation of small molecules from proteins and then linker cleavage. For example, for the ADC utilizing an enzyme-sensitive dipeptide Val-Cit linker (e.g., brentuximab vedotin), the release of payload can be achieved by digestion with proteases such as cathepsin B and papain [67,68,93,94,120–122]. For the ADC with a disulfide bond linker (e.g., coltuximab ravtansine), reducing agent such as DTT and TCEP is employed for cleavage [123,124]. Conventionally, conjugated antibody and conjugated payload are measured by two independent assays using two aliquots of the same samples. Xu et al. [125] introduced an LC-MS approach enabling simultaneous measurement of total antibody and antibody-conjugated drug in plasma samples, followed by immunocapture enrichment. The strategy utilizes sequentially enzymatic digestion with cathepsin B and then Lys-C to release conjugated payload and then signature peptide of the antibody component. The assay platform was further applied in another ADC containing a polymer linker via an ester bond, which was cleaved by sodium hydroxide [99].

As mentioned previously, quantification of conjugated payloads of ADCs with cleavable linkers can be achieved after linker cleavage, which is an alternative method to intact LC-MS-based DAR measurement in biological samples [67,68,91,93,94]. The average DAR is calculated as the molar ratio of conjugated payload vs. total antibody, and the change of average DAR could indicate ADC deconjugation in vivo [94]. However, a highly specific immunoaffinity enrichment is commonly required to isolate free payload with conjugated ADCs, which not only is feasible in many projects, but also impedes conjugated payload quantification in tissue samples. An alternative and simpler method is using protein precipitation followed by on-pellet linker cleavage [91].

By comparison, given the inherent feature of non-cleavable linker, payloads conjugated by non-cleavable linkers are often indirectly determined by multiplying in vivo average DAR measure using intact LC-MS with total antibody concentration [57]. That being said, direct quantification of small-molecule forms of payloads conjugated with non-cleavable linkers has recently been explored, where the target analytes are payload-linker-amino-acids or payload-linker-peptides after extensive or site-specific digestion [93]. Such attempts are currently limited to ADCs with site-specific conjugation. Hyung et al. [126] developed an LC-MS method for quantification of conjugated payload of an engineered, cysteine-conjugated ADC with non-cleavable linkers in plasma sample. After a rough enrichment using protein A, the ADC was subjected to tryptic digestion, which produced a unique peptide-linker-payload moiety for quantification. In another case, an ADC that contained maytansinoid tubulin inhibitor DM1 conjugated to engineered cysteine residues through a tri-glycine-containing peptide linker (CX1) was investigated [127]. A tryptic peptide containing cystine-linker-payload was selected as the surrogate for quantification of the conjugated payload.

Apart from investigations on unconjugated and conjugated payloads, it appears that protein-payload adduct has attracted increasing attention, especially for cysteine-maleimide-based ADCs (e.g., brentuximab vedotin, T-DM1) which might undergo thiol-exchange reactions with matrix proteins [128]. The protein-payload adduct could originate from thiol-exchange reactions between matrix proteins and unconjugated payloads or conjugated payloads of maleimide-linker-containing ADCs. Characterization of these products provides important information on plasma stability of the ADC product [98].

4. Future perspective

The past decade has witnessed growing interest and accelerating development in ADCs. Although these agents have demonstrated improved clinical outcomes, the relationship between structural features of ADCs and clinical efficacy/toxicity is still poorly understood owing to the complicated nature of this therapeutic system. A comprehensive, integrated characterization of ADCs and the related pharmaceutical system is highly valuable in evaluating efficacy/safety of these agents as well as in directing both therapeutic and engineering efforts, which requires reliable analytical approaches to answering quantitative and qualitative questions from a wide range of aspects.

Among the techniques applicable for ADCs analysis, LC-MS emerges as a highly valuable and versatile tool. Over the past few

years, a growing number of LC-MS strategies at protein-, subunit-, peptide-, and payload levels have been developed, which permitted a significantly improved understanding of the molecular characteristics and pharmacokinetic/pharmacodynamic of ADCs, and provided novel insights into the complicated albeit interesting therapeutic system. Additionally, these new analytical methods have discovered novel information that profoundly affects the efficacy and safety of ADCs, for example, the identification and quantification of albumin-adduct formation which accounts for a new mechanism for DAR loss in maleimide-containing ADCs [120,128,129].

Despite these tremendous technical advancements, challenges remain. To name a few: i) Analysis of ADCs in tissues is highly critical to understanding drug effects, but is still difficult; ii) lack of an optimal method to analyze conjugated payload for ADCs with non-cleavable linkers; iii) problems associated with analysis of various products of biotransformation and catabolism; and iv) suboptimal robustness and accuracy are often an intractable problem. Addressing these challenges would greatly accelerate drug discovery and development, and facilitate clinical efforts of ADCs. Consequently, we anticipate that in the near future, intense efforts will be directed toward the development of new LC-MS-based analytical strategies in order to meet these challenges. Conceivably, such efforts will also be markedly fueled by the ever-increasing requirements of defining new parameters of ADCs (e.g., average DAR in vivo, charge heterogeneity, and positional isomers) and the evolution of new ADC modalities (e.g., ADC for non-oncology indications, antibody-dual-drug conjugates, and biparatopic ADC) [4,12,94,130]. Finally, given the rapid advancement of LC-MS techniques, LC-MS will continue to improve as the most powerful tool for ADC analysis.

Conflicts of interest

The authors declare that there are no conflicts of interest.

References

[1] Wikipedia, Antibody-drug conjugate. https://en.wikipedia.org/wiki/Antibody-drug_conjugate, 2020, 202011.
[2] L. Ducry (Ed.), Antibody-drug Conjugates, Humana Press, New York, 2013.
[3] N. Jain, S.W. Smith, S. Ghone, et al., Current ADC linker chemistry, Pharm. Res. (N. Y.) 32 (2015) 3526–3540.
[4] A. Wagh, H. Song, M. Zeng, et al., Challenges and new frontiers in analytical characterization of antibody-drug conjugates, mAbs 10 (2018) 222–243.
[5] A. Wakankar, Y. Chen, Y. Gokarn, et al., Analytical methods for physicochemical characterization of antibody drug conjugates, mAbs 3 (2011) 161–172.
[6] X. Duan, L. Abuqayyas, L. Dai, et al., High-throughput method development for sensitive, accurate, and reproducible quantification of therapeutic monoclonal antibodies in tissues using orthogonal array optimization and nano liquid chromatography/selected reaction monitoring mass spectrometry, Anal. Chem. 84 (2012) 4373–4382.
[7] E. Nouri-Nigjeh, M. Zhang, T. Ji, et al., Effects of calibration approaches on the accuracy for LC-MS targeted quantification of therapeutic protein, Anal. Chem. 86 (2014) 3575–3584.
[8] H. Donaghy, Effects of antibody, drug and linker on the preclinical and clinical toxicities of antibody-drug conjugates, mAbs 8 (2016) 659–671.
[9] P.K. Mahalingaiah, R. Ciurlionis, K.R. Durbin, et al., Potential mechanisms of target-independent uptake and toxicity of antibody-drug conjugates, Pharmacol. Ther. 200 (2019) 110–125.
[10] R. Mandler, H. Kobayashi, E.R. Hinson, et al., Herceptin-geldanamycin immunoconjugates, Canc. Res. 64 (2004) 1460.
[11] C.A. Boswell, E.E. Mundo, C. Zhang, et al., Impact of drug conjugation on pharmacokinetics and tissue distribution of anti-STEAP1 antibody-drug conjugates in rats, Bioconjugate Chem. 22 (2011) 1994–2004.
[12] C. Wei, D. Su, J. Wang, et al., LC–MS challenges in characterizing and quantifying monoclonal antibodies (mAb) and antibody-drug conjugates (ADC) in biological samples, Curr. Pharmacol. Rep. 4 (2018) 45–63.
[13] A. Beck, E. Wagner-Rousset, D. Ayoub, et al., Characterization of therapeutic antibodies and related products, Anal. Chem. 85 (2013) 715–736.
[14] K. Sandra, I. Vandenheede, P. Sandra, Modern chromatographic and mass spectrometric techniques for protein biopharmaceutical characterization, J. Chromatogr. A 1335 (2014) 81–103.
[15] J. Bergquist, M. Palmblad, M. Wetterhall, et al., Peptide mapping of proteins in human body fluids using electrospray ionization Fourier transform ion cyclotron resonance mass spectrometry, Mass Spectrom. Rev. 21 (2002) 2–15.
[16] B. Bobaly, S. Fleury-Souverain, A. Beck, et al., Current possibilities of liquid chromatography for the characterization of antibody-drug conjugates, J. Pharmaceut. Biomed. Anal. 147 (2018) 493–505.
[17] M. Kallsten, R. Hartmann, K. Artemenko, et al., Qualitative analysis of antibody-drug conjugates (ADCs): an experimental comparison of analytical techniques of cysteine-linked ADCs, Analyst 143 (2018) 5487–5496.
[18] T. Mouchahoir, J.E. Schiel, Development of an LC-MS/MS peptide mapping protocol for the NISTmAb, Anal. Bioanal. Chem. 410 (2018) 2111–2126.
[19] L. Chen, L. Wang, H. Shion, et al., In-depth structural characterization of Kadcyla(R) (ado-trastuzumab emtansine) and its biosimilar candidate, mAbs 8 (2016) 1210–1223.
[20] K.J. Arlotta, A.V. Gandhi, H.N. Chen, et al., In-depth comparison of lysine-based antibody-drug conjugates prepared on solid support versus in solution, Antibodies 7 (2018) 6.
[21] H. Sang, G. Lu, Y. Liu, et al., Conjugation site analysis of antibody-drug-conjugates (ADCs) by signature ion fingerprinting and normalized area quantitation approach using nano-liquid chromatography coupled to high resolution mass spectrometry, Anal. Chim. Acta 955 (2017) 67–78.
[22] G. Wu, Y. Gao, D. Liu, et al., Study on the heterogeneity of T-DM1 and the analysis of the unconjugated linker structure under a stable conjugation process, ACS Omega 4 (2019) 8834–8845.
[23] M.C. Janin-Bussat, M. Dillenbourg, N. Corvaia, et al., Characterization of antibody drug conjugate positional isomers at cysteine residues by peptide mapping LC-MS analysis, J. Chromatogr. B 981 (2015) 9–13.
[24] O. Hernandez-Alba, S. Houel, S. Hessmann, et al., A case study to identify the drug conjugation site of a site-specific antibody-drug-conjugate using middle-down mass spectrometry, J. Am. Soc. Mass Spectrom. 30 (2019) 2419–2429.
[25] O.V. Friese, J.N. Smith, P.W. Brown, et al., Practical approaches for overcoming challenges in heightened characterization of antibody-drug conjugates with new methodologies and ultrahigh-resolution mass spectrometry, mAbs 10 (2018) 335–345.
[26] O.O. Dada, Y. Zhao, N. Jaya, et al., High-resolution capillary zone electrophoresis with mass spectrometry peptide mapping of therapeutic proteins: peptide recovery and post-translational modification analysis in monoclonal antibodies and antibody-drug conjugates, Anal. Chem. 89 (2017) 11236–11242.
[27] K. Sandra, J. Vandenbussche, I. Vandenheede, et al., Peptide mapping of monoclonal antibodies and antibody-drug conjugates using micro-pillar array columns combined with mass spectrometry, LC-GC Eur. 31 (2018) 155–166.
[28] Y. Wang, X. Li, Y.H. Liu, et al., Simultaneous monitoring of oxidation, deamidation, isomerization, and glycosylation of monoclonal antibodies by liquid chromatography-mass spectrometry method with ultrafast tryptic digestion, mAbs 8 (2016) 1477–1486.
[29] M.R. Larsen, M.B. Trelle, T.E. Thingholm, et al., Analysis of posttranslational modifications of proteins by tandem mass spectrometry, Biotechniques 40 (2006) 790–798.
[30] O.N. Jensen, Modification-specific proteomics: characterization of post-translational modifications by mass spectrometry, Curr. Opin. Chem. Biol. 8 (2004) 33–41.
[31] L.W. Dick Jr., D. Mahon, D. Qiu, et al., Peptide mapping of therapeutic monoclonal antibodies: improvements for increased speed and fewer artifacts, J. Chromatogr. B 877 (2009) 230–236.
[32] D. Ren, G.D. Pipes, D. Liu, et al., An improved trypsin digestion method minimizes digestion-induced modifications on proteins, Anal. Biochem. 392 (2009) 12–21.
[33] D.P. Donnelly, C.M. Rawlins, C.J. DeHart, et al., Best practices and benchmarks for intact protein analysis for top-down mass spectrometry, Nat. Methods 16 (2019) 587–594.
[34] L.E. Kilpatrick, E.L. Kilpatrick, Optimizing high-resolution mass spectrometry for the identification of low-abundance post-translational modifications of intact proteins, J. Proteome Res. 16 (2017) 3255–3265.
[35] S. Kotapati, D. Passmore, S. Yamazoe, et al., Universal affinity capture liquid chromatography-mass spectrometry assay for evaluation of biotransformation of site-specific antibody drug conjugates in preclinical studies, Anal. Chem. 92 (2020) 2065–2073.
[36] T. Botzanowski, S. Erb, O. Hernandez-Alba, et al., Insights from native mass spectrometry approaches for top- and middle- level characterization of site-specific antibody-drug conjugates, mAbs 9 (2017) 801–811.
[37] D. Su, C. Ng, M. Khosraviani, et al., Custom-designed affinity capture LC-MS F(ab')2 assay for biotransformation assessment of site-specific antibody drug conjugates, Anal. Chem. 88 (2016) 11340–11346.
[38] J. He, S.F. Yu, S. Yee, et al., Characterization of in vivo biotransformations for trastuzumab emtansine by high-resolution accurate-mass mass spectrometry, mAbs 10 (2018) 960–967.
[39] K. Xu, L. Liu, R. Dere, et al., Characterization of the drug-to-antibody ratio distribution for antibody–drug conjugates in plasma/serum, Bioanalysis 5 (2013) 1057–1071.
[40] K. Xu, L. Liu, O.M. Saad, et al., Characterization of intact antibody-drug

conjugates from plasma/serum in vivo by affinity capture capillary liquid chromatography-mass spectrometry, Anal. Biochem. 412 (2011) 56–66.

[41] A. Ehkirch, V. D'Atri, F. Rouviere, et al., An online four-dimensional HICxSEC-IMxMS methodology for proof-of-concept characterization of antibody drug conjugates, Anal. Chem. 90 (2018) 1578–1586.

[42] Y.Q.Y. Henry Shion, Weibin Chen, Analytical Scale Native SEC-MS for Antibody-Drug Conjugates (ADCs) Characterization, Waters Application Note, 2018.

[43] E. Wagner-Rousset, M.C. Janin-Bussat, O. Colas, et al., Antibody-drug conjugate model fast characterization by LC-MS following IdeS proteolytic digestion, mAbs 6 (2014) 173–184.

[44] D. Firth, L. Bell, M. Squires, et al., A rapid approach for characterization of thiol-conjugated antibody-drug conjugates and calculation of drug-antibody ratio by liquid chromatography mass spectrometry, Anal. Biochem. 485 (2015) 34–42.

[45] Y. Tang, F. Tang, Y. Yang, et al., Real-time analysis on drug-antibody ratio of antibody-drug conjugates for synthesis, process optimization, and quality control, Sci. Rep. 7 (2017) 7763.

[46] A.C. Lazar, L. Wang, W.A. Blattler, et al., Analysis of the composition of immunoconjugates using size-exclusion chromatography coupled to mass spectrometry, Rapid Commun. Mass Spectrom. 19 (2005) 1806–1814.

[47] L. Grafmuller, C. Wei, R. Ramanathan, et al., Unconjugated payload quantification and DAR characterization of antibody–drug conjugates using high-resolution MS, Bioanalysis 8 (2016) 1663–1678.

[48] W. Jin, L. Burton, I. Moore, LC-HRMS quantitation of intact antibody drug conjugate trastuzumab emtansine from rat plasma, Bioanalysis 10 (2018) 851–862.

[49] J.F. Kellie, M.Z. Karlinsey, Review of approaches and examples for monitoring biotransformation in protein and peptide therapeutics by MS, Bioanalysis 10 (2018) 1877–1890.

[50] L. Kang, N. Weng, W. Jian, LC-MS bioanalysis of intact proteins and peptides, Biomed. Chromatogr. 34 (2019), e4633.

[51] A. Beck, G. Terral, F. Debaene, et al., Cutting-edge mass spectrometry methods for the multi-level structural characterization of antibody-drug conjugates, Expert Rev. Proteomics 13 (2016) 157–183.

[52] M. Damelin (Ed.), Innovations for Next-Generation Antibody-Drug Conjugates, Humana Press, New York, 2018.

[53] K.J. Hamblett, S.D. Barnscher, R.H. Davies, et al., Abstract P6-17-13: ZW49, a HER2 targeted biparatopic antibody drug conjugate for the treatment of HER2 expressing cancers, Canc. Res. 79 (2019), 17-13.

[54] T. Chen, Y. Chen, C. Stella, et al., Antibody-drug conjugate characterization by chromatographic and electrophoretic techniques, J. Chromatogr. B 1032 (2016) 39–50.

[55] M.M.C. Sun, K.S. Beam, C.G. Cerveny, et al., Reduction– alkylation strategies for the modification of specific monoclonal antibody disulfides, Bioconjugate Chem. 16 (2005) 1282–1290.

[56] J. Tang, X. Zhang, T. Chen, et al., Removal of half antibody, hole-hole homodimer and aggregates during bispecific antibody purification using MMC ImpRes mixed-mode chromatography, Protein Expr. Purif. 167 (2020) 105529.

[57] R.Y. Huang, G. Chen, Characterization of antibody-drug conjugates by mass spectrometry: advances and future trends, Drug Discov. Today 21 (2016) 850–855.

[58] C. Wang, B. Vemulapalli, M. Cao, et al., A systematic approach for analysis and characterization of mispairing in bispecific antibodies with asymmetric architecture, mAbs 10 (2018) 1226–1235.

[59] L. Schachner, G. Han, M. Dillon, et al., Characterization of chain pairing variants of bispecific IgG expressed in a single host cell by high-resolution native and denaturing mass spectrometry, Anal. Chem. 88 (2016) 12122–12127.

[60] R.J. Woods, M.H. Xie, T.S. Von Kreudenstein, et al., LC-MS characterization and purity assessment of a prototype bispecific antibody, mAbs 5 (2013) 711–722.

[61] R.A. Gomes, C. Almeida, C. Correia, et al., Exploring the analytical power of the QTOF MS platform to assess monoclonal antibodies quality attributes, PloS One 14 (2019), e0219156.

[62] L. Wang, G. Amphlett, W.A. Blattler, et al., Structural characterization of the maytansinoid-monoclonal antibody immunoconjugate, huN901-DM1, by mass spectrometry, Protein Sci. 14 (2005) 2436–2346.

[63] S. Panowski, S. Bhakta, H. Raab, et al., Site-specific antibody drug conjugates for cancer therapy, mAbs 6 (2014) 34–45.

[64] R. Dere, J.-H. Yi, C. Lei, et al., PK assays for antibody–drug conjugates: case study with ado-trastuzumab emtansine, Bioanalysis 5 (2013) 1025–1040.

[65] K. Tsuchikama, Z. An, Antibody-drug conjugates: recent advances in conjugation and linker chemistries, Protein Cell 9 (2018) 33–46.

[66] B. Gorovits, S.C. Alley, S. Bilic, et al., Bioanalysis of antibody–drug conjugates: american association of pharmaceutical scientists antibody–drug conjugate working group position paper, Bioanalysis 5 (2013) 997–1006.

[67] R.J. Sanderson, M.A. Hering, S.F. James, et al., In vivo drug-linker stability of an anti-CD30 dipeptide-linked auristatin immunoconjugate, Clin. Canc. Res. 11 (2005) 843–852.

[68] R.J. Sanderson, N.D. Nicholas, C. Baker Lee, et al., Antibody-conjugated drug assay for protease-cleavable antibody–drug conjugates, Bioanalysis 8 (2016) 55–63.

[69] S.C. Alley, K.E. Anderson, Analytical and bioanalytical technologies for characterizing antibody-drug conjugates, Curr. Opin. Chem. Biol. 17 (2013) 406–411.

[70] L.A. Khawli, S. Goswami, R. Hutchinson, et al., Charge variants in IgG1: isolation, characterization, in vitro binding properties and pharmacokinetics in rats, mAbs 2 (2010) 613–624.

[71] S. Fekete, A. Beck, J.-L. Veuthey, et al., Ion-exchange chromatography for the characterization of biopharmaceuticals, J. Pharmaceut. Biomed. Anal. 113 (2015) 43–55.

[72] S.J. Harrington, R. Varro, T.M. Li, High-performance capillary electrophoresis as a fast inprocess control method for enzyme-labelled monoclonal antibody conjugates, J. Chromatogr. A 559 (1991) 385–390.

[73] I.S. Krull, X. Liu, J. Dai, et al., HPCE methods for the identification and quantitation of antibodies, their conjugates and complexes, J. Pharmaceut. Biomed. Anal. 16 (1997) 377–393.

[74] D.A. Michels, O. Salas-Solano, C. Felten, Imaged capillary isoelectric focusing for charge-variant analysis of biopharmaceuticals, BioProcess. Int. 9 (2011) 48–54.

[75] K.J. Hamblett, P.D. Senter, D.F. Chace, et al., Effects of drug loading on the antitumor activity of a monoclonal antibody drug conjugate, Clin. Canc. Res. 10 (2004) 7063–7070.

[76] R.E. Birdsall, H. Shion, F.W. Kotch, et al., A rapid on-line method for mass spectrometric confirmation of a cysteine-conjugated antibody-drug-conjugate structure using multidimensional chromatography, mAbs 7 (2015) 1036–1044.

[77] E.A. Redman, J.S. Mellors, J.A. Starkey, et al., Characterization of intact antibody drug conjugate variants using microfluidic capillary electrophoresis-mass spectrometry, Anal. Chem. 88 (2016) 2220–2226.

[78] M. Qu, B. An, S. Shen, et al., Qualitative and quantitative characterization of protein biotherapeutics with liquid chromatography mass spectrometry, Mass Spectrom. Rev. 36 (2017) 734–754.

[79] C.J. Krusemark, B.L. Frey, P.J. Belshaw, et al., Modifying the charge state distribution of proteins in electrospray ionization mass spectrometry by chemical derivatization, J. Am. Soc. Mass Spectrom. 20 (2009) 1617–1625.

[80] S. Rogstad, A. Faustino, A. Ruth, et al., A retrospective evaluation of the use of mass spectrometry in FDA biologics license applications, J. Am. Soc. Mass Spectrom. 28 (2016) 786–794.

[81] J.F. Valliere-Douglass, W.A. McFee, O. Salas-Solano, Native intact mass determination of antibodies conjugated with monomethyl Auristatin E and F at interchain cysteine residues, Anal. Chem. 84 (2012) 2843–2849.

[82] F. Debaene, A. Boeuf, E. Wagner-Rousset, et al., Innovative native MS methodologies for antibody drug conjugate characterization: high resolution native MS and IM-MS for average DAR and DAR distribution assessment, Anal. Chem. 86 (2014) 10674–10683.

[83] H. Shion, R. Birdsall, F.W. Kotch, et al., Development of Integrated Informatics Workflows for the Automated Assessment of Comparability for Antibody Drug Conjugates (ADCs) Using LC/UV and LC/UV/MS, Poster Session Presented at the 62nd Annual Conference on Mass Spectrometry and Allied Topics, Baltimore, MD, 2014.

[84] B. Chen, Y. Peng, S.G. Valeja, et al., Online hydrophobic interaction chromatography−mass spectrometry for top-down proteomics, Anal. Chem. 88 (2016) 1885–1891.

[85] M. Sarrut, A. Corgier, S. Fekete, et al., Analysis of antibody-drug conjugates by comprehensive on-line two-dimensional hydrophobic interaction chromatography x reversed phase liquid chromatography hyphenated to high resolution mass spectrometry. I - optimization of separation conditions, J. Chromatogr. B 1032 (2016) 103–111.

[86] A.C. Leney, A.J. Heck, Native mass spectrometry: what is in the name? J. Am. Soc. Mass Spectrom. 28 (2017) 5–13.

[87] J.A. Davis, M. Kagan, J. Read, et al., Immunoprecipitation middle-up LC−MS for in vivo drug-to-antibody ratio determination for antibody−drug conjugates, Bioanalysis 9 (2017) 1535–1549.

[88] J.F. Kellie, A.S. Thomson, S. Chen, et al., Biotherapeutic antibody subunit LC-MS and peptide mapping LC-MS measurements to study possible biotransformation and critical quality attributes in vivo, J. Pharmaceut. Sci. 108 (2019) 1415–1422.

[89] B. Rago, T. Clark, Lindsay King, et al., Calculated conjugated payload from immunoassay and LC−MS intact protein analysis measurements of antibody-drug conjugate, Bioanalysis 8 (2016) 2205–2217.

[90] J. Pu, B. An, F. Vazvaei, et al., Enrichment of protein therapeutics and biomarkers for LC−MS quantification, Bioanalysis 10 (2018) 979–982.

[91] X. Zhu, B. An, M. Zhang, et al., Investigation of Ocular Tissue Disposition of Antibody-Drug Conjugates Using Novel LC-MS-based Strategies, Poster Session Presented at the 66th Annual Conference on Mass Spectrometry and Allied Topics, 2019. San Diego, CA, USA.

[92] H. Myler, V.S. Rangan, J. Wang, et al., An integrated multiplatform bioanalytical strategy for antibody−drug conjugates: a novel case study, Bioanalysis 7 (2015) 1569–1582.

[93] A. Liu, A. Kozhich, D. Passmore, et al., Quantitative bioanalysis of antibody-conjugated payload in monkey plasma using a hybrid immuno-capture LC−MS/MS approach: assay development, validation, and a case study, J. Chromatogr. B 1002 (2015) 54–62.

[94] J. Wang, H. Gu, A. Liu, et al., Antibody−drug conjugate bioanalysis using LB-LC−MS/MS hybrid assays: strategies, methodology and correlation to ligand-binding assays, Bioanalysis 8 (2016) 1383–1401.

[95] G.A. Eiceman, Z. Karpas, H.H. Hill Jr., Ion Mobility Spectrometry, 3rd ed., CRC

press, New York, 2013.

[96] E. Kraynov, A.V. Kamath, M. Walles, et al., Current approaches for absorption, distribution, metabolism, and excretion characterization of antibody-drug conjugates: an industry white paper, Drug Metab. Dispos. 44 (2016) 617—623.

[97] M. Faria, M. Peay, B. Lam, et al., Multiplex LC-MS/MS assays for clinical bioanalysis of MEDI4276, an antibody-drug conjugate of tubulysin analogue attached via cleavable linker to a biparatopic humanized antibody against HER-2, Antibodies 8 (2019) 11.

[98] L. Dong, C. Li, C. Locuson, et al., A two-step immunocapture LC/MS/MS assay for plasma stability and payload migration assessment of cysteine-maleimide-based antibody drug conjugates, Anal. Chem. 90 (2018) 5989—5994.

[99] L. Xu, Z. Zhang, S. Xu, et al., Simultaneous quantification of total antibody and antibody-conjugated drug for XMT-1522 in human plasma using immunocapture-liquid chromatography/mass spectrometry, J. Pharmaceut. Biomed. Anal. 174 (2019) 441—449.

[100] J. Qu, R.M. Straubinger, Improved sensitivity for quantification of proteins using triply charged cleavable isotope-coded affinity tag peptides, Rapid Commun. Mass Spectrom. 19 (2005) 2857—2864.

[101] R. Jenkins, J.X. Duggan, A.-F. Aubry, et al., Recommendations for validation of LC-MS/MS bioanalytical methods for protein biotherapeutics, AAPS J. 17 (2015) 1—16.

[102] J. Cao, V.M. Covarrubias, R.M. Straubinger, et al., A rapid, reproducible, on-the-fly orthogonal array optimization method for targeted protein quantification by LC/MS and its application for accurate and sensitive quantification of carbonyl reductases in human liver, Anal. Chem. 82 (2010) 2680—2689.

[103] X. Duan, L. Dai, S.-C. Chen, et al., Nano-scale liquid chromatography/mass spectrometry and on-the-fly orthogonal array optimization for quantification of therapeutic monoclonal antibodies and the application in preclinical analysis, J. Chromatogr. A 1251 (2012) 63—73.

[104] B. An, M. Zhang, R.W. Johnson, et al., Surfactant-aided precipitation/on-pellet-digestion (SOD) procedure provides robust and rapid sample preparation for reproducible, accurate and sensitive LC/MS quantification of therapeutic protein in plasma and tissues, Anal. Chem. 87 (2015) 4023—4029.

[105] E. Nouri-Nigjeh, M. Zhang, T. Ji, et al., Effects of calibration approaches on the accuracy for LC-MS targeted quantification of therapeutic protein, Anal. Chem. 86 (2014) 3575—3584.

[106] S. Shen, B. An, X. Wang, et al., Surfactant cocktail-aided extraction/precipitation/on-pellet digestion strategy enables efficient and reproducible sample preparation for large-scale quantitative proteomics, Anal. Chem. 90 (2018) 10350—10359.

[107] B. An, M. Zhang, J. Pu, et al., High-throughput, sensitive LC-MS quantification of biotherapeutics and biomarkers using antibody-free, peptide-level, multiple-mechanism enrichment via strategic regulation of pH and ionic and solvent strengths, Anal. Chem. 91 (2019) 3475—3483.

[108] M. Zhang, B. An, Y. Qu, et al., Sensitive, high-throughput, and robust trapping-micro-LC-MS strategy for the quantification of biomarkers and antibody biotherapeutics, Anal. Chem. 90 (2018) 1870—1880.

[109] L.A. Vasicek, X. Zhu, D.S. Spellman, et al., Direct quantitation of therapeutic antibodies for pharmacokinetic studies using immuno-purification and intact mass analysis, Bioanalysis 11 (2019) 203—213.

[110] W. Jian, L. Kang, L. Burton, et al., A workflow for absolute quantitation of large therapeutic proteins in biological samples at intact level using LC-HRMS, Bioanalysis 8 (2016) 1679—1691.

[111] N. de Mel, S.H.R. Mulagapati, M. Cao, et al., A method to directly analyze free-drug-related species in antibody-drug conjugates without sample preparation, J. Chromatogr. B 1116 (2019) 51—59.

[112] L.N. Tumey (Ed.), Antibody-Drug Conjugates: Methods and Protocols, Humana Press, New York, 2020.

[113] H.H. Gong, N. Ihle, M.T. Jones, et al., Control strategy for small molecule impurities in antibody-drug conjugates, AAPS PharmSciTech 19 (2018) 971—977.

[114] K. Lin, J. Tibbitts, Pharmacokinetic considerations for antibody drug conjugates, Pharm. Res. (N. Y.) 29 (2012) 2354—2366.

[115] Y. Fujiwara, M. Furuta, S. Manabe, et al., Imaging mass spectrometry for the precise design of antibody-drug conjugates, Sci. Rep. 6 (2016) 1—8.

[116] B.-Q. Shen, D. Bumbaca, O. Saad, et al., Catabolic fate and pharmacokinetic characterization of trastuzumab emtansine (T-DM1): an emphasis on preclinical and clinical catabolism, Curr. Drug Metabol. 13 (2012) 901—910.

[117] D. Wei, M. Sullivan, O. Espinosa, et al., A sensitive LC—MS/MS method for the determination of free maytansinoid DM4 concentrations—method development, validation, and application to the nonclinical studies of antitumor agent DM4 conjugated hu-anti-Cripto MAb B3F6 (B3F6-DM4) in rats and monkeys, Int. J. Mass Spectrom. 312 (2012) 53—60.

[118] Y. Liu, F. Zhou, H. Sang, et al., LC-MS/MS method for the simultaneous determination of Lys-MCC-DM1, MCC-DM1 and DM1 as potential intracellular catabolites of the antibody-drug conjugate trastuzumab emtansine (T-DM1), J. Pharmaceut. Biomed. Anal. 137 (2017) 170—177.

[119] S. Kaur, K. Xu, O.M. Saad, et al., Bioanalytical assay strategies for the development of antibody—drug conjugate biotherapeutics, Bioanalysis 5 (2013) 201—226.

[120] B. Rago, L.N. Tumey, C. Wei, et al., Quantitative conjugated payload measurement using enzymatic release of antibody—drug conjugate with cleavable linker, Bioconjugate Chem. 28 (2017) 620—626.

[121] A. Liu, Immuno-capture LC-MS/MS hybrid assay methodology in ADC bioanalysis, Immunome Res. 12 (2016) 54.

[122] Y. Li, C. Gu, J. Gruenhagen, et al., An enzymatic deconjugation method for the analysis of small molecule active drugs on antibody-drug conjugates, mAbs 8 (2016) 698—705.

[123] T. Chen, D. Su, J. Gruenhagen, et al., Chemical de-conjugation for investigating the stability of small molecule drugs in antibody-drug conjugates, J. Pharmaceut. Biomed. Anal. 117 (2016) 304—310.

[124] A. Hussain, B. Gorovits, M. Leal, et al., PK of immunoconjugate anticancer agent CMD-193 in rats: ligand-binding assay approach to determine in vivo immunoconjugate stability, Bioanalysis 6 (2013) 21—32.

[125] L. Xu, L.E. Packer, C. Li, et al., A generic approach for simultaneous measurements of total antibody and cleavable antibody-conjugated drug by LC/MS/MS, Anal. Biochem. 537 (2017) 33—36.

[126] S.-J. Hyung, D. Li, N. Koppada, et al., Method development of a novel PK assay for antibody-conjugated drug measurement of ADCs using peptide-linker drug analyte, Anal. Bioanal. Chem. 411 (2019) 2587—2596.

[127] C. Shi, S. Goldberg, T. Lin, et al., Bioanalytical workflow for novel scaffold protein—drug conjugates: quantitation of total Centyrin protein, conjugated Centyrin and free payload for Centyrin—drug conjugate in plasma and tissue samples using liquid chromatography—tandem mass spectrometry, Bioanalysis 10 (2018) 1651—1665.

[128] C. Wei, G. Zhang, T. Clark, et al., Where did the linker-payload go? A quantitative investigation on the destination of the released linker-payload from an antibody-drug conjugate with a maleimide linker in plasma, Anal. Chem. 88 (2016) 4979—4986.

[129] B.Q. Shen, K. Xu, L. Liu, et al., Conjugation site modulates the in vivo stability and therapeutic activity of antibody-drug conjugates, Nat. Biotechnol. 30 (2012) 184—189.

[130] A. Beck, L. Goetsch, C. Dumontet, et al., Strategies and challenges for the next generation of antibody-drug conjugates, Nat. Rev. Drug Discov. 16 (2017) 315—337.

Review paper

Current status of *in vivo* bioanalysis of nano drug delivery systems

Tingting Wang [a, c], Di Zhang [c], Dong Sun [d, e, **], Jingkai Gu [b, c, *]

[a] *Clinical Laboratory, The First Hospital, Jilin University, Changchun, 130061, PR China*
[b] *Research Institute of Translational Medicine, The First Hospital, Jilin University, Changchun, 130061, PR China*
[c] *Research Center for Drug Metabolism, College of Life Science, Jilin University, Changchun, 130012, PR China*
[d] *Department of Biopharmacy, College of Life Science, Jilin University, Changchun, 130012, PR China*
[e] *Key Laboratory of Molecular Pharmacology and Drug Evaluation, Ministry of Education, Yantai University, Yantai, 264005, PR China*

ARTICLE INFO

ABSTRACT

The development of nano drug delivery systems (NDDSs) provides new approaches to fighting against diseases. The NDDSs are specially designed to serve as carriers for the delivery of active pharmaceutical ingredients (APIs) to their target sites, which would certainly extend the benefit of their unique physicochemical characteristics, such as prolonged circulation time, improved targeting and avoiding of drug-resistance. Despite the remarkable progress achieved over the last three decades, the understanding of the relationships between the in vivo pharmacokinetics of NDDSs and their safety profiles is insufficient. Analysis of NDDSs is far more complicated than the monitoring of small molecular drugs in terms of structure, composition and aggregation state, whereby almost all of the conventional techniques are inadequate for accurate profiling their pharmacokinetic behavior in vivo. Herein, the advanced bio-analysis for tracing the in vivo fate of NDDSs is summarized, including liquid chromatography tandem-mass spectrometry (LC-MS/MS), Förster resonance energy transfer (FRET), aggregation-caused quenching (ACQ) fluorophore, aggregation-induced emission (AIE) fluorophores, enzyme-linked immunosorbent assay (ELISA), magnetic resonance imaging (MRI), radiolabeling, fluorescence spectroscopy, laser ablation inductively coupled plasma MS (LA-ICP-MS), and size-exclusion chromatography (SEC). Based on these technologies, a comprehensive survey of monitoring the dynamic changes of NDDSs in structure, composition and existing form in system (i.e. carrier polymers, released and encapsulated drug) with recent progress is provided. We hope that this review will be helpful in appropriate application methodology for investigating the pharmacokinetics and evaluating the efficacy and safety profiles of NDDSs.

1. Introduction

In the past 30 years, the development of nanotechnology was fruitful and many novel technologies have been applied to disease diagnosis, pharmaceutical discovery and tissue engineering [1–3]. NDDS is a rapidly developing and most remarkable nanomedicine technique. Doxil®, liposomal doxorubicin (DOX), was the first approved NDDS in 1995 for the treatment of AIDS-related Kaposi's and ovarian cancer with reduced side effects and passive tumor targeting effect [4]. In recent years, many types of NDDSs, such as liposomes, micelles, polymer-based nanoparticles (NPs), nano-emulsions, nanogels, inorganic NPs and inorganic/organic (core/shell) NPs, have been subjected to preclinical and clinical studies [5].

In NDDSs, small molecular drugs or biotherapeutics are entrapped or chemically bonded onto nanoparticles. Different from traditional pharmaceuticals, NDDSs exhibit material physico-chemical characteristics related to drug delivering properties after administration [6,7]. The NDDS enhances pharmacological and pharmaceutical properties of the parent drugs by prolonging circulation time, improving efficacy and targeting, overcoming drug-resistance, reducing immunogenicity and toxicity [8,9].

The superiority of NDDSs attracted global investment, so the research funding in nanomedicine from the US National Institutes of Health (NIH) from 2011 to 2019 is around 623 million US dollars

[10,11]. However, only 51 nanomedical products have been approved by the Food and Drug Administration (FDA) till recently [12]. The low clinical transition ratio was partially due to the incomplete understanding of the pharmacokinetic properties of NDDSs [13]. The biological fate of NDDSs remains elusive. The conventional pharmacokinetic studying methods, such as fluorescence labeling, could not track or distinguish in vivo nanocarriers and payloads simultaneously.

Herein, we review the recent advances of the bioanalytical techniques for pharmacokinetic research on NDDSs for the first time. The measurement strategies and results for the released and encapsulated drug as to the carrier polymer of NDDSs and their biodistribution are enumerated, and obstacles and perspectives of these technologies are discussed.

2. Classical NDDS

NDDSs such as liposomes, micelles, polymer-based NPs, nanoemulsions, nanogels, inorganic NPs and inorganic/organic (core/shell) NPs have long been developed for delivering APIs to the specific site of action. Nowadays increased number of NDDSs appear in preclinical and clinical phases [14].

2.1. Liposomes

Liposomes are lipid-based concentric bilayer vesicles (particle size ≈ 400 nm) comprising either synthetic or natural phospholipids [15]. The phospholipid molecules typically consist of a polar phosphate group and two hydrophobic fatty acid chains, which can spontaneously form a closed, bilayer structure by self-assembling in an aqueous environment [16]. The hydrophilic phosphate groups are exposed on the outer and inner surfaces of the liposomes and the hydrophobic fatty chains are packed and piled up in between [17]. Hence, liposomes are utilized for carrying water-soluble APIs in the cavity or lipophile APIs within the lipid bilayer (Fig. 1A). Because of their size, hydrophobic character and surface electrical charge, liposomes can be rapidly recognized and cleared by the mononuclear phagocyte system (MPS) [18]. One of the solutions to overcoming this issue is to modify the surface of liposome with amphiphilic polymers, such as poly (ethylene glycol) (PEG). The PEG coating can protect the liposome from enzymatic and immunologic clearance, hence called "stealth properties". Therefore, modifying with PEG (PEGylation) has become a widely applied strategy to reduce opsonization and prolong circulation time of liposomes [19]. The approved Doxil® in 1995 has adopted this surface-bound methoxy polyethylene glycol liposomal formulation (STEALTH®), and a half-life of approximately 55 h in humans has been achieved.

2.2. Polymeric micelles

Polymeric micelles are solid spherical aggregates with size ranging from 10 nm to 100 nm, composed of amphiphilic copolymers containing hydrophobic and hydrophilic blocks [20]. The micelles can be formed spontaneously by self-assembly when the concentration of amphiphilic copolymers exceeds the critical micelle concentration (CMC). With a hydrophobic core and a hydrophilic shell layer or corona, polymeric micelles have been used as carriers for various lipophilic drugs, which significantly increase the drug concentration in an aqueous medium (Fig. 1B) [21]. After injection, polymeric micelles are susceptible to being diluted below the CMC in the blood. This may lead to the dissociation of micelles into unimers [22]. The CMC is dependent on the factors such as chemical structure of the polymer as well as the molecular weight (MW) of each polymeric block. The marketed Nanoxel-PM® is docetaxel provided in an mPEG-PDLLA micellar formulation [23]. Furthermore, Genexol®-PM is paclitaxel loaded PEG-PLA micelle.

2.3. Polymeric NPs

Polymeric particles in size of 40—400 nm are capable of carrying APIs in the polymeric matrix or on the surface of the particle by absorption or conjugation [24]. Polymeric NPs are solid systems classified into nanospheres and nanocapsules depending on the
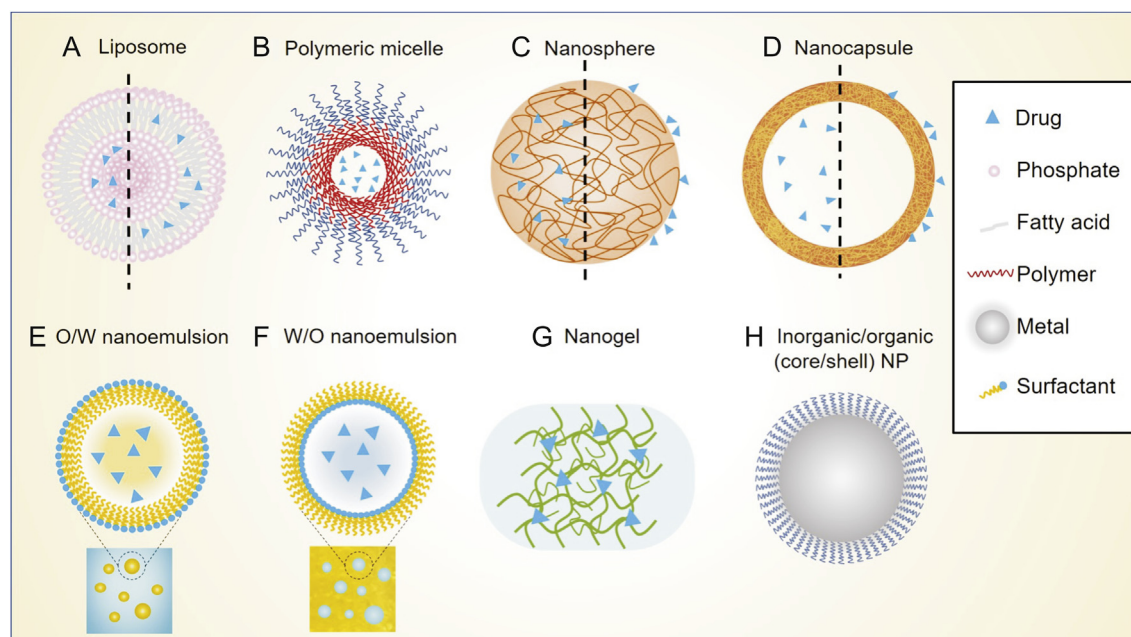
Fig. 1. Classical nano drug delivery system (NDDSs) used in drug delivery, including: (A) liposome, (B) polymeric micelle, (C) nanosphere, (D) nanocapsule, (E) O/W nanoemulsion, (F) W/O nanoemulsion, (G) nanogel, and (H) inorganic/organic (core/shell) nanoparticle (NP).

type of polymer, the localization of APIs and the production procedure [25,26]. Nanospheres are essentially monolithic systems having a solid matrix, whereby the APIs can be either loaded onto the surface or dissolved within it (Fig. 1C). In contrast, nanocapsules are reservoir systems composed of a polymeric shell, and the APIs are confined in the inner liquid core or adsorbed on the surface (Fig. 1D) [27]. Polymeric NPs can be produced from natural polymers such as chitosan or dextran, as well as from synthetic polymers, such as poly(lactide) (PLA), poly (lactide-co-glycolide) (PLGA), poly(alkylcyanoacrylates) or poly(epsilon-caprolactone) [28—30]. Synthetic polymers such as PEG, PLA and PLGA have been approved by FDA for human use over decades [31]. The 2018 approved lipid NP drug Onpattro® contains two kinds of lipids: heptatriaconta-6,9,28,31-tetraen-19-yl-4-(dimethylamino) butanoate (DLin-MC3-DMA) and α-(3'-{[1,2-di(myristyloxy)proponoxy] carbonylamino} propyl)-ω-methoxy, polyoxyethylene (PEG$_{2000}$-C-DMG) [32].

2.4. Nanoemulsions

Nanoemulsions are oil-in-water (O/W) or water-in-oil (W/O) dispersion of two kinds of immiscible liquids. One is dispersed as droplets in the other one and stabilized by an amphiphilic surfactant [33] (Fig. 1 E and F). The diameter of attained droplet is usually of 10—600 nm in size. This nanocarrier is adequate for the delivery of both hydrophilic and hydrophobic drugs, which is ideal for improving the solubility of hydrophobic drugs in aqueous media and protecting them from hydrolysis and enzymatic degradation. Drug release process from nanoemulsion involves solute partitioning from droplets into surfactant layer and then diffusing into surrounding phase. Nanoemulsions prepared by low-energy emulsification frequently require large amounts of surfactants for stabilization. High dose of surfactant will cause cell membrane fluidization. Therefore, the major disadvantages of nanoemulsions are their limited stability and low adhesivity. The oil-in-water nanoemulsion Restasis®, cyclosporine A in castor oil droplets with polysorbate 80 as the emulsifying agent, has been approved by FDA in 2002 for the treatment of keratoconjunctivitis sicca [34].

2.5. Nanogels

Nanogels are nanoscale hydrogel particles with size ranging from 100 nm to 200 nm, composed of cross-linked hydrophilic polymer network [35]. Nanogels are capable of absorbing water up to a thousand-fold of their dry weight. The swollen hydrogel forms a gigantic 3D framework, which can be utilized for entrapping drugs, polymers and dispersed phase of liquid (Fig. 1G). Nanogels are mainly used as drug carriers for delivery of both hydrophilic and hydrophobic drugs [36]. Owing to their swelling/shrinking property, flexibility in form, large surface area and highly water content, a controlled and sustained release manner can be achieved. Many nanogels formulations are available on the market; most of them are cosmetic remedies, a number of them are toothpaste formulation and several formulations are personal skin care products [37,38].

2.6. Inorganic NPs and inorganic/organic (core/shell) nanoparticles

Inorganic NPs include metal and metal oxides, such as gold (Au), silver (Ag), platinum (Pt), iron oxide (Fe$_3$O$_4$), titanium oxide (TiO$_2$), copper oxide (CuO) and zinc oxide (ZnO) [39]. Many of the inorganic NPs have long been used in clinic for various therapeutic applications, such as platinum compounds for cancer therapy and silver as antibacterial agents. Similar to organic pharmaceuticals, inorganic pharmaceuticals can also benefit from NDDSs by

improving their pharmacokinetic performance, such as enhanced targeting, drug loading, and immune system evasion.

Inorganic/organic (core/shell) nanoparticles are complexation of inorganic NPs with an organic polymer shell (Fig. 1H) [40]. The polymeric protective shell can promote purely steric repulsions so as to reduce the range and strength of electrostatic and van der Waals interactions between the colloids. The hybrid aggregates are typically in the size around 100 nm and have remarkable colloidal stability even against ionic strength variations. Ferumoxytol (Feraheme®) are iron oxide nanoparticles coated with poly-glucose sorbitol carboxy-methyl-ether, which have been approved by FDA for treatment of iron deficiency in adults with chronic kidney disease in 2009 [41].

3. Quantification of the in vivo trafficking of NDDSs

To exert the desired biologically effect, the encapsulated/embedded APIs must be released from NPs and reach their target site. Although NDDSs have been applied as drug carriers for over twenty years, pharmacokinetics studies have always been focused on the total drug concentrations and the polymers have often been overlooked. Furthermore, the characterization of the systematic release profile for the drug loaded particles remains incomplete. Different from the traditional pharmacokinetic studies of APIs, beside the released drug, the key aspects of the pharmacokinetic studies on NDDSs further include encapsulated drug and carrier polymers. The polymer quantitation and differentiation between released and encapsulated drug were the main technical difficulties bothering the bioanalysis of NDDS. With the technology development, methods have been merged for distinguishing the released and encapsulated drugs in vivo, such as LC-MS/MS, FRET, ACQ and AIE fluorophores and ELISA (Table S1).

3.1. Quantitation methods for the released and encapsulated drug in vivo

The NDDS encapsulation preserves the payloads drugs and endows them with prolonged circulation time and solubilization, which is therefore often referred to as a circulating "reservoir" of drug. To date, numerous efforts have been dedicated to reveal the release profiling of NDDSs.

3.1.1. LC-MS/MS

LC-MS/MS is a standard bioanalysis method for small molecule drugs, which recently is also considered as the preferred choice for profiling the drug release process of NDDSs in vivo. Distinguishing the released and encapsulated drug by LC-MS/MS is a critical challenge. Smits et al. [42] were the first to report an LC-MS/MS method for the differential quantification of released and encapsulated drug of prednisolone phosphate loaded liposomes in whole blood and liver tissue. Since released prednisolone phosphate will be immediately dephosphorylated by phosphatases in vivo, the prednisolone was utilized as surrogate analyte for the released drug. Similarly, the determination of released drug from polymeric micelles was reported in Braal et al.'s study [43]. CriPec® is a docetaxel-temporarily covalently conjugated micelle (approximately 65 nm). This conjugate is stable at pH 5.0 at room temperature. The quantitation of the released docetaxel can be therefore measured free from the interference of the conjugated drug. For the quantitation of the conjugated docetaxel, the drug needs to be detached from micelles at 37 °C and pH 7.4 for three days. Since the LC-MS/MS method alone cannot differentiate the detached drug from the previously released drug, the drug-loaded micelles should be separated first.

Solid phase extraction (SPE) is widely applied to separate the
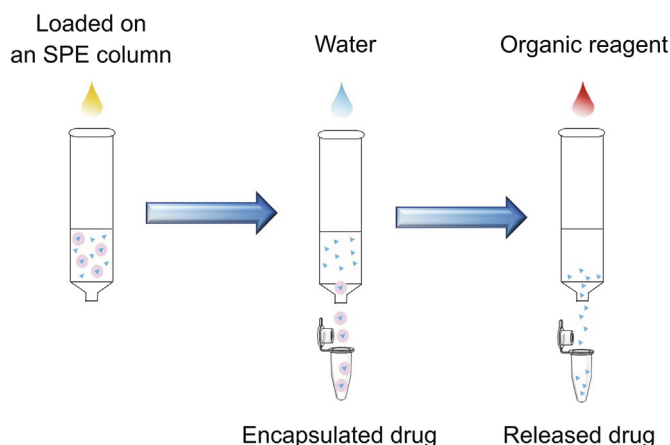
Fig. 2. Procedure for the separation of released and encapsulated drug in liposomes by solid phase extraction (SPE) in plasma sample.

Fig. 3. Illustration of the Förster resonance energy transfer (FRET) that is being developed for tracking the bio-distribution of nano drug delivery system (NDDSs).

released and encapsulated drug. A common SPE procedure is as follows: 1) sample loading; 2) water washing (liposomes with hydrophilic surface will not be retained on SPE column); and 3) hydrophobic solvent washing (the adsorbed released drug will be then eluted) (Fig. 2). Deshpande et al. [44], Su et al. [45] and Xie et al. [46] have utilized SPE separation method for profiling the pharmacokinetic behavior of amphotericin B and DOX liposomes in vivo. A similar approach was adopted by Wang et al., whereby the release and uptake processes of DOX liposome in health tissues and in tumors were profiled [47]. This SPE separation method has also been conditionally applied to separate polymeric NPs. Song et al. [48] were the first to utilize a similar separation method for the quantitation of gedatolisib released from PLA-PEG NPs. The concentration of encapsulated gedatolisib was calculated by subtracting the released gedatolisib values from the total values. In consideration of the properties of the payload drug, here an MCX SPE column was employed instead of an HLB SPE column.

Ultrafiltration was also considered as a separation method for liposomal released and encapsulated drug. Xie et al. [46] investigated the accuracy of this separation method using DOX liposomes as test sample. The recovery rate of DOX separated by ultrafiltrate was no more than 10%, which may be related to the adsorption of DOX to device and plasma proteins.

A new class of separation techniques was developed by Chen et al. [49]. Based on the specific binding of biotin and streptavidin, streptavidin-Fe$_3$O$_4$@PDA was utilized as the separation nanoprobes to separate biotin-DTX-liposomes from plasma in the presence of a magnetic field, and 75% recovery efficiency has been achieved.

3.1.2. FRET

FRET is a new tool to reveal the biological fate of NDDSs in vivo. Its principle involves energy transfer between a donor fluorophore in its electronic excited state and an adjacent acceptor fluorophore (1–10 nm) (Fig. 3) [50]. A spectrum overlap between the donor and acceptor greater than 30% is necessary for an efficiently energy transfer [51]. In the FRET-based strategies for investigating the stability and drug release of NDDSs, a FRET pair (donor and acceptor) should be co-encapsulated in the core of micelles [52,53]. FRET signal decays rapidly regarding exceeding of the energy transfer distance, which corresponds to the payload release [50].

However, the payload release can be made either by FRET pair diffusion or by micelles dissociation. In a recent study by Sun et al., the in vivo stability of the micelles has been investigated by immobilizing the FRET pair on the hydrophobic end of the carrier
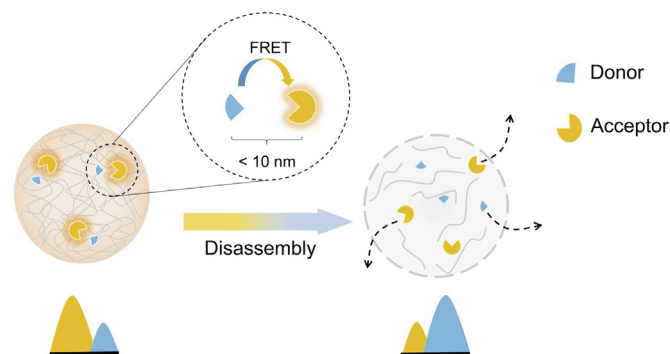
polymers. The FRET pair loaded polymers were then transformed into micelle. Therefore, the signal decreasing in vivo is merely correlated to micelles dissociation (Fig. 4). [54]. To minimize the impact of FRET fluorophore on micelle properties, only a small percentage of the hydrophobic ends were loaded with the FRET pair (1% for both), and the loading of drug is not influenced.

The FRET method has some restrictions of its own: 1) Re-illumination caused by repartitioning into hydrophobic constructs. The FRET pairs are generally highly hydrophobic compounds, prefer to repartition into hydrophobic constructs such as membranes, hydrophobic cavities of biomacromolecules or hydrophobic cores of physiological micelles. 2) Low sensitivity. Since the acceptor can be only excited by the donor indirectly, generally the fluorescence intensity of the FRET system is relatively weak.

3.1.3. ACQ fluorophores

ACQ fluorophores possess excellent fluorescent properties when dispersed in solution. The fluorescence can be turned off by fluorescent quenching, in case the fluorophores aggregated and formed stable π-π stack [55]. ACQ fluorophores are usually conjugated aromatic systems with strong hydrophobicity, which is prone to aggregate in a hydrophilic solvent, such as water. Based on this characteristic, ACQ probes are encapsulated in the hydrophobic core of nanocarriers. The fluorescence emission indicates a dispersed state of ACQ, which represents intact nanocarriers (Fig. 5A). Once the nanocarriers are dissociated, the fluorescence is quenched immediately accompanying with the ACQ probes aggregating in the aqueous medium. The tiny aggregates can be dispersed in the solvent and appear as homogenous solutions without precipitation. This aggregating process is reversible. When new micelles are introduced, the aggregates can dissolve or disperse into monomers again in the hydrophobic domains and regain their fluorescence. Although the ACQ probes are originally designed for imaging, He et al. applied this strategy for quantitation of mPEG−PDLLA polymeric micelles in vivo. The near-infrared aza-BODIPY fluorescent probe P2 was encapsulated in the hydrophobic core of the polymeric micelles. Excellent linearity of fluorescent response versus polymeric micelle concentration over the range of 9.77−625 μg/mL was observed [56]. The result of pharmacokinetic study in rat indicates that ACQ can be an alternative for the bio-analysis of NDDSs. The major drawback of ACQ method is re-illumination. Additionally, the application of ACQ is restricted in hydrophobic NDDSs.

3.1.4. AIE fluorophores

In contrast to ACQ, AIE fluorophores exhibit hardly emission in dilute solvent. In aggregate state, the free rotation of dye molecules is restricted, which dramatically boosts emission (Fig. 5B). In the
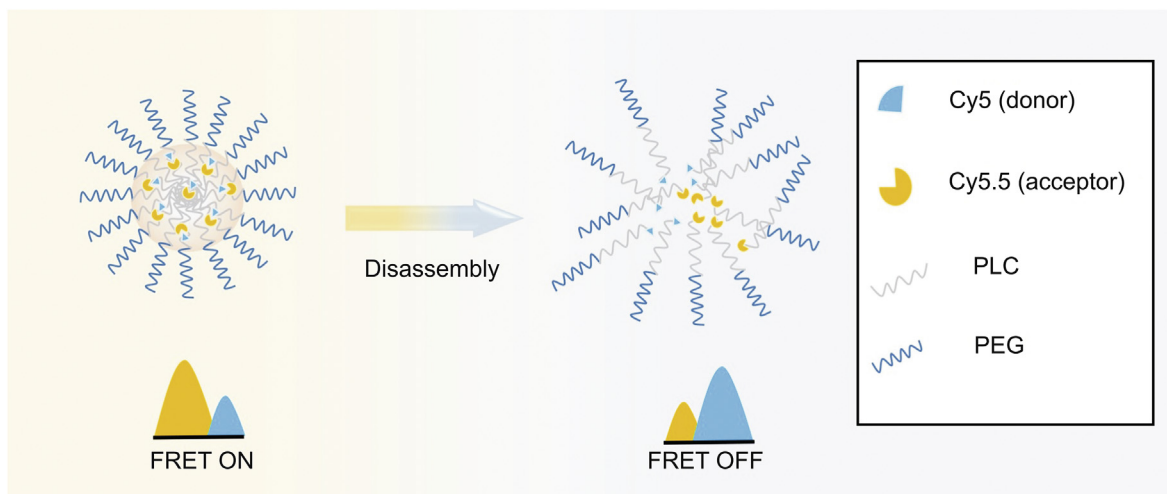
Fig. 4. Design and working principle of the Förster resonance energy transfer (FRET) micelles.
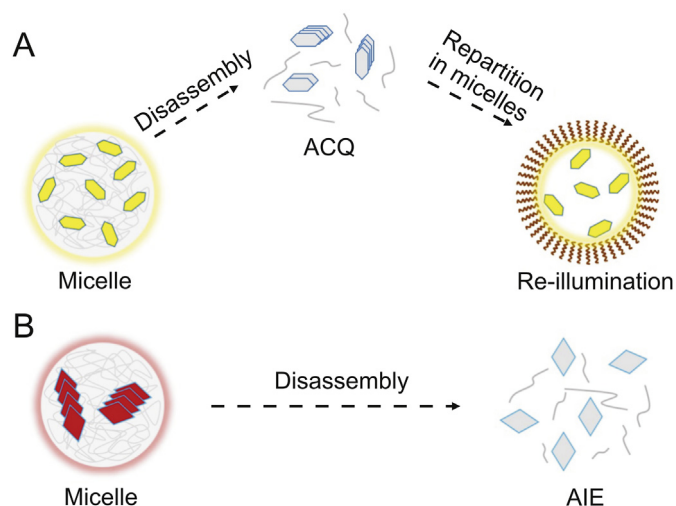
Fig. 5. Illustration of (A) aggregation-caused quenching (ACQ) and (B) aggregation-induced emission (AIE) that are being developed for tracking the drug encapsulated in nano drug delivery system (NDDSs).

case of nanocarrier dissociation, the fluorescence of leaked AIE probes is extremely weak in the environment. Therefore, the AIE probes can be employed to indicate the state of nanoparticles in vivo. Till recently, not many reports about monitoring the in vivo fate of NDDSs with AIE strategy are available. Conventional short-wavelength one-photon excited AIE material has some drawbacks in application, such as toxicity, short penetration depth (<100 mm), interference of tissue autofluorescence and photobleaching phenomenon. Furthermore, AIE is hindered by scattering, which relates to the long-wavelengths of the exciting light and high signal-noise ratio at a deep focal plane. By comparison, two-photon excited AIE has the advantages of low biological damage, low-energy irradiation, high-energy fluorescence, reduction of autofluorescence and excellent penetration depth. Most recently, Zhuang et al. employed a two-photon excitable AIE fluorescence probe to compare the pharmacokinetic behaviors of DOX and DOX-loaded micelles in vivo [57]. The doped TBIS fluorophore endowed mPEG-SS-Poly (AEMA-co-TBIS) (mPEATss) micelles with great AIE feature without influencing the drug loading.

3.1.5. ELISA

The ELISA is an immunological assay for detection of biological molecules such as proteins, antibodies, hormones and cytokines. ELISA has been also applied in investigating the release profile of the biomacromolecule loaded nanoparticles. The most prevalent ELISA method is known as "sandwich" ELISA, for the analyst antigen is stuck between two kinds of antibodies. Wherein, a primary antibody is first immobilized to the surface of the plate for capturing the analyst antigen in the serum; therefore, the primary antibody is also known as capture antibody. The captured antigens can be followed and recognized by an enzyme-linked antigen-specific antibody, which is referred as detecting antibody. The coupled enzyme serves here for an optical detection, signal amplification and quantitation of the captured analyst antigen [58].

In a study by Wang et al., the sandwich ELISA method was employed for quantifying the released payloads stromal cell-derived factor 1 (SDF-1) and bone morphogenetic protein 2 (BMP-2) to evaluate the encapsulation efficiency and release kinetics of the chitosan oligosaccharide/heparin (CSO/H) NPs in vitro [59]. In the work of Azie et al., latent transforming growth-factor beta (TGF-β) was conjugated to superparamagnetic iron oxide nanoparticles (SPIONs). The release profile of the active TGF-β from the SPIONs was subsequently monitored by ELISA [60]. However, the ELISA has the advantage in sensitivity, but it also has certain limitations, such as limited varieties of commercial ELISA kits, narrow linear ranges and cross-reactivity issue.

3.2. Quantitation methods for polymer

After the administration, the polymeric material of NDDSs may subject to disassembly, distribution, metabolism and excretion. In contrast to the payload drug, the knowledge to the in vivo fate of the polymeric materials is insufficient. The pharmaceutical polymer excipients are the main component of NDDS and are generally considered to be inert ingredients. However, the polymer related adverse drug reaction (ADR) reports on iatrogenic illnesses keep increasing, such as hypersensitivity reactions [61], cell vacuolation [62] or splenomegaly [63]. The accumulation of polymer may have potential toxicity and has aroused attention of regulatory authorities. Several analytical techniques have been developed for the bioanalysis of the polymeric material in NPs. Nuclear magnetic resonance (NMR) [64], colorimetric methods [65,66], SEC [67] and high-performance liquid chromatography (HPLC) [68–71]

technologies are inadequate in sensitivity. The LC-MS/MS and ELISA are currently employed techniques for in vivo polymer quantitation (Table S1).

3.2.1. LC-MS/MS

LC-MS/MS is a common analysis technique in the small molecular drug, which has recently made a great improvement in bioanalysis of polymers. The major challenge for the quantitative analysis of polymers by LC-MS/MS lies primarily in their polydispersity, which includes series of homologues with different degrees of polymerization and MWs. To overcome this challenge, several mass spectroscopy data acquisition strategies, such as selected ion monitoring (SIM), multiple reaction monitoring (MRM), in-source collision induced dissociation (CID) and MS^{ALL}, were applied to the polymer analysis in biological matrices. In this review, bioanalytical strategies for detecting several important pharmaceutical polymers are enumerated, including PEG, PLA, hyaluronan (HA), chitosan, and cyclodextrin (CD).

3.2.1.1. PEG. PEG is one of the most meaningful synthetic polymers in the pharmaceutical industry, which are produced commercially from ethylene oxide monomers (Fig. 6A) [72]. It is widely used as solubilizer, stabilizer, release-modifier or conjugated with drug molecules (PEGylation) and drug delivery vehicles (liposomes, micelle and nanoparticles). PEGylation, which can prolong drug half-life, enhance bioavailability, and reduce immunogenicity of the vehicle, has been approved by FDA for human use over a decade [73].

In 2004, Zhang et al. [74] developed a flow injection MS method for the quantitation of PEG300 in drug formulations under SIM mode. SIM is a variation of an MRM scanning mode, in which only the selected precursor ions will be transmitted through the quadrupole mass analyzer Q1 and Q3, and the collision energy (CE) of Q2 should be set to the level without causing obvious fragmentation (Fig. 7A). This method provided a better sensitivity in lower limits of quantitation (LLOQ, 136 ng/mL) than previously published methods: gas chromatography-mass spectrometry (GC-MS) (1 mg/mL) [75], semi-preparative HPLC (0.73 mg/mL) [69], HPLC (50 μg/mL) [68] and SEC (1.15 mg/mL) [67]. SIM methods are not routinely utilized to analyze biological samples because of the reduced selectivity and high background noise. Ashiru et al. [76] developed the first specific LC-MS/MS method for the quantitation of PEG400 in biological samples. Due to the limited selectivity of SIM, this method was prone to interference from endogenous substances, and the obtained LLOQ (2.5 μg/mL) was higher than that of the previously flow injection MS method.

MRM is a sensitive and selective scan mode, which is commonly used in the LC-MS/MS bioanalysis of small-molecular drugs. Under MRM mode, the precursor ions of the analyte are selected by the first mass spectrometer Q1 and effectively fragmented in Q2. Form the multiple product ions, a highly specific product ion is selected by the second mass spectrometer Q3 for detection. With the aids of the analyte-specific product ion, the selectivity and the signal-noise ratio could be greatly improved (Fig. 7B). A bioanalytical assay for PEG400 using MRM analysis in plasma has been exploited by Bhaskar et al. [77]. In this study, the nine most abundant oligomers and their common product ion (at *m/z* 89) were monitored in Q1 and Q3, respectively. Analyte peaks were then summed up to estimate the total amount of PEG400 in plasma with an LLOQ of 1.01 μg/mL. This approach may be appropriate for low MW PEGs. High MW PEGs contain a wide range of homologues and multi-charged ions, and only a fraction of the ions can be monitored by MRM, which is inadequate for quantitation.

Warrack et al. [78] reported a combined strategy for the quantitation of high MW PEG (1.4-40 kDa) in biological samples. The polymers first undergo in-source CID, which generates fragment ions by the declustering potential (DP) in the ion source (Fig. 7C). The generated fragment ions are subjected to the following MRM as surrogate precursor ions. However, detection is still limited by insufficient fragmentation under DP in the ion source, which ultimately limits the sensitivity of the following MRM scan. The LLOQ with in-source CID is 300 ng/mL for PEG.

To improve the fragmentation efficiency, Zhou et al. [79] developed an MS^{ALL} based approach for the quantitative analysis of PEG by liquid chromatography triple-quadrupole/time-of-flight mass spectrometry (LC-Q-TOF MS). Q-TOF MS is a hybrid MS consisting of Q1, Q2 and a high-resolution TOF mass analyzer. MS^{ALL} scan mode allows all precursor ions to pass through Q1, being fragmented in Q2. Consequentially, all the product ions were scanned by the high-resolution TOF analyzer (Fig. 7D). Compared to previous approaches, MS^{ALL} is an effective strategy for quantitation of PEGs in biological samples. Therefore, this approach is also applied in quantitative analysis of PEG and PEGylated drug simultaneously, such as PEGylated DOX, paclitaxel and gemcitabine [80–82].

3.2.1.2. PLA. Benefiting from its biocompatibility and low toxicity, PLA is one of the most widely used biodegradable polymers (Fig. 6B) [83,84]. Various types of PLA, such as poly-L-lactic acid (PLLA), poly-D-lactic acid (PDLA), and poly-DL-lactic acid (PDLLA), are commercially available for medical applications. PLA usually copolymerized with PEG to produce amphiphilic copolymer, which can self-assemble into micelles for encapsulating drugs in their hydrophobic cores. Based on in-source CID technique, Shi et al. [85] developed an analytical method for quantitation of PEG-PLA in plasma. The PLA-specific fragment ions were generated in source, consequentially further fragmented into specific product ions in Q2 (*m/z* 505.0 → 217.0). Due to their higher sensitivity, these PLA-specific product ions were selected for the quantitation of PEG-PLA. The PEG-specific fragment ions were MRM transition monitored for PEG-PLA. This approach was successfully applied to the pharmacokinetic study of mPEG2000-PDLLA2500-COOH in rats.

3.2.1.3. HA. HA is a linear polysaccharide made up of D-glucuronic acid and N-acetyl-D-glucosamine, which is abundant in different types of vertebrate tissues, including connective tissues and extracellular matrix (Fig. 6C) [86,87]. This polymer is very promising due to its hydrophilicity, biocompatible, biodegradable, non-toxic and non-immunogenic features. HA usually interacts with proteins strongly and exhibits a low ionization efficiency, which challenges the biological sample preparation and quantitative analysis by LC-MS/MS. Šimek et al. [88] developed an LC-MS/MS method for the detection of DOX and oleyl hyaluronan (HA-C18:1) in plasma and tissue homogenates. The sample preparation for HA-C18:1 involved two enzymatic work-up procedures by protease and hyaluronate lyase, respectively. Digestion by a protease can release HA from protein-binding in the biological samples. Shortening HA chain by hyaluronate lyase is to achieve a sufficient ionization efficiency. The developed method was applied to the pharmacokinetic studies of DOX and HA-C18:1 after i.v. administration of DOX loaded HA-C18:1 polymeric micelle. The different pharmacokinetic profiles of DOX and HA-C18:1 indicated a premature disruption of HA micelles in vivo.

3.2.1.4. Chitosan. Chitosan is a linear polysaccharide composed of β-1,4-linked D-glucosamine and N-acetyl-D-glucosamine. Chitosan is produced by deacetylation of chitin under alkaline or enzymatic conditions (Fig. 6D) [89,90]. High MW chitosan generally exhibits less solubility, lower degradation rate and higher toxicity than low MW chitosan [89,91]. Chitosan with an MW less than 3.9 kDa has a
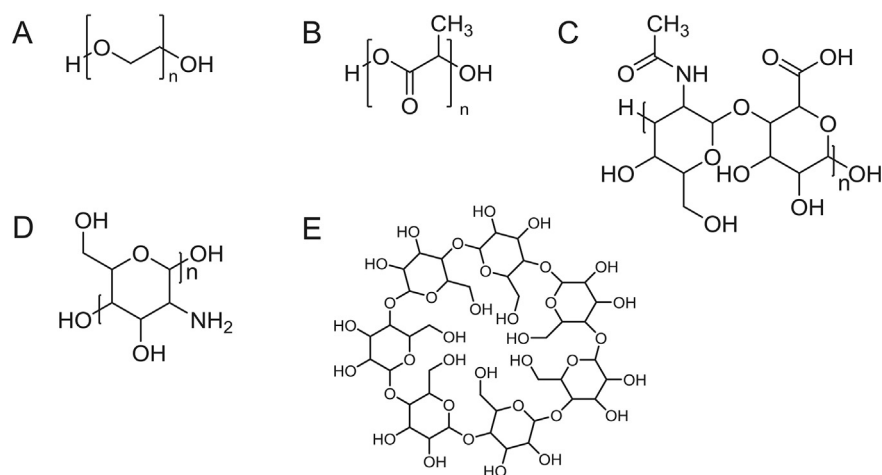
Fig. 6. Structures of (A) poly (ethylene glycol) (PEG), (B) poly(lactide) (PLA), (C) hyaluronan (HA), (D) Chitosan, and (E) β-cyclodextrin (β-CD).
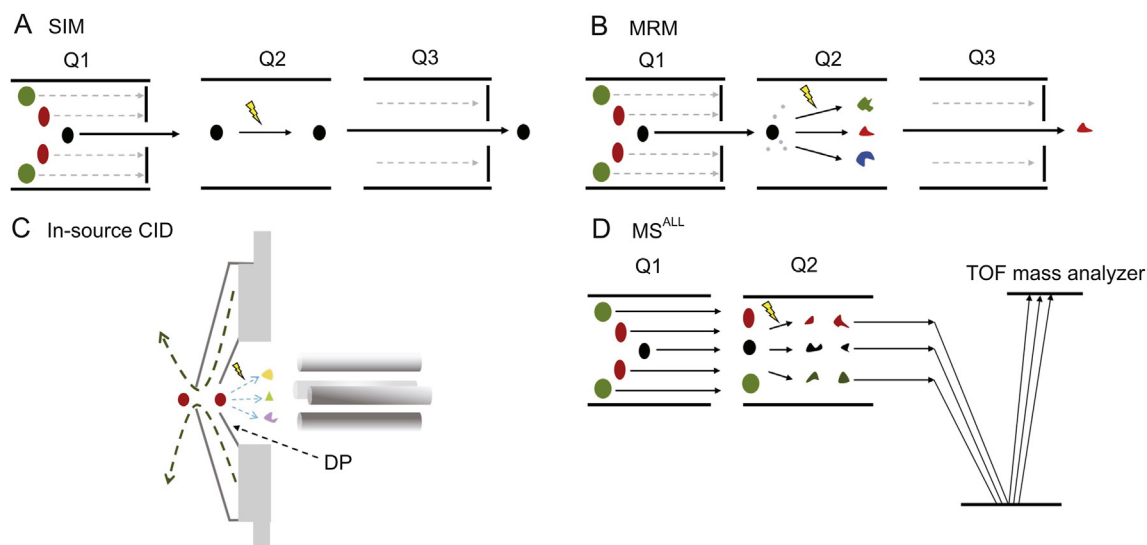
Fig. 7. Description of variety scan modes for quantitative analysis of polymers, including: (A) selected ion monitoring (SIM), (B) multiple reaction monitoring (MRM), (C) In-source collision induced dissociation (CID), and (D) MS^{ALL}.

common name called chitooligosaccharide (COS). Nowadays, the studies for investigating chitosan by LC-MS/MS are mainly focused on the characterizing of COS oligomers. Li et al. [92] reported an MRM method for the simultaneous determination of COS oligomers (D-glucosamine monomer to heptamer) in the chitosan samples. Since chitosan was susceptible to fragmentation in an ESI source, an in-source CID method (without fragment in Q2) was developed for detection of chitosan (139.7 ± 6.0 kDa), which showed excellent linearity (r > 0.99) with the LC concentration in a range of 20−10,000 ng/mL.

3.2.1.5. CD. CDs are cyclic oligosaccharides formed by six (αCD), seven (βCD) or eight (γCD) α-1,4-linked glucose units. The hydrophobic cone-like cavity of CD was found capable of loading drugs. Therefore, formed CD-drug complex is water-soluble and can improve the physicochemical properties of the loaded drug (Fig. 6E) [93]. The 2-hydroxypropyl-β-CD (HP-β-CD), a hydroxyalkyl derivative of βCD, is widely used as pharmaceutical excipient. HP-β-CD is a mixture of series of homologues and isomers with 2-hydroxypropyl groups randomly in position and amount

(2,097,151 possible homologues) [94]. Jiang et al. [95] developed a 2D-LC-IF-MS/MS method and an RP-UPLC-MS/MS method for the detection of HP-β-CD in human plasma and CSF. HP-β-CD prefers to form sodium adducts with poor fragmentation efficiency. In this study, ammonium salt was added into the mobile phase to suppress the formation of sodium adducts. In the UPLC-MS/MS method, the MRM transition at m/z 1326.5 → 383 was selected for the quantification of HP-β-CD. An LLOQ of 50 ng/mL and 5 μg/mL was achieved for HP-β-CD in human plasma and CSF, respectively. In the 2D-LC-MS/MS method, the detection is based on in-source CID and MRM with the LLOQ in human plasma and CSF of 10 ng/mL and 100 ng/mL, respectively. The HP-β-CD undergoes an in-source CID and generates 2-hydroxypropyl substituted dihydro-pyrylium fragment at m/z 203. With this ion as surrogate precursor ion, a fragmentation transition to the product ion of 4-hydroxypyrylium at m/z 97 was identified and monitored by MRM. The separation of HP-β-CD was first performed on a HILIC column. However, it was found that the glycerophosphocholine species in plasma suppressed the detection of HP-β-CD in plasma samples [96]. To overcome this matrix interference, the chromatography was

sequentially performed on a C_{18} guard column and a HILIC column for the 1D and 2D separation. The 2D-LC-MS/MS method was more sensitive, while the UPLC-MS/MS method with shorter runtime could improve the throughput. Both these methods were successfully applied to the pharmacokinetic study of HP-β-CD in humans.

3.2.2. ELISA

The development of antibodies that specifically bind to PEG-conjugates enables the application of ELISA method in PEGylated drugs detection. The binding affinity of the anti-PEG antibodies to free PEGs is much weaker than to PEG-conjugates [97]. Richter and Akerblom were the first scientists who proposed generating antibodies against PEG by immunizing rabbits. The prepared polyclonal antibodies provide an LLOQ of PEGylated drugs down to about 1 μg/mL [98]. To further improve the sensitivity, the mouse monoclonal antibodies were prepared later, which were capable of binding PEG-conjugates specifically without differentiating their conjugates [99–102]. The concentrations of PEG-conjugates in complex biological samples can be therefore determined via sandwich ELISA. With the help of anti-PEG sandwich ELISA, detection of PEG at a concentration as low as 1.2 ng/mL has been achieved.

Danika et al. [103] developed a sensitive LC-MS/MS method (LLOQ 0.125 μg/mL) for the determination of PCK3145 in mouse plasma. Although LC-MS/MS has been utilized for quantitative bioanalysis of peptides, this technique still faces significant challenges for analysis of PEGylated peptides, such as high polydispersity of PEG, high MW and poor ionization efficiency. They developed an indirect ELISA method for the detection of PEG-PCK3145 by PEGylated protein ELISA kit (Enzo Life Sciences). The concentration of PCK3145 was obtained from the quantification of PEG-PCK3145. Anti-PEG sandwich ELISA achieved a higher sensitivity (LLOQ 0.132 ng/mL) and widely applications for PEG-conjugates. The specificity of this technology remains to be confirmed. Moreover, ELISA method is not suitable for the analysis of free PEGs, which is a limitation for its application in monitoring the biological fate of PEG-based NDDSs.

3.3. Quantitation methods for the NPs

The NDDSs delivery-related activity and their uptake mechanism are still unclear, but an increased cell uptake of nanostructures has been verified by several in vitro and in vivo studies. The enhanced cell uptake may affect the biodistribution of payload drugs and therefore has gained great attention in the field of NDDSs. The MRI, radiolabeling, fluorescence spectroscopy and LA-ICP-MS are currently employed techniques for in vivo NPs quantitation (Table S1).

3.3.1. MRI

MRI, one of the most commonly used medical diagnostic techniques, possesses unique features including noninvasiveness, no exposure to ionizing radiation, high contrast in soft tissues and high spatial resolution [104]. MRI scanner utilizes pulses of radio waves for exciting hydrogen nuclear and records the emitted radio frequency during the relaxation processes from the excited hydrogen atoms. Since hydrogen atoms in form of water are abundant in human tissues and they are different in location, amount and bonding status, spatially localized spectra of the tissues in terms of the hydrogen nuclear density can be generated. According to the different relaxation properties between the hydrogen atoms in different body fluids and tissues, different contrasts will be generated. MRI often requires the use of contrast agents for better image

quality. Gd-based contrast agents are the only FDA approved contrast agents for MRI to be used on patients with all types of cancers [105].

The intrinsic/background signals will interfere drug distribution signals, so Gd MRI is not suitable for quantitative clinical measures of NPs. ^{19}F-MRI offers a quantifiable signal, but the sensitivity is far from ideal. Magnetic particle imaging (MPI) is a new non-invasive imaging modality. Employing superparamagnetic nanoparticles (SPNs) as contrast agents, MPI has been applied to monitor the biodistribution of NDDSs. MPI can provide a wide range of imaging depths, linearly quantifiable signals, high sensitivity, and real-time imaging. Zhu et al. [106] designed a superparamagnetic Fe_3O_4 nanocluster@poly (lactide-co-glycolide acid) core-shell nanocomposite loaded with DOX, which serves not only as a drug delivery system but also as an MPI quantification tracer. The nanocomposite can be degraded under a mild acidic microenvironment (pH = 6.5), which leads to a sustained release of DOX and gradual decomposition of the Fe_3O_4 nanocluster. The decomposition-induced MPI signal decay is proportional to the release rate of DOX over time ($R^2 = 0.99$). A quantitative monitoring procedure of the drug release process in cell culture has been successfully established.

3.3.2. Radiolabeling

Labeling nanoparticles with radionuclides allows tracing the nanoparticles in vivo and investigating their biodistribution, drug targeting and clearance quantitatively. Classical methods for radiolabeling NPs generally involve functionalizing the particle surface, core or coating with radio-tag [107]. A main concern of the classical radiolabeling methods is the introduction of a bulky lipophilic prosthetic tag or charged metal ion chelate-tag into the system, which may affect the pharmacokinetic and toxicity profiles of the original NPs [108]. Efforts have been made to explore alternative radiolabeling methods for NPs in order to avoid alerting their surface properties. The newly emerging labeling methods include radiochemical doping, physisorption, direct chemisorption, isotope exchange, cation exchange, particle beam or reactor activation and cavity encapsulation [109]. The in vivo biodistribution of radiolabeled NDDSs can be obtained by modern imaging techniques, such as positron emission tomography (PET). In Engudar et al.'s study, liposomes were remote loaded ^{124}I and evaluated by PET/CT imaging in vivo. A prolonged blood circulation half-life of 19.5 h was observed for the radiolabeled liposomes. Lower accumulation of radiolabeled liposomes in the spleen, liver, kidney and tumors was observed than usually long-circulating liposomes [110].

3.3.3. Fluorescence spectroscopy

Recently, semiconductor NPs, also known as quantum dots (QDs), have been extensively applied in fluorescence spectroscopy [111,112]. Fluorescence technology is an efficient approach to studying the biodistributions of nanostructures in cells and tissues. Compared with the conventional organic dyes, QDs have optical transitions in the near-infrared region, where the tissue absorption is minimal [113]. Kenesei et al. [114] applied spectral imaging fluorescence microscopy to monitor the distribution of fluorescent polystyrene nanoparticles modified with PEG or carboxylic acid groups in male and pregnant female mice. Spectral imaging combined with post hoc spectrum analysis allowed visualizing nanoparticles in various tissues and helped to overcome the limitations caused by the high autofluorescence of native tissues.

3.3.4. LA-ICP-MS

ICP-MS has been regarded as a sensitive analytical method for the determination of ultra-trace levels of metals and metalloids [115]. LA-ICP-MS is a derived technology of ICP-MS, which is equipped with a laser ablation system for vaporizing the sample [116]. By rastering a laser beam across the surface of a cryosectioning tissue sample, an LA-ICP-MS imaging is performed, which can provide a high spatial resolution of the absorbed metallic NPs in different tissues. Elci et al. [117] developed an LA-ICP-MS method to quantitatively image the biodistributions of PEGylated AuNPs. This imaging approach will provide important tissue/organ distribution data, which will greatly facilitate the design and study of nanomaterials for biomedical applications.

3.4. Metabolite profiling methods for NDDSs

The metabolism and elimination of the polymer material are very important features of NDDSs. The accumulation of the polymers or their metabolites in tissue or in organs such as liver, spleen or kidneys, is a potential source of iatrogenic illness. Polymers such as PLA and HA are biodegradable, which can be degraded into low MW monomers or oligomers and be relative rapidly eliminated from the body. For non-biodegradable polymers like PEG, the MW and shape have critical influences on the glomerular filtration and thereby affect the elimination routes and rate. Copolymer, consisting of biodegradable and non-biodegradable polymer blocks, is a compromise solution for polymer excipients to balance their performance and excretion. For example, PEG-PLA block copolymer consists of low MW PEG and PLA polymers alternate in sequence, which can be degraded in vivo to non-biodegradable PEG-segments below the renal excretion cut-off [118]. Therefore, monitoring the synthetic polymers according to ADME concept is of great significance for early detection of progressive accumulation and for prevention of iatrogenic illnesses.

Determining the excretion routes and identifying metabolites are two important features of the polymer mass balance study. Hereby, the eliminated polymers in urine, bile or feces should be analyzed regarding their MW and quantity. These bio-samples can be subjected to solid-phase or liquid extraction techniques for recovering and enriching of polymer components. Subsequently, SEC or LC-MS techniques are generally used to analyze the MW distribution of the eliminated polymers (Table S1). The aforementioned fluorescence and radiometric techniques are also applicable for the quantitation of polymers in excreta samples. Since both the fluorescence- and radio-labeling techniques are surrogate analysis methods, they are generally used in conjugation with SEC for the quantitation of polymers. With the help of radio labeling, the degradation of poloxamer 188 [119], and HA [120] were investigated. Meanwhile, the degradation of chitosan [121] and PVA [122] were studied by means of fluorescence. Polymers usually do not have strong chromophores for UV detection. Refractive index (RI) is an alternative detection for the quantitation of polymers at high concentration and of high purity. The quantitation of the degraded PLGA [123], PLA [124], chitosan [121,125] and HA [126] were performed by SEC or HPLC in combination with RI.

4. Conclusion and perspectives

The ideal NDDSs should provide APIs with the properties of sustained release, prolonged circulation time, improved stability, solubility and targeting. Annually, a great deal of pharmacokinetic information about drug-loaded NDDSs has been reported.

However, the approved nanotechnology-based products are limited. The low drug pass-through rate may partially attribute to the inadequate understanding of their pharmacokinetic properties. The present review discusses the recent advances in the bioanalysis of NDDSs, including technological progress in the analysis of the released and encapsulated drug respectively. Besides identifying their pharmacokinetics activities, the bioanalysis of the polymer material of NDDSs is also discussed. Among the enumerated analytical methods, LC-MS/MS is the most comprehensive approach for either profiling the pharmacokinetic behavior of NDDSs in clinical trial or for polymer quantitation in vivo.

Because of the huge gap between the released (in-)active ingredients and NPs in their pharmacokinetics, a comprehensive understanding of the in vivo fate of NDDSs is necessary to ensure their safe clinical applications. There has been a continued demand for developing efficient bioanalytical methods toward this goal. We hope this review will contribute to critical implications in the evaluation of NDDSs in vivo.

Conflicts of interest

The authors declare that there are no conflicts of interest.

Acknowledgments

Appendix A. Supplementary data

Supplementary data to this article can be found online at https://doi.org/10.1016/j.jpha.2020.05.002.

References

[1] B. Halamoda-Kenzaoui, U. Holzwarth, G. Roebben, et al., Mapping of the available standards against the regulatory needs for nanomedicines, Wiley Interdiscip. Rev.-Nanomed. Nanobiotechnol. 11 (2019) e1531.

[2] S. Talebian, J. Foroughi, S.J. Wade, et al., Biopolymers for antitumor implantable drug delivery systems: recent advances and future outlook, Adv. Mater. 30 (2018), e1706665.

[3] H. Cabral, K. Miyata, K. Osada, et al., Block copolymer micelles in nanomedicine applications, Chem. Rev. 118 (2018) 6844–6892.

[4] Y. Barenholz, Doxil®–the first FDA-approved nano-drug: lessons learned, J. Contr. Release 160 (2012) 117–134.

[5] X. Chen, S.S. Gambhir, J. Cheon, Theranost. Nanomed., Acc. Chem. Res. 44 (2011) 841.

[6] K. Siddiqui, A. Waris, H. Akber, et al., Physicochemical modifications and nano particulate strategies for improved bioavailability of poorly water soluble drugs, Pharm. Nanotechnol. 5 (2017) 276–284.

[7] P.N. Navya, A. Kaphle, S.P. Srinivas, et al., Current trends and challenges in cancer management and therapy using designer nanomaterials, Nano. Converg. 6 (2019) 23.

[8] Y. Malam, M. Loizidou, A.M. Seifalian, Liposomes and nanoparticles: nanosized vehicles for drug delivery in cancer, Trends Pharmacol. Sci. 30 (2009) 592–599.

[9] D. Chen, S. Lian, J. Sun, et al., Design of novel multifunctional targeting nano-carrier drug delivery system based on CD44 receptor and tumor microenvironment pH condition, Drug Deliv. 23 (2016) 808–813.

[10] A. Dickherber, S.A. Morris, P. Grodzinski, NCI investment in nanotechnology: achievements and challenges for the future, Wiley Interdiscip. Rev.-Nanomed. Nanobiotechnol. 7 (2015) 251–265.

[11] M.A.W. Eaton, L. Levy, O.M.A. Fontaine, Delivering nanomedicines to patients: a practical guide, Nanomed. Nanotechnol. Biol. Med. 11 (2015) 983–992.

[12] J.K. Patra, G. Das, L.F. Fraceto, et al., Nano based drug delivery systems: recent developments and future prospects, J. Nanobiotechnol. 16 (2018) 71.

[13] D.L. Stirland, J.W. Nichols, S. Miura, et al., Mind the gap: a survey of how cancer drug carriers are susceptible to the gap between research and practice, J. Contr. Release 172 (2013) 1045—1064.

[14] L. Yan, F. Zhao, J. Wang, et al., A safe-by-design strategy towards safer nanomaterials in nanomedicines, Adv. Mater. 31 (2019), e1805391.

[15] L. Sercombe, T. Veerati, F. Moheimani, et al., Advances and challenges of liposome assisted drug delivery, Front. Pharmacol. 6 (2015) 286.

[16] T.X. Nguyen, L. Huang, M. Gauthier, et al., Recent advances in liposome surface modification for oral drug delivery, Nanomedicine 11 (2016) 1169—1185.

[17] Y. Malam, M. Loizidou, A.M. Seifalian, Liposomes and nanoparticles: nano-sized vehicles for drug delivery in cancer, Trends Pharmacol. Sci. 30 (2009) 592—599.

[18] A. Samad, Y. Sultana, M. Aqil, Liposomal drug delivery systems: an update review, Curr. Drug Deliv. 4 (2007) 297—305.

[19] M.L. Immordino, F. Dosio, L. Cattel, Stealth liposomes: review of the basic science, rationale, and clinical applications, existing and potential, Int. J. Nanomed. 1 (2006) 297—315.

[20] B. He, H.Y. Hu, T. Tan, et al., IR-780-loaded polymeric micelles enhance the efficacy of photothermal therapy in treating breast cancer lymphatic metastasis in mice, Acta Pharmacol. Sin. 39 (2018) 132—139.

[21] J.L. Markman, A. Rekechenetskiy, E. Holler, et al., Nanomedicine therapeutic approaches to overcome cancer drug resistance, Adv. Drug Deliv. Rev. 65 (2013) 1866—1879.

[22] T.D. Langridge, R.A. Gemeinhart, Toward understanding polymer micelle stability: density ultracentrifugation offers insight into polymer micelle stability in human fluids, J. Contr. Release 319 (2020) 157—167.

[23] E. Bernabeu, M. Cagel, E. Lagomarsino, et al., Paclitaxel: what has been done and the challenges remain ahead, Int. J. Pharm. 526 (2017) 474—495.

[24] X. Zhang, X. Li, H. Hua, et al., Cyclic hexapeptide-conjugated nanoparticles enhance curcumin delivery to glioma tumor cells and tissue, Int. J. Nanomed. 12 (2017) 5717—5732.

[25] P. Szabo, R. Zelko, Formulation and stability aspects of nanosized solid drug delivery systems, Curr. Pharmaceut. Des. 21 (2015) 3148—3157.

[26] X. Yan, L. Xu, C. Bi, et al., Lactoferrin-modified rotigotine nanoparticles for enhanced nose-to-brain delivery: LESA-MS/MS-based drug biodistribution, pharmacodynamics, and neuroprotective effects, Int. J. Nanomed. 13 (2018) 273—281.

[27] N. Erdoğar, S. Akkın, E. Bilensoy, Nanocapsules for drug delivery: an updated review of the last decade, Recent Pat. Drug Deliv, Formulary 12 (2018) 252—266.

[28] W.H. De Jong, P.J.A. Borm, Drug delivery and nanoparticles: applications and hazards, Int. J. Nanomed. 3 (2008) 133—149.

[29] Z. Liu, Y. Jiao, Y. Wang, et al., Polysaccharides-based nanoparticles as drug delivery systems, Adv. Drug Deliv. Rev. 60 (2008) 1650—1662.

[30] C. Bi, A. Wang, Y. Chu, et al., Intranasal delivery of rotigotine to the brain with lactoferrin-modified PEG-PLGA nanoparticles for Parkinson's disease treatment, Int. J. Nanomed. 11 (2016) 6547—6559.

[31] Y. Jiang, F. Wang, H. Xu, et al., Development of andrographolide loaded PLGA microspheres: optimization, characterization and in vitro-in vivo correlation, Int. J. Pharm. 475 (2014) 475—484.

[32] S.M. Hoy, Patisiran: first global approval, Drugs 78 (2018) 1625—1631.

[33] M. Pandey, H. Choudhury, O.C. Yeun, et al., Perspectives of nanoemulsion strategies in the improvement of oral, parenteral and transdermal chemo-therapy, Curr. Pharmaceut. Biotechnol. 19 (2018) 276—292.

[34] G.W. Jerkins, G.R. Pattar, S.R. Kannarr, A review of topical cyclosporine a formulations-a disease-modifying agent for keratoconjunctivitis sicca, Clin. Ophthalmol. 14 (2020) 481—489.

[35] Y. Yin, B. Hu, X. Yuan, et al., Nanogel: a versatile nano-delivery system for biomedical applications, Pharmaceutics 12 (2020) 290.

[36] D. Chen, H. Yu, K. Sun, et al., Dual thermoresponsive and pH-responsive self-assembled micellar nanogel for anticancer drug delivery, Drug Deliv. 21 (2014) 258—264.

[37] B. Ashrafi, M. Rashidipour, A. Marzban, et al., Mentha piperita essential oils loaded in a chitosan nanogel with inhibitory effect on biofilm formation against S. mutans on the dental surface, Carbohydr. Polym. 212 (2019) 142—149.

[38] Y. Mao, X. Chen, B. Xu, et al., Eprinomectin nanoemulgel for transdermal delivery against endoparasites and ectoparasites: preparation, in vitro and in vivo evaluation, Drug Deliv. 26 (2019) 1104—1114.

[39] S. Bayda, M. Hadla, S. Palazzolo, et al., Inorganic nanoparticles for cancer therapy: a transition from lab to clinic, Curr. Med. Chem. 25 (2018) 4269—4303.

[40] T.A. Esquivel-Castro, M.C. Ibarra-Alonso, J. Oliva, et al., Porous aerogel and core/shell nanoparticles for controlled drug delivery: a review, Mater. Sci. Eng. C Mater. Biol. Appl. 96 (2019) 915—940.

[41] M. Auerbach, G.M. Chertow, M. Rosner, Ferumoxytol for the treatment of iron deficiency anemia, Expet Rev. Hematol. 11 (2018) 829—834.

[42] E.A. Smits, J.A. Soetekouw, I. van Doormalen, et al., Quantitative LC-MS determination of liposomal encapsulated prednisolone phosphate and non-encapsulated prednisolone concentrations in murine whole blood and liver tissue, J. Pharmaceut. Biomed. Anal. 115 (2015) 552—561.

[43] C.L. Braal, P. de Bruijn, F. Atrafi, et al., A new method for the determination of total and released docetaxel from docetaxel-entrapped core-crosslinked polymeric micelles (CriPec(R)) by LC-MS/MS and its clinical application in plasma and tissues in patients with various tumours, J. Pharmaceut. Biomed. Anal. 161 (2018) 168—174.

[44] N.M. Deshpande, M.G. Gangrade, M.B. Kekare, et al., Determination of free and liposomal amphotericin B in human plasma by liquid chromatography-mass spectroscopy with solid phase extraction and protein precipitation techniques, J. Chromatogr. B Analyt. Technol. Biomed. Life Sci. 878 (2010) 315—326.

[45] C. Su, H. Yang, H. Sun, et al., Bioanalysis of free and liposomal amphotericin B in rat plasma using solid phase extraction and protein precipitation followed by LC-MS/MS, J. Pharmaceut. Biomed. Anal. 158 (2018) 288—293.

[46] Y. Xie, N. Shao, Y. Jin, et al., Determination of non-liposomal and liposomal doxorubicin in plasma by LC-MS/MS coupled with an effective solid phase extraction: in comparison with ultrafiltration technique and application to a pharmacokinetic study, J. Chromatogr. B Analyt. Technol. Biomed. Life Sci. 1072 (2018) 149—160.

[47] H. Wang, M. Zheng, J. Gao, et al., Uptake and release profiles of PEGylated liposomal doxorubicin nanoparticles: a comprehensive picture based on separate determination of encapsulated and total drug concentrations in tissues of tumor-bearing mice, Talanta 208 (2020) 120358.

[48] W. Song, J.A. Tweed, R. Visswanathan, et al., Bioanalysis of targeted nano-particles in monkey plasma via LC-MS/MS, Anal. Chem. 91 (2019) 13874—13882.

[49] Y. Chen, L. Wang, D. Guo, et al., A rapid and efficient technique for liposomal and nonliposomal drug pharmacokinetics studies using magnetic nanop-robes and its application to leakage kinetics of liposomes, J. Chromatogr. A 1580 (2018) 2—11.

[50] T. Chen, B. He, J. Tao, et al., Application of forster resonance energy transfer (FRET) technique to elucidate intracellular and in vivo biofate of nano-medicines, Adv. Drug Deliv. Rev. 143 (2019) 177—205.

[51] J.F. Lovell, J. Chen, M.T. Jarvi, et al., FRET quenching of photosensitizer singlet oxygen generation, J. Phys. Chem. B 113 (2009) 3203—3211.

[52] M. Miteva, K.C. Kirkbride, K.V. Kilchrist, et al., Tuning PEGylation of mixed micelles to overcome intracellular and systemic siRNA delivery barriers, Biomaterials 38 (2015) 97—107.

[53] R. Bouchaala, L. Mercier, B. Andreiuk, et al., Integrity of lipid nanocarriers in bloodstream and tumor quantified by near-infrared ratiometric FRET imag-ing in living mice, J. Contr. Release 236 (2016) 57—67.

[54] X. Sun, G. Wang, H. Zhang, et al., The blood clearance kinetics and pathway of polymeric micelles in cancer drug delivery, ACS Nano 12 (2018) 6179—6192.

[55] M.S.T. Gonçalves, Fluorescent labeling of biomolecules with organic probes, Chem. Rev. 109 (2009) 190—212.

[56] H. He, J. Zhang, Y. Xie, et al., Bioimaging of intravenous polymeric micelles based on discrimination of integral particles using an environment-responsive probe, Mol. Pharm. 13 (2016) 4013—4019.

[57] W. Zhuang, B. Ma, J. Hu, et al., Two-photon AIE luminogen labeled multi-functional polymeric micelles for theranostics, Theranostics 9 (2019) 6618—6630.

[58] H. Kaur, S.R. Bhagwat, T.K. Sharma, et al., Analytical techniques for charac-terization of biological molecules - proteins and aptamers/oligonucleotides, Bioanalysis 11 (2019) 103—117.

[59] B. Wang, Y. Guo, X. Chen, et al., Nanoparticle-modified chitosan-agarose-gelatin scaffold for sustained release of SDF-1 and BMP-2, Int. J. Nanomed. 13 (2018) 7395—7408.

[60] O. Azie, Z.F. Greenberg, C.D. Batich, et al., Carbodiimide conjugation of latent transforming growth factor β1 to superparamagnetic iron oxide nano-particles for remote activation, Int. J. Mol. Sci. 20 (2019).

[61] R. Ali, A. Farah, Z. Binkhathlan, Development and characterization of methoxy poly(ethylene oxide)-block-poly(ε-caprolactone) (PEO-b-PCL) mi-celles as vehicles for the solubilization and delivery of tacrolimus, Saudi Pharmaceut. J. 25 (2017) 258—265.

[62] A.M. Fletcher, P. Tellier, J. Douville, et al., Adverse vacuolation in multiple tissues in cynomolgus monkeys following repeat-dose administration of a PEGylated protein, Toxicol. Lett. 317 (2019) 120—129.

[63] A.M. Fletcher, P. Tellier, J. Douville, et al., Adverse vacuolation in multiple tissues in cynomolgus monkeys following repeat-dose administration of a PEGylated protein, Toxicol. Lett. 317 (2019) 120—129.

[64] K. Yoncheva, E. Lizarraga, J.M. Irache, PEGylated nanoparticles based on poly(methyl vinyl ether-co-maleic anhydride): preparation and evaluation of their bioadhesive properties, Eur. J. Pharmaceut. Sci. 24 (2005) 411—419.

[65] T.W. Chung, C.H. Chung, Y.F. Lue, A colorimetric method for determining distearoylphosphatidylethanolamine- polyethylene glycol 2000 in blood suspension, Anal. Biochem. 285 (2000) 264—267.

[66] F.M. Veronese, O. Schiavon, G. Pasut, et al., PEG-doxorubicin conjugates: influence of polymer structure on drug release, in vitro cytotoxicity, bio-distribution, and antitumor activity, Bioconjugate Chem. 16 (2005) 775—784.

[67] S. Loret, G. Nollevaux, R. Remacle, et al., Analysis of PEG 400 and 4000 in urine for gut permeability assessment using solid phase extraction and gel permeation chromatography with refractometric detection, J. Chromatogr. B Analyt. Technol. Biomed. Life Sci. 805 (2004) 195—202.

[68] G.O. Young, D. Ruttenberg, J.P. Wright, Measurement of polyethylene glycol 400 in urine by direct-injection high-performance liquid chromatography, Clin. Chem. 36 (1990) 1800–1802.

[69] C.M. Ryan, M.L. Yarmush, R.G. Tompkins, Separation and quantitation of polyethylene glycols 400 and 3350 from human urine by high-performance liquid chromatography, J. Pharmacol. Sci. 81 (1992) 350–352.

[70] H.A. Schwertner, W.R. Patterson, J.H. Cissik, et al., New extraction procedure and high-performance liquid chromatographic method for analyzing polyethylene glycol-400 in urine, J. Chromatogr. 578 (1992) 297–301.

[71] I.M. Kinahan, M.R. Smyth, High-performance liquid chromatographic determination of PEG 600 in human urine, J. Chromatogr. 565 (1991) 297–307.

[72] A. Kolate, D. Baradia, S. Patil, et al., PEG — a versatile conjugating ligand for drugs and drug delivery systems, J. Contr. Release 192 (2014) 67–81.

[73] K. Knop, R. Hoogenboom, D. Fischer, et al., Poly(ethylene glycol) in drug delivery: pros and cons as well as potential alternatives, Angew Chem. Int. Ed. Engl. l49 (2010) 6288–6308.

[74] J. Zhang, J. Lin, T.A. Anderson, A flow injection analysis/mass spectrometry method for the quantification of polyethylene glycol 300 in drug formulations, Int. J. Pharm. 282 (2004) 183–187.

[75] J.B. Bouska, S.F. Phillips, Simple method for gas–liquid chromatographic analysis of polyethylene glycol 400 in biological fluids, J. Chromatogr. 183 (1980) 72–77.

[76] D.A. Ashiru, K. Karu, M. Zloh, et al., Relative quantification of polyethylene glycol 400 excreted in the urine of male and female volunteers by direct injection electrospray-selected ion monitoring mass spectrometry, Int. J. Pharm. 414 (2011) 35–41.

[77] V. Vijaya Bhaskar, A. Middha, S. Tiwari, et al., Liquid chromatography/tandem mass spectrometry method for quantitative estimation of polyethylene glycol 400 and its applications, J. Chromatogr. B Analyt. Technol. Biomed. Life Sci. 926 (2013) 68–76.

[78] B.M. Warrack, B.P. Redding, G. Chen, et al., Determination of the molecular weight of poly(ethylene glycol) in biological samples by reversed-phase LC–MS with in-source fragmentation, Anal. Bioanal. Chem. 405 (2013) 4283–4287.

[79] X. Zhou, X. Meng, L. Cheng, et al., Development and application of an MS[ALL]-based approach for the quantitative analysis of linear polyethylene glycols in rat plasma by liquid chromatography triple-quadrupole/time-of-flight mass spectrometry, Anal. Chem. 89 (2017) 5193–5200.

[80] L. Yin, C. Su, T. Ren, et al., MS[All] strategy for comprehensive quantitative analysis of PEGylated-doxorubicin, PEG and doxorubicin by LC-high resolution q-q-TOF mass spectrometry coupled with all window acquisition of all fragment ion spectra, Analyst 142 (2017) 4279–4288.

[81] H. Sun, Q. Zhang, Z. Zhang, et al., Simultaneous quantitative analysis of polyethylene glycol (PEG), PEGylated paclitaxel and paclitaxel in rats by MS/MS[ALL] technique with hybrid quadrupole time-of-flight mass spectrometry, J. Pharmaceut. Biomed. Anal. 145 (2017) 255–261.

[82] L. Yin, T. Ren, S. Zhao, et al., Comparative pharmacokinetic study of PEGylated gemcitabine and gemcitabine in rats by LC-MS/MS coupled with precolumn derivatization and MS[ALL] technique, Talanta 206 (2020) 120184.

[83] M. Alizadeh-Osgouei, Y. Li, C. Wen, A comprehensive review of biodegradable synthetic polymer-ceramic composites and their manufacture for biomedical applications, Bioact. Mater. 4 (2019) 22–36.

[84] Y. Shi, W. Huang, R. Liang, et al., Improvement of in vivo efficacy of recombinant human erythropoietin by encapsulation in PEG-PLA micelle, Int. J. Nanomed. 8 (2013) 1–11.

[85] M. Shi, H. Jiang, L. Yin, et al., Development of an UPLC-MS/MS method coupled with in-source CID for quantitative analysis of PEG-PLA copolymer and its application to a pharmacokinetic study in rats, J. Chromatogr. B Analyt. Technol. Biomed. Life Sci. 1125 (2019) 121716.

[86] F. Abbruzzese, F. Basoli, M. Costantini, et al., Hyaluronan: an overview, Univ. Mich. Med. Cent. J. 31 (2017) 9–22.

[87] M.K. Cowman, T.A. Schmidt, P. Raghavan, et al., Viscoelastic Properties of Hyaluronan in Physiological Conditions, vol. 4, 2015, p. 622. F1000Res.

[88] M. Šimek, M. Hermannova, D. Smejkalova, et al., LC-MS/MS study of in vivo fate of hyaluronan polymeric micelles carrying doxorubicin, Carbohydr. Polym. 209 (2019) 181–189.

[89] U. Garg, S. Chauhan, U. Nagaich, et al., Current advances in chitosan nanoparticles based drug delivery and targeting, Adv. Pharmaceut. Bull. 9 (2019) 195–204.

[90] Q. Meng, A. Wang, H. Hua, et al., Intranasal delivery of Huperzine A to the brain using lactoferrin-conjugated N-trimethylated chitosan surface-modified PLGA nanoparticles for treatment of Alzheimer's disease, Int. J. Nanomed. 13 (2018) 705–718.

[91] K. Nagpal, S.K. Singh, D.N. Mishra, Chitosan nanoparticles: a promising system in novel drug delivery, Chem. Pharm. Bull. 58 (2010) 1423–1430.

[92] J. Li, L. Chen, Z. Meng, et al., Development of a mass spectrometry method for the characterization of a series of chitosan, Int. J. Biol. Macromol. 121 (2019) 89–96.

[93] T. Loftsson, P. Saokham, A.R. Sa Couto, Self-association of cyclodextrins and cyclodextrin complexes in aqueous solutions, Int. J. Pharm. 560 (2019) 228–234.

[94] L. Szente, J. Szejtli, Highly soluble cyclodextrin derivatives: chemistry, properties, and trends in development, Adv. Drug Deliv. Rev. 36 (1999) 17–28.

[95] H. Jiang, R. Sidhu, H. Fujiwara, et al., Development and validation of sensitive LC-MS/MS assays for quantification of HP-beta-CD in human plasma and CSF, J. Lipid Res. 55 (2014) 1537–1548.

[96] J.L. Little, M.F. Wempe, C.M. Buchanan, Liquid chromatography-mass spectrometry/mass spectrometry method development for drug metabolism studies: examining lipid matrix ionization effects in plasma, J. Chromatogr. B Analyt. Technol. Biomed. Life Sci. 833 (2006) 219–230.

[97] K. Shiraishi, M. Yokoyama, Toxicity and immunogenicity concerns related to PEGylated-micelle carrier systems: a review, Sci. Technol. Adv. Mater. 20 (2019) 324–336.

[98] A.W. Richter, E. Akerblom, Antibodies against polyethylene glycol produced in animals by immunization with monomethoxy polyethylene glycol modified proteins, Int. Arch. Allergy Appl. Immunol. 70 (1983) 124–131.

[99] N.M. Tsai, T.L. Cheng, S.R. Roffler, Sensitive measurement of polyethylene glycol-modified proteins, Biotechniques 30 (2001) 396–402.

[100] T.L. Cheng, C.M. Cheng, B.M. Chen, et al., Monoclonal antibody-based quantitation of poly(ethylene glycol)-derivatized proteins, liposomes, and nanoparticles, Bioconjugate Chem. 16 (2005) 1225–1231.

[101] Y.C. Su, B.M. Chen, K.H. Chuang, et al., Sensitive quantification of PEGylated compounds by second-generation anti-poly(ethylene glycol) monoclonal antibodies, Bioconjugate Chem. 21 (2010) 1264–1270.

[102] D.A. Wunderlich, M. Macdougall, D.V. Mierz, et al., Generation and characterization of a monoclonal IgG antibody to polyethylene glycol, Hybridoma 26 (2007) 168–172.

[103] C. Danika, M.A. El Mubarak, I. Leontari, et al., Development and validation of analytical methodologies for the quantification of PCK3145 and PEG-PCK3145 in mice, Anal. Biochem. 564–565 (2019) 72–79.

[104] H. Cai, X. Dai, X. Wang, et al., A nanostrategy for efficient imaging-guided antitumor therapy through a stimuli-responsive branched polymeric prodrug, Adv. Sci. 7 (2020) 1903243.

[105] M.S. Usman, M.Z. Hussein, S. Fakurazi, et al., Gadolinium-based layered double hydroxide and graphene oxide nano-carriers for magnetic resonance imaging and drug delivery, Chem. Cent. J. 11 (2017) 47.

[106] X. Zhu, J. Li, P. Peng, et al., Quantitative drug release monitoring in tumors of living subjects by magnetic particle imaging nanocomposite, Nano Lett. 19 (2019) 6725–6733.

[107] P. Datta, S. Ray, Nanoparticulate formulations of radiopharmaceuticals: strategy to improve targeting and biodistribution properties, J. Label. Compd. Radiopharm. (2020), https://doi.org/10.1002/jlcr.3839.

[108] C. Su, C. Liu, Y. He, et al., Analytical methods for investigating in vivo fate of nanoliposomes: a review, J. Pharm. Anal. 8 (2018) 219–225.

[109] J. Lamb, J.P. Holland, Advanced methods for radiolabeling multimodality nanomedicines for SPECT/MRI and PET/MRI, J. Nucl. Med. 59 (2018) 382–389.

[110] G. Engudar, H. Schaarup-Jensen, F.P. Fliedner, et al., Remote loading of liposomes with a [124]I-radioiodinated compound and their in vivo evaluation by PET/CT in a murine tumor model, Theranostics 8 (2018) 5828–5841.

[111] O. Tagit, N. Hildebrandt, Fluorescence sensing of circulating diagnostic biomarkers using molecular probes and nanoparticles, ACS Sens. 2 (2017) 31–45.

[112] H. Liu, Y. Zhang, C. Huang, Development of nitrogen and sulfur-doped carbon dots for cellular imaging, J. Pharm. Anal. 9 (2019) 127–132.

[113] C. Li, P. Wu, Cu-doped quantum dots: a new class of near-infrared emitting fluorophores for bioanalysis and bioimaging, Luminescence 34 (2019) 782–789.

[114] K. Kenesei, K. Murali, Á. Czéh, et al., Enhanced detection with spectral imaging fluorescence microscopy reveals tissue- and cell-type-specific compartmentalization of surface-modified polystyrene nanoparticles, J. Nanobiotechnol. 14 (2016) 55.

[115] T. Cavey, M. Ropert, O. Loréal, et al., Metals: common clinical applications in inductively coupled plasma mass spectrometry, Ann. Biol. Clin. (Paris) 77 (2019) 495–504.

[116] R. Weiskirchen, S. Weiskirchen, P. Kim, et al., Software solutions for evaluation and visualization of laser ablation inductively coupled plasma mass spectrometry imaging (LA-ICP-MSI) data: a short overview, J. Cheminf. 11 (2019) 16.

[117] S.G. Elci, B. Yan, S.T. Kim, et al., Quantitative imaging of 2 nm monolayer-protected gold nanoparticle distributions in tissues using laser ablation inductively-coupled plasma mass spectrometry (LA-ICP-MS), Analyst 141 (2016) 2418–2425.

[118] E. Markovsky, H. Baabur-Cohen, A. Eldar-Boock, et al., Administration, distribution, metabolism and elimination of polymer therapeutics, J. Contr. Release 161 (2012) 446–460.

[119] J.M. Grindel, T. Jaworski, O. Piraner, et al., Distribution, metabolism, and excretion of a novel surface-active agent, purified poloxamer 188, in rats, dogs, and humans, J. Pharmacol. Sci. 91 (2002) 1936–1947.

[120] M. Laznicek, A. Laznickova, D. Cozikova, et al., Preclinical pharmacokinetics of radiolabelled hyaluronan, Pharmacol. Rep. 64 (2012) 428–437.

[121] W. Dong, B. Han, Y. Feng, et al., Pharmacokinetics and biodegradation mechanisms of a versatile carboxymethyl derivative of chitosan in rats:

in vivo and in vitro evaluation, Biomacromolecules 11 (2010) 1527–1533.

[122] Y. Kaneo, S. Hashihama, A. Kakinoki, et al., Pharmacokinetics and bio-disposition of poly(vinyl alcohol) in rats and mice, Drug Metabol. Pharma-cokinet. 20 (2005) 435–442.

[123] A.K. Mohammad, J.J. Reineke, Quantitative detection of PLGA nanoparticle degradation in tissues following intravenous administration, Mol. Pharm. 10 (2013) 2183–2189.

[124] T. Beslikas, I. Gigis, V. Goulios, et al., Crystallization study and comparative in vitro-in vivo hydrolysis of PLA reinforcement ligament, Int. J. Mol. Sci. 12 (2011) 6597–6618.

[125] W. Dong, B. Han, K. Shao, et al., Effects of molecular weights on the ab-sorption, distribution and urinary excretion of intraperitoneally adminis-trated carboxymethyl chitosan in rats, Journal of materials science, J. Mater. Sci. Mater. Med. 23 (2012) 2945–2952.

[126] M. Kimura, T. Maeshima, T. Kubota, et al., Absorption of orally administered hyaluronan, J. Med. Food 19 (2016) 1172–1179.

Original article

Ultra-sensitive bioanalysis of the therapeutic peptide exenatide for accurate pharmacokinetic analyses at effective plasma concentrations utilizing UPLC-MS/MS

Max Sauter, Philipp Uhl, Jürgen Burhenne[*], Walter E. Haefeli

Department of Clinical Pharmacology and Pharmacoepidemiology, Heidelberg University Hospital, Im Neuenheimer Feld 410, 69120, Heidelberg, Germany

ABSTRACT

Exenatide is the first approved glucagon-like peptide 1 receptor agonist subcutaneously or intramuscularly injected for the treatment of type 2 diabetes mellitus. Typical therapeutic plasma concentrations are in the low pg/mL range, therefore requiring ultra-sensitive quantification. To enable the accurate evaluation of pharmacokinetic studies, we established a UPLC-MS/MS assay with a lower limit of quantification (LLOQ) of 5 pg/mL (1.2 pM) using 200 μL of plasma, validated according to FDA's and EMA's pertinent guidelines. Exenatide was isolated from plasma with solid phase extraction utilizing anion-exchange sorbent. Quantification was performed with positive electrospray ionization tandem mass spectrometry in the selected reaction monitoring mode. The calibrated concentration range of 5 −10,000 pg/mL was linear showing correlation coefficients >0.99. Interday and intraday accuracy ranged from 97.5% to 105.4% with corresponding precision of <10.9%. Accuracy at the LLOQ ranged from 93.0% to 102.5% with corresponding precision of <15.9%. Because of the validity of a 10-fold dilution QC (accuracy 111.2%), the assay is suitable for exenatide quantification up to 100,000 pg/mL. The ultra-sensitive assay's applicability was demonstrated by the quantification of exenatide plasma concentrations and pharmacokinetics after intravenous and nasal administration to beagle dogs.

© 2020 Xi'an Jiaotong University. Production and hosting by Elsevier B.V. This is an open access article under the CC BY-NC-ND license (http://creativecommons.org/licenses/by-nc-nd/4.0/).

1. Introduction

Glucagon-like peptide 1 (GLP-1) receptor agonists are recommended early in the management of type 2 diabetes mellitus (T2DM) [1]. Exenatide (synthetic exendin-4), a 39-amino acid peptide with an amide C-terminus (sequence: H G E G T F T S D L S K Q M E E E A V R L F I E W L K N G G P S S G A P P P S; $C_{184}H_{282}N_{50}O_{60}S$, 4,186.6 g/mol), originates from the saliva of the Gila monster [2,3] and is the first approved GLP-1 receptor agonist. In patients with T2DM, glycemic control is improved by exenatide, which reduces fasting and postprandial glucose-concentrations through glucose-dependent insulinotropic and glucagonostatic effects and increase of β-cell mass, while further fostering weight loss via reduction of energy intake by inducing satiety and delaying gastric emptying [2,4–6].

Exenatide is available as immediate release subcutaneous injection for twice daily administration (Byetta®) [7] and as extended release weekly subcutaneous injection formulated in microspheres (Bydureon®) [8] which frequently cause injection site reactions [9–14]. Exenatide exerts efficacy in the low picomolar range showing a half maximal effective concentration (EC_{50}) on fasting plasma glucose of 56.8 pg/mL (~14 pM) [15], and typical peak (for the therapeutic 10 μg dose) and steady-state plasma concentrations around 200 to 300 pg/mL (~50 to 70 pM) [2,15–19]. With the latest approval of the first oral GLP-1 receptor agonist semaglutide (Rybelsus®) [20,21], investigations aiming at the development of alternative routes of exenatide administration to avoid the frequently associated injection site reactions are anticipated to receive increased attention.

Because of today's availability of sufficiently sensitive tandem mass spectrometers, quantification of peptides is increasingly performed by MS/MS methodologies due to their advantages of a wider dynamic range, often great accuracy, and especially superior specificity due to the lack of cross-reactivity in comparison to the traditionally performed immunoassays. However, the sensitive bioanalysis of large peptides using MS/MS is challenging because of their high molecular weight, multiple charge distribution, and

Peer review under responsibility of Xi'an Jiaotong University.

* Corresponding author.
  E-mail address: juergen.burhenne@med.uni-heidelberg.de (J. Burhenne).

typical lack of intense, specific fragments in collision-induced dissociation (CID) sourcing from the multitude of possible bond breakages.

Thus far, only few assays for the bioanalysis of exenatide have been published that rely on LC-MS methodologies and none is suitable for accurate pharmacokinetic analyses in the therapeutic range [22–24]. Such assays require lower limits of quantification (LLOQ) that are at least tenfold lower than observed peak plasma concentrations. The lowest reported LLOQ of LC-MS-based assays is 50 pg/mL (24 pM) for an LC-HRMS assay avoiding CID [23], while the lowest LLOQ for immunologic exenatide quantification is 10 pg/mL [5,18].

To enable reliable pharmacokinetic investigations of exenatide and allow formulation development for alternative routes of administration, we established an ultra-sensitive UPLC-MS/MS assay for plasma exenatide quantification with a remarkably low LLOQ of 5 pg/mL (1.2 pM). The assay was validated according to the pertinent recommendations of the US Food and Drug Administration (FDA) and European Medicines Agency (EMA) [25,26]. Its suitability for pharmacokinetic studies and formulation development was demonstrated by the quantification of plasma exenatide after nasal and intravenous administration to beagle dogs enabling the determination of exenatide's absolute nasal bioavailability (F).

2. Materials and methods

2.1. Beagle dog study and plasma sample generation

The study was carried out at Citoxlab France (Evreux, France) in accordance with national and European guidelines for the care and use of laboratory animals (European regulations 2010/63/EU and the French decret No. 2013-118 on the protection of animals used for scientific purposes). The project (#4786; animal facility D-2741001) has been approved by the French Ministry of Higher Education and Research (Ministère de l'Enseignement Supérieur et de la Recherche) under the ethical committee number C2EA-48. Four male beagle dogs received an intravenous bolus injection of 1 mL of a 0.1 mg/mL solution of exenatide (100 μg) in phosphate buffered saline followed after a wash-out of one week by one nasal spray puff of 100 μL of a 0.6 mg/mL exenatide solution (60 μg) in phosphate buffered saline. Blood samples were drawn into heparinized tubes (2 mL) before administration and 0.25, 0.5, 1, 2, 4, 6, 12, and 24 h after administration, immediately centrifuged at 2,500 ×g for 10 min while refrigerated to 4 °C, and the plasma was stored at -80 °C until analysis.

2.2. Drugs, chemicals, solvents, and materials

Exenatide acetate (92.6%) was obtained from Bachem AG (Bubendorf, Switzerland). Isotopically labeled internal standard (IS) [$^{13}C_6$,^{15}N]-Leu(10,21,26)-exenatide, which has all leucines in the sequence isotopically labeled (resulting mass difference 21 Da), was purchased from Peptide Specialty Laboratories GmbH (Heidelberg, Germany). Remaining reagents and solvents (water, methanol (MeOH), acetonitrile (ACN), and formic acid (FA)) were purchased from Biosolve (Valkenswaard, The Netherlands) in the highest available purity. Blank beagle plasma, supplied by Innovative Research (Novi, MI, USA), was obtained from Dunn Labortechnik GmbH (Asbach, Germany).

2.3. Standard solutions

For preparing calibration and QC stock solutions, exenatide was independently weighed into plastic (polypropylene) reaction tubes to circumvent adsorption observed for glass vessels, and

subsequently dissolved in 4 mL ACN/water (1/1, v/v) + 0.1% FA. Solutions were then diluted 100-fold with ACN/water (1/1, v/v) + 0.1% FA. Calibration spike-solutions were prepared from the diluted stock at concentrations of 40, 120, 480, 1,600, 6,400, 20,000, and 80,000 pg/mL in ACN/water (1/1, v/v) + 0.1% FA (corresponding to sample concentrations of 5, 15, 60, 200, 800, 2,500, and 10,000 pg/mL). QC spike solutions were prepared accordingly at 120, 4,800, 60,000, and 160,000 pg/mL (corresponding to sample concentrations of 15, 600, 7,500, and 20,000 pg/mL for QC A, B, C, and D, respectively). The IS spike solution was prepared at 25,000 pg/mL (corresponding to a sample concentration of 3,125 pg/mL). Solutions were kept at 4 °C and were stable for at least 2 months.

2.4. Plasma sample preparation

To 200 μL of plasma in 2 mL reaction tubes, 25 μL of IS spike solution and 25 μL of the respective calibration or QC spike solution was added for the preparation of calibration and QC samples. Study plasma samples (200 μL) were spiked with 25 μL of IS and 25 μL of ACN/water (1/1, v/v) + 0.1% FA for volume compensation. To enable the determination of plasma concentrations above the calibrated range, which are anticipated to occur early after intravenous injection, a dilution QC was validated. Dilution QC D samples were generated by preparing QC D samples without addition of IS by addition of 25 μL of QC D spike solution to 175 μL of plasma and the subsequent dilution of 20 μL of these samples with 180 μL of blank plasma, which were then spiked similar to study samples. For extraction, samples were treated with 75 μL of 25% aqueous ammonia, transferred to wells of an Oasis® MAX μElution Plate (anion exchange; Waters, Milford, MA, USA), and loaded onto the sorbent by applying positive pressure (positive pressure unit; Waters, Milford, MA, USA). Wells were washed with 100 μL of ACN/water (1/1, v/v) containing 5% ammonia followed by 100 μL of ACN/water (1/4, v/v) + 0.05% FA. Subsequently, exenatide was eluted from the solid phase into wells of a 96-well collection plate (800 μL; Waters, Milford, MA, USA) with two times 30 μL of ACN/water/MeOH (2/1/1, v/v/v) containing 5% FA. To the wells of the collection plate, 40 μL of water was added, the plate was sealed, shaken, and samples were injected onto the UPLC-MS/MS system.

2.5. Instrumental analysis parameters

A UPLC-MS/MS system (Waters, Milford, MA, USA) consisting of a triple stage quadrupole mass spectrometer (Waters Xevo TQ-XS with Z-spray source) equipped with an Acquity classic UPLC® system (Waters, Milford, MA, USA) was used for mass spectrometric detection. Chromatographic separation was performed on a Waters Acquity BEH C_{18} peptide column (300 Å, 2.1 mm × 50 mm, 1.7 μm) heated to 80 °C using a flow rate of 0.5 mL/min and an injection volume of 20 μL. The eluent consisted of 0.1% (v/v) aqueous FA with 5% ACN (aqueous eluent; A) and ACN including 0.1% FA (ACN eluent; B). Initial conditions of 80% A/20% B were kept for 0.1 min followed by a change to 67% A/33% B within 1.9 min. Subsequently, the ratio was changed to 5% A/95% B within 0.5 min, adjusted to 50% A/50% B in 0.5 min, changed back to 5% A/95% B within 0.5 min and kept for an additional 0.5 min before returning to starting conditions in 0.5 min. The initial conditions were kept for equilibration while the subsequent injection was prepared (1 min), which resulted in a total cycle time of 5.5 min.

The Z-spray ionization parameters were manually optimized and the Xevo TQ-XS was tuned to exenatide and the IS using the MassLynx V4.2 system software (Waters, Milford, MA, USA) with integrated IntelliStart procedures. Selected reaction monitoring (SRM) measurements were performed utilizing Ar for CID in

Table 1
Optimized parameters for the detection of exenatide using UPLC-MS/MS with positive heated ESI and SRM.

Parameter	Exenatide	[$^{13}C_6$,^{15}N]-Leu(10,21,26)-exenatide
Spray voltage (V)	700	700
Cone voltage (V)	20	20
Source temperature (°C)	150	150
Desolvation gas flow (N_2) (L/h)	1,000	1,000
Desolvation temperature (°C)	600	600
SRM transition (m/z)	838.3 → 948.7	842.5 → 954.0
Dwell time (ms)	100	100
Collision energy (V)	18	18
Collision gas flow (Ar) (mL/min)	0.15	0.15

ESI: Electrospray ionization; SRM: selected reaction monitoring.

positive ion mode. Mass spectrometric characteristics are shown in Table 1.

2.6. Validation of the analytical methods

The assay was validated following the pertinent recommendations published by the FDA and EMA [25,26]. Accuracy (expressed in percent) was calculated as the ratio of mean concentrations measured in individual batches divided by the nominal value. Precision (expressed in percent) was determined from the ratio of standard deviation (SD) and mean measured concentration. Validity of the assay was demonstrated by analysis of three validation batches with each batch containing at least eight calibration samples and at least 24 QC samples at different concentrations (LLOQ, QC A, B, and C, as well as additional dilution QC D; six-fold each). Blank plasma samples from six different beagle dogs, which were processed without addition of analyte and IS, were used for testing the assay's selectivity by evaluating the baseline at the retention time of the analyte.

Extraction recovery rates from plasma were assessed from QC samples A to C in three-fold determinations by the ratio of their respective peak areas and the respective peak areas from blank plasma spiked after extraction (representing 100% analyte amount in identical matrix). Matrix effects were determined also in three-fold determination for QC A to C by comparing peak areas of blank plasma samples spiked after extraction with the respective peak areas of matrix-free solvent spiked with the identical amount [27].

Short-term and long-term stability of exenatide in plasma at room temperature and -40 °C has already been demonstrated [22]. However, during validation, the stability of exenatide in the pg/mL range was assessed for plasma samples stored at -25 °C for 3 weeks, which well covers the storage time of the beagle dog study plasma samples, as well as in three freeze-and-thaw cycles using QC samples A to C. Stability of the extracts in the autosampler was evaluated by repeated analysis of QC A to C after remaining in the autosampler at 10 °C for 24 h.

To evaluate the assay's applicability to human studies, specificity, recovery, and matrix effect were also determined in human plasma (citrate).

2.7. Calculations and statistical methods

Calibration curves were calculated with weighted linear regressions ($1/x^2$) from the peak area ratios of the analyte and IS of calibration samples using Waters TargetLynx V4.2 software (Waters, Milford, MA, USA). Non-compartmental pharmacokinetic parameters were determined utilizing Thermo Kinetica Version 5.0 (Thermo Fisher Scientific, Waltham, MA, USA); maximum plasma concentration (C_{max}) and time to C_{max} (t_{max}) was directly obtained from the raw data, terminal elimination half-life ($t_{1/2}$), AUC extrapolated to infinity, apparent volume of distribution at steady state (V_{ss}/F), and apparent oral clearance (Cl/F) were calculated by a mixed log-linear model. Absolute exenatide bioavailability was calculated as AUC(nasal) ÷ AUC(intravenous) × Dose(intravenous) ÷ Dose(nasal) × 100%. Standard calculations were performed with Microsoft Office Excel 2010 (Mountain View, CA, USA).

3. Results and discussion

3.1. Mass spectrometric and chromatographic characteristics

Positive electrospray ionization of exenatide (4,186.6 Da) yielded the [M+5H]$^{5+}$ signal at m/z 838.3 as most intense ion (m/z 842.5 for the IS). In contrast to most peptides that usually show immonium ions of single amino acids as most abundant product ions (especially at high collision energy) as well as a multitude of larger fragments in CID, exenatide shows two large fragments (apart from water loss observed at m/z 834.7) as explicitly most intense CID product ions that both correspond to the identical dissociation-reaction (Fig. 1). These product ions were observed at m/z 948.7 and at m/z 396.2, respectively, and constituted the b_{35} fragment (z = 4) and the y_4 fragment (z = 1), respectively. Their identity and charge were confirmed by high-resolution mass spectrometric analysis (deviation to calculated m/z value < 20 ppm) on a Waters Xevo G2-XS QTof mass spectrometer (Waters, Milford, MA, USA). Fig. 1 depicts the product spectra of the [M+5H]$^{5+}$ signal of exenatide (m/z 838.3) and the dissociation reaction corresponding to the selected quantifier transition m/z 838.3 → m/z 948.7. For the isotopically labeled IS, the corresponding mass transition was monitored at m/z 842.5 → m/z 954.0. The mass shift of 5.3 Da of the CID fragment of the IS was in line with the z = 4 signal of the b_{35}-fragment comprising all three [$^{13}C_6$,^{15}N]-leucines (mass difference 21 Da; Fig. 1).

The superior intensity of the two abundant product ions (b_{35} and y_4 fragment) indicates that one peptide bond in exenatide is substantially more labile and predestined for dissociation in CID. As a consequence of the favored single dissociation-reaction, exenatide can be quantified ultra-sensitively by MS/MS despite its high molecular weight and numerous peptide bonds.

Chromatographic separation of exenatide was performed on a Waters BEH peptide C_{18} UPLC® column with a pore width of 300 Å which together with heating to 80 °C facilitated interaction of the large peptide exenatide with the solid phase to achieve sharp chromatographic peaks. A gradient from 80% to 67% aqueous eluent and a parallel increase of the ACN eluent proportion from 20% to 33% within 2 min resulted in a fast separation gradient and a peak width at baseline of 5 s. Dwell times of 100 ms for analyte and IS transition yielded approximately 25 data points per peak and, hence, well resolved single mass traces (Fig. 2). Because of initially observed carry-over affecting successive analyses, a second gradient for cleaning purposes was implemented into the
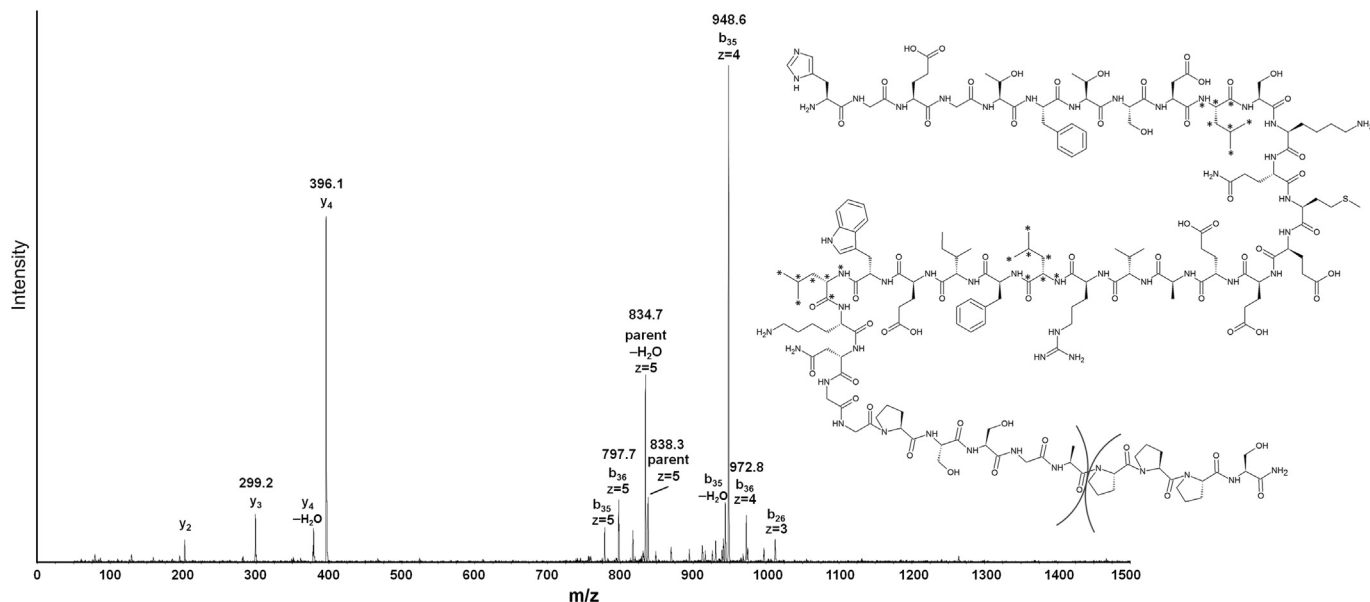
Fig. 1. Positive product spectrum of exenatide using collision-induced decomposition at 18 V. The grey brackets in the exenatide structure depict the preferred dissociation reaction corresponding to the m/z 838.3 → m/z 948.7 (b_{35}) and m/z 838.3 → m/z 396.2 (y_4) transition. The positions of the isotopic labels in the corresponding internal standard are marked with an asterisk.

chromatographic method, which reduced the carry-over to levels well below the required 20% peak area of the LLOQ signal.

3.2. Extraction by protein precipitation

Exenatide is an acidic peptide bearing more carboxyl functions than amino groups, rendering it accessible to anion exchange chromatography, similar to the GLP-1 receptor agonist liraglutide

[28]. Therefore, isolation of exenatide from plasma was performed by solid phase extraction (SPE) using mixed mode strong anion exchange and reverse phase sorbent, which yielded quantitative recovery (99.9% to 110.8% for QC A to C). SPE anion exchange isolation of exenatide allowed rigorous washing and resulted in little remaining matrix interference, which could be separated by optimized chromatographic conditions. The matrix effect for QC A to C was negligible with determined values between −7.1% and
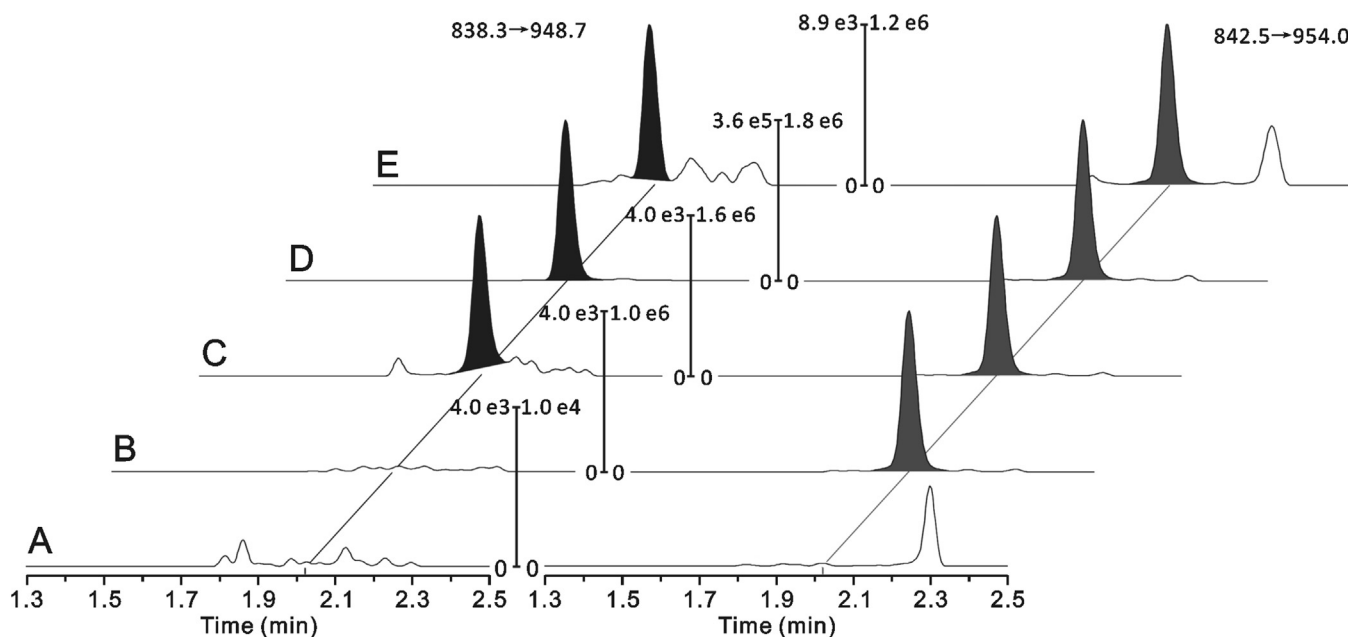
Fig. 2. Selected UPLC-MS/MS chromatograms of processed plasma samples with exenatide quantifier transition on the left (black filling) and IS transition on the right (grey filling). Intensities were normalized to the highest signal except for the exenatide quantifier transition of blank and IS spiked plasma which were normalized to the intensity of the lower limit of quantification (LLOQ) signal. (A) blank plasma sample, (B) plasma sample with added IS, (C) plasma sample at LLOQ concentration (representing 5 pg/mL), (D) plasma sample at QC B concentration (representing 600 pg/mL), and (E) plasma sample of beagle dog #1 15 min after nasal administration of 60 μg exenatide (quantified exenatide concentration 15.8 pg/mL).

Table 2
Summary of quality control results for exenatide in plasma.

Batch	Parameters	LLOQ (5.00 pg/mL)	QC A (15.0 pg/mL)	QC B (600 pg/mL)	QC C (7,500 pg/mL)
Within-batch					
1	Mean (pg/mL)	4.65	15.0	603	7,680
	Accuracy (%)	93.0	100.0	100.5	102.4
	Precision (%CV)	15.2	3.37	4.21	2.83
2	Mean (pg/mL)	4.85	14.9	614	7,905
	Accuracy (%)	97.0	99.4	102.3	105.4
	Precision (%CV)	9.07	8.32	2.66	2.68
3	Mean (pg/mL)	5.13	14.6	606	7,693
	Accuracy (%)	102.5	97.5	100.9	102.6
	Precision (%CV)	15.9	10.9	7.06	8.66
Batch-to-batch					
	Mean (pg/mL)	4.86	14.8	607	7,763
	Accuracy (%)	97.2	98.9	101.2	103.5
	Precision (%CV)	13.4	7.64	4.83	5.01

CV: Coefficient of variation; LLOQ: Lower limit of quantification; QC: Quality control.
$n = 5$ replicates at LLOQ and each QC concentration.

Table 3
Results of the incurred sample reanalysis of 9 plasma samples after intravenous administration.

Sample	Original analysis (pg/mL)	Incurred reanalysis (pg/mL)	Deviation (%)
Dog1 15 min	31,984	26,739	−16.4
Dog1 30 min	18,693	17,741	−5.1
Dog2 15 min	38,013	37,203	−2.1
Dog2 30 min	22,063	22,774	3.2
Dog3 15 min	33,936	39,227	15.6
Dog3 30 min	26,266	23,743	−9.6
Dog3 60 min	13,172	12,829	−2.6
Dog4 15 min	40,817	39,019	−4.4
Dog4 30 min	22,412	21,165	−5.6

3.6%.

Anion-exchange purification of peptides conveys the significant advantage of yielding acidic extracts, which is beneficial for peptide stability. Therefore, neutralization and excessive dilution steps can be avoided which, combined with the utilization of the μ-elution format, resulted in concentrated sample extracts suitable for ultra-sensitive quantification.

3.3. Validation results

The anion exchange extraction combined with UPLC-MS/MS quantification of exenatide was in complete compliance with the pertinent guidelines of FDA and EMA [25,26]. Selectivity was demonstrated in blank matrices from six individual beagle dogs by absence of signals at the analytes' retention times. Fig. 2 shows typical chromatograms of blank plasma as well as plasma samples spiked with IS, at LLOQ concentration, at QC B concentration, and one beagle dog plasma sample 15 min after nasal administration of 60 μg exenatide. The correlation coefficients (r^2) of all calibration curves were >0.99. Intraday accuracies (QC A to C) varied between 97.5% and 105.4% with corresponding precisions <10.9% while interday accuracies ranged from 98.9% to 103.5% with corresponding precisions <7.7%. The accuracy at the LLOQ varied between 93.0% and 102.5% intraday and was 97.2% interday. The corresponding precisions were <15.9% and 13.4%, respectively. A summary of the quality control results during validation is given in Table 2.

For quantification of higher exenatide plasma concentrations occurring early after intravenous administration, a 10-fold dilution with blank plasma (QC D) was validated using 20 μL of plasma.
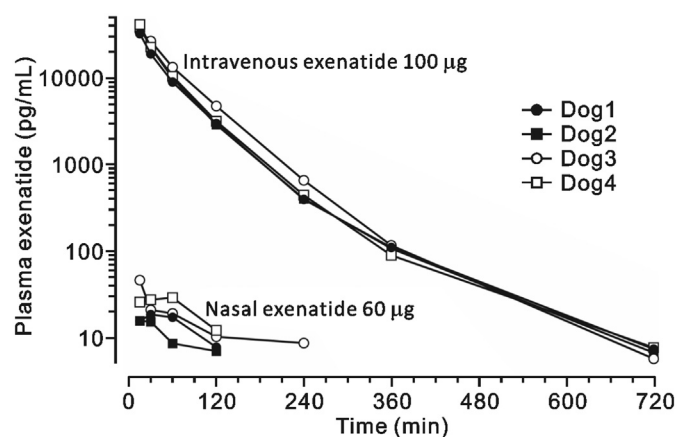
Fig. 3. Exenatide plasma concentration-time profiles in beagle dogs after intravenous (100 μg) and nasal (60 μg) administration.

Accuracy of the dilution QC D was 111.2% with corresponding precision of 1.09%, proving the assay's applicability to quantify plasma exenatide up to 100,000 pg/mL (100 ng/mL). The reliability of exenatide quantification was demonstrated by an incurred sample reanalysis of 9 study samples originating from all four exposed beagle dogs which all showed deviations of <16.5% (2.1%–16.4%) compared to the original analysis, being well within the requirements of the FDA and EMA (Table 3).

Due to the utilization of an isotopically labeled IS, which accurately accounts for recovery and matrix effects, the assay is in principle applicable to human plasma determinations. Therefore,

Table 4
Single dose pharmacokinetics of exenatide in beagle dogs after intravenous bolus injection and after nasal administration.

Exenatide dose and route of administration	Weight of dog (kg)	C_{max} (pg/mL)	AUC (pg/mL · h)	V_Z (L/kg)	Cl (mL/min)	$t_{1/2}$ (min)	F (%)
Intravenous	1 (10.1)	31,984	25,394	0.62	65.6	66.5	100
100 µg	2 (10.2)	38,013	28,483	0.54	58.5	65.1	100
	3 (9.5)	33,936	34,397	0.44	48.5	59.9	100
	4 (9.1)	40,817	30,024	0.58	55.5	65.3	100
Nasal	1 (10.1)	18.7	37.4	0.48	64.1	52.7	0.24
60 µg	2 (10.2)	15.9	27.3	0.30	58.6	36.3	0.16
	3 (9.5)	46.6	74.3	0.49	48.5	67.2	0.36
	4 (9.1)	29.3	57.9	0.42	55.3	47.8	0.32

AUC: area under the concentration-time curve; Cl: clearance corrected for F; C_{max}: maximal plasma concentration; F: absolute bioavailability calculated as AUC(oral) ÷ AUC(iv) × 100 % × dose(iv) ÷ dose(oral); $t_{1/2}$: half-life; V_Z: volume of distribution corrected for F.

the possible LLOQ of our assay in human plasma and the required plasma volume are primarily dependent on the extraction characteristics and matrix interferences. Because the extraction characteristics of exenatide in human plasma (recovery of 84.0% to 87.8% and a matrix effect of −9.3% to −5.8%) are similar to beagle plasma and due to the absence of interfering signals in blank plasma from six different individuals, applicability of the presented assay is indicated also for plasma exenatide quantification in human studies.

3.4. Stability

Stability of plasma exenatide was demonstrated by accurate quantification of freeze-and-thaw samples of QC A to C, which showed accuracies between 93.8% and 101.7%. Additionally, QC samples A to C stored at −25 °C for 3 weeks showed accuracies ranging from 105.4% to 112.0%, confirming plasma exenatide stability for storage under these conditions. Stability in plasma has already been demonstrated for 1 month at −40 °C and 2 h at room temperature [22].

Plasma extracts were stable after remaining in the Sampler Manager for 24 h, which is sufficient for the course of analysis also for large batches and favorable for high throughput quantification of pharmacokinetic samples. The stability of exenatide in the stock and standard solutions was confirmed by the quantification of freshly prepared QC A to C samples (from an independent new weighing) with calibration solutions stored at 4 °C for 2 months, which revealed accuracies of 106.0% to 111.7%.

3.5. Pharmacokinetics of exenatide after intravenous and nasal administration to beagle dogs

Fig. 3 shows the exenatide plasma concentration-time profiles after intravenous and nasal administration to four beagle dogs (bodyweight 9.1 to 10.2 kg) and the corresponding non-compartmental pharmacokinetic analyses are given in Table 4. After intravenous bolus injection of 100 µg, exenatide's mean volume of distribution was 0.54 L/kg (range: 0.44–0.62) and mean clearance 57.0 mL/min (48.5–65.6) resulting in an average half-life ($t_{1/2}$) of 64.2 min (59.9–66.5) (Table 4). Nasal administration of 60 µg exenatide resulted in detectable plasma concentrations with an average C_{max} of 27.6 pg/mL (15.9–46.6), reached (t_{max}) 30 min (15–60) after nasal administration (Fig. 3). These values were in good agreement with models for allometric scaling of exenatide pharmacokinetics [29].

Because only few sampling points with detectable plasma concentrations were observed, extrapolation of AUC values to infinity was less reliable after nasal administration (extrapolated fraction 22%–28%) and, therefore, nasal pharmacokinetics are less well established and give only preliminary indication on accurate

nasal availability of the peptide. However, these data clearly show that nasal absorption is minimal. Nevertheless, the determined volume of distribution of 0.42 L/kg (0.30–0.49), the clearance of 56.6 mL/min (48.5–64.1), and the $t_{1/2}$ of 51.0 min (36.3–67.2) after nasal administration were comparable to those of intravenous exenatide. Absolute nasal bioavailability was calculated at 0.27% (0.16%–0.36%), indicating minimal nasal absorption, which may be explained by the large size of exenatide leading to poor intrinsic membrane penetration.

4. Conclusion

Only few assays for exenatide bioanalysis relying on LC-MS methodologies have been reported with the most sensitive having an LLOQ of 50 pg/mL, hence lacking sensitivity for pharmacokinetic analyses in the therapeutic range. Having an LLOQ of 5 pg/mL (1.2 pM), the presented ultra-sensitive UPLC-MS/MS assay for exenatide quantification in plasma is the first LC-MS-based assay suitable for the pharmacokinetic characterization of exenatide in its intended therapeutic range, which even exhibits superior sensitivity compared to previously reported immunoassays. The assay's dynamic range spans more than three orders of magnitude while concurrently being accurate and precise. The utilization of anion exchange plasma extraction of exenatide performed in a µ-elution format resulted in concentrated extracts, supporting sensitive quantification and rendering the assay suitable for high sample throughput. Using this UPLC-MS/MS assay, absolute nasal bioavailability of native exenatide was found to be very low (bioavailability well below 1%), demonstrating the assay's applicability for pharmacokinetic studies and future formulation development for alternative routes of administration.

Conflicts of interest

The authors declare that there are no conflicts of interest.

References

[1] A.J. Garber, M.J. Abrahamson, J.I. Barzilay, et al., Consensus statement by the American association of clinical endocrinologists and American college of endocrinology on the comprehensive type 2 diabetes management algorithm - 2018 executive summary, Endocr. Pract. 24 (2018) 91–120.
[2] F.K. Knop, A. Bronden, T. Vilsboll, Exenatide: pharmacokinetics, clinical use, and future directions, Expert Opin. Pharmacother. 18 (2017) 555–571.
[3] J. Eng, W. Kleinman, L. Singh, et al., Isolation and characterization of exendin-

4, an exendin-3 analogue, from Heloderma suspectum venom. Further evidence for an exendin receptor on dispersed acini from Guinea pig pancreas, J. Biol. Chem. 267 (1992) 7402–7405.

[4] C.M.B. Edwards, S.A. Stanley, R. Davis, et al., Exendin-4 reduces fasting and postprandial glucose and decreases energy intake in healthy volunteers, Am. J. Physiol. Endocrinol. Metab. 281 (2001) E155–E161.

[5] M.S. Fineman, T.A. Bicsak, L.Z. Shen, et al., Effect on glycemic control of exenatide (synthetic exendin-4) additive to existing metformin and/or sulfonylurea treatment in patients with type 2 diabetes, Diabetes Care 26 (2003) 2370–2377.

[6] L.L. Nielsen, A.A. Young, D.G. Parkes, Pharmacology of exenatide (synthetic exendin-4): a potential therapeutic for improved glycemic control of type 2 diabetes, Regul. Pept. 117 (2004) 77–88.

[7] BYETTA (Exenatide) Injection: US Prescribing Information, AstraZeneca Pharmaceuticals LP, Wilmington, DE, 2018.

[8] BYDUREON (Exenatide Extended-Release) for Injectable Suspension: US Prescribing Information, AstraZeneca Pharmaceuticals LP, Wilmington, DE, 2018.

[9] I. Andrés-Ramos, S. Blanco-Barrios, E. Fernández-López, et al., Exenatide-induced eosinophil-rich granulomatous panniculitis: a novel case showing injected microspheres, Am. J. Dermatopathol. 37 (2015) 801–802.

[10] N.C. Boysen, M.S. Stone, Eosinophil-rich granulomatous panniculitis caused by exenatide injection, J. Cutan. Pathol. 41 (2014) 63–65.

[11] S.C. Jones, D.L. Ryan, V.S. Pratt, et al., Injection-site nodules associated with the use of exenatide extended-release reported to the US Food and Drug administration adverse event reporting system, Diabetes Spectr. 28 (2015) 283–288.

[12] K. Riswold, V. Flynn, Persistent injection site nodules from exenatide: successful treatment with intralesional triamcinolone, JAAD Case Rep. 4 (2018) 830–832.

[13] S.-J. Shan, Y. Guo, Exenatide-induced eosinophilic sclerosing lipogranuloma at the injection site, Am. J. Dermatopathol. 36 (2014) 510–512.

[14] C.I. Vidal, S. Chaudhry, N.M. Burkemper, Exenatide-induced panniculitis: utility of the acid-fast stain to identify injected microspheres, Am. J. Dermatopathol. 40 (2018) 867–869.

[15] M. Fineman, S. Flanagan, K. Taylor, et al., Pharmacokinetics and pharmacodynamics of exenatide extended-release after single and multiple dosing, Clin. Pharmacokinet. 50 (2011) 65–74.

[16] Y.M. Cui, X.H. Guo, D.M. Zhang, et al., Pharmacokinetics, safety, and tolerability of single- and multiple-dose exenatide once weekly in Chinese patients with type 2 diabetes mellitus, J. Diabetes 5 (2013) 127–135.

[17] O.G. Kolterman, D.D. Kim, L. Shen, et al., Pharmacokinetics, pharmacodynamics, and safety of exenatide in patients with type 2 diabetes mellitus, Am.

J. Health Syst. Pharm. 62 (2005) 173–181.

[18] P.A. Kothare, H. Linnebjerg, Y. Isaka, et al., Pharmacokinetics, pharmacodynamics, tolerability, and safety of exenatide in Japanese patients with type 2 diabetes mellitus, J. Clin. Pharmacol. 48 (2008) 1389–1399.

[19] J. Malloy, E. Capparelli, M. Gottschalk, et al., Pharmacology and tolerability of a single dose of exenatide in adolescent patients with type 2 diabetes mellitus being treated with metformin: a randomized, placebo-controlled, single-blind, dose-escalation, crossover study, Clin. Therapeut. 31 (2009) 806–815.

[20] FDA Approves First Oral GLP-1 Treatment for Type 2 Diabetes, US Department of Health and Human Services Food and Drug Administration, 2019. https://www.fda.gov/news-events/press-announcements/fda-approves-first-oral-glp-1-treatment-type-2-diabetes.

[21] C. Granhall, M. Donsmark, T.M. Blicher, et al., Safety and pharmacokinetics of single and multiple ascending doses of the novel oral human GLP-1 analogue, oral semaglutide, in healthy subjects and subjects with type 2 diabetes, Clin. Pharmacokinet. 58 (2019) 781–791.

[22] J.F. Zhang, C.J. Sha, Y. Sun, et al., Ultra-high-performance liquid chromatography for the determination of exenatide in monkey plasma by tandem quadrupole mass spectrometry, J. Pharm. Anal. 3 (2013) 235–240.

[23] L.-P. Morin, J.-N. Mess, F. Garofolo, Large-molecule quantification: sensitivity and selectivity head-to-head comparison of triple quadrupole with Q-TOF, Bioanalysis 5 (2013) 1181–1193.

[24] J.R. Kehler, C.L. Bowen, S.L. Boram, et al., Application of DBS for quantitative assessment of the peptide Exendin-4; comparison of plasma and DBS method by UHPLC–MS/MS, Bioanalysis 2 (2010) 1461–1468.

[25] Guidance for Industry, Bioanalytical Method Validation, US Department of Health and Human Services Food and Drug Administration, 2018. http://www.fda.gov/downloads/Drugs/GuidanceComplianceRegulatoryInformation/Guidances/ucm070107.pdf.

[26] Guideline on Validation of Bioanalytical Methods, EMEA/CHMP/EWP/192217/2009, European Medicines Agency, 2009. http://www.ema.europa.eu/docs/en_GB/document_library/Scientific_guideline/2011/00/WC500109686.pdf.

[27] B. Matuszewski, M. Constanzer, C. Chavez-Eng, Strategies for the assessment of matrix effect in quantitative bioanalytical methods based on HPLC– MS/MS, Anal. Chem. 75 (2003) 3019–3030.

[28] M. Sauter, P. Uhl, M. Majewsky, et al., An ultrasensitive UPLC–MS/MS assay for the quantification of the therapeutic peptide liraglutide in plasma to assess the oral and nasal bioavailability in beagle dogs, Bioanalysis 11 (2019) 887–898.

[29] T. Chen, D.E. Mager, L. Kagan, Interspecies modeling and prediction of human exenatide pharmacokinetics, Pharm. Res. (N. Y.) 30 (2013) 751–760.

Original article

Software-aided detection and structural characterization of cyclic peptide metabolites in biological matrix by high-resolution mass spectrometry

Ming Yao [a], Tingting Cai [b, *], Eva Duchoslav [c], Li Ma [a], Xu Guo [c], Mingshe Zhu [a, d, **]

[a] *Pharmaceutical Candidate Optimization, Bristol-Myers Squibb, Princeton, NJ, USA*
[b] *XenoBiotic Labs, WuXi AppTec, Nanjing, China*
[c] *SCIEX, Concord, ON, L4K 4V8, Canada*
[d] *MassDefect Technologies, Princeton, NJ, USA*

ARTICLE INFO

ABSTRACT

Compared to their linear counterparts, cyclic peptides show better biological activities, such as anti-bacterial, immunosuppressive, and anti-tumor activities, and pharmaceutical properties due to their conformational rigidity. However, cyclic peptides could form numerous putative metabolites from potential hydrolytic cleavages and their fragments are very difficult to interpret. These characteristics pose a great challenge when analyzing metabolites of cyclic peptides by mass spectrometry. This study was to assess and apply a software-aided analytical workflow for the detection and structural characterization of cyclic peptide metabolites. Insulin and atrial natriuretic peptide (ANP) as model cyclic peptides were incubated with trypsin/chymotrypsin and/or rat liver S9, followed by data acquisition using TripleTOF® 5600. Resultant full-scan MS and MS/MS datasets were automatically processed through a combination of targeted and untargeted peak finding strategies. MS/MS spectra of predicted metabolites were interrogated against putative metabolite sequences, in light of a, b, y and internal fragment series. The resulting fragment assignments led to the confirmation and ranking of the metabolite sequences and identification of metabolic modification. As a result, 29 metabolites with linear or cyclic structures were detected in the insulin incubation with the hydrolytic enzymes. Sequences of twenty insulin metabolites were further determined, which were consistent with the hydrolytic sites of these enzymes. In the same manner, multiple metabolites of insulin and ANP formed in rat liver S9 incubation were detected and structurally characterized, some of which have not been previously reported. The results demonstrated the utility of software-aided data processing tool in detection and identification of cyclic peptide metabolites.

© 2020 Xi'an Jiaotong University. Production and hosting by Elsevier B.V. This is an open access article under the CC BY-NC-ND license (http://creativecommons.org/licenses/by-nc-nd/4.0/).

1. Introduction

Cyclic peptides are a class of peptides containing cyclic ring structure, which can be formed by folding the peptide chain with an amide bond, or other chemically stable bonds such as lactone, ether, thioether, disulfide bond [1,2]. In the past decades, several cyclic peptide drugs have been developed for clinical therapy [3],

like cyclosporine A, gramicidin-S, vasopressin, oxytocin, vancomycin, and insulin [4–8]. As a feature in these therapeutic compounds, peptide cyclization can improve the potency [9,10] and proteolysis stability of peptides [11,12], as well as pharmacokinetic property and intracellular activity such as membrane permeability [13]. Apart from the advantageous conformational rigidity, the special structures of cyclic peptides also lead to great challenge for the detection and identification of cyclic peptide metabolites with mass spectrometry (MS). Firstly, the flexible starting point as well as the stochastic fragment lengths of a cyclic peptide would derive numerous possibilities of generating metabolites via peptide hydrolysis. For example, based on simulation, insulin could generate over 46000 metabolites via hydrolysis (Fig. S1) and each of these metabolites could generate multiple molecular ions of different

---

charge states. These vast amounts of potential metabolites make it impossible to rely on manpower to search for predicted metabolites of cyclic peptides. Furthermore, for the linear peptides, the fragmentation under gas phase collision induced dissociation (CID) is well understood [14,15]. CID, electron transfer dissociation (ETD) and electron capture dissociation (ECD) are the regular ways to produce b/y, a/x, c/z fragment ions from linear peptides [16,17]. As the most commonly used activation technique in tandem mass spectrometry, CID produces a series of b/y ions, which are widely used in peptide sequencing and proteomics study [18–21]. Many software and databases are capable of efficiently determining sequences and structures of linear peptides [22–24]. However, for the cyclic peptides, the C-terminus and N-terminus may not be present due to the complex cyclization types. In addition, cyclic peptides with disulfide bond [25,26] or other linkage structures [27] will resist CID fragmentation at lower collisional energy, while in high-collision energy condition they generate only nonspecific small immonium ions that are not suitable for spectral interpretation. Thus, the in-silico tools developed for the analysis of linear peptide sequences and modifications in proteomics studies are not useful for the assignment of sequence and modification sites of cyclic peptide metabolites [28–32].

In this study, we evaluated and applied a recently implemented MetabolitePilot Software for the automatic detection and structure characterization of cyclic peptide metabolites. Insulin and atrial natriuretic peptide (ANP), which are biologically active cyclic peptides formed with three and one disulfide bonds, respectively (Fig. 1) [33,34], were selected as model cyclic peptides. Like LC/MS analysis of cyclic peptides with a variety of linkage structures, studying metabolism of both insulin and ANP faced the same challenges: enormous potential metabolites could be formed via peptide bond hydrolysis and product ion spectra are very difficult to interpret. The first experiment was to detect and structurally characterize metabolites formed in the incubation of insulin with a combination of trypsin and chymotrypsin [35,36]. Since peptide hydrolytic sites by these enzymes are known and metabolites from the incubations are predicable, results from this experiment can allow us to evaluate the effectiveness of the data processing workflow (Fig. 2) in studying metabolism of cyclic peptides in vitro. The second experiment was to investigate unknown metabolites of insulin and ANP formed in incubations with rat liver S9 that have a

variety of peptide hydrolytic enzymes. Results from this study demonstrated that the novel data processing workflow was able to rapidly detect and characterize metabolites of cyclic peptides formed in biological matrix.

2. Experimental section

2.1. Chemicals and reagents

Human insulin and ANP (Fig. 1) were purchased from Sigma-Aldrich (Burlington, MA). Pooled rat liver S9 was obtained from Sekisui XenoTech, LLC (Kansas City, KS, USA). Trypsin and chymotrypsin were purchased from Sigma-Aldrich (Burlington, MA, USA). Ammonium bicarbonate and 0.1 M HCl were from Sigma-Aldrich (Burlington, MA, USA). Acetonitrile (ACN) methanol and water of LC-MS grade were from Merck (Kenilworth, NJ, USA). Ultrapure water was freshly prepared with Millipore purification system (Massachusetts, USA).

2.2. Enzymatic digestion of insulin

The enzymatic digestion of insulin was carried out in 200 μL of 50 mM ammonium bicarbonate (pH 7.4). Insulin was dissolved in 50 mM ammonium bicarbonate with droplet adding 0.1 M HCl until completely dissolved. In the final system, 20 μM of insulin was incubated with trypsin and chymotrypsin (5 μg/mL) under 37 °C for 0, 1, 2 and 3 h. After incubation, 500 μL of ACN was added to quench the reaction and centrifuged at 21,000 g for 10 min. The supernatant was collected and dried down under a gentle stream of N_2 gas. The samples were reconstituted in LC/MS grade water (100 μL) for further liquid chromatography high resolution mass spectrometry (LC-HRMS) analysis.

2.3. Metabolism of insulin and ANP in liver S9

Insulin and ANP were incubated with rat liver S9 respectively in 200 μL of 50 mM ammonium bicarbonate (pH 7.4) for 0 and 3 h. Rat liver S9 was added prior to the addition of insulin or ANP, and pre-incubated on ice for 5 min. The final enzymatic system contained 1 mg/mL of rat liver S9 and 20 mM of insulin or ANP. After incubation, 500 μL of ACN was added to quench the reaction and
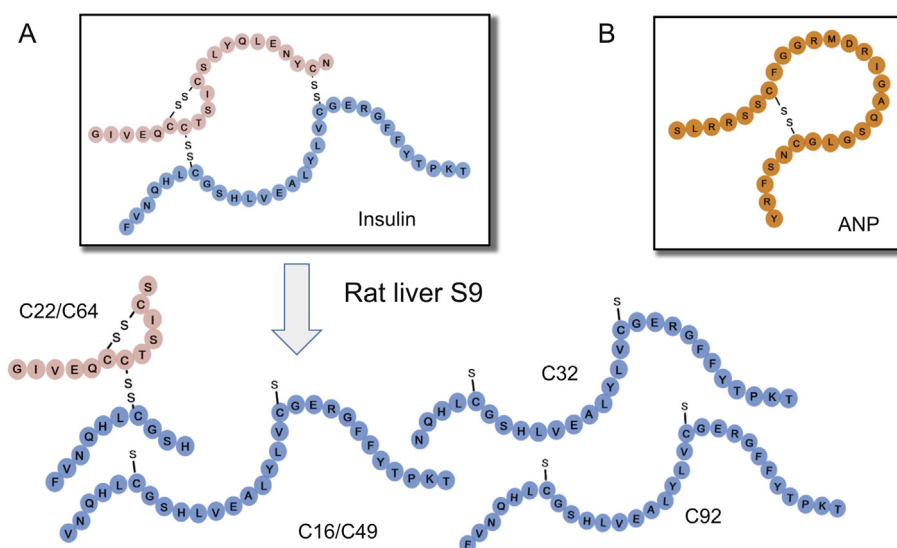
Fig. 1. (A) Structures of insulin and its metabolites formed in liver S9 incubation. (B) Structures of ANP.
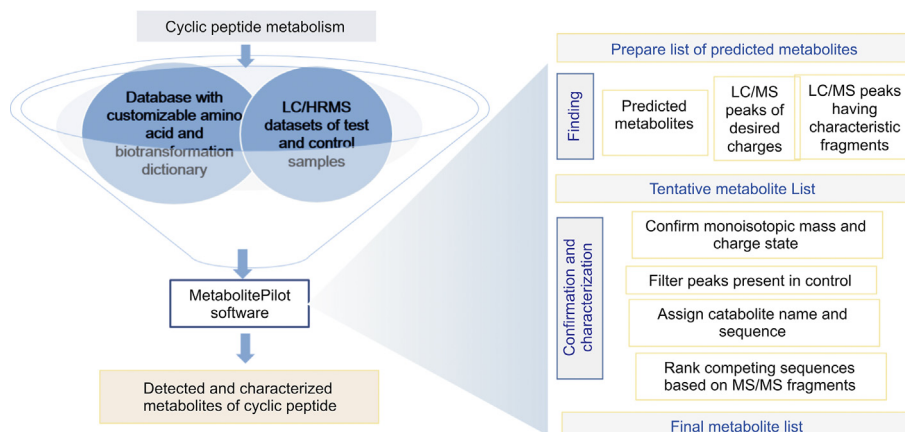
Fig. 2. Workflow for detection, confirmation and identification of cyclic peptides metabolites using a newly developed software-aided data processing tool.

centrifuged at 21,000 *g* for 10 min. The supernatant was collected and dried down under a gentle stream of N_2 gas. The samples were reconstituted in LC/MS grade water (100 μL) for further LC-HRMS analysis.

2.4. Data acquisition for metabolites of insulin and ANP

An Agilent 1290 Infinity II LC system (Agilent Technologies, Santa Clara, US) was connected to a TripleTOF® 5600 mass spectrometer (SCIEX, Framingham, MA) for all LC-MS analysis. Mobile phase A was H_2O with 0.1% formic acid and mobile phase B was acetonitrile with 0.1% formic acid. 10 μL of sample was injected onto a C_{18} column (Waters Acquity UPLC, BEH C18; 2.1 mm × 100 mm, 1.7 μm) for each run at a flow rate of 400 μL/min. The chromatography commenced at a solvent composition of 2% B and 98% A for 2 min, and then increased to 45% B at 45 min, and reached 90% B at 45.1 min and held until 47 min. Thereafter, the column was re-equilibrated back to the starting solvent conditions of 2% B and 98% A at 47.1 min, and held to the end of the gradient (54 min).

To maximize the information acquired on the mass spectrometer for each sample, a full MS scan (*m/z* 300–2000) was acquired followed by top 20 information dependent acquisition (IDA) MS/MS scans (*m/z* 100–1600) in positive ion mode. The parameters for curtain plate (CUR), declustering potential (DP), collision energy (CE); ionspray voltage IS, Gas1, Gas2 in full MS scan mode was 30psi, 80V, 10V, 5500V, 55 psi, and 55 psi. Source temperature was set to 450 °C and tray temperature was set to 22 °C. The criteria for the IDA precursor selection were as follows: top 20 most intense peaks with charge states from 2 to 5 and intensities greater than 50 were selected. Previous candidates within the mass tolerance of 50 mDa were excluded for the duration of 3 s after 1 occurrence. Dynamic background subtraction was activated. Rolling collision energy for multiply charged peptides was enabled. Divert Valco valve was used to switch LC flow to MS between 2 and 50 min.

2.5. Data processing with MetabolitePilot™ software

The liquid chromatography/high resolution mass spectrometry (LC/HRMS) data were processed with MetabolitePilot Software 2.0; this tool facilitates automated LC/MS data processing for the characterization of therapeutic peptides, including non-linear, cross-linked and cyclic structures. This software could also deal with non-natural amino acids and modifications, targeted searching of predicted hydrolytic cleavages, calculating and assigning a-, b-, y- and internal fragments for linear and non-linear peptides. The

strategies used for finding the peptide-related material were as follows: peak finding in accurate extracted ion chromatograms of hypothetical catabolites, generic LC/MS peak finding followed with charge filter that removed singly-charged peaks, and finding peaks that yielded characteristic accurate mass fragments in MS/MS data. In order to remove false positive measurements, the peak finding was followed by comparison of the data against that of a control sample; only peaks that were either absent or significantly smaller (0.5 or less) in the control sample were kept. The LC/MS peaks were matched with putative peptide catabolite names based on mass tolerance of 10 ppm and TOF isotope pattern agreement within 20%. MS and MS/MS spectra as well as metabolite chromatographic traces were saved with the peak finding results. The sequences of putative catabolites were confirmed by MS/MS annotation using theoretical a,b,y, y|a and y|b fragments and an mass tolerance of 5 ppm.

3. Results and discussion

3.1. Workflow for detection and characterization of cyclic peptides metabolites

The high-level workflow for detection and characterization of metabolites of cyclic peptides using LC/HRMS data processing software tool is shown in Fig. 2. The input for the software processing comprises the LC/HRMS data, preferentially a test sample and a control sample, and the processing instructions. The processing method combines the information regarding the peak finding strategies and settings, the studied cyclic peptide sequence in combination with the amino acid and biotransformation dictionary, and the details on potential metabolites to be considered in the target search. Since for larger cyclic peptides, the monoisotopic mass is not the most intense peak in the isotope cluster, the target extracted ion chromatography (XIC)-based search in the MetabolitePilot™ Software uses the mass to charge of the most intense peak in the cluster for the accurate ion chromatogram extraction. If the MS/MS spectrum of the studied peptide is available, it can be loaded to the method and used in untargeted peak finding strategies, such as a search for characteristic fragments.

The actual data processing has a few parts: first, all LC/MS peaks found by any chosen strategy are merged. Then the unique peaks are confirmed; peaks outside processing settings and isotope peaks leading to duplicate entries are removed. Confirmed peaks are then potentially assigned names and putative sequences, based on accurate mass. If MS/MS data are available, the sequence assignments

are confirmed or ranked. In case of peptide biotransformation that can be located on multiple amino-acid residues, the interpretation considers all of these possibilities, and ranks the putative metabolite sequences based on the completeness for MS/MS peptide fragment annotation.

3.2. Metabolite identification of insulin incubated with hydrolytic enzymes

The software-aided workflow was applied to the detection and characterization of the insulin metabolites formed in the incubation with a combination of trypsin and chymotrypsin, which targeted at peptide bond between lysine and arginine, and peptide bonds with aromatic amino acids, such as tyrosine, phenylalanine, and tryptophan, respectively. As a result, 29 insulin metabolites with cyclic or linear structures were directly detected and characterized without reducing disulfide bond (Table 1). The structures of these insulin metabolites are consistent with hydrolytic sites of trypsin and chymotrypsin, which validated the effectiveness of this software-aided approach in studying biotransformation of cyclic peptides in vitro. These metabolites were initially found using multiple detection mechanisms described and further confirmed based on their MS/MS spectral data (Fig. 2). In addition, scoring and ranking of putative amino-acid sequences pointed to predicted insulin digest products. The extracted ion chromatograms of these metabolites shown in Fig. 3 indicated the relative intensities of the insulin metabolites. The accurate full-scan MS and MS/MS spectra of M4, a representative metabolite of insulin, are shown in Fig. 4.

The charge state was assigned based on the isotope cluster in TOF MS, and the structure of metabolite was confirmed based on the exact masses of protonated molecule ions (Fig. 4A) product ions (Fig. 4B).

3.3. Metabolite identification of insulin and ANP formed in incubations with rat liver S9

Insulin and ANP were further incubated with rat liver S9, which contained a variety of peptide hydrolases, followed by direct generation of accurate mass full-scan MS and MS/MS datasets. Major metabolites of insulin and ANP are characterized and listed in Table 2 and Table 3, some of which have not been reported in the literature. The MS responses of the metabolites relative to the parent drug increased with the incubation time. The extracted ion chromatograms of insulin and ANP metabolites are illustrated in Fig. 5. The structures of the six major insulin metabolites formed in rat liver S9 are displayed in Fig. 1. The mass spectra and proposed structures of C92 and C108, the most abundant metabolites of ANP in liver S9 incubation, are depicted in Fig. S2 and Fig. S3.

3.4. The software features for the peak finding and confirmation of minor peptide metabolites

As a majority of therapeutic peptides entering clinical development have twenty or more amino acid residues [37], the monoisotopic peak in the theoretical isotope pattern of a typical therapeutic peptide is not the most intense peak; its relative

Table 1
Insulin metabolites detected and characterized in enzymatic incubation.

ID	Name	Neutral mass	m/z	Charge	RT (min)	Peak area	MS/MS assigned	Sequence type
P	Parent [M+5H]$^{5+}$	5803.62	1161.7320	5	27.3	5.96E+05	✓	C
M1	YTPKT	608.32	305.1688	2	5.4	4.26E+05	✓	L
M2	QLENYC [*3]N/VC [*3]GER	1442.60	722.3065	2	9.8	1.71E+04		LL
M3	FYTPKT	755.39	378.7036	3	11.8	3.21E+05	✓	L
M4	QLENYC [*3]N/LVC [*3]GER	1555.69	519.5699	3	12.4	6.45E+06	✓	LL
M5	GIVEQC [*1]CT/IC [*1]SLYQ + Loss of Water	1556.66	779.3393	2	12.9	5.19E+04		OR
M6	QLENYC [*3]N/YLVC [*3]GER	1718.75	573.9243	3	14.9	1.62E+05	✓	LL
M7	QLENYC [*3]N/LVC [*3]GER + Loss of Water	1537.67	769.8426	2	15.5	5.29E+05	✓	LL
M8	NYC [*3]N/LVC [*3]GERGFF + Hydrogenation	1538.66	770.3349	2	16.1	4.92E+05	✓	LL
M9	QLENYC [*3]N/LVC [*3]GERGF	1759.77	880.8916	2	16.4	5.28E+04		LL
M10	GFFYTPK	858.43	430.2247	2	17.7	9.40E+05	✓	L
M11	GFFYTPKT	959.48	480.7492	2	18.2	8.15E+05	✓	L
M12	SLYQLENYC [*3]N/LYLVC [*3]G	1909.86	637.6257	3	19.4	2.54E+04	✓	LL
M13	QLENYC [*3]N/LVC [*3]GERGFF	1906.84	954.4265	2	20.3	8.16E+04	✓	LL
M14	GIVEQC [*1]C [*2]TSIC [*1]SL/LC [*2]GSHLVE + Loss of Water	2188.97	730.6647	3	21.0	2.27E+04	✓	RLL
M15	SLYQLENYC [*3]N/LYLVC [*3]GERGFFY	2709.24	678.3180	4	21.2	1.46E+04	✓	LL
M16	GIVEQC [*1]C [*2]TSIC [*1]SLY/FVNQHLC [*2]GSHL	2767.23	692.8140	4	22.4	5.88E+04	✓	RLL
M17	GIVEQC [*1]C [*2]TSIC [*1]SL/FVNQHLC [*2]GSHL	2604.14	869.0542	3	24.9	2.47E+05	✓	RLL
M18	GIVEQC [*1]C [*2]TSI/C [*1]SLYQLENYC [*3]N/FVNQHLC [*2]GSHLVEALYLVC [*3]GER	4880.18	814.3705	6	25.0	2.55E+04	✓	C
M19	GIVEQC [*1]C [*2]TSIC [*1]S/FVNQHLC [*2]GSHLVEALYL	3179.46	795.8729	4	25.0	1.76E+05	✓	RLL
M20	GIVEQC [*1]C [*2]TSIC [*1]SLY/HLC [*2]GSHLVEALY	2854.28	952.4339	3	25.1	2.58E+04		RLL
M21	GIVEQC [*1]C [*2]TSIC [*1]SLY/FVNQHLC [*2]GSHLVEALY	3342.53	836.6388	4	25.4	1.07E+07	✓	RLL
M22	GIVEQC [*1]C [*2]TSIC [*1]SLY/LC [*2]GSHLVEALY	2717.23	906.7501	3	25.6	2.72E+04	✓	RLL
M23	GIVEQC [*1]C [*2]TSIC [*1]SLY/FVNQHLC [*2]GSHLVEALY	3342.52	836.6369	4	26.0	3.79E+04	✓	RLL
M24	GIVEQC [*1]C [*2]TSIC [*1]SLYQLENYC [*3]N/FVNQHLC [*2]GSHLVEALYLVC [*3]GER	4862.17	973.4418	5	26.2	7.62E+04		C
M25	CSLYQLENYC [*3]N/GSHLVEALYLVC [*3]GERGFFY	3505.58	1169.5354	3	26.2	4.44E+04		LL
M26	GIVEQC [*1]C [*2]TSIC [*1]SLY/FVNQHLC [*2]GSHLVEALY	3342.52	836.6381	4	27.0	1.82E+05		RLL
M27	GIVEQC [*1]C [*2]TSIC [*1]SLY/FVNQHLC [*2]GSHLVEALYL	3455.60	864.9078	4	27.4	1.18E+05		RLL
M28	GIVEQC [*1]C [*2]TSIC [*1]SLYQLENYC [*3]N/FVNQHLC [*2]GSHLVEALYLVC [*3]GERGFF	5213.33	1043.6723	5	28.0	2.32E+05		C
M29	GIVEQC [*1]C [*2]TSIC [*1]SLYQLENYC [*3]N/FVNQHLC [*2]GSHLVEALYLVC [*3]GERGFFY	5376.40	1076.2866	5	28.0	2.75E+05		C

Insulin metabolite amino-acid sequences are outlined in column Name. In the sequence representation, the chains are separated by "/" and the cysteine di-sulfide bonds are represented by shared indices in cysteine modification suffix "[*]". Sequence type column indicates type of metabolite peptide sequence: cyclic (C), linear (L), linked linear (LL), open ring (OR), linked linear with ring (RLL).
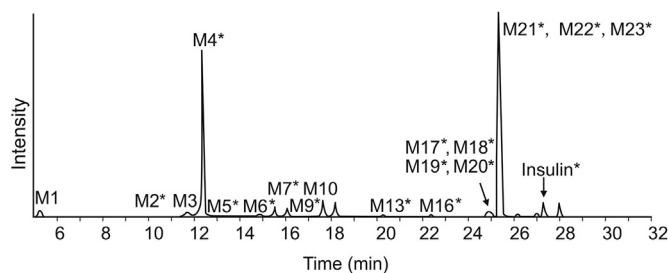
Fig. 3. Metabolite profile of insulin incubated with hydrolytic enzymes (1 h); *represents the metabolite containing disulfide bond.
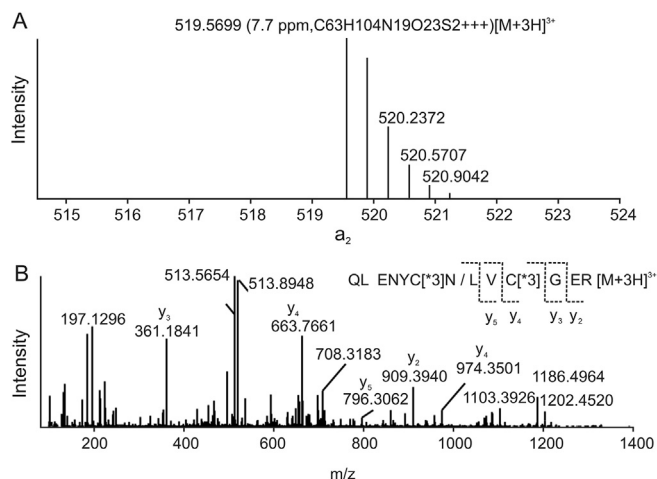
Fig. 4. Full-scan MS (A) and MS/MS (B) spectra of insulin metabolite M4 from enzymatic incubation.

abundance decreases with the increase of size of studied peptides. To support data mining for such larger molecules, one of unique features in MetabolitePilot™ software is to consider the isotopic

distribution of the predicted metabolites and use the most intense isotope for LC/MS peak finding in XIC. Once a peak is found in an XIC trace, TOF MS confirmation includes review of the anticipated isotope pattern. In Table 4, peak index column outlines the index of the peptide isotope peak which was used for XIC extraction when finding metabolites. The monoisotopic peak index is 0, and the respective isotope indices are 1, 2, 3, etc. Once a peak is found with the base peak other than 0, the XIC trace of the base peak is provided in the result workspace. Moreover, since series of multiply-charged isotope peaks are selected in the 1 Da isolation window in the first quadrupole of mass spectrometer (Q1) and fragmented in parallel, peptide fragments exhibit isotope patterns and these patterns aid in confident MS/MS annotation. The isotopic signal of fragments improves signal to noise (S/N) of minor multiply charged peptide fragments and enables their contribution to sequence confirmation. For example, the contribution of doubly charged fragments of insulin to the overall assignment would be raised from 3.6% to 6.9% of total MS/MS ion count.

3.5. The software features for the structure confirmation of isobaric metabolites and modification site

For metabolite identification, one of challenges is to determine isobaric and isomeric metabolites that pose ambiguity even with high resolution mass spectrometry [38]. For large peptides, hydrolytic cleavages may have identical molecular weight, but their sequences could be different. In Table 5, for an ANP metabolite eluted by 17.01 min, two possible isobaric metabolite sequences (RIGAQSGLGCNSF or IGAQSGLGCNSFR) were proposed based on TOF MS data interpretation. For further sequence identification, MetabolitePilot™ software enabled the MS/MS information to match characterized fragments in the spectrum with predicted theoretical ones. Therefore, based on more assigned fragments (provided in Table S1), RIGAQSGLGCNSF was claimed as a "Winner" metabolite sequence, with 23.8% of total ion count that could be directly assigned to sequence fragments.

The MS/MS data also aid in the characterization of cyclic peptide modifications. One of common approaches to enhancing the

Table 2
Time dependent metabolism of insulin in rat liver S9.

ID	Name	m/z	RT(min)	MS area			
				T0	T0.5h	T1.5h	T3h
Insulin	Parent [M+5H]$^{5+}$	1161.737	27.24	3.50E06	2.08E06	1.20E06	6.83E05
C16	VNQHLCGSHLVEALYLVCGERGFFYTPKT + Desaturation [M+4H]$^{4+}$	820.6582	25.9	ND	1.03E05	2.77E05	2.38E05
C22	GIVEQC [*1]C [*2]TSIC [*1]S/FVNQHLC [*2]GSH [M+2H]$^{2+}$	1189.9946	25.92	4.02E04	4.45E+05	5.49E05	4.57E05
C32	NQHLCGSHLVEALYLVCGERGFFYTPKT + Desaturation [M+4H]$^{4+}$	795.8898	26.17	ND	2.68E04	1.66E05	3.10E05
C49	VNQHLCGSHLVEALYLVCGERGFFYTPKT + Desaturation [M+3H]$^{3+}$	1093.8723	26.22	ND	2.03E05	5.67E05	6.60E05
C64	GIVEQC [*1]C [*2]TSIC [*1]S/FVNQHLC [*2]GSH [M+2H]$^{2+}$	1189.9919	26.33	8.67E04	9.42E05	1.31E06	1.27E06
C92	FVNQHLCGSHLVEALYLVCGERGFFYTPKT + Desaturation [M+4H]$^{4+}$	857.4257	26.96	4.00E05	2.73E06	2.29E06	1.35E06

As shown in Fig. 1, C22 and C64 were a pair of isomers. C16 and C49 were another pair of isomes.
ND: Not detected.

Table 3
Time dependent metabolism of ANP in rat liver S9.

ID	Name	m/z	RT (min)	MS area	
				T0	T3h
ANP	Parent [M+5H]$^{5+}$	616.6964	17.54	7.59E06	1.70E06
C94	SLRRSSC [*1]FGGRMDRIGAQSGLGC [*1]NSF [M+4H]$^{4+}$	690.8263	18.09	7.80E04	8.13E04
C96	RSSC [*1]FGGRMDRIGAQSGLGC [*1]NSFRY [M+4H]$^{4+}$	681.5643	18.41	3.52E04	7.44E04
C108	SSC [*1]FGGRMDRIGAQSGLGC [*1]NSFRY [M+4H]$^{4+}$	642.5375	19.8	ND	1.44E05
C109	SC [*1]FGGRMDRIGAQSGLGC [*1]NSFRY [M+4H]$^{4+}$	620.7803	19.97	ND	7.32E04
C111	SSC [*1]FGGRMDRIGAQSGLGC [*1]NSF [M+3H]$^{3+}$	749.9938	20.4	ND	9.74E03
C112	SC [*1]FGGRMDRIGAQSGLGC [*1]NSF [M+3H]$^{3+}$	720.9815	20.46	ND	9.96E03

ND: Not detected.

Fig. 5. Metabolite profile of cyclic peptides incubated in rat liver S9. (A) Insulin; (B) ANP. *represents the metabolite containing disulfide bond.

Table 4
The representative identification of ANP metabolites in rat liver S9 with isotopic MS1 ions.

Peak ID	Name	m/z	Charge	Peak index	% Score
1	FGGRMD [M+2H]$^{2+}$	341.6519	2	0	57.1
2	Loss of 1611.8223 [M+3H]$^{3+}$	489.8823	3	0	0.8
3	Loss of 2594.2036 [M+H]$^{+}$	485.2511	1	0	0
4	RIGAQSGLGCNS [M+2H]$^{2+}$	581.7858	2	0	52.1
5	Loss of 2691.2006 [M+H]$^{+}$	388.2541	1	0	0
6	Loss of 2647.1743 [M+H]$^{+}$	432.2804	1	0	0
7	Loss of 2603.1491 [M+H]$^{+}$	476.3056	1	0	0
8	Loss of 2767.2596 [M+H]$^{+}$	312.1951	1	0	0
9	Loss of 2559.1217 [M+H]$^{+}$	520.333	1	0	0
10	SLRRSSC [*1]FGGRMDRIGAQSGLGC [*1]NS [M+4H]$^{4+}$	654.0593	4	1	54.4
11	SLRRSSC [*1]FGGRMDRIGAQSGLGC [*1]NS + Loss of Water [M+5H]$^{5+}$	519.8473	5	1	50
12	SLRRSSC [*1]FGGRMDRIGAQSGLGC [*1]NS [M+5H]$^{5+}$	523.4488	5	1	50.9
13	SLRRSSC [*1]FGGRMDRIGAQSGLGC [*1]NS [M+3H]$^{3+}$	871.7447	3	1	53
14	RSSC [*1]FGGRMDRIGAQSGLGC [*1]NS [M+4H]$^{4+}$	565.0045	4	1	48.4
15	Loss of 2626.1117 [M+H]$^{+}$	453.343	1	0	0
16	SLRRSSC [*1]FGGRMDRIGAQSGLGC [*1]NSFR [M+5H]$^{5+}$	584.0816	5	1	45.1
17	Loss of 2515.0960 [M+H]$^{+}$	564.3587	1	0	0
18	RIGAQSGLGCNSF [M+2H]$^{2+}$	655.3193	2	0	53.4
19	Parent [M+5H]$^{5+}$	616.6947	5	1	51

Table 5
The sequence identification of an ANP metabolite M4 based on fragments assignment.

Auto-generated	Rank	MSMS peak area assigned (%)	Proposed sequences	AA index	Apply to results	Fragments assigned
TRUE	1	23.80	RIGAQSGLGCNSF	AA (10—22)	TRUE	9
TRUE	2	4.80	IGAQSGLGCNSFR	AA (11—23)	FALSE	3

stability of therapeutic peptides is the structural modification; considering potential modifications and their sites will increase the number of potential metabolites to be searched for. For instance, MetabolitePilot™ Software proposed five potential metabolite sequences listed in Table 6, and four of them were linear peptides with serine amino acid residue replaced with oxoalanine at various locations. By utilizing the MS/MS spectrum information, metabolite sequence SSC [*1]FGGRMDRIGAQSGLGC [*1]NSFRY, having a disulfide bond between cysteines at positions 3 and 19, was selected

with 37 fragments matched.

4. Conclusions

Detection and structural characterization of cyclic peptide metabolites in biological matrices represent great analytical challenges. The expanded MetabolitePilot™ Software 2.0 offers multiple mechanisms for targeted and non-targeted searching for intact cyclic peptide metabolites with cyclic or linear structures

Table 6
The characterization of ANP metabolite C108 (Table 3) based on fragment assignments to isomeric linear and non-linear sequences.

Auto-generated	Rank	TIC intensity assigned	MSMS peak area assigned (%)	Proposed sequences	Fragments assigned
TRUE	1	483.6	7.20	SSC [*1]FGGRMDRIGAQSGLGC [*1]NSFRY	37
TRUE	2	403.6	6.00	SSCFGGRMDRIGAQS [SOa]GLGCNSFRY	19
TRUE	2	403.6	6.00	SSCFGGRMDRIGAQSGLGCNS [SOa]FRY	19
TRUE	3	356	5.30	S [SOa]SCFGGRMDRIGAQSGLGCNSFRY	18
TRUE	3	356	5.30	SS [SOa]CFGGRMDRIGAQSGLGCNSFRY	18

through processing LC/HRMS data sets, followed by automated sequence confirmation and structural identification of these metabolites (Fig. 2). Results from analyzing predicted metabolites of insulin formed by the hydrolysis of trypsin and chymotrypsin demonstrated that the approach is capable of rapidly finding and identifying metabolic products of cyclic peptides. Additionally, the features and characterization tools integrated in the software allowed for the confirmation of metabolite sequences and ranking of competing assignments. The example of applying the HRMS-based data processing tool for the direct detection and identification of unknown metabolites of insulin and ANP in rat liver S9 without reducing their disulfide bond or enzymatic hydrolysis, further indicated that it is useful for studying in vitro biotransformation of cyclic peptides with a variety of linkage structures. Potential applications of the analytical approach at the stage of drug discovery include metabolic soft spot analysis of cyclic peptides in lead optimization and in vitro metabolism comparison across species in clinical candidate characterization. The effectiveness of this workflow for analyzing in vivo metabolites of cyclic peptides remains to be evaluated, which will face additional challenges due to the interference by a large number of endogenous peptides.

Conflicts of interest

The authors declare that there are no conflicts of interest.

Appendix A. Supplementary data

Supplementary data to this article can be found online at https://doi.org/10.1016/j.jpha.2020.05.012.

References

[1] S.H. Joo, Cyclic Peptides as therapeutic agents and biochemical tools, Biomol. Ther. 20 (2012) 19—26. http://doi:10.4062/biomolther.2012.20.1.019.
[2] T.B. Andrew, M.M. Cayla, R.S. Lokey, Form and function in cyclic peptide natural products: a pharmacokinetic perspective, Curr. Top. Med. Chem. 13 (2013) 821—836, https://doi.org/10.2174/1568026611313070005.
[3] T. Anthi, M. Minos-Timotheos, S. Carmen, et al., Review cyclic peptides on a merry-go-round: towards drug design, Peptide Sci 104 (2015) 453—461. http://doi:10.1002/bip.22669.
[4] A. Fahr, Cyclosporin clinical pharmacokinetics, Clin. Pharmacokinet. 24 (1993) 472—495. http://10.2165/00003088-199324060-00004.
[5] S.A. Kates, N.A. Solé, C.R. Johnson, et al., A novel, convenient, three-dimensional orthogonal strategy for solid-phase synthesis of cyclic peptides, Tetrahedron Lett. 34 (1993) 1549—1552, https://doi.org/10.1016/0040-4039(93)85003-F.
[6] R.G. Hall, K.D. Payne, A.M. Bain, et al., Multicenter evaluation of vancomycin dosing: emphasis on obesity, Am. J. Med. 121 (2008) 515—518. http://doi:10.1016/j.amjmed.2008.01.046.
[7] E. Emanuele, M. Arra, S. Pesenti, Vasopressin and oxytocin as neurohormonal mediators of MDMA (ecstasy) sociosexual behavioural effects, Med. Hypotheses 67 (2006) 1250—1251. http://doi:10.1016/j.mehy.2006.05.021.
[8] S. Bellary, A.H. Barnett, Inhaled insulin: new technology, new possibilities, Int. J. Clin. Pract. 60 (2006) 728—734. http://doi:10.1111/j.1742-1241.2006.00976.x.
[9] S.K. Sia, P.A. Carr, A.G. Cochran, et al., Short constrained peptides that inhibit HIV-1 entry, Proc. Natl. Acad. Sci. U.S.A. 99 (2002) 14664—14669, https://doi.org/10.1073/pnas.232566599.
[10] Y. Gao, T. Kodadek, Direct comparison of linear and macrocyclic compound libraries as a source of protein ligands, ACS Comb. Sci. 17 (2005) 190—195. http://doi:10.1021/co500161c.
[11] G. Luca, M.R. De, C. Lucia, Chemical modifications designed to improve peptide stability: incorporation of non-natural amino acids, pseudo-peptide bonds, and cyclization, Curr. Pharmaceut. Des. 16 (2010) 3185—3203, https://doi.org/10.2174/138161210793292555.
[12] L. Di, Strategic approaches to optimizing peptide ADME properties, AAPS J. 17 (2015) 134—143. http://doi:10.1208/s12248-014-9687-3.
[13] T. Rezai, B. Yu, G.L. Millhauser, et al., Testing the conformational hypothesis of passive membrane permeability using synthetic cyclic peptide diastereomers, J. Am. Chem. Soc. 128 (2006) 2510—2511. http://doi:10.1021/ja0563455.
[14] K.B. Christopher, A.J.O. Richard, Gas-phase peptide fragmentation: how understanding the fundamentals provides a springboard to developing new chemistry and novel proteomic tools, J. Mass Spectrom. 43 (2008) 1301—1319. http://doi:10.1002/jms.1469.
[15] G.H. Alex, To b or not to b: the ongoing saga of peptide b ions, Mass Spectrom. Rev. 28 (2009) 640—654. http://doi:10.1002/mas.20228.
[16] H. Chi, H. Chen, K. He, et al., pNovo+: de novo peptide sequencing using complementary HCD and ETD tandem mass spectra, J. Proteome Res. 12 (2013) 615—625.
[17] L.D. Quan, M. Liu, CID, ETD and HCD fragmentation to study protein post-translational modifications, Mod. Chem. Appl. 1 (2013) e102. http://doi:10.4172/2329-6798.1000e102.
[18] K.F. Medzihradszky, J.M. Campbell, M.A. Baldwin, et al., The characteristics of peptide collision-induced dissociation using a high-performance MALDI-TOF/TOF tandem mass spectrometer, Anal. Chem. 72 (2000) 552—558. http://doi:10.1021/ac990809y.
[19] V.H. Wysocki, K.A. Resing, Q. Zhang, et al., Mass spectrometry of peptides and proteins, Methods 35 (2005) 211—222, https://doi.org/10.1016/j.ymeth.2004.08.013.
[20] A.P. Ioannis, The interpretation of collision-induced dissociation tandem mass spectra of peptides, Mass Spectrom. Rev. 14 (1995) 49—73. http://doi:10.1002/mas.1280140104.
[21] P. Béla, S. Sándor, Fragmentation pathways of protonated peptides, Mass Spectrom, Rev 24 (2005) 508—548. http://doi:10.1002/mas.20024.
[22] M. Strohalm, D. Kavan, P. Novák, et al., mMass 3: a cross-platform software environment for precise analysis of mass spectrometric data, Anal. Chem. 82 (2010) 4648—4651.
[23] F. Rusconi, massXpert 2: a cross-platform software environment for polymer chemistry modelling and simulation/analysis of mass spectrometric data, Bioinformatics 25 (2009) 2741—2742. http://doi:10.1093/bioinformatics/btp504.
[24] J. Swaminathan, S. Varatharajan, Peptide fragment ion analyzer (PFIA): a simple and versatile tool for the interpretation of tandem mass spectrometric data and de novo sequencing of peptides, Rapid Commun. Mass Spectrom. 21 (2007) 3033—3038. http://doi:10.1002/rcm.3179.
[25] E. Ciccimaro, A. Ranasinghe, C. D'Arienzo, et al., Strategy to improve the quantitative LC-MS analysis of molecular ions resistant to gas-phase collision dissociation: application to disulfide-rich cyclic peptides, Anal. Chem. 86 (2014) 11523—11527, https://doi.org/10.1021/ac502678y.
[26] Y.Q. Xia, E. Ciccimaro, N. Zheng, et al., Differential mobility spectrometry combined with multiple ion monitoring for bioanalysis of disulfide-bonded peptides with inefficient collision-induced dissociation fragmentation, Bioanalysis 9 (2017) 183—192. http://doi:10.4155/bio-2016-0190.
[27] Y. Fu, Y. Xia, J. Flarakos, et al., Differential mobility spectrometry coupled with multiple ion monitoring in regulated LC-MS/MS bioanalysis of a therapeutic cyclic peptide in human plasma, Anal. Chem. 88 (2016) 3655—3661, https://doi.org/10.1021/acs.analchem.5b04408.
[28] R.J. Arnold, N. Jayasankar, D. Aggarwal, et al., A machine learning approach to predicting peptide fragmentation spectra, P. Pac. Symp. Biocomput. 11 (2006) 219—230, https://doi.org/10.1142/9789812701626_0021.
[29] A.M. Frank, Predicting intensity ranks of peptide fragment ions, J. Proteome Res. 8 (2009) 2226—2240. http://doi:10.1021/pr800677f.
[30] B.J.M. Webb-Robertson, W.R. Cannon, Current trends in computational inference from mass spectrometry-based proteomics, Briefings Bioinf. 8 (2007) 304—317. http://doi:10.1093/bib/bbm023.
[31] S. Li, R.J. Arnold, H. Tang, et al., On the accuracy and limits of peptide fragmentation spectrum prediction, Anal. Chem. 83 (2011) 790—796, https://doi.org/10.1021/ac102272r.
[32] Z. Zhang, Prediction of low-energy collision-induced dissociation spectra of peptides, Anal. Chem. 76 (2004) 3908—3922, https://doi.org/10.1021/ac049951b.
[33] I.B. Hirsch, Insulin analogues, N. Engl. J. Med. 352 (2005) 174—183. http://doi:10.1056/NEJMra040832.
[34] R.B. Philippe, Structure activity in the atrial natriuretic peptide (ANP) family, Med. Res. Rev. 10 (1990) 115—142. http://doi:10.1002/med.26.
[35] J.V. Olsen, S. Ong, M. Mann, Trypsin cleaves exclusively C-terminal to arginine and lysine residues, Mol. Cell. Proteomics 3 (2004) 608—614. http://doi:10.1074/mcp.T400003-MCP200.
[36] J. Feher, 8.5 Digestion and Absorption of the Macronutrients, Quantitative Human Physiology, second ed., Academic Press, Boston, 2017, pp. 821—833.
[37] J.L. Lau, M.K. Dunn, Therapeutic peptides: historical perspectives, current development trends, and future directions, Bioorg. Med. Chem. 26 (2018) 2700—2707, https://doi.org/10.1016/j.bmc.2017.06.052.
[38] M. Yao, B. Chen, W. Zhao, et al., LC-MS differential analysis for fast and sensitive determination of biotransformation of therapeutic proteins, Drug Metab. Dispos. 46 (2018) 451—457. Epub 2018 Jan 31, https://doi: 10.1124/dmd.117.077792.

Original article

Quantitation of DNA by nuclease P1 digestion and UPLC-MS/MS to assess binding efficiency of pyrrolobenzodiazepine

Yong Ma[*], Buyun Chen, Donglu Zhang[**]

Drug Metabolism and Disposition, Genentech, 1 DNA Way, South San Francisco, CA, 94080, USA

A B S T R A C T

Accurate DNA quantitation is a prerequisite in many biomedical and pharmaceutical studies. Here we established a new DNA quantitation method by nuclease P1 digestion and UPLC-MS/MS analysis. DNA fragments can be efficiently hydrolyzed to single deoxyribonucleotides by nuclease P1 in a short time. The decent stabilities of all the four deoxyribonucleotides were confirmed under different conditions. Deoxyadenosine monophosphate (dAMP) was selected as the surrogate for DNA quantitation because dAMP showed the highest sensitivity among the four deoxyribonucleotides in the UPLC-MS/MS analysis. The linear range in DNA quantitation by this method is 1.2–5000 ng/mL. In the validation, the inter-day and intra-day accuracies were within 90%–110%, and the inter-day and intra-day precision were acceptable (RSD < 10%). The validated method was successfully applied to quantitate DNA isolated from tumors and organs of a mouse xenograft model. Compared to the quantitation methods using UV absorbance, the reported method provides an enhanced sensitivity, and it allows for the accurate quantitation of isolated DNA with contamination of RNA and ribonucleotide.
© 2020 Xi'an Jiaotong University. Production and hosting by Elsevier B.V. This is an open access article under the CC BY-NC-ND license (http://creativecommons.org/licenses/by-nc-nd/4.0/).

1. Introduction

As the carrier of genetic information, DNA is essentially involved in a lot of modern chemical, biological and pharmacological studies. The methods of DNA isolation from different organisms have been maturely developed, and various commercial kits are available to provide a convenient and productive DNA isolation. In general, accurate quantitation of isolated DNA is not always necessary before the sequential step of characterization or application. For example, polymerase chain reaction (PCR) and PCR-based DNA sequencing usually characterize DNA qualitatively or only semi-quantitatively. Meanwhile, DNA itself is also a therapeutic target of drugs including intercalating agents, alkylating agents, DNA cutters and many more [1]. The inhibition of DNA replication can serve as an efficacious therapeutic strategy in the treatment of multiple diseases including cancers and virus infections. Pyrrolo-benzodiazepine (PBD-dimer) is a DNA minor groove binder that forms covalent DNA interstrand cross-links in a sequence-dependent manner (Fig. 1) and exhibits broad-spectrum sub-nanomolar antiproliferative activities against a variety of cancer cell lines [2]. In the studies involving DNA alkylating agents like PBD-dimer, accurate quantitation of DNA becomes necessary in evaluating DNA adduct occurrence [2]. Conventionally, the concentrations of DNA solutions can be roughly determined by UV absorbance [3]. Although the integrity of DNA fragments is kept by the UV absorbance method, the limitations of this method are also prominent: its low sensitivity and lack of robustness [4]. The UV absorbance method usually tends to overestimate DNA concentrations, especially when isolated DNA is contaminated by RNA or ribonucleotides [5,6]. Fluorescent dyes can help determine low DNA concentrations, but the sensitivity and accuracy are impacted by the various binding affinities between dyes and DNA fragments [7].

DNA adducts are usually released via DNA hydrolysis, making the post-hydrolysis quantitation of DNA feasible. The method can be easily integrated with the steps of DNA adducts isolation and quantitation [2]. DNA quantitation methods by hydrolysis, either chemically or enzymatically, have been introduced previously. Chemical hydrolysis of DNA usually requires harsh conditions which may change the structure of DNA adducts. Therefore, enzymatic digestion of DNA under physiological conditions is preferred in some cases. After digestion, DNA hydrolysis products can be

---

Peer review under responsibility of Xi'an Jiaotong University.

* Corresponding author.
** Corresponding author.
   E-mail addresses: yongma87@gmail.com (Y. Ma), zhangd38@gene.com (D. Zhang).
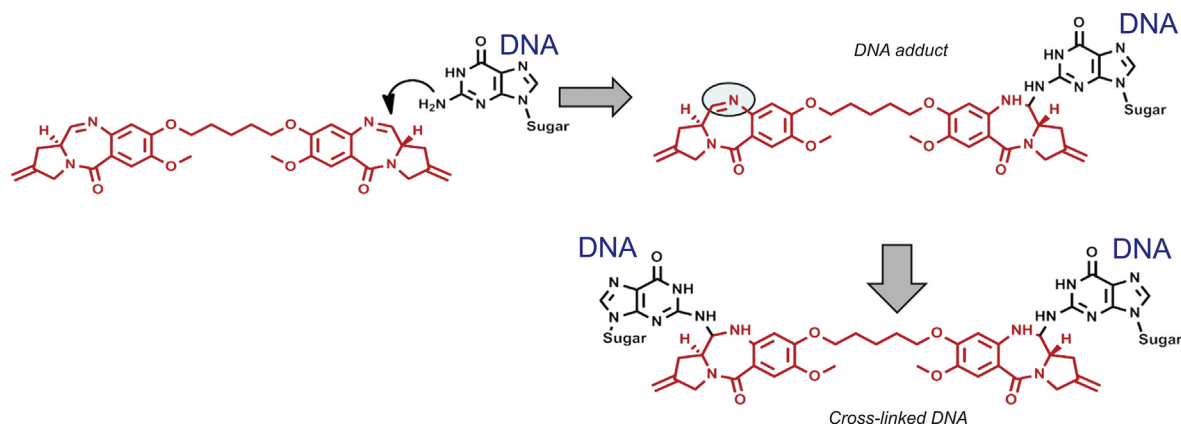
Fig. 1. The scheme of DNA alkylkation by pyrrolobenzodiazepine (PBD-dimer).

analyzed by high performance liquid chromatography (HPLC) coupled with a UV detector. For example, Shimelis et al. [4] and Li et al. [8] established a nuclease P1 digestion/HPLC-UV method to quantitate DNA, and the DNA concentrations determined by this method were almost identical to those determined by the acid hydrolysis/HPLC-UV method. The hydrolysis/HPLC-UV methods were also found to be more reliable than non-hydrolysis methods including the dye-binding or direct UV spectrophotometric assays [4]. Herein, by coupling tandem mass spectrometer (MS/MS) with nuclease P1 hydrolysis and reversed-phase UPLC, we developed a sensitive and efficient method to determine DNA concentration. The method has been fully validated and demonstrated to be useful in the quantitation of DNA isolated from tumors and organs in a mouse xenograft model, and it has been successfully applied to assess the DNA-alkylating efficiency of the PBD-dimer.

2. Experimental

2.1. Chemicals and reagents

Calf thymus (CT) DNA was purchased from Rockland Immuno-chemicals (Pottstown, PA, USA). Deoxyadenosine monophosphate (dAMP), thymidine monophosphate (TMP), deoxycytidine mono-phosphate (dCMP), deoxyguanosine monophosphate (dGMP), adenosine monophosphate (AMP), uridine monophosphate (UMP), cytidine monophosphate (CMP), guanosine monophosphate (GMP), nuclease P1 and deoxyribonuclease I (DNase I) were pur-chased from Sigma-Aldrich (St. Louis, MO, USA). Inosine mono-phosphate (IMP) was purchased from Cayman Chemical (Ann Arbor, MI, USA). DNeasy Blood & Tissue Kit was purchased from Qiagen (Valencia, CA, USA). Acetonitrile and water (MS grade) were purchased from EMD (Gibbstown, NJ, USA).

2.2. DNA digestion efficiency by enzymes

The DNA digestion by DNase I or nuclease P1 was initially characterized to determine whether they can digest DNA polymer to single deoxyribonucleotides. To test the DNA digestion efficiency of DNase I, 10 μg/mL CT DNA was incubated with 300 unit/mL DNase I for 2 h. The DNA digestion efficiency of nuclease P1 was further investigated to determine the amount of enzyme used and incubation time length. 190 μL of CT DNA solution (10 or 100 μg/mL) was mixed with different concentrations of nuclease P1 in 10 μL of water (0.1, 0.01 or 0.001 unit) and then incubated at 37 °C for different time lengths (0, 1, 2, 3, and 4 h). After digestion, the samples were diluted 200-fold in water. An aliquot of 200 μL

diluted samples was mixed with 50 μL IMP in water (50 ng/mL) as the internal standard (IS) before UPLC-MS/MS analysis.

2.3. UPLC-MS/MS quantitation

The deoxyribonucleotides produced from DNA hydrolysis were analyzed on a Shimadzu Nexera HPLC system (Columbia, MD, USA) coupled to a Sciex API 6500 triple quadrupole mass spectrometer with an IonDrive Turbo V source (Sciex, Foster City, CA, USA) in positive ion mode. The conditions were as follows: column, Phe-nomenex XB-C_{18} (100 mm × 2.1 mm, 2.6 μm); mobile phase A, water with 0.1% formic acid; mobile phase B, acetonitrile with 0.1% formic acid; gradient, 0–1.0 min, 0% B, 1.0–2.0 min, 0%–5% B, 2.0–2.5 min, 5%–95% B, 2.5–3.0 min, 95% B, 3.0–3.5 min, 95%–0% B, 3.5–4.0 min, 0% B; flow rate, 1.0 mL/min; column temperature, 50 °C; and injection volume, 10 μL.

The deoxyribonucleotides were quantitated in the multiple re-action monitoring (MRM) scan in the positive mode. The compound-dependent parameters are listed in Table 1, and the main instrument-dependent parameters were set as follows: ion-spray voltage, 5500 V; ion source temperature, 500 °C; collision gas (CAD), -3; curtain gas (CUR), 30; nebulizer gas (GS1), 60; and turbo gas (GS2), 60.

2.4. Method validation

2.4.1. Stability and sensitivity of deoxyribonucleotides

Stability of the four deoxyribonucleotides in water was deter-mined by analyzing QC samples ($n = 6$) under different tempera-ture conditions (at 90 °C for 30 min and at −80 °C for 14 days) or through three freeze-thaw cycles (−80 °C–25 °C). A signal-to-noise ratio of at least 10:1 was used as the principle criterion to deter-mine the lower limit of quantification (LLOQ). Among the four de-oxyribonucleotides, one with adequate stability and best sensitivity in MS analysis will be selected as a surrogate in DNA quantitation.

2.4.2. Calibration curve of DNA

Different concentrations of CT DNA in water were prepared as the standard samples to establish a calibration curve. After diges-tion by nuclease P1 and UPLC-MS/MS analysis, the peak area ratios of dAMP to IS were calculated and correlated with CT DNA con-centrations by a least-squares linear regression method with $1/x^2$ weighting ($R^2 > 0.9995$).

2.4.3. Precision and accuracy

In the method validation, the precision and accuracy was

Table 1
Compound-dependent parameters in MS/MS analysis of mono-deoxyribonucleotides.

Analyte	Q1(m/z)	Q3(m/z)	Dwell times (ms)	DP(V)	EP(V)	CE(V)	CXP(V)
dAMP	332	136	50	41	10	21	10
dTMP	323	207	50	26	10	9	14
dCMP	308	112	50	31	10	15	8
dGMP	348	152	50	31	10	17	12
IMP	349	137	50	41	10	17	12

evaluated by quantitating the QC samples prepared at the concentrations ($n = 6$ for each concentration). The inter-day and intra-day precision and accuracy were calculated from the results of QC sample quantification on the same day and on three different days, respectively.

2.5. DNA extraction from tumors and organs of xenograft mice

The establishment of subcutaneous xenograft mouse model, administration of an anti-CD22 THIOMAB™ antibody pyrrolo-benzodiazepine (PBD)-dimer conjugate (with a cyclobutyl-containing disulfide linker), and sample collection were described previously [2,9]. The tumor, liver, lung and kidney were weighed and then homogenized in 4-fold weight of ice-cold PBS. DNA from 75 μL of homogenates was isolated by DNeasy Blood & Tissue Kit following instructions with modifications. After the first loading of tissue lysate, the flow-through was loaded two more times to ensure the best column binding of DNA. The columns were washed sequentially by two wash buffers (containing approximately 50% ethanol) provided in the kit. In the last step, DNA column was eluted with 200 μL water twice and the elute was combined.

2.6. Release of PBD-dimer from DNA and quantitation

To digest DNA, 0.001 unit of nuclease P1 in 10 μL water was added to 190 μL of mouse organ or tumor DNA sample and then incubated at 37 °C for 1 h. Digested samples were heated at 90 °C for 30 min to release the PBD-dimer.

The post-heating samples were aliquoted for the separate quantitation of DNA and PBD-dimer. For DNA quantitation, an aliquot of the post-heating samples was diluted in water by 200-fold. Before LC-MS/MS injection, 200 μL of diluted sample was mixed with 50 μL of 50 ng/mL IMP in water as the IS. CT DNA was dissolved in water at various concentrations between 5 and 5000 ng/mL to serve as the standard curve for the DNA quantitation. For the quantitation of PBD-dimer, a standard curve of PBD-dimer can be made in either pure water or 100 μg/mL CT solution. The standard curve samples made in CT DNA were incubated at 37 °C for 1 h before digestion and heating to ensure completion of DNA alkylation [2,9]. It was observed that two standard curves in water and DNA solutions superimposed each other very well, indicating that the presence of deoxyribonucleotides did not impact the recovery and quantitation of PBD-dimer. Also, PBD-dimer was confirmed to be stable in the absence of DNA, as well as at high temperature (90 °C). Thus, quantitative recovery of PBD-dimer from tissue DNA samples can be expected after the digestion and heating process. The LC-MS/MS method for PBD-dimer has been described previously [2,9].

The calculation of PBD-DNA adducts abundance is based on the results of DNA and PBD-dimer quantitation. The mass of DNA was converted to the number of base pairs, based on an average DNA base pair molecular weight as 650 Da. The final results were shown as the adduct numbers per 10^6 base pairs.

2.7. DNA quantitation by UV

The absorbance readings of DNA or DNA/nucleotides samples at different wavelengths (230, 260, and 280 nm) were determined by a NanoDrop 8000 spectrophotometer (NanoDrop Technologies Inc., Wilmington, DE, USA). The DNA concentrations were calculated from the absorbance reading at 260 nm (1 OD260 unit = 50 μg/mL pure DNA).

3. Results and discussion

3.1. Chromatography and mass spectrometry

MRM transitions and parameters for the quantitation of de-oxyribonucleotides were determined by manual tuning (Table 1). For a better ionization in the source, 0.1% formic acid in water and 0.1% formic acid in acetonitrile were used as the mobile phase A and B, respectively. Multiple reversed-phase columns were tested and Phenomenex XB-C$_{18}$ column (100 mm × 2.1 mm, 2.6 μm) was selected to provide the best retention and peak shape. To improve the peak shape of hydrophilic analytes, the column temperature was set as 50 °C and the flow rate was set as 1 mL/min. In the liquid chromatography, the retention times of dAMP, TMP, dCMP and dGMP were 1.41, 0.98, 0.54 and 1.22 min, respectively. IMP, a ribonucleotide with a similar structure, was selected as the internal standard in the quantitation. The retention time of IMP is 0.80 min (Fig. 2A).

3.2. The DNA digestion efficiency of nuclease P1

Incubation with nuclease P1 completely digested CT DNA to single deoxyribonucleotides (Fig. 2B). To figure out whether nuclease P1 can be substituted by another commonly used DNA-cutting enzyme, DNase I, the cleavage of CT DNA by DNase I was also tested. The result showed that no single deoxyribonucleotides were released, indicating that DNase I can only cut DNA into smaller fragments or oligos (Fig. 2E).

The DNA digestion efficiency of nuclease P1 was investigated to determine the amount of nuclease P1 needed to digest certain unit weight of DNA and the appropriate incubation time as well. Relatively high concentration DNA solutions (10 or 100 μg/mL) was digested by different concentrations of nuclease P1 (final concentrations as 0.5, 0.05 and 0.005 unit/mL) for various periods of time (0, 1, 2, 3 and 4 h). Based on the peak areas of deoxyribonucleotides, it was observed that the digestion of DNA by nuclease P1 was completed very quickly in all the incubations (Fig. 3). With the lowest enzyme concentration tested (0.005 unit/mL), the digestion of 100 μg/mL DNA was finished within 1 h of incubation at 37 °C. With 0.5 or 0.05 unit/mL nuclease P1, the digestion was almost 100% completed even before the 37 °C incubation began, indicating the great efficiency of nuclease P1 in DNA digestion. Therefore, 0.005 unit/mL nuclease P1 and 1 h, 37 °C incubation were selected as the conditions for DNA digestion.
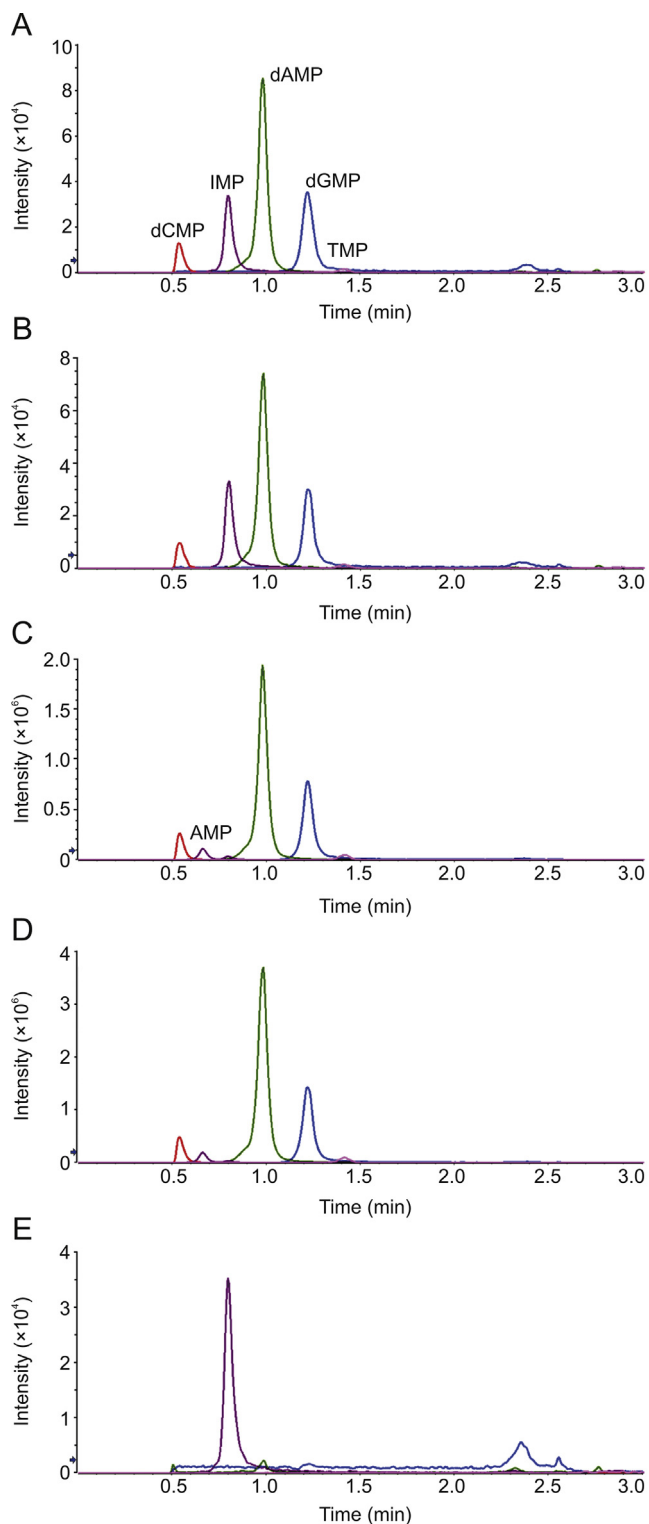
Fig. 2. Representative chromatograms in UPLC-MSMS analysis: (A) 20 ng/mL equimolar mixture of the 4 deoxyribonucleotides; (B) 20 ng/mL CT DNA after nuclease P1 digestion; (C) 100 μg/mL CT DNA spiked with 100 μg/mL ribonucleotide equimolar mixture, after nuclease P1 digestion (200-fold diluted before injection); (D) DNA isolated from mouse tumor, after nuclease P1 digestion (200-fold diluted before injection); (E) 20 ng/mL CT DNA after DNase I digestion.
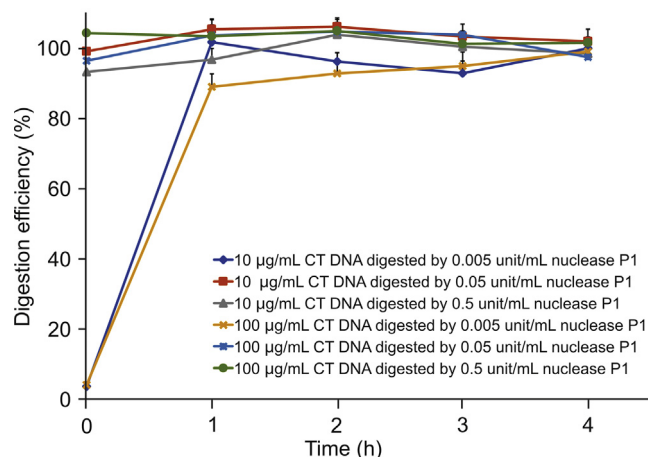
Fig. 3. The time course of calf thymus DNA digestion by nuclease P1. 10 or 100 μg/mL calf thymus DNA was incubated with 0.005–0.5 units/mL nuclease P1 for up to 4 h to determine the digestion efficiency.

3.3. Method validation

3.3.1. Stability of deoxyribonucleotides

The stability of deoxyribonucleotides was investigated under different conditions, including at high temperature for a short time (90 °C for 30 min), low temperature for long-term storage (−80 °C for 14 days), and undergoing repeated freeze-thaw action (3 cycles). These conditions were selected to assess the potential impact of practical operations on post-digestion DNA quantitation. In all the tests, the four deoxyribonucleotides exhibited excellent stability, with almost 100% remaining after all the treatments (Table 2). The confirmed stability of dAMP, TMP, dCMP, and dGMP indicated that deoxyribonucleotides derived from DNA digestion can serve as solid surrogates in DNA.

3.3.2. Sensitivity and linearity

Using authentic deoxyribonucleotides as standards, the LC-MS/MS method was found to be with various sensitivities in detecting each of them. The LLOQs for dAMP, TMP, dCMP, and dGMP were determined as 0.3, 4.8, 1.2 and 1.2 ng/mL, respectively. Therefore, dAMP was selected as the surrogate after DNA hydrolysis by nuclease P1, and the linear range for DNA quantitation was determined as 1.2–5000 ng/mL. DNA isolated from cell or tissue samples with a concentration higher than 5000 ng/mL should be appropriately diluted before quantitation.

3.3.3. Accuracy and precision

Six replicate CT DNA samples at three concentrations (10, 100, and 1000 ng/mL) as QC were measured to determine the intra-day and inter-day accuracy and precision. The results shown in Table 3 indicate that for both intra-day and inter-day, the accuracies were always between 90%–110% and the precisions were within the acceptable range (relative standard deviation lower than 10%).

3.4. The quantitation of DNA isolated from tissue samples

In addition to the enhanced sensitivity, the superiority of DNA quantitation by nuclease P1 digestion and UPLC-MS/MS over the

Table 2
LC retention times, LC-MS linear ranges, and stabilities of deoxyribonucleotides.

Analyte	Retention time (min)	Linear range (ng/mL)	Concentration (ng/mL)	Stability (%)		
				90 °C, 30 min	−80 °C, 14 days	Freeze-thaw 3 cycles
dAMP	1.41	0.3–1250	2.5	106.2 ± 3.7	99.7 ± 4.4	100.8 ± 5.1
			25	106.4 ± 5.0	98.7 ± 3.0	99.1 ± 3.3
			250	105.0 ± 5.3	97.0 ± 2.8	99.5 ± 3.3
TMP	0.98	4.8–1250	2.5	90.4 ± 9.5	102.3 ± 7.0	89.1 ± 10.9
			25	101.8 ± 6.1	96.4 ± 4.5	96.7 ± 4.3
			250	104.2 ± 2.3	98.1 ± 1.6	100.6 ± 2.5
dCMP	0.54	1.2–1250	2.5	100.7 ± 6.3	96.9 ± 2.3	97.6 ± 4.7
			25	102.3 ± 5.0	99.5 ± 1.9	100.5 ± 3.3
			250	105.3 ± 3.1	99.3 ± 2.6	100.4 ± 2.4
dGMP	1.22	1.2–1250	2.5	95.5 ± 8.2	102.6 ± 2.6	95.4 ± 4.2
			25	100.0 ± 5.8	99.3 ± 1.3	96.7 ± 4.4
			250	104.1 ± 4.1	99.0 ± 1.0	100.4 ± 2.5

Table 3
Method validation for LC-MS/MS analysis of DNA.

Analyte	Linear range (ng/mL)	Concentration (ng/mL)	Intra-day		Inter-day	
			Accuracy (bias, %)	Precision (RSD[b], %)	Accuracy (bias, %)	Precision (RSD[b], %)
CT DNA[a]	1.2–5000	10	107.8	5.1	110.0	7.0
		100	95.7	6.8	105.4	9.0
		1000	101.8	4.9	101.3	4.3

[a] CT DNA, calf thymus DNA.
[b] RSD, relative standard deviation.

traditional UV absorbance method was further examined. DNA isolated by commercial kits is often contaminated by RNA unless the samples are pre-treated with RNase before extraction [10,11]. In the presence of RNA or RNA-derived ribonucleotides, a higher UV absorbance can be expected and it will lead to an overestimation of DNA concentrations. For example, after samples containing known concentrations of CT DNA were spiked with ribonucleotides, the accurate DNA concentration could not be determined by the UV absorbance method (Table 4). The direct quantitation of DNA by UV absorbance relies on both relatively high DNA concentration and good DNA purity. The HPLC-UV method may exclude the inferences from RNA or ribonucleotides by separating the peaks in the chromatography, which takes more efforts in the LC method

development. Quantitation of DNA by digestion and LC-MS/MS is not limited by the purity of DNA samples. CT DNA was still accurately quantitated by this method after spiked with ribonucleotides (Fig. 2C), indicating that the signal channels of deoxyribonucleotides in mass spectrometry were not impacted by the presence of RNA or ribonucleotides (Table 4).

3.5. The PBD-DNA abundance in the mouse tumors and organs

Previously, we reported the in vitro and in vivo characterization of antibody-drug conjugates (ADCs) bearing a PBD-dimer as the cytotoxic payload [2,9]. To fully assess the anti-tumor efficacy of the ADCs in a mouse xenograft model, the abundance of DNA-PBD

Table 4
Comparative quantitation of DNA by UV and LC-MS/MS of dAMP after DNA hydrolytic digestion.

Sample	UV absorbance				Concentration determined by LC-MS/MS (µg/mL)
	A260	A260/230	A260/A280	Concentration determined by UV (µg/mL)	
100 µg/mL CT DNA[a]	1.99	2.40	1.70	99.4	102.2
100 µg/mL CT DNA + 50 µg/mL XMP mix	3.34	2.51	1.85	166.8	108.1
100 µg/mL CT DNA + 100 µg/mL XMP mix	4.67	2.55	1.94	233.7	109.2
500 µg/mL CT DNA	9.76	2.41	1.72	488.1	504.8
500 µg/mL CT DNA + 250 µg/mL XMP mix	16.93	2.52	1.84	846.5	529.2
500 µg/mL CT DNA + 500 µg/mL XMP mix	23.38	2.52	1.94	1169.0	492.9
DNA extracted from mouse lung 1	3.52	1.99	2.04	176.0	61.6
DNA extracted from mouse lung 2	1.55	1.98	1.94	77.7	71.2
DNA extracted from mouse liver 1	10.09	2.11	2.05	504.3	50.4
DNA extracted from mouse liver 2	15.84	2.12	2.05	791.8	84.0
DNA extracted from mouse kidney 1	7.25	2.02	2.02	362.5	150.4
DNA extracted from mouse kidney 2	7.32	2.11	2.06	365.8	109.1
DNA extracted from mouse tumor 1	8.39	2.11	1.99	419.7	191.1
DNA extracted from mouse tumor 2	16.92	2.14	2.01	846.2	262.2

[a] CT DNA, calf thymus DNA.
[b] XMP mix, equimolar mixture of AMP, UMP, CMP, and GMP.

Table 5
DNA isolation and PBD-dimer recovery in tumor and major organs from xenograft mice after the administration of an anti-CD22 THIOMAB™ antibody PBD-dimer conjugate (with a cyclobutyl-containing disulfide linker).

ADC	Time (h)	DNA extracted (mg/g tissue)				PBD-dimer recovered (pmol/g tissue)			
		Tumor	Liver	Kidney	Lung	Tumor	Liver	Kidney	Lung
Cyclobutyl-containing	24	5.5	2.1	2.0	1.9	73.7	2.8	< LLOQ	3.2
ADC	96	3.8	2.3	1.8	1.8	234.5	3.1	< LLOQ	2.8

LLOQ, 0.030 pM for PBD-dimer after DNA digestion.

adducts in tumor or organs was investigated. As shown in Table 4, the DNA concentrations isolated from mouse tumors and tissues were all overvalued by UV absorbance in varying degrees, probably due to the contamination of RNA or ribonucleotides. In contrast, the digestion and UPLC-MS/MS method excluded the interferences from RNA or ribonucleotides (Fig. 2D). In addition, this method can be integrated with UPLC-MS/MS quantitation of DNA alkylators or adducts, providing a convenient and comprehensive way to determine the DNA adduct occurrence. By employing this method in our studies, the accurate numbers of DNA adducts formed per million base pairs have been successfully determined and correlated with the anti-tumor efficacy of the ADCs (Table 5).

4. Conclusions

Digestion by nuclease P1 can efficiently convert DNA fragments to single deoxyribonucleotides. The stability of deoxyribonucleotides was confirmed in various conditions and the results demonstrated that they can serve as the surrogate of DNA for the quantitation purpose. Here, DNA digestion and UPLC-MS/MS analysis of post-digestion deoxyribonucleotides constitute an accurate, sensitive and convenient method to quantitate DNA. More importantly, this method can exclude the interferences by RNA or ribonucleotides when DNA samples contain such impurities. The analytical method we described here can be used for the accurate DNA quantitation, which can be crucial for many downstream experiments to study DNA. Since DNA is an important drug target in oncology, this method can be highly useful in determining the DNA adduct abundance in tumor cells and help understand the mechanism of action of DNA alkylating agents (like PBD-dimer).

Conflicts of interest

The authors declare that there are no conflicts of interest.

References

[1] P. Imming, C. Sinning, A. Meyer, Drugs, their targets and the nature and number of drug targets, Nat. Rev. Drug Discov. 5 (2006) 821–834.

[2] Y. Ma, D. Zhang, S.-F. Yu, et al., Chemical structure and concentration of intratumor catabolites determine efficacy of antibody drug conjugates, Drug Metab. Dispos. 44 (2016) 1517–1523.

[3] S.R. Gallagher, P.R. Desjardins, Quantitation of DNA and RNA with absorption and fluorescence spectroscopy, Curr. Protoc. Protein Sci. 52 (2008) A.4K.1-A.4K.21.

[4] O. Shimelis, R.W. Giese, Nuclease P1 digestion/high-performance liquid chromatography, a practical method for DNA quantitation, J. Chromatogr. A 1117 (2006) 132–136.

[5] K.A. Haque, R.M. Pfeiffer, M.B. Beerman, et al., Performance of high-throughput DNA quantification methods, BMC Biotechnol. 3 (2003) 20.

[6] K.A. Boesenberg-Smith, M.M. Pessarakli, D.M. Wolk, Assessment of DNA yield and purity: an overlooked detail of PCR troubleshooting, Clin. Microbiol. Newsl. 34 (2012) 1–6.

[7] Y. Nakayama, H. Yamaguchi, N. Einaga, et al., Pitfalls of DNA quantification using DNA-binding fluorescent dyes and suggested solutions, PLoS One 11 (2016) e0150528.

[8] G. Li, O. Shimelis, X. Zhou, et al., Scaled-down nuclease P1 for scaled-up DNA digestion, Biotechniques 34 (2003) 908.

[9] Y. Ma, S.C. Khojasteh, C.E.C.A. Hop, et al., Antibody drug conjugates differentiate uptake and DNA alkylation of pyrrolobenzodiazepines in tumors from organs of xenograft mice, Drug Metab. Dispos. 44 (2016) 1958–1962.

[10] S.C. Tan, B.C. Yiap, DNA, RNA, and protein extraction: the past and the present, J. Biomed. Biotechnol. 2009 (2009) 574398.

[11] A. Dhaliwal, DNA extraction and purification, Mater. Methods 3 (2013) 191.

Original article

Rapid bioluminescence assay for monitoring rat CES1 activity and its alteration by traditional Chinese medicines

Jun Zhang [a], Dandan Wang [b], Liwei Zou [b], Min Xiao [a], Yufeng Zhang [a], Ziwei Li [a], Ling Yang [b], Guangbo Ge [b], Zhong Zuo [a, *]

[a] School of Pharmacy, Faculty of Medicine, The Chinese University of Hong Kong, Hong Kong, China
[b] Institute of Interdisciplinary Medicine, Shanghai University of Traditional Chinese Medicine, Shanghai, 201203, China

ARTICLE INFO

ABSTRACT

In traditional Chinese medicine herbs (TCM), including *Radix Salviae Miltiorrhizae* (Danshen), *Radix Puerariae Lobatae* (Gegen), *Radix Angelicae Sinensis* (Danggui), and *Rhizoma Chuanxiong* (Chuanxiong) are widely used for the prevention and treatment of cardiovascular diseases and also often co-administered with Western drugs as a part of integrative medicine practice. Carboxylesterase 1 (CES1) plays a pivotal role in the metabolisms of pro-drugs. Since (*S*)-2-(2-(6-dimethylamino)-benzothiazole)-4,5-dihydro-thiazole-4-carboxylate (NLMe) has recently been identified by us as a selective CES1 bioluminescent sensor, we developed a rapid method using this substrate for the direct measurement of CES1 activity in rats. This bioluminescence assay was applied to determine CES1 activity in rat tissues after a two-week oral administration of each of the four herbs noted above. The results demonstrated the presence of CES1 enzyme in rat blood and all tested tissues with much higher enzyme activity in the blood, liver, kidney and heart than that in the small intestine, spleen, lung, pancreas, brain and stomach. In addition, the four herbs showed tissue-specific effects on rat CES1 expression. Based on the CES1 biodistribution and its changes after treatment in rats, the possibility that Danshen, Gegen and Danggui might alter CES1 activities in human blood and kidney should be considered. In summary, a selective and sensitive bioluminescence assay was developed to rapidly evaluate CES1 activity and the effects of orally administered TCMs in rats.

1. Introduction

Carboxylesterase (CES) belongs to a widespread α,β-hydrolase-fold superfamily of proteins. This superfamily shares a highly conserved catalytic triad of amino acid and plays a pivotal role in the biotransformation of a wide variety of endogenous and exogenous compounds, including esters, thioesters, carbamates, and amides to their corresponding free acids and alcohols [1]. It has been noted that about 20% of drugs and 50% of prodrugs are metabolised by CES [2]. The main CES isozymes involved in drug metabolism are CES1 and CES2, both of which are expressed extensively in human, dog, and rat liver [3,4]. In human liver, CES1 (hCE1) contributes about 80–95% of the total hydrolytic activity [5]. In rat liver, the dominant CES1 family includes four different

isozymes: hydrolase A, hydrolase B, hydrolase C and rat egasyn, among which hydrolase A is the closest in catalytic function to human hCE1, with about 78% sequence similarity [6,7].

Four traditional Chinese medicine (TCM) herbs, *Radix Salviae Miltiorrhizae* (Red sage root, Danshen, DS) [8–10], *Radix Puerariae Lobatae* (Kudzu root, Gegen, GG) [10–12], *Radix Angelicae Sinensis* (Angelica root, Danggui, DG) [9,13] and *Rhizoma Chuanxiong* (Szechuan lovage rhizome, Chuanxiong, CX) [9,13] are widely used for the prevention and treatment of cardiovascular diseases. Thus, they have a high potential to be co-administered with Western drugs [9,12]. For instance, in a real-world study of 84,697 patients with coronary heart disease, 43.46% of patients in antiplatelet therapy also took TCMs at the same time [14]. In addition, TCM was used with P2Y 12 receptor inhibitors, such as clopidogrel or ticagrelor, to minimize adverse effects, drug intolerances, thrombotic risk, and socioeconomic issues [15,16]. The effect of TCM herbs on rat CES1 activity in blood and tissue S9 fractions has not been addressed. Our recent findings suggested that co-administration of

---

GG and DG could lead to altered pharmacokinetics of clopidogrel and aspirin with significant inhibition of CES activity [17]. Considering that CES serves as the major hydrolysing enzyme for a large number of drugs, especially pro-drugs such as enalapril, oseltamivir and clopidogrel [18], and that the pharmacokinetics of drugs determined by preclinical experiments in rats are widely used as a reference for clinical studies, further clarification of the distribution of CES1 and the tissue-specific impact of TCMs on CES1 activity in rats is needed not only for interpretation of preclinical drug pharmacokinetics but also for the safe use of drugs in the practice of integrative medicine.

In modern TCM practice Chinese materia medica (CMM) formula granules have become popular as an alternative to decoction preparations. Since these granules not only retain the properties but also address the common problems of quality control, preparation, and administration, their clinical use has gradually increased worldwide. In China there are more than 600 types of herb granule preparations and 200 kinds of herbal formulae [19]. In addition, there are more than 400 herbal granule preparations in Japan [20] and 300 types in South Korea [21]. A recent review of 56 clinical trials demonstrated no significant difference in effectiveness and safety between granules and decoctions of Chinese herbal medicine [22]. Thus, herbal granule preparations of the four studied TCMs were adopted for our current study.

The activity of CES is measured as the reduction of a specific substrate or formation of its respective metabolites during a given time using recombinant CES enzymes, liver microsomes, S9 fractions and plasma from different species. Activity is measured by photometric assay, fluorometric assay, and chromatography assay to detect a signal generated by the substrates or the products formed [23–26]. In these methods, *p*-nitrophenyl acetate, *p*-iodonitrophenyl tetrazolium violet, butanilicaine, acyl-CoA, 5,5′-dithiobis-(2-nitrobenzoic acid), phenacetin, acetanilide and clopidogrel are substrates commonly used. In our previous study we reported two selective sensors (2-(2-benzoyloxy-3-methoxyphenyl)benzothiazole) (BMBT) and (*S*)-4,5-dihydro-2-(6-hydroxy-2-benzothiazolyl)-4-thiazolecarboxylic acid-methyl ester (DME), both of which could be used for the quantitative detection of hCE1 activity in human liver microsomes [26,27]. However, it was found that the BMBT-based fluorescent assay suffered from strong background interference and potential phototoxicity. Based on the chemical structure backbone of BMBT and DME, (*S*)-2-(2-(6-dimethylamino)-benzothiazole)-4,5-dihydro-thiazole-4-carboxylate (NLMe), a new specific substrate of hCE1 with minimum background interference and no phototoxicity was developed and the synthesis method, identification and application of NLMe and its hydrolysed product (*S*)-2-(2-(6-dimethylamino)-benzothiazole)-4,5-dihydro-thiazole-4-carboxylic acid (NL) were reported in our previous studies [27–29]. The design of NLMe as a bioluminescent sensor for detecting enzyme activity was based on the strategy that the firefly luciferin-luciferase reaction is the most important and widely used system in bioluminescence detection, and the free luciferin can be masked with distinctive substitutes [29]. NLMe is an ester derivative of luciferin that contains a large carboxyl group and a small alcohol group and thus may serve as a good substrate for CES1, as CES1 preferentially hydrolyses substrates with small alcohol groups and large acyl groups, while CES2 prefers substrates with large alcohol groups and small acyl groups [30]. NLMe was found to be a specific substrate for CES1 and could be specifically metabolised by hCE1 to NL, while other hydrolases such as acetylcholinesterase, butyrylcholinesterase, human paraoxonase 1, human paraoxygen phosphate 2, carbonic anhydrase, bovine albumin, lipase, C-reactive protein, myoglobin, transgenic ferritin, lysozyme, pepsin, trypsin, human albumin, prion protein, human carboxylesterase 2 and phosphate buffer could not catalyze the reaction. The hydrolysis of NLMe in liver microsomes could be suppressed markedly by the

specific carboxylesterase inhibitor BNPP but not by other esterase inhibitors such as piperazine, huperzine A, galantamine and ethylenediamine tetraethylammonium [28]. The rate of NLMe metabolism in microsomes from human lung, kidney, intestine and liver in a preliminary bioluminescent test was found to be consistent with hCE1 expression in the corresponding microsomes by Western blot assay, demonstrating the specificity of NLMe as a substrate for CES1 [28]. The current study further develops and validates a comprehensive bioluminescence assay using NLMe as a probe for direct detection of CES1 activity in different biomatrices such as plasma and various tissues in rats. Based on this assay the distribution profile of CES1 activity was obtained, providing important information for the preclinical development of pro-drugs and also enabling us to directly monitor CES1 activity and changes due to drug and/or herbal treatment, thereby facilitating better prediction of herb/drug interactions to ensure their safe use.

2. Experimental

2.1. Materials and instruments

NLMe and NL (Fig. 1) were synthesized by our group with a purity of >98%. Phosphate buffered saline (PBS) tablets, a Bicinchoninic Acid (BCA) Protein Assay kit and rat liver microsomes (RLM) were purchased from Sigma-Aldrich (St. Louis, MO, USA). Luciferin detection reagent (LDR), a product of Promega Corporation (Madison, WI, USA), was prepared by adding reconstitution buffer to the lyophilized luciferin reagent and gently swirling to dissolve. Rehydration of the reagent at room temperature for 1 h before use was necessary. Bis-*p*-nitrophenyl phosphate (BNPP), fluoxetine and loperamide were purchased from TCI (Tokyo, Japan). Ultrapure water was generated by a Milli-Q ultrapure water system from Millipore (Milford, MA, USA). Nunc™ F96 white polystyrene plates were from Thermo Scientific (Rockford, IL USA). Ultra-Turrax T25 Disperser (IKA, Boutersem, Belgium) and a CT15RT versatile refrigerated centrifuge (Techcomp Ltd., Shanghai, China) were used in the animal study. A CLARIOstar® microplate reader (BMG LABTECH, Ortenberg, Germany) was used for total protein concentration determination and bioluminescence assay.

The CMM granules of DS (Batch No. 1007), GG (Batch No. 1027), CX (Batch No. 1019) and DG (Batch No. 1017) were kindly provided by PuraPharm International Limited (Hong Kong). The herb to herbal granule concentration ratio was 5:1 for DS granules, GG granules, CX granules, and 3:1 for DG granules. The contents of the represented bioactive marker compounds in the granules were determined in our previous study [17] as follows: 25 mg/g salvianolic acid in DS granule, 114 mg/g puerarin in GG granule, 0.63 mg/g Ferulic acid in DG granule and 1.81 mg/g Ferulic acid in CX granule. Specific quality controls were strictly followed as is described for the four selected TCM herbs in both the Chinese Pharmacopoeia of the People's Republic of China [31] and the Hong Kong Chinese Materia Medica Standards [32]. The voucher specimens for the four herbal granules were kept in the School of Pharmacy, the Chinese University of Hong Kong, China.

2.2. Development and validation of the bioluminescence assay

2.2.1. Verification of NLMe as CES1 substrate in rat plasma

In contrast to the lack of CES in human plasma, high expression of CES in rat plasma has been reported [33]. Since NLMe had been demonstrated to be a selective hCES1 substrate, to validate the specificity of NLMe towards CES1 in rat plasma, potential inhibition assays of various CES inhibitors on NLMe hydrolysis were conducted in blank rat plasma. Assessment was done by comparing activity in the presence or absence of various reported CES

A

B
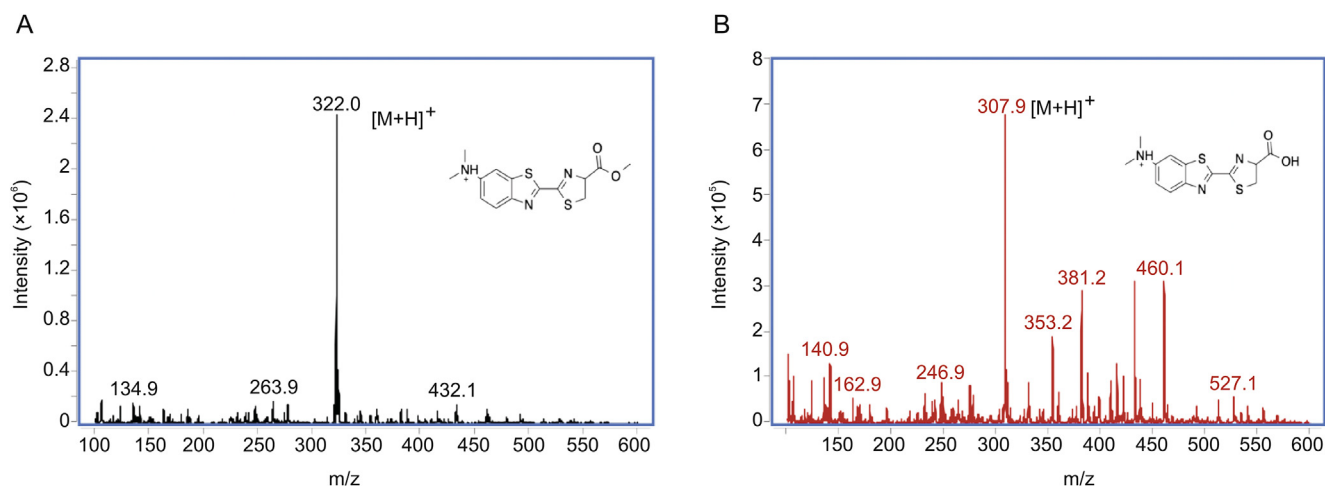
Fig. 1. Structure and MS/MS spectra of (A) NLMe and (B) NL.

inhibitors including BNPP (a general CESs inhibitor) [34], fluoxetine (a selective CES1 inhibitor) [35] and loperamide (a selective CES2 inhibitor) [36]. The study was conducted in a 96-well microplate in a total volume of 100 μL. BNPP was dissolved in dimethyl sulfoxide, and fluoxetine and loperamide were dissolved in ethanol to obtain stock solutions with a concentration of 40 mM. Serial dilutions with PBS (100 mM, pH 7.4) were done to achieve solutions of 0.5, 1.0, 2.0, 3.9, 7.8, 15.6, 31.3, 62.5, 125 and 250 μM. A 25 μL volume of the diluted solution was pre-incubated with 25 μL of rat plasma (protein concentration of 4 μg/mL) at 37 °C for 60 min and then 25 μL of NLMe solution (500 ng/mL) was added to initiate the reaction. Ten min after incubation at 37 °C the reaction was terminated by adding 25 μL of LDR. After another 20 min incubation of the mixture, the bioluminescent signals generated were measured with the CLAR-IOstar® microplate reader to measure CES1 activity. Solvent vehicles and control samples without the inhibitors were also employed. The residual activity (%) representing the percentage of CES1 activity from different treatment groups compared to that of the control was obtained and compared. To evaluate the inhibitory effects of CES inhibitors such as BNPP and fluoxetine, a half-maximal inhibitory concentration (IC_{50}) was estimated based on their concentration-response curves using GraphPad 7.0 software (GraphPad Software Inc, San Diego, CA, USA).

2.2.2. Determination of NL by the bioluminescence assay

As illustrated in Fig. 2, NLMe could be hydrolysed by CES1 to NL, which served as a specific substrate of luciferase and could be quantified by measuring the bioluminescence generated from reactions with LDR. Briefly, to a 25 μL aliquot of NL standard solution, 50 μL of PBS (100 mM, pH 7.4) was added followed by incubating the mixture at 37 °C with gentle shaking for 10 min. Subsequently, 25 μL of LDR was added to the reaction mixture followed by a 20 min incubation at 37 °C. The bioluminescent signals generated were measured with the CLARIOstar® microplate reader.

2.2.3. Validation of the bioluminescence assay

The developed bioluminescence assay was validated for specificity, linearity, precision, accuracy and robustness. Specificity of the assay was assessed by detecting possible interference via scanning the emission spectra of NLMe, NL and enzyme (RLM) reaction mixtures. Linearity was evaluated by analysing standard solutions of NL at concentrations of 15.62, 31.25, 62.5, 125, 250, 500 and 1000 ng/mL in triplicate; the standard solutions were freshly prepared by serial dilutions of 2 mg/mL NL stock solution with 100 mM PBS buffer. The bioluminescent signals were plotted versus NL concentration and the calibration equation was obtained using weighted linear regression analysis. The limit of detection (LOD) and limit of quantification (LOQ) were respectively calculated using
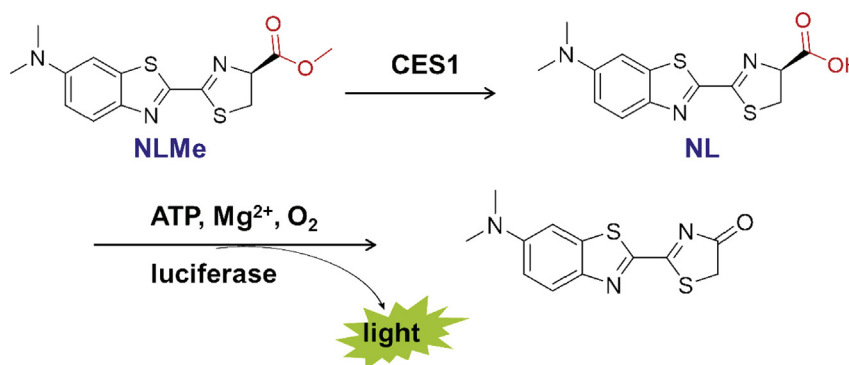
Fig. 2. Illustration of the current CES1 mediated enzymatic reaction of NLMe and bioluminescent assay of the formed NL.

the slope (S) of the calibration curve and the standard deviation of response (σ) with the following formulas: LOD = 3.3 σ/S and LOQ = 10 σ/S. Precision was evaluated by intra- and inter-day precision and expressed as the relative standard deviation (RSD %). Intra-day precision was evaluated by performing three repeated analyses of NL standard solutions at concentrations of 125, 500 and 1000 ng/mL on the same day. As for inter-day precision, the same analyses were performed on three different days. Accuracy was expressed as a percentage of deviation between the nominal and measured concentrations of the sample with ±15% as acceptance criteria.

Since the assays were all performed in 96-well microplates, robustness assessment was conducted on three days with three plates processed each day. Each plate layout consisted of NL standard solutions at 125, 500 and 1000 ng/mL to mimic the low, middle and high bioluminescent signals, respectively. The low, middle and high signal samples were distributed within the plates in an interleaved-signal format with different column-wise order: high-middle-low for plate A, low-high-middle for plate B and middle-low-high for plate C (n = 32). The signals measured were then used to calculate the coefficient of variations (CV), signal window (SW) and Z' value for robustness assessment (see Supplementary Information: S1) [37].

2.3. Evaluation of CES1 activity after oral administration of selected TCM herbs with the bioluminescence assay

2.3.1. Animal treatment

To evaluate the effects of selected TCM herbs on CES1 activities in rats, thirty male Sprague Dawley rats (12—14 weeks, 150—200 g) were randomly divided into nine groups (G1 to G9, n = 6 for G1, n = 3 for G2-G9). G1 served as the control group, in which rats were orally administered 1 mL saline twice a day for 14 days, while rats in G2 to G9 received a human equivalent dose of herbal granules twice a day for 14 days.

Based on the recommended human dose (60 kg per person) for the four herbs (DS dried herb: 10—15 g; GG dried herb: 10—15 g; DG dried herb: 6—12 g; and CX dried herb: 3—10 g) [31] and the dose correction factor for rats based on body surface area as recommended by the US FDA [38], the equivalent herbal doses in rats (g/kg) were calculated to be 1.03 g/kg of DS (G2, DSL), 1.55 g/kg of DS (G3, DSH), 1.03 g/kg of GG (G4, GGL), 1.55 g/kg of GG (G5, GGH), 0.62 g/kg of DG (G6, DGL), 1.24 g/kg of DG (G7, DGH), 0.31 g/kg of CX (G8, CXL) and 1.03 g/kg of CX (G9, CXH). Based on the herb to herbal granule extraction ratio provided by the manufacturer (5:1 for DS granules, GG granules and CX granules; 3:1 for DG granules), doses of the CMM granules in each treatment group were calculated to be: 0.21 g/kg of DS granule (G2, DSL), 0.31 g/kg of DS granule (G3, DSH), 0.21 g/kg of GG granule (G4, GGL), 0.31 g/kg of GG granule (G5, GGH), 0.21 g/kg of DG granule (G6, DGL), 0.41 g/kg of DG granule (G7, DGH), 0.062 g/kg of CX granule (G8, CXL) and 0.21 g/kg of CX granule (G9, CXH). The selected amount of each herbal granule was suspended in 30 mL warm water followed by 30 min sonication at room temperature to prepare a stock solution of 0.0441 g/mL for DSL, GGL, DGL and CXH, 0.0651 g/mL for DSH and GGH, 0.0882 g/mL for DGH, and 0.0130 g/mL for CX (based on a 210 g rat). The final oral gavage volume of the stock solution for each rat (ranging from 0.4 to 0.8 mL) was further adjusted based on body weight.

All the animal experiments were carried out after approval by the Animal Ethics Committee of The Chinese University of Hong Kong (Ref No. 14-171-MIS) and Sprague Dawley rats were supplied by the Laboratory Animal Service Centre at The Chinese University of Hong Kong.

2.3.2. Sample collection and treatment

Blood samples were collected on Day 0, Day 2, Day 4, Day 6, Day 8, Day 10, and Day 12 from the tail vein of each rat. On day 14 all rats were killed 2 h after their last dosing, blood was sampled via cardiac puncture, and the heart, liver, kidney, spleen, lung, pancreas, intestine, brain and stomach were collected after quick cardiac perfusion with 200 mL saline. Plasma samples were separated from blood by immediate centrifugation at 8000g for 3 min. Plasma and all collected tissue samples were frozen at −80 °C. To prepare S9 fractions of each collected tissue, the frozen tissues were thawed in ice-cold homogenization buffer (0.1 mM Tris-HCl, 10 mM EDTA and 150 mM KCl) and then homogenized in an ice-water bath. The homogenates were then centrifuged at 10,000 g for 20 min at 4 °C to obtain the supernatants (S9 fractions) with storage at -80 °C. The total protein concentration of the plasma and prepared S9 fractions was determined with the microplate reader using a BCA protein assay kit as described in the technical bulletin accompanying the kit.

2.3.3. CES1 activity determination by the bioluminescence assay

CES1 activity in the biomatrices was determined by the formation of NL from NLMe in an optimized incubation system. In brief, 25 μL sample solutions with optimum protein concentrations were pre-incubated in 25 μL PBS (100 mM, pH 7.4) at 37 °C with gentle shaking for 10 min. Thereafter the reactions were initiated by adding 25 μL NLMe (500 ng/mL) and further incubated for 10 min. Finally, the CES1 activity of the S9 fraction samples obtained from section 2.4.2 was expressed as the formation rate of NL by the newly developed bioluminescence assay.

2.4. Data analyses

To determine CES1 activity, background bioluminescent signals obtained from control samples ($n = 3$) containing NLMe and PBS were subtracted from the signals obtained from the biomatrix samples. Data are presented as mean ± SD (standard deviation of mean) of three independent experiments. To compare the CES1 activity between different treatment groups, Welch's t-test was used with a $p < 0.05$ considered statistically significant.

3. Results and discussion

While changes in enzyme activity are not always the result of changes in enzyme levels [39], changes in expression are the most common means by which cells regulate enzyme activity. The bioluminescence assay developed here allows the rapid determination of CES1 enzyme activity in a variety of tissues, preparations, blood and plasma. To ensure that changes in activity were normalized to protein content in each biomatrice, the protein concentration of each biomatrix sample was determined by BCA assay. An optimized protein concentration for determining CES1 activity was selected for each tissue or blood sample based on the linear range and the intensity of the signal response by using a plot of protein concentration versus the luminescent signal produced by NLMe hydrolysis. With this optimized protein concentration for each plasma/tissue, the CES1 activity of each organ was determined as the NL formation rate after adjustment of the protein concentration (mM/mg protein/min).

In previous studies photometric, fluorometric and chromatography methods were utilized to measure CES activities [23—26]. The photometric assay was considered to be simple and rapid (1 or 2 min) but lack of specificity for CES1 activity was a problem [23]. The fluorometric assay using a fluorescent probe for hCE1 provided high sensitivity with a LOD of 1.29 ng/mL, but suffered from interference caused by impurities and the instability of products

when exposed to light [26]. The chromatographic analyses using HPLC or UPLC are selective and sensitive but time-consuming, requiring up to 30 min for each sample run [25,26]. Our newly developed bioluminescence assay has the advantages of a simpler procedure, a stable signal, shorter sample analysis time and lower cost. In addition, the current method provides higher selectivity and sensitivity with an LOD as low as 1.15 ng/mL, 8-fold more sensitive than our previously reported DME-based bioluminescent method (LOD of 10 ng/mL) [27]. We have applied this CES1 activity assay to measure changes in CES1 activity in rat biomatrices after TCM treatment.

Species variation exists for almost every enzyme including CES. Previous reports based on substrate levels changes have demonstrated species variations in CES activities. For example, for the prodrug diethylene triamine pentaacetic acid the degree of its CES-mediated hydrolysis and resultant metabolic profile in human and dog liver S9 fractions were vastly different from that in rats [40]. Significant variation in clopidogrel hydrolysis in different species as determined by the formation rate of the inactive metabolite clopidogrel carboxylic acid also was noticed [41]. Since changes in substrate levels could result from metabolic pathways other than CES-mediated hydrolysis, it is expected that our bioluminescence assay will provide more accurate and direct monitoring of CES activity changes.

3.1. Bioluminescence assay development and validation

3.1.1. Optimization of the bioluminescence assay conditions and method validation

The maximum bioluminescent emission wavelength of NL and the enzymatic reaction solution were both at 618 nm with no bioluminescent signal interference from NLMe (Fig. 3A), indicating that the determination method was specific. Since a 20 min incubation generated the strongest signal, stable for up to 50 min, it was considered the optimum incubation time (Fig. 3B). It was also found the intensity of the bioluminescent signal generated was proportional to NL concentration up to 1000 ng/mL at the studied three incubation temperatures, with 37 °C generating higher signal intensity than 25 °C and 30 °C. Thus, incubation at 37 °C was selected for sample analyses (Fig. 3C).

Analysis of CES1 activity using the bioluminescence assay required a standard curve plotting the bioluminescence intensity against the corresponding NL concentration. A weighted (1/x weighting) least squares linear regression model was adopted to obtain a calibration curve. The relationship between bioluminescence intensity and NL concentration was linear over its concentration range of 15.63–1000 ng/mL with a squared Pearson correlation coefficient (r^2) of 0.9996. The calculated LOD and LOQ of NL were 1.15 and 3.48 ng/mL respectively, demonstrating exceptional sensitivity for the current assay. Table 1 shows that the accuracy and precision determined at the three concentration levels of NL on three different days were all within 15%, confirming the reliability of the developed assay. The robustness evaluations were based on plate uniformity and signal variability assessment. Table 2 indicates that CV values were all less than 20%, SW and Z' values were all no less than 2 and 0.4 respectively, verifying that the assay was reliable with sufficient robustness.

3.1.2. Optimization of CES1 enzymatic reaction conditions

CES1 activity was evaluated by determining the rate of CES1-mediated NLMe hydrolysis, which was a substrate of luciferin and could generate bioluminescence during reaction with LDR (Fig. 2). Serial dilution samples of in vitro enzymatic reactions were conducted to optimize the conditions. As shown in Fig. 4A, the percentage of NLMe consumption increased linearly when the protein
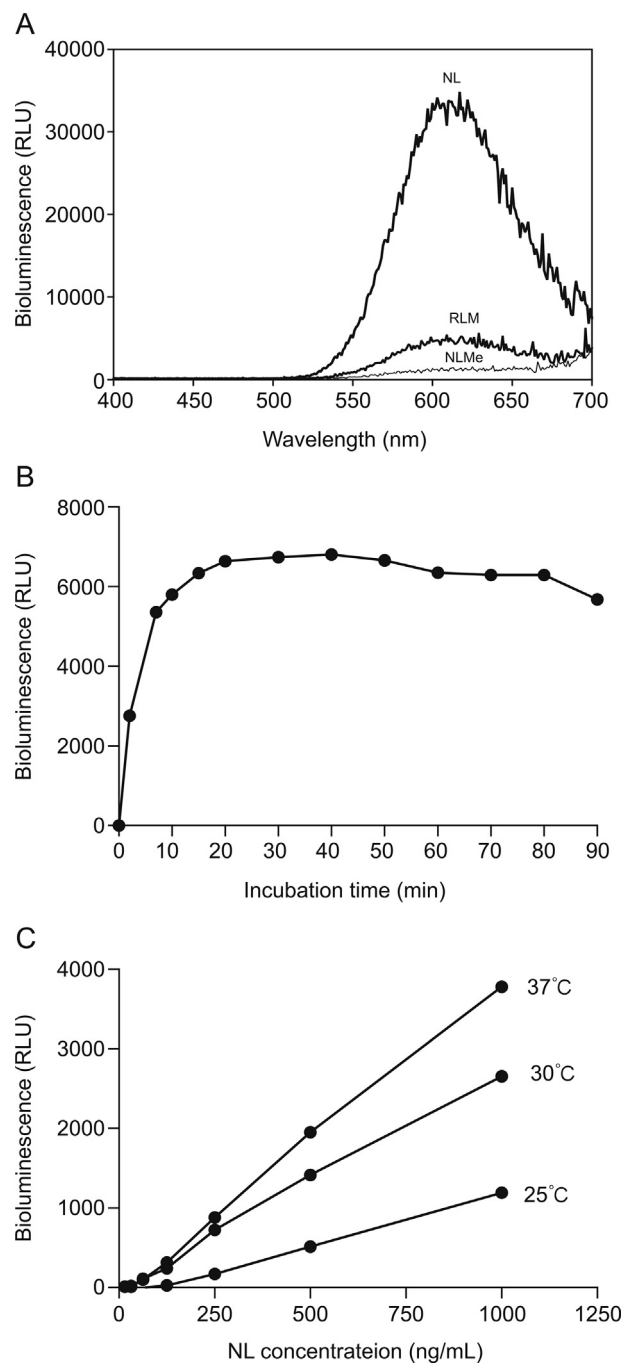
Fig. 3. Optimization of the bioluminescent assay with demonstrations of (A) bioluminescent spectra (400–700 nm) of NL (500 ng/mL), NLMe (500 ng/mL) and incubation mixture of enzyme (RLM, 2 μg/mL), relationships between bioluminescent intensity and (B) incubation time (0–90 min) and (C) NL concentrations and incubation temperatures (25 °C, 30 °C and 37 °C).

concentration of RLM was lower than 16 μg/mL and tended to reach a plateau when it was higher than 40 μg/mL. Based on the obtained linear range and the intensity of signal response, 2 μg/mL protein concentration was considered to be sufficient for the enzymatic reaction. Similarly, protein concentrations were optimized for the plasma samples (4 μg/mL) and S9 samples of heart (20 μg/mL), liver (6 μg/mL), kidney (10 μg/mL), spleen (50 μg/mL), lung (20 μg/mL), pancreas (10 μg/mL), intestine (20 μg/mL), brain (50 μg/mL) and stomach (30 μg/mL). Under the above optimized reaction conditions, the enzyme hydrolysis reaction was found to be very quick

Table 1
Accuracy and precision of the developed assay (mean ± SD, $n = 3$).

Test	Nominal conc. (ng/mL)	Measured conc. (ng/mL)	Accuracy (%)	Precision (CV, %)
Intra-day	125	140 ± 8.96	112 ± 7.17	6.41
	500	515 ± 15.89	103 ± 3.18	3.08
	1000	958 ± 5.88	96 ± 0.59	0.61
Inter-day	125	145 ± 9.39	116 ± 7.51	6.46
	500	526 ± 29.76	105 ± 5.95	5.65
	1000	995 ± 37.83	99 ± 3.78	3.80

Table 2
Robustness of the developed assay in 96 well-plates.

Test	Day	Plate	CV (%)			SW	Z'
			Low signals (125 ng/mL)	Middle signals (500 ng/mL)	High signals (1000 ng/mL)		
Intra-day	1	A	0.50	0.45	1.27	5	1.0
		B	1.17	0.48	0.60	5	1.0
		C	0.73	1.13	0.46	5	1.0
	2	A	0.52	0.62	1.02	5	1.0
		B	1.18	0.45	0.63	6	1.0
		C	0.56	1.03	0.50	5	1.0
	3	A	0.47	0.48	1.37	6	1.0
		B	1.05	0.41	0.57	6	1.0
		C	0.63	1.21	0.38	7	1.0
Inter-day	NA	NA	0.18	0.22	0.40	2	1.0

NA: not applicable.

with the NL formation rate stabilized after 10 min (Fig. 4B). Therefore, 10 min was considered as the optimum reaction time. On the other hand, the NL formation rate increased linearly when the substrate NLMe concentration increased from 7.81 ng/mL to 500 ng/mL (Fig. 4C). In order to maximize the generated signal without affecting the linearity of the response, 500 ng/mL of NLMe was selected as the optimum substrate concentration.

3.1.3. Verification of the selectivity of NLMe for CES1 in rat plasma

To further validate the selectivity of NLMe for CES1 in rat plasma, an inhibition assay of various carboxylesterase inhibitors was performed. As shown in Fig. 5, among the selected compounds, both BNPP and fluoxetine exhibited a significant inhibitory effect on the hydrolysis of NLMe with an IC_{50} of 5.1 μM and 2.6 μM, respectively. Loperamide, the selective CES2 inhibitor, demonstrated no effect on NLMe hydrolysis at its final concentrations up to 62.5 μM, further suggesting the specificity of NLMe as CES1 substrate.

3.2. Impact of orally administered TCMs on CES1 activity in rats

3.2.1. Effect of TCM treatment on CES1 activity in plasma and different tissues

Understanding the tissue distribution of CES isoenzymes is critical for predicting CES-mediated metabolism of drugs. Using our developed bioluminescent method, we measured the expression of CES1 in rat plasma and major tissues after a two-week administration of selected TCMs. In the current study CES1 activity in S9 fractions instead of microsomal fractions was monitored. Notably, S9 fractions contain both microsomal and cytosolic fractions and CES1 enzymes have been found to be highly expressed in both human and rat liver cytosol [42].

As shown in Fig. 6, the CES1 enzyme was found in plasma and all tested tissues including heart, liver, kidney, spleen, lung, pancreas, intestine, brain and stomach. Consistent with previous reports [43,44], CES1 enzyme expression in liver, kidney and plasma was found to be higher than that in the small intestine. In addition, CES1 activity was detected in heart and brain. In summary, CES1 activity

in plasma, heart, liver and kidney was much higher than that in spleen, lung, pancreas, intestine, brain and stomach. Furthermore, the effect of two-week TCM treatment (except for DSL and DSH groups) on rat CES1 activity proved to be tissue-specific: in the GGL group a significant increase was found in lung and in the GGH group no significant differences were found. Moreover, a significant decrease in CES1 activity was found in the kidney in both the DGL and DGH groups. In the DGL group CES1 activity tended to decrease in plasma and all assayed tissues, but without statistical significance. In the DGH group significantly decreased CES1 activity was also found in the spleen. Finally, significant increases in CES1 activity were found in the lung in both the CXL and CXH groups, while CES1 activity significantly decreased in spleen in the CXH group. Such tissue-specific alterations in CES1 activity with different TCM treatments could be due to differing tissue distribution of the TCM components that affect CES1 expression or activity. It has been reported that tanshinone from *Salvia miltiorrhiza* (DS) [45] and flavonoids such as baicalin, baicalein, chrysin and galangin can inhibit CES [46].

In our previous study [17] the impacts of these herbs on rat liver CES1 activity after co-administration with clopidogrel and aspirin were studied. Similar findings were observed after administration of DSL, DSH, GGL, DGL, DGH and CXL. However, instead of decreased CES1 activity in liver, increased CES1 activity was found for both GGH and CXH in this current study. Such discrepancies could be due to the different approaches adopted for CES1 activity determination. Our previous study used clopidogrel as the probe substrate for CES1, whereas the current study utilized a more specific and direct measurement for CES1 activity. NLMe used in our current study was a specific substrate hydrolysed only by the CES1 enzyme, whereas clopidogrel used in our previous study had two competitive metabolic pathways: a primarily pathway for hydrolysis by hCE1 to clopidogrel carboxylic acid and a secondary oxidation pathway by CYP enzymes to clopidogrel thiolactone, which could then be hydrolysed to the carboxylic acid of thiolactone by hCE1 [47]. Our current bioluminescence assay has greater specificity as well as direct monitoring of CES1 activity, making the altered CES1 activities after TCM treatment *in vivo* more
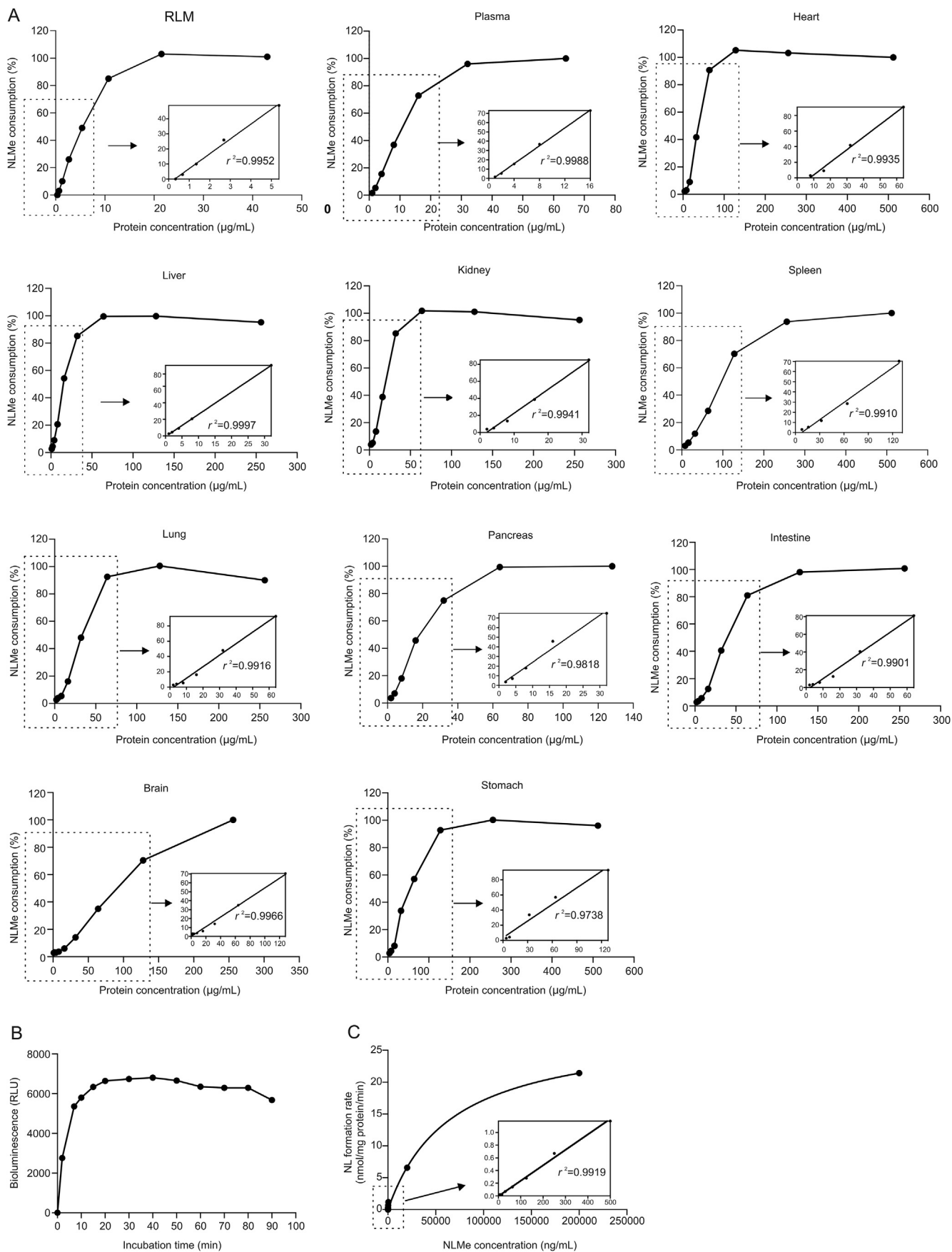
Fig. 4. Optimization of enzymatic reaction conditions on (A) protein concentration of RLM, plasma, S9 of heart, liver, kidney, spleen, lung, pancreas, intestine, brain and stomach respectively, (B) Reaction time (2−80 min), and (C) NLMe concentrations (7.81 ng/mL−200 μg/mL).

relevant.

3.2.2. Rat plasma CES1 activity changes during the two-week TCM treatment

Based on the high expression level of CES1 in rat plasma, blood samples from all treatment groups were collected every two days until Day 14 to monitor the changes in CES1 activity during the treatment period (Fig. 7). Plasma CES1 activity changes during the 14 days of treatment are shown in Fig. 7A. For fair comparison of the rat plasma CES1 activity changes by different orally administered TCMs during the two-week treatment, the fold-change in CES 1 activity is expressed relative to Day 0, based on which z-scores (see Supplementary Information: S2) were calculated for the plot of a heatmap (Fig. 7B).

As shown in Fig. 7A, compared to that in control group, the plasma CES1 activity in DSL, DSH, GGL and GGH-treated groups was mostly decreased during the period of treatment with significant decreases observed in the DSL, DSH and GGL groups on Day 8, suggesting that long-term oral administration of DS and GG would have the potential to inhibit plasma CES1 activity in rats. On the other hand, plasma CES1 activity in the DG and CX-treated groups fluctuated during the treatment period with a significant increase in CES1 activity observed in the DGL group on Day 8 and in the CXH group on Day 2 and Day 8, with no significant difference on Day 14.

Besides, compared with that on Day 0, it was noticed that plasma CES1 activity of the control, DSL, GGH and CXH groups fluctuated on the first few days and showed a trend of a steady decrease after Day 8 (Fig. 7B) with only the DSL group demonstrating significant decreased CES1 activity on Day 8, Day 10, Day 12 and Day 14 (Fig. 7A), with no significant differences on Day 14 in the GGH and CXH groups. For other groups, including DSH, GGL, DGL, DGH and CXL, consistent decrease in plasma CES1 activity was observed after Day 2 (Fig. 7B) with significant decreases found in the DGH and CXL groups on Day 10, in the DGL group on Day 10 and Day 12 and no significant differences for all groups on Day 14 (Fig. 7A).

To statistically analyse the differences in CES1 activity in the biomatrices of rats from different treatment groups, Welch's t-test, an adaption of Student's t-test [48], was adopted in our current study. Welch's t-test performs better on control of Type 1 errors than Student's t-test when sample sizes are unequal and performs similarly when sample sizes and variances are equal [48–50]. Our analysis procedure was as follows: First, the assumption of normality was checked using the Shapiro-Wilk normality test because of the small sample size of control group ($n = 6$) and TCM-dosed groups ($n = 3$). We found that all data sets of rat plasma CES1 activity in all groups followed normal distributions. Secondly, assumptions of homogeneity of variance were verified using the F-test: e.g., the variance of data sets of rat plasma CES1 activity in the DSL group on Day 2 $vs.$ Day 0 ($n = 3$) (scenario A) was found to be equal ($p = 0.892$), whereas that in the DSH group on Day 10 vs. Day 0 ($n = 3$) (scenario B) was unequal ($p = 0.006$). Finally, the data sets were analysed using both Student's t-test and Welch's t-test. For scenario A, it was found that there was no significant difference between the two data sets ($p = 0.409$ in both tests) with the same t value ($t = 0.9218$) and degree of freedom (df) (df = 4) from both tests; for scenario B, different results were found between the two data sets by the two tests: Student's t-test: $p = 0.019$, $t = 3.828$, df = 4; Welch's t-test: $p = 0.061$, $t = 3.828$, df = 2. Since when variances were unequal across groups, Student's t-test could be severely biased and lead to unreliable results [49], while Welch's t-test provides better control of Type 1 error rates [48–50], Welch's t-test was selected in our study.

In summary, among the four TCM herbs, DS and GG tended to have the greatest effect on plasma CES1 activity, with a decrease in plasma CES1 activity after long-term oral administration, whereas

DG and CX affected CES1 activity in organs including kidney, spleen and lung. Based on the CES1 distribution and changes in its activity after treatment with the four TCM herbs, we suggest that DS, GG and DG might significantly alter CES1 activity in tissues where it is most abundantly expressed, including blood and kidney. Among the tested organs, CES1 activity in heart, liver, pancreas, intestine, brain and stomach was barely affected by the two-week orally administered TCM herbs. Considering the above-mentioned impact, the abundance of CES1 expression and the convenience for sampling, plasma CES1 could serve as a biomarker in monitoring the alteration in CES1 activities in rats.

4. Conclusions

A novel and rapid bioluminescence assay with sufficient sensitivity and convenience has been developed and validated for monitoring CES1 activity in various tissues. For the first time, the distribution profiles of CES1 activity in rat tissues are fully characterized with our bioluminescence assay. We found that the CES1 enzyme was present in plasma and all tested organs in rats with much higher levels in plasma, heart, liver and kidney. The four studied TCM herbs showed tissue-specific effects on CES1 activity after two-week oral administration in rats at human-equivalent
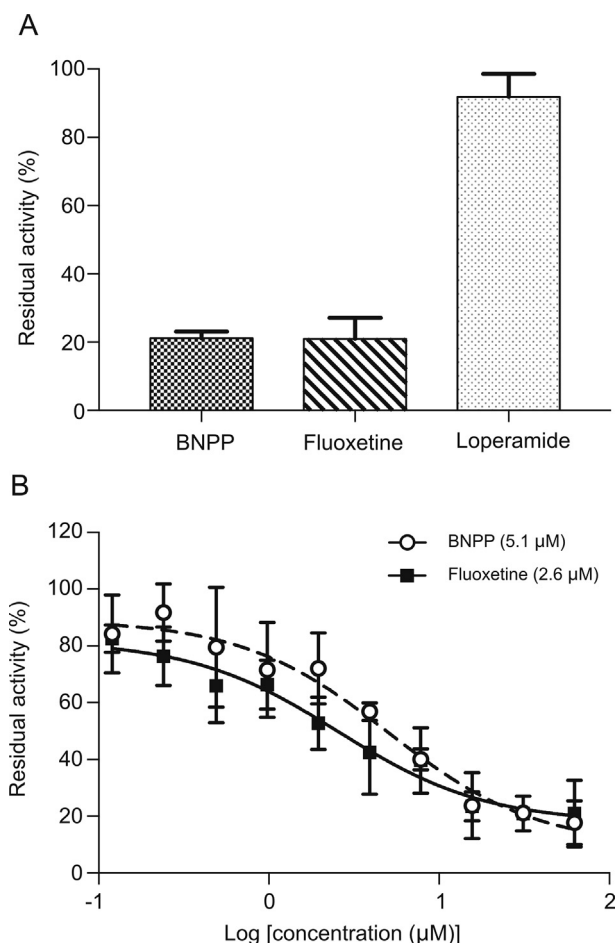
Fig. 5. An assessment of potential inhibitory effects of the selected compounds on the hydrolysis of NLMe in rat plasma. Data are means ± SD, $n = 3$. (A) Histogram of residual activities compared to control for BNPP, fluoxetine and loperamide at final concentrations of 31.25 μM; (B) Dose-inhibition curves of BNPP and fluoxetine, IC_{50} values were presented in the parenthesis.
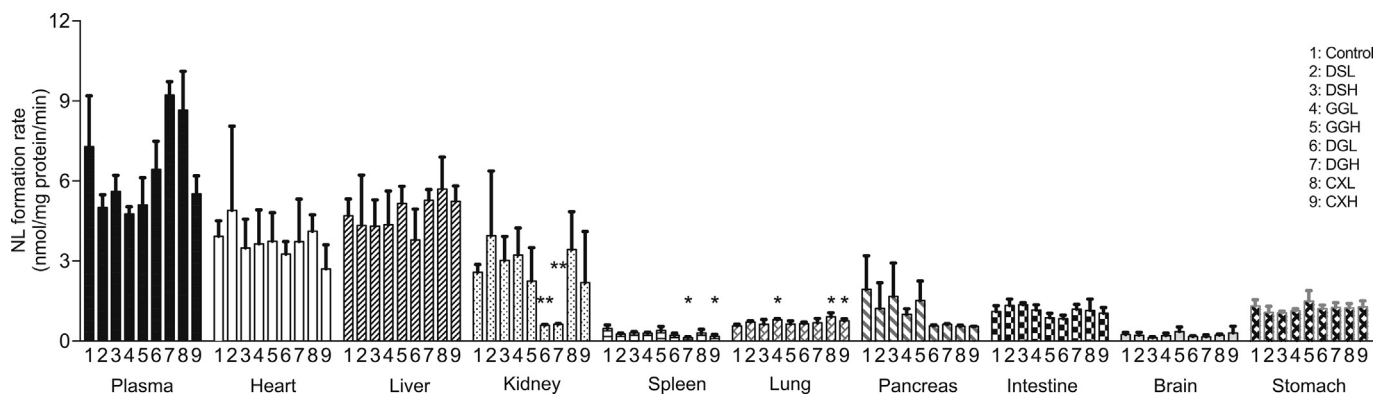
Fig. 6. Histogram for the CES1 activities in plasma and tissues after the two-week TCM administrations. in rats. Data are means ± SD, $n = 6$ for control group and $n = 3$ for TCM dosed groups. *$P < 0.05$, **$P < 0.01$ compared with control.
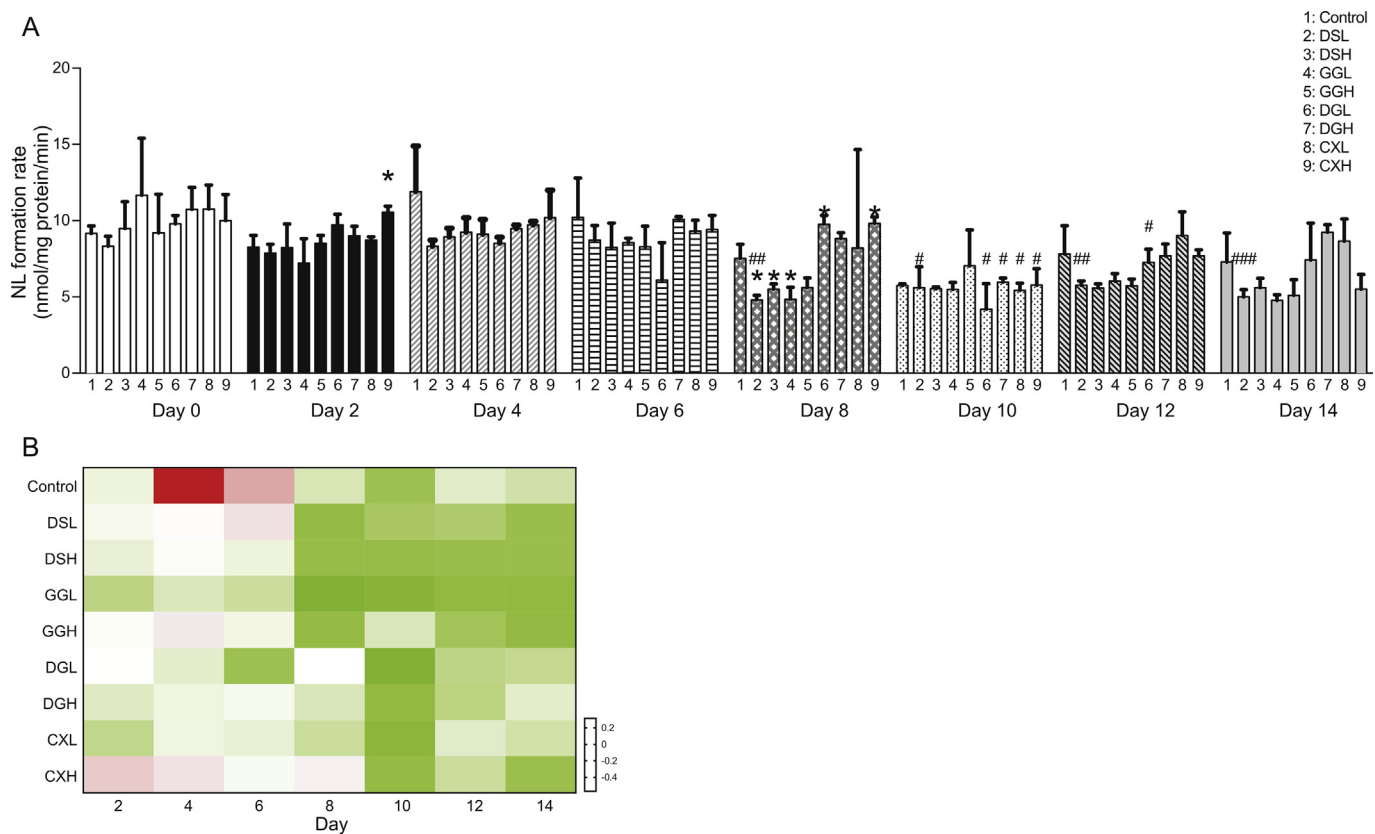
Fig. 7. CES1 activities in plasma of rats during the two-week TCM administrations. (A) Histogram for the CES1 activities in rats on Day 0, 2, 4, 6, 8, 10, 12 and 14. Data are means ± SD, $n = 6$ for control group and $n = 3$ for TCM dosed groups. *$p < 0.05$, **$P < 0.01$ compared with control. #$P < 0.05$, ##$P < 0.01$, ###$P < 0.001$ compared with Day 0. (B) Heatmap for z-scored fold change of CES1 activities in rats on Day 2, 4, 6, 8, 10, 12 and 14 relative to Day 0, respectively.

doses with DS and GG affecting CES1 activity in plasma to the greatest extent, while DG and CX affected activity in tissues to a greater extent. DS/GG treatment resulted in a trend of decreased CES1 activity in plasma, while DG and CX treatment led to a significant decrease in CES1 activity in kidney and lung, respectively. Our bioluminescence assay not only provided comprehensive in vivo tissue distribution profiles for CES1 in rats but also could be used for the identification of potential CES1 inhibitors or inducers and for monitoring CES1 activity during drug/drug and drug/herb treatments in clinical practice.

Conflicts of interest

The authors declare that there are no conflicts of interest.

Acknowledgments

Appendix A. Supplementary data

Supplementary data to this article can be found online at https://doi.org/10.1016/j.jpha.2020.05.006.

References

[1] S.C. Laizure, V. Herring, Z. Hu, et al., The role of human carboxylesterases in drug metabolism: have we overlooked their importance? Pharmacotherapy 33 (2013) 210–222.

[2] D. Li, The impact of carboxylesterases in drug metabolism and pharmacokinetics, Curr. Drug Metabol. 19 (2018) 91–102.

[3] T. Satoh, P. Taylor, W.F. Bosron, et al., Current progress on esterases: from molecular structure to function, Drug Metab. Dispos. 30 (2002) 488–493.

[4] D.D. Wang, L.W. Zou, Q. Jin, et al., Human carboxylesterases: a comprehensive review, Acta Pharm. Sin. B 8 (2018) 699–712.

[5] H.J. Zhu, J.S. Markowitz, Carboxylesterase 1 (CES1) genetic polymorphisms and oseltamivir activation, Eur. J. Clin. Pharmacol. 69 (2013) 733–734.

[6] T. Imai, Y. Takase, H. Iwase, et al., Involvement of carboxylesterase in hydrolysis of propranolol prodrug during permeation across rat skin, Pharmaceutics 5 (2013) 371–384.

[7] M. Hosokawa, Structure and catalytic properties of carboxylesterase isozymes involved in metabolic activation of prodrugs, Molecules 13 (2008) 412–431.

[8] L. Zhou, Z. Zuo, M.S. Chow, Danshen: an overview of its chemistry, pharmacology, pharmacokinetics, and clinical use, J. Clin. Pharmacol. 45 (2005) 1345–1359.

[9] Z.X. Chen, X.Q. Liu, W.Y. Gao, et al., Studies on pharmacology, toxicology and pharmacokinetics of the chemical constituents in hemorrheologic agent, Asian J. Pharmacodyn. Pharmacokinet. 8 (2008) 15–30.

[10] W.Y. Tam, P. Chook, M. Qiao, et al., The efficacy and tolerability of adjunctive alternative herbal medicine (Salvia miltiorrhiza and Pueraria lobata) on vascular function and structure in coronary patients, J. Alternative Compl. Med. 15 (2009) 415–421.

[11] Z. Zhang, T.N. Lam, Z. Zuo, Radix Puerariae: an overview of its chemistry, pharmacology, pharmacokinetics, and clinical use, J. Clin. Pharmacol. 53 (2013) 787–811.

[12] B. Ge, Z. Zhang, Z. Zuo, Radix Puerariae lobatae (Gegen) suppresses the anticoagulation effect of warfarin: a pharmacokinetic and pharmacodynamics study, Chin. Med. 11 (2016) 7.

[13] Z. Wen, Z. Wang, S. Wang, et al., Discovery of molecular mechanisms of traditional Chinese medicinal formula Si-Wu-Tang using gene expression microarray and connectivity map, PloS One 6 (2011), e18278.

[14] G.H. Li, H.Y. Jiang, Y.M. Xie, et al., Preliminary study on integration of traditional Chinese medicine and western medicine in patients with coronary heart disease in real world, Zhongguo Zhongyao Zazhi 39 (2014) 3474–3478.

[15] F. Rollini, F. Franchi, D.J. Angiolillo, Switching P2Y12-receptor inhibitors in patients with coronary artery disease, Nat. Rev. Cardiol. 13 (2016) 11–27.

[16] M. Valgimigli, H. Bueno, R.A. Byrne, et al., ESC focused update on dual antiplatelet therapy in coronary artery disease developed in collaboration with eacts: the task force for dual antiplatelet therapy in coronary artery disease of the European Society of Cardiology (ESC) and of the european association for cardio-thoracic surgery (EACTS), Eur. Heart J. 39 (2017) 213–260, 2018.

[17] M. Xiao, C. Qian, X. Luo, et al., Impact of the Chinese herbal medicines on dual antiplatelet therapy with clopidogrel and aspirin: pharmacokinetics and pharmacodynamics outcomes and related mechanisms in rats, J. Ethnopharmacol. 235 (2019) 100–110.

[18] J. Oh, S. Lee, H. Lee, et al., The novel carboxylesterase 1 variant c.662A>G may decrease the bioactivation of oseltamivir in humans, PloS One 12 (2017), e0176320.

[19] J. Wei, L.X. Zhang, Natural Products: Drug Discovery and Therapeutic Medicine, Humana Press, Totowa, 2005, pp. 229–250.

[20] L.C. Edwin, Y. Nobuo, Complementary and Alternative Approaches to Biomedicine, Kluwer Academic/Plenum Publishers, New York, 2004, pp. 27–28.

[21] B.G. Zhang, X.L. Wang, Q.F. Liu, Current status and development of Chinese herbal medicine granules, Chin. Pharmaceut. J. 35 (2000) 487–489.

[22] H. Luo, Q. Li, A. Flower, et al., Comparison of effectiveness and safety between granules and decoction of Chinese herbal medicine: a systematic review of randomized clinical trials, J. Ethnopharmacol. 140 (2012) 555–567.

[23] M. Hosokawa, T. Satoh, Measurement of carboxylesterase (CES) activities, Curr. Protoc. Toxicol. (Suppl. 10) (2002) 4 7.1–4.7.14.

[24] J.A. Crow, A. Borazjani, P.M. Potter, M.K. Ross, Hydrolysis of pyrethroids by human and rat tissues: examination of intestinal, liver and serum carboxylesterases, Toxicol. Appl. Pharmacol. 221 (2007) 1–12.

[25] M.K. Ross, A. Borazjani, Enzymatic activity of human carboxylesterases, Curr.

[26] D.D. Wang, Q. Jin, J. Hou, et al., Highly sensitive and selective detection of human carboxylesterase 1 activity by liquid chromatography with fluorescence detection, J. Chromatogr. B 1008 (2016) 212–218.

[27] D.D. Wang, Q. Jin, L.W. Zou, et al., A bioluminescent sensor for highly selective and sensitive detection of human carboxylesterase 1 in complex biological samples, Chem. Commun. (Camb.) 52 (2016) 3183–3186.

[28] L. Yang, D.D. Wang, G.B. Ge, et al., Bioluminescence Detection Kit for hCE1 (Human Carboxylesterase 1) as Well as Use Method and Application of Bioluminescence Detection Kit, CN107271432A, China, 2017.

[29] L. Yang, L.W. Zou, G.B. Ge, et al., Bioluminescence Probe Substrate for Human Carboxylesterase 1 and Preparation Method and Application Thereof, CN105712987A, China, 2016.

[30] T. Imai, M. Hosokawa, Prodrug approach using carboxylesterases activity: catalytic properties and gene regulation of carboxylesterase in mammalian tissue, J. Pestic. Sci. 35 (2010) 229–239.

[31] Pharmacopoeia of the People's Republic of China, ume I, China Medical Science and Technology Press, Beijing, 2015. Edition, 2015, pp. 44 (Chuanxiong), 77 (Danshen), 133 (Dangui), 333 (Gegen).

[32] Hong Kong Chinese Medica Materia Standards, Volume 1: Danggu, Danshen; Volume 2: Chuanxiong; Volume 3: Gegen, D.o.H. Chinese Medicine Division, the Government of the Hong Kong Special Administrative Region, the People's Republic of China, Hongkong, 2012. https://www.cmro.gov.hk/htmL/eng/GCMTI/hkcmms/volumes.htmL.

[33] B. Li, M. Sedlacek, I. Manoharan, et al., Butyrylcholinesterase, paraoxonase, and albumin esterase, but not carboxylesterase, are present in human plasma, Biochem. Pharmacol. 70 (2005) 1673–1684.

[34] H. Eng, M. Niosi, T.S. McDonald, et al., Utility of the carboxylesterase inhibitor bis-para-nitrophenylphosphate (BNPP) in the plasma unbound fraction determination for a hydrolytically unstable amide derivative and agonist of the TGR5 receptor, Xenobiotica 40 (2010) 369–380.

[35] H.J. Zhu, D.I. Appel, Y.K. Peterson, et al., Identification of selected therapeutic agents as inhibitors of carboxylesterase 1: potential sources of metabolic drug interactions, Toxicology 270 (2010) 59–65.

[36] S.K. Quinney, S.P. Sanghani, W.I. Davis, et al., Hydrolysis of capecitabine to 5'-deoxy-5-fluorocytidine by human carboxylesterases and inhibition by loperamide, J. Pharmacol. Exp. Therapeut. 313 (2005) 1011–1016.

[37] P.W. Iversen, B. Beck, Y.F. Chen, et al., HTS Assay Validation: Assay Guidance Manual [Internet], Eli Lilly & Company and the National Center for Advancing Translational Sciences, Bethesda, 2012. https://www.ncbi.nlm.nih.gov/books/NBK83783/.

[38] Guidance for Industry Estimating the Maximum Safe Starting Dose in Initial Clinical Trials for Therapeutics in Adult Healthy Volunteers, U.S. Department of Health and Human Services, 2015. Food and Drug Administration, Center for Drug Evaluation and Research (CDER), https://www.fda.gov/media/72309/download.

[39] M.K. Ross, A. Borazjani, R. Wang, et al., Examination of the carboxylesterase phenotype in human liver, Arch. Biochem. Biophys. 522 (2012) 44–56.

[40] J. Fu, E. Pacyniak, M.G.D. Leed, et al., Interspecies differences in the metabolism of a multiester prodrug by carboxylesterases, J. Pharm. Sci. 105 (2016) 989–995.

[41] Y.Q. Wang, X.F. Shang, L. Wang, et al., Interspecies variation of clopidogrel hydrolysis in liver microsomes from various manmmals, Chem. Biol. Interact. 315 (2020) 108871.

[42] T. Tabata, M. Katoh, S. Tokudome, et al., Identification of the cytosolic carboxylesterase catalyzing the 5'-deoxy-5-fluorocytidine formation from capecitabine in human liver, Drug Metab. Dispos. 32 (2004) 1103–1110.

[43] T. Satoh, M. Hosokawa, The mammalian carboxylesterases: from molecules to functions, Annu. Rev. Pharmacol. Toxicol. 38 (1998) 257–288.

[44] T. Satoh, M. Hosokawa, Carboxylesterases: structure, function and polymorphism in mammals, J. Pestic. Sci. 35 (2010) 488–493.

[45] M.J. Hatfield, L.G. Tsurkan, J.L. Hyatt, et al., Modulation of esterified drug metabolism by tanshinones from *Salvia miltiorrhiza* ("Danshen"), J. Nat. Prod. 76 (2013) 36–44.

[46] D.X. Sun, G.B. Ge, P.P. Dong, et al., Inhibition behavior of fructus psoraleae's ingredients towards human carboxylesterase 1 (hCES1), Xenobiotica 46 (2016) 503–510.

[47] K. Hagihara, M. Kazui, H. Ikenaga, et al., Comparison of formation of thiolactones and active metabolites of prasugrel and clopidogrel in rats and dogs, Xenobiotica 39 (2009) 218–226.

[48] B.L. Welch, The generalization of "Student's" problem when several different population variances are involved, Biometrika 34 (1947) 28–35.

[49] M. Delacre, D. Lakens, C. Leys, Why psychologists should by default use Welch's t-test instead of Student's t-test, Int. Rev. Soc. Psychol. 30 (2017) 92–101.

[50] G.V. Glass, P.D. Peckham, J. R Sanders, Con-sequences of failure to meet assumptions underlying the fixed effects analyses of variance and covariance, Rev. Educ. Res. 42 (1972) 237–288.

Original article

An ultra-sensitive and easy-to-use assay for sensing human UGT1A1 activities in biological systems

Ya-Di Zhu [a, b], Hui-Lin Pang [c], Qi-Hang Zhou [a], Zi-Fei Qin [d], Qiang Jin [a], Moshe Finel [e], Yi-Nan Wang [a], Wei-Wei Qin [f], Yin Lu [b], Dan-Dan Wang [a, **], Guang-Bo Ge [a, b, *]

[a] Institute of Interdisciplinary Integrative Medicine Research, Shanghai University of Traditional Chinese Medicine, Shanghai, 201203, China
[b] Jiangsu Key Laboratory for Pharmacology and Safety Evaluation of Chinese Materia Medica, School of Pharmacy, Nanjing University of Chinese Medicine, Nanjing, 210023, China
[c] School of Life Science and Medicine, Dalian University of Technology, Panjin, 124221, China
[d] Department of Pharmacy, The First Affiliated Hospital of Zhengzhou University, Zhengzhou, China
[e] Division of Pharmaceutical Chemistry and Technology, Faculty of Pharmacy, University of Helsinki, 00014, Finland
[f] Department of Pharmacy, Huashan Hospital, Fudan University, Shanghai, China

ARTICLE INFO

ABSTRACT

The human UDP-glucuronosyltransferase 1A1 (UGT1A1), one of the most essential conjugative enzymes, is responsible for the metabolism and detoxification of bilirubin and other endogenous substances, as well as many different xenobiotic compounds. Deciphering UGT1A1 relevance to human diseases and characterizing the effects of small molecules on the activities of UGT1A1 requires reliable tools for probing the function of this key enzyme in complex biological matrices. Herein, an easy-to-use assay for highly-selective and sensitive monitoring of UGT1A1 activities in various biological matrices, using liquid chromatography with fluorescence detection (LC-FD), has been developed and validated. The newly developed LC-FD based assay has been confirmed in terms of sensitivity, specificity, precision, quantitative linear range and stability. One of its main advantages is lowering the limits of detection and quantification by about 100-fold in comparison to the previous assay that used the same probe substrate, enabling reliable quantification of lower amounts of active enzyme than any other method. The precision test demonstrated that both intra- and inter-day variations for this assay were less than 5.5%. Furthermore, the newly developed assay has also been successfully used to screen and characterize the regulatory effects of small molecules on the expression level of UGT1A1 in living cells. Overall, an easy-to-use LC-FD based assay has been developed for ultra-sensitive UGT1A1 activities measurements in various biological systems, providing an inexpensive and practical approach for exploring the role of UGT1A1 in human diseases, interactions with xenobiotics, and characterization modulatory effects of small molecules on this conjugative enzyme.

1. Introduction

UDP-glucuronosyltransferases1A1 (UGT1A1) is one of the most essential enzymes responsible for the biotransformation and detoxification of the endogenous toxin bilirubin, and metabolic clearance of a variety of crucial therapeutic drugs and other xenobiotics [1,2]. Multiple evidences have indicated that dysfunction or potent inhibition of hepatic UGT1A1 may result in a disorder of bilirubin metabolism, causing different degrees of hyperbilirubinemia, liver disorders, and other diseases [3,4]. In addition, reduced expression/activities of UGT1A1 may trigger clinically relevant drug/herbs-drug interactions by affecting the pharmacokinetic behaviors of the UGT1A1-substrate drugs [5–7]. Due to the vital roles of UGT1A1 in biotransformation of both endogenous compounds (particularly bilirubin conjugation) and drugs, the European Medicines Agency (EMA) and the US Food and Drug Administration (FDA) have recommended that the inhibition

potency of new drug candidates or phytochemical products on UGT1A1 activities should be tested before marketing approval [8].

A panel of analytical methods have already been reported for studying the inhibition potency of different drug candidates or phytochemical products on the human UGT1A1, either employing the recombinant enzyme or liver preparations, such as microsomes [9]. However, most of the previously reported methods had considerable limitations in sensing UGT1A1 activities in biological samples that vary from instability of the substrate under the assay conditions, to poor selectivity towards UGT1A1 over other hepatic UGTs, to low sensitivity unless liquid chromatography-tandem mass spectrometry (LC-MS/MS) is used as the analytical tool [10,11]. Usually, the LC-MS/MS based assays are costly and labor-intensive, because the expensive instruments and skillful operators are always required.

Recently, we have developed two isoform-specific fluorogenic substrates for the human UGT1A1, which provide alternative methods for high-throughput detection of this key enzyme, using fluorescence-based assays [12,13]. In particular, a recent investigation has clearly demonstrated that N-butyl-4-(4-hydroxyphenyl)-1,8-naphthalimide (NHPN) is an isoform-specific fluorogenic probe for UGT1A1 (Fig. 1A), which binds at the bilirubin binding site on this key enzyme, is highly suitable for replacing bilirubin for measuring UGT1A1 activities and investigating UGT1A1-ligand interactions in tissue preparations [13,14]. Nevertheless, even though the specificity of NHPN for UGT1A1 is high, the fluorogenic properties of this probe are not good enough, mainly due to short emission wavelength of its O-glucuronide (<520 nm). This is a problem since some endogenous compounds and phytochemicals emit fluorescence signals at visible wavelengths (400−600 nm), leading to a high background fluorescence

that may strongly affect the detection of NHPN O-glucuronide, lowering its sensitivity and accuracy. Hence, it is necessary to develop a practical and accurate method for highly selective and ultra-sensitive probing of UGT1A1 activities in complex biological matrix. The practical approach is to take advantage of the high specificity of NHPN and combine it with improved analytical assays that include advanced fluorescence detection, allowing taking full benefits of this newly developed fluorogenic substrate for UGT1A1.

In the present study, a reliable and easy-to-use assay for high sensitivity and selectivity probing of UGT1A1 activities in various biological systems is presented in details. To this end, NHPN was used as the fluorogenic substrate, while liquid chromatography with fluorescence detection (LC-FD) was used to separate the target analytes without interference from the endogenous matrix. The assay was fully validated in terms of sensitivity, specificity, precision, quantitative linear range and stability. Furthermore, the newly developed LC-FD based assay was successfully used to measure UGT1A1 activities in tissue preparations, as well as to screen and characterize the regulatory effects of small molecules on this conjugative enzyme in living cells. Collectively, these findings provided a practical and reliable assay for probing UGT1A1 activities, which would strongly facilitate UGT1A1-associated studies in both academic and industrial fields.

2. Methods and experimental

2.1. Reagents and materials

The fluorogenic probe substrate N-butyl-4-(4-hydroxyphenyl)-1,8-naphthalimide (NHPN) and its O-glucuronide (NHPNG) were synthesized and purified (purity≥98%) according to the previously reported scheme [13]. Nilotinib and chrysin were from Dalian Meilun Biotech Co., Ltd. (Meilun, Dalian, China). The tissue preparations, including pooled human liver microsomes (HLM), pooled human intestine microsomes (HIM), pooled human kidney microsomes (HKM), and pooled human lung microsomes (HLuM) were purchased from Celsis Inc. (Baltimore, MD, USA). Recombinant human UGT1A1 was from BD Biosciences (Woburn, MA, USA). Stably transfected HeLa cells (named HeLa-UGT1A1 cells) were constructed as previously reported [15−17]. The uridine diphosphate-glucuronic acid (UDPGA), polyethylene glycol hexadecyl ether (Brij 58) and anti-GAPDH antibody (G8795) were purchased from Sigma-Aldrich (St. Louis, MO, USA). Anti-UGT1A1 antibody (ab194697) was obtained from Abcam (Cambridge, MA). The reagents for the SimpleWestern blotting system were purchased from ProteinSimple (San Jose, CA). Ultrapure water purified by Milli-Q® Integral Water Purification System (Millipore, USA) was used throughout, while LC grade methanol, acetonitrile, and formic acid were ordered from Tedia (Fairfield, USA).

2.2. Chromatography and analytical conditions

Both NHPN and NHPNG were analyzed by a UFLC system (Shimadzu, Kyoto, Japan), equipped with a CBM-20A communications bus module, two LC-20AD pumps, a DGU-20A5R vacuum degasser, a SIL-20AC autosampler, a CTO-20AC column oven, and an RF-20A fluorescence detector. A Shim-pack VP-ODS C_{18} column (4.6 mm × 150 mm, 5 μm, Shimadzu) was used in this study, and the column temperature was maintained at 40 °C. The fluorescence signals of NHPN and NHPNG were recorded with the excitation wavelength at 370 nm, while the emission wavelength was set at 520 nm [13]. The mobile phase was a mixture of acetonitrile (A) and 0.2% formic acid (B). The following gradient elution program was used: 0−0.5 min, 40%−20% B; 0.5−1.8 min, 20%−5% B; 1.8−3.8 min, 5% B; 3.8−5 min, 20%−40% B; and 5−6 min, balance to 40% B.
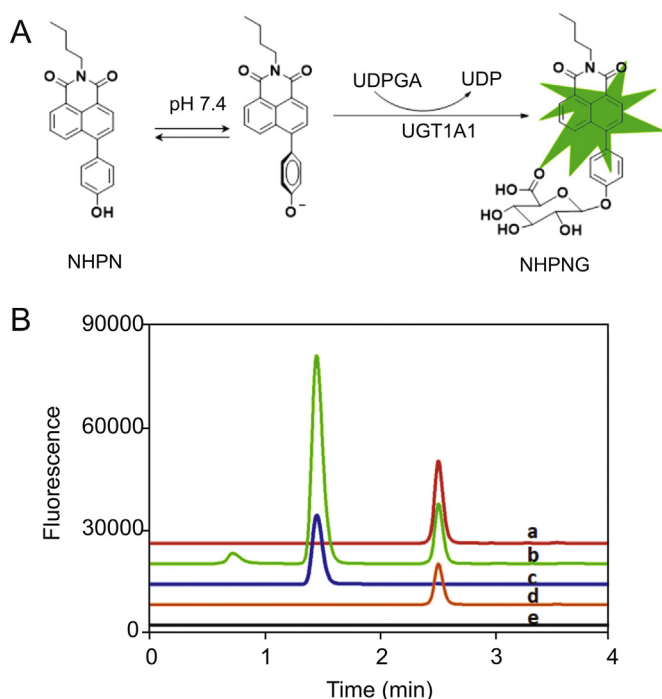
Fig. 1. The chemical structure of NHPN and its mechanism for sensing UGT1A1 activity (A). Liquid chromatography-fluorescence detection (LC-FD) chromatograms of NHPN and NHPNG (B). (a) NHPN only, (b) NHPN was co-incubated with UDPGA in the presence of activated HLM (0.5 mg/mL) at 37 °C for 20 min, (c) NHPNG only, (d) NHPN was co-incubated with HLM (0.5 mg/mL) but without UDPGA, (e) buffer only. The fluorescence signals of NHPN and NHPNG were recorded using excitation wavelength of 370 nm and emission wavelength of 520 nm.

2.3. Method validation

In this study, the limit of detection (LOD), the limit of quantification (LOQ), the linear range for UGT1A1 activities detection, matrix effects, as well as the precision and stability of the newly developed LC-FD based assay were carefully investigated. LOD and LOQ were determined as the fluorescence signals of NHPNG that produces three and ten folds of the baseline noise, respectively. Standard curves were constructed by using seven concentrations of both NHPN and NHPNG. The linearity of the method was evaluated by linear regression analysis. The inter-day and intra-day precision of the newly identified LC-FD based method was assessed by analyzing three different batches of samples and different concentrations of NHPN (0.2 μM, 1 μM and 8 μM) and NHPNG (2 nM, 20 nM, 80 nM). To assess intra-day precision, the NHPN and NHPNG concentrations in each sample were measured within 24 h. For inter-day assays, NHPN and NHPNG in each sample were quantified for three consecutive days. The overall precision was expressed using relative standard deviation (%, RSD). Stability was evaluated by analyzing the concentrations of NHPNG in UGTs reaction mixtures stored for 24 h or 48 h at 4 °C.

2.4. Enzymatic activities and kinetic analyses

The activities and kinetic behavior of NHPN-O-glucuronidation were investigated in both recombinant human UGT1A1 and pooled HLM. Prior to kinetic analyses, the linear fluorescent responses with respect to protein concentration and reaction time in each type of sample were investigated. After that, the kinetic plots of recombinant UGT1A1-mediated NHPN-O-glucuronidation were constructed using the following NHPN concentrations 0, 0.1, 0.5, 1, 2, and 5 μM. The protein concentrations were 0.01 mg/mL for both recombinant UGT1A1 and HLM. The relationship between the substrate concentration [S] and the rate of formation NHPNG [V] was plotted, and the Hill kinetic equation (Eq. 1) was employed to calculate the kinetic parameters.

$$V = V_{max} S^n / (S_{50}^n + S^n) \qquad (1)$$

Here, V is the O-glucuronidation rate, V_{max} is the maximum O-glucuronidation rate, S is the NHPN concentration, S_{50} is the NHPN concentration resulting in 50% of V_{max}, and n is the Hill coefficient.

2.5. Determination of UGT1A1 activities and protein level in biological samples

The UGT1A1 activities in tissue preparations from different human samples, including HLM, HIM, HKM and HLuM, were measured by the newly developed LC-FD assay. Tissue preparations (0.2 mg/mL, final protein concentration) were first activated by pre-incubation with Brij 58 on ice for 20 min. Subsequently, a total volume of 90 μL incubation system consisting of NHPN (5 μM, final concentration), Tris-HCl buffer (50 mM, pH 7.4), MgCl$_2$ (5 mM), and the tissue preparation (mixed with Brij 58) was pre-incubated at 37 °C for 3 min, and then reaction was initiated by the addition of UDPGA (dissolved in water) to a final concentration of 4 mM. Following incubation at 37 °C for 30 min, 100 μL ice-cold acetonitrile was added to terminate the reaction. Following centrifugation at 20,000 g for 20 min, the supernatant was subjected to LC-FD analysis. Meanwhile, the UGT1A1 protein levels in HLM, HIM, HKM and HLuM could be assayed by the SimpleWestern blotting system. For the latter, in brief, 3 μL of total protein lysate (0.4 mg/mL, final concentration) was loaded into a SimpleWes assay plate (12- to 230-kDa, ProteinSimple, USA) and 400 nL of each sample was withdrawn through a capillary according to the manufacturer's instruction.

2.6. UGT1A1 inhibition assays using various enzyme sources

Nilotinib (a known human UGT1A1 inhibitor) was used for testing the efficiency of the newly developed LC-FD based assay to monitor the O-glucuronidation rates of NHPN in UGT1A1 inhibition assays by various biological systems [18,19]. HLM (0.05 mg/mL, final concentration) was first pre-incubated with the same concentration of Brij 58 on ice for 20 min and then at 37 °C for 3 min. Thereafter, an incubation system was conducted as described in Section 2.5 with or without nilotinib (DMSO only). Following incubation for 30 min at 37 °C, 100 μL ice-cold acetonitrile was added to the incubation system to terminate the reaction. Subsequently, the reaction mixture was centrifuged at 20,000 g for 20 min. The supernatant was subjected to LC-FD analysis. As for UGT1A1 inhibition assays in living cells, Hela-UGT1A1 cell lines were grown in DMEM/high glucose medium supplemented with 10% fetal bovine serum (FBS), in a humidified atmosphere (95% air and 5% CO$_2$) at 37 °C. Hela-UGT1A1 cells were seeded in 96-well plates. When cells in 96-well plates were about 50% confluent, they were treated with nilotinib for 1 h. After that, cells were treated with NHPN (50 μM, final concentration) for 3 h, then terminated by adding the equal volume of ice-cold acetonitrile. The reaction mixture was centrifuged at 20,000 g for 20 min. The supernatant was subjected to LC-FD analysis. The IC$_{50}$ values of nilotinib on UGT1A1-mediated NHPN-O-glucuronidation in HLM and in recombinant UGT1A1 were estimated by using GraphPad Prism V6.0 (Graphpad Software Inc., La Jolla, USA).

2.7. UGT1A1 induction assays in living cells

Chrysin was used as a positive inducer of UGT1A1 [20,21]. Here we used it to try and induce UGT1A1 in living cells. In brief, Caco-2 cells were cultured in DMEM/high glucose medium, supplemented with 10% FBS and 1% penicillin-streptomycin solution, in a humidified atmosphere (95% air and 5% CO$_2$) at 37 °C. The cells were seeded in 6-well plates and 96-well plates, respectively. Chrysin was added into the cell culture system, at the final concentrations of either 2 μM, 10 μM, or 25 μM. Following 72 h co-incubation with chrysin, the cells were collected for mRNA assay and UGT1A1 activities assay. For mRNA level assay, the cells were collected with RNAiso Plus reagent and the total RNA was extracted as previously described [22]. The cDNA was synthesized from total RNA using RNA PCR kit. Real-time PCR experiments were performed on an ABI 7500 real-time PCR System. The primers used are listed in Table S1 [23,24]. For UGT1A1 activities assay, after the final day of induction treatment, the cell medium was discarded and the cultured cells were incubated with 50 μM NHPN in a serum-free medium. After 3 h incubation, 50 μL of the medium in each well was mixed with ice-cold acetonitrile (50 μL). The mixture was then centrifuged at 20,000 g for 20 min, and the supernatant was subjected to LC-FD analysis.

3. Results and discussion

3.1. Method development

As mentioned above, we are looking for a way to avoid the interference of endogenous substances and some tested drugs or other xenobiotics which may affect the fluorescence output of the substrate NHPN and its NHPNG [13]. To this end, an LC-FD based assay was developed via integration of the advantages of both chromatographic separation and fluorescence detection. As shown in Fig. 1B, at the excitation wavelength of 370 nm, both NHPN and
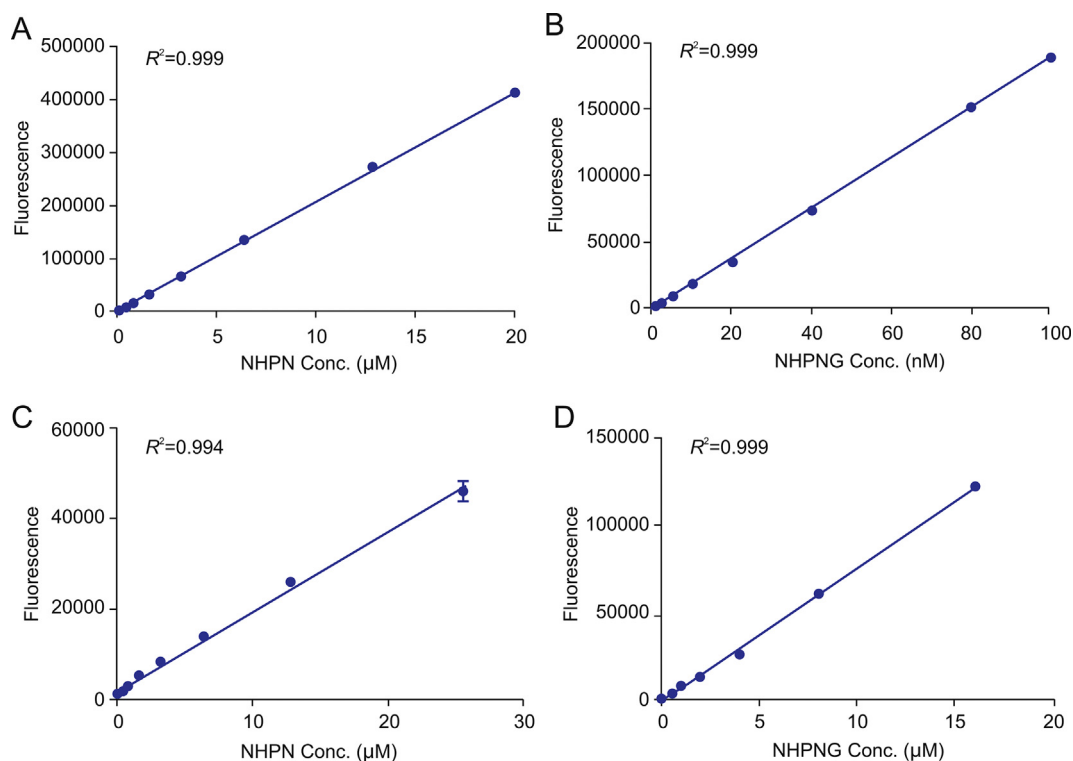
Fig. 2. The standard curves of NHPN (A) and NHPNG (B) in Tris-HCl and acetonitrile (1:1, v/v), by using LC-FD based assay. The standard curves of NHPN (C) and NHPNG (D) in Tris-HCl and acetonitrile (1:1, v/v), by using microplate reader based assay.

Table 1
The linear range, LOD, and LOQ of NHPNG using microplate reader and LC-FD.

Method	Analyte	Linear (nM)	LOD (nM)	LOQ (nM)
Microplate reader	NHPNG	100–30000	40	100
LC-FD	NHPNG	1–100	0.5	1

NHPNG exhibited good fluorescence response and could be well separated within 3.0 min. The chromatographic separation using acetonitrile (A) and 0.2% formic acid-water (B) as the mobile to generate the mobile phase and the suitable gradient resulted in very high resolution and separation of NHPN and NHPNG (Fig. S1). Notably, most of the endogenous compounds could already be eluted from the ODS column within the first minute (near the dead time), which greatly reduced the interference from endogenous matrix during fluorescence analysis of the two aim analytes (the retention times of the aim analytes were 2.51 min and 1.53 min, for NHPN and NHPNG, respectively). The specificity of the newly developed LC-FD method for detection of NHPN or NHPNG is very high. By the way, as shown in Fig. S2, no interference peaks were

Table 2
Intra- and inter-day variability of the LC-FD based assay for quantitative determination of NHPN and NHPNG.

Compound	Theoretical concentrations	Intra-day ($n = 3$)		Inter-day ($n = 3$)	
		Measured concentration	RSD (%)	Measured concentration	RSD (%)
NHPN	0.2 μM	0.19 μM	0.71	0.18 μM	3.90
	1 μM	1.07 μM	1.96	0.99 μM	5.03
	8 μM	7.76 μM	1.12	7.29 μM	5.33
NHPNG	2 nM	2.52 nM	3.69	2.38 nM	1.91
	20 nM	19.95 nM	1.10	18.92 nM	4.40
	80 nM	81.86 nM	1.74	79.70 nM	1.52

Table 3
Stability of the main product NHPNG in reaction mixtures.

Analyte	Enzyme source	Conditions	Initial conc. (nM)	Measured conc. (nM)	Recovery (%)
NHPNG	HLM	4 °C, 24 h	4.52	4.33	95.79
	HLM	4 °C, 48 h	4.52	4.35	96.23
	HLM	4 °C, 24 h	39.92	39.16	98.10
	HLM	4 °C, 48 h	39.92	38.94	97.54
	HLM	4 °C, 24 h	81.01	80.19	98.98
	HLM	4 °C, 48 h	81.01	78.86	97.34
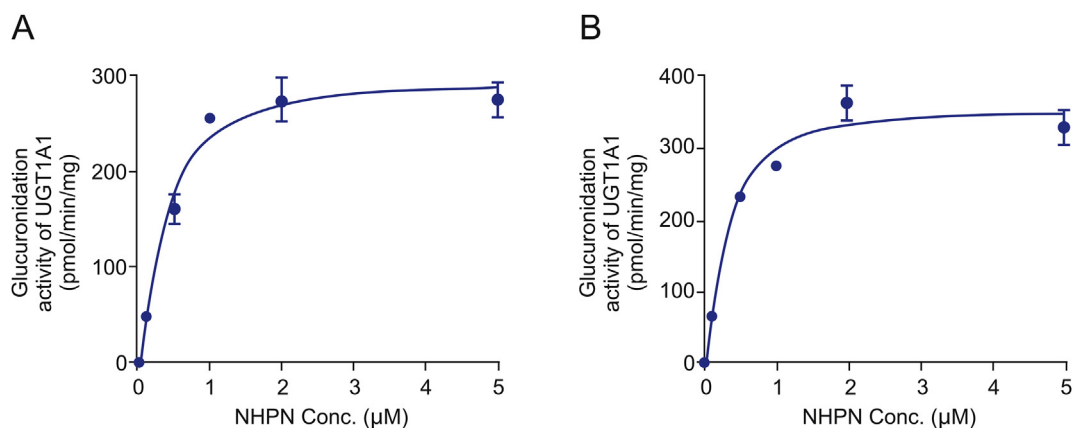
Fig. 3. Enzymatic kinetic plots of NHPN-*O*-glucuronidation in HLM (A) and in recombinant human UGT1A1 (B).
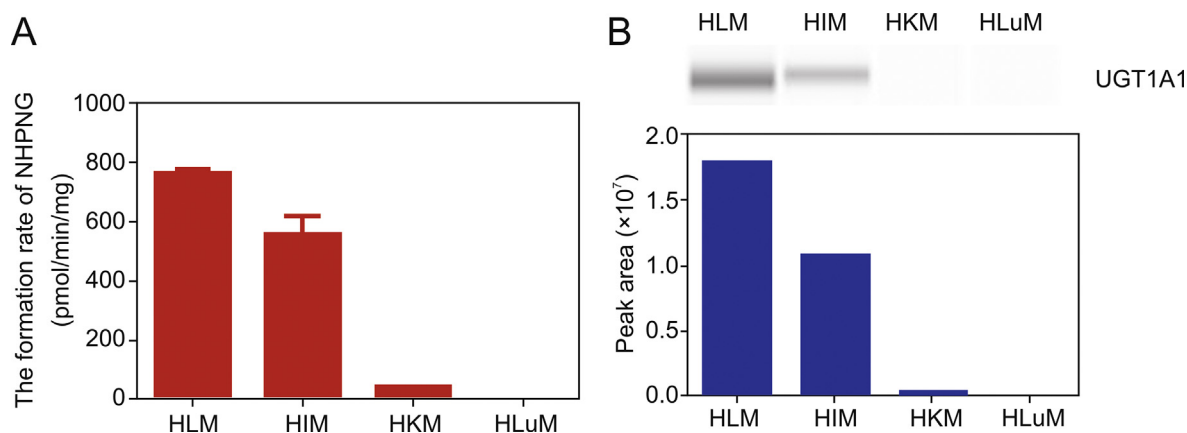
Fig. 4. NHPN-*O*-glucuronidation activities (A) and protein levels (B) of UGT1A1 in HLM, HIM, HKM and HLuM.

detected in blank tissue samples in the retention time of NHPN or NHPNG.

3.2. Method validation

The newly developed LC-FD based assay was rigorously validated in terms of linear range, precision, accuracy and stability. As depicted in Figs. 2A and B, the calibration curves of both NHPN and NHPNG exhibited good linearity between peak areas and concentrations while using this newly developed LC-FD based assay, within the linear range of 0.1—20 μM and 2—100 nM, for NHPN and NHPNG, respectively. Meanwhile, as shown in Figs. 2C and D, the calibration curves were also constructed for NHPN and NHPNG and it showed satisfactory linearity between the fluorescence response and the concentration within the range of 0—25 μM and 0—16 μM, respectively. The linear fluorescence responses with increasing concentrations of recombinant hUGT1A1 were also investigated and are presented in Fig. S3. Notably, the LOQ of NHPNG was calculated as low as 1 nM (Table 1), which was equivalent to that of the generated NHPNG in 0.16 μg/mL of hUGT1A1 under optimized conditions (1 μM NHPN was incubated with hUGT1A1 for 30 min at 37 °C). To the best of our knowledge, the described LC-FD based method is currently the most sensitive UGT1A1 activities assay. The intra-day and inter-day variabilities of this assay were also determined via quantification of the two main analytes in different samples. As shown in Table 2, the relative standard deviation (RSD) for quantification of the two analytes was less than 5.5% and 5.0%,

for NHPN and NHPNG, respectively. Furthermore, as shown in Table 3, the stability of NHPNG in different reaction mixtures was tested by analyzing the samples stored at 4 °C for different storage time (0 h, 24 h and 48 h). The results clearly showed that NHPNG in the reaction mixture was stable after storage of 48 h, with over 90% recovery. These findings suggested that the newly developed LC-FD based assay is highly sensitive and reliable, making it is suitable for sensing UGT1A1 activities in biological samples.

3.3. Kinetic analyses using the LC-FD based assay

Enzymatic kinetic behavior of the maker reaction is an important indication for sensing the real activities of the target enzyme in biological samples [25]. Unfortunately, kinetic plots of NHPN-*O*-glucuronidation could hardly be examined by the microplate reader-based assay, owing to the limited sensitivity at low substrate concentrations. In the present study, this problem has been solved and the kinetic plots of NHPN-*O*-glucuronidation in HLM and in recombinant hUGT1A1 were carefully analyzed using the newly developed LC-FD based method. The kinetic curves of NHPN-*O*-glucuronidation in both recombinant hUGT1A1 and HLM are displayed in Fig. 3. It is clear that the kinetic behaviors of NHPN-*O*-glucuronidation in both HLM and UGT1A1 are well-fitted to the Hill equation, and the derived kinetic constants are listed in Table S2. Hence, NHPN-*O*-glucuronidation in both HLM and UGT1A1 exhibited similar kinetic behaviors, with quite similar S_{50} values (0.27 μM in recombinant UGT1A1 and 0.41 μM in HLM) and similar
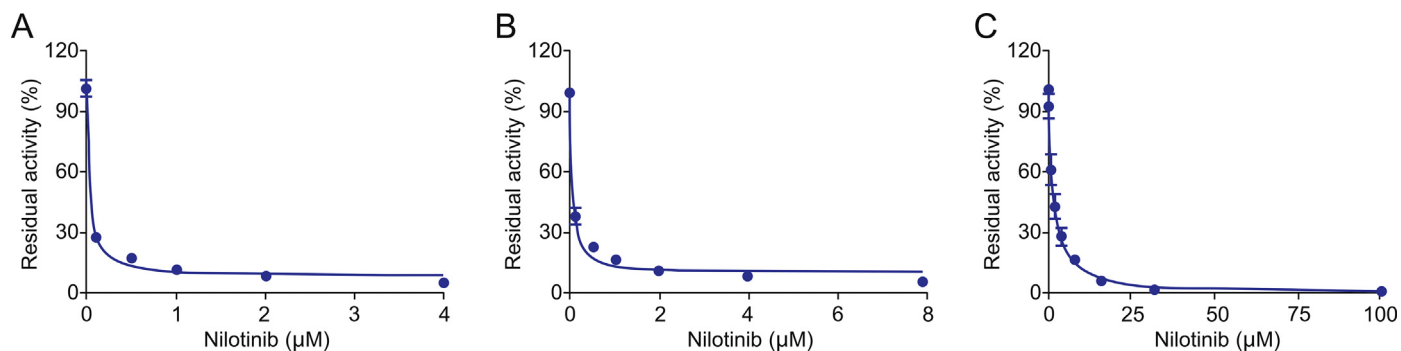
Fig. 5. The dose-inhibition curves of nilotinib against UGT1A1-catalyzed NHPN-*O*-glucuronidation in various enzyme sources, including recombinant UGT1A1 (A), HLM (B) and Hela-UGT1A1 living cells (C).
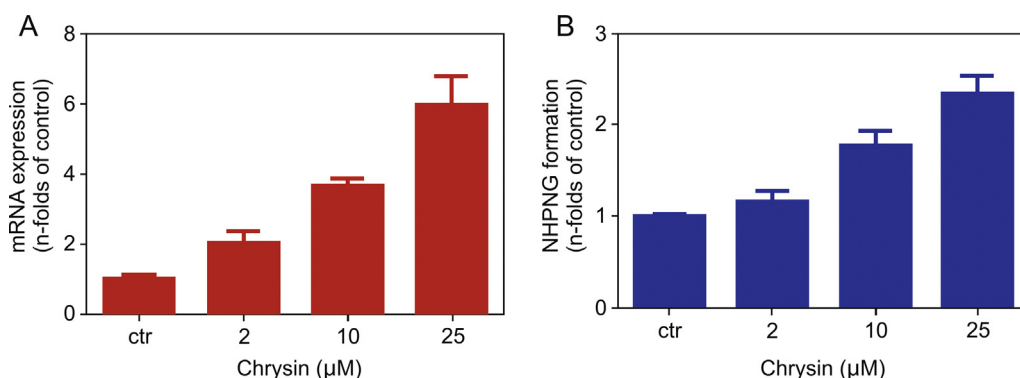
Fig. 6. Induction of UGT1A1 by different doses of chrysin (0 μM, 2 μM, 10 μM, 25 μM) in living Caco-2 cells. (A) The UGT1A1 mRNA levels were monitored by real-time PCR, and (B) the UGT1A1 activity was determined by the LC-FD based assay.

V_{max} values (330.1 pmol/min/mg protein in recombinant UGT1A1 and 307.6 pmol/min/mg protein in HLM). These findings clearly demonstrated that NHPN is a very high-affinity substrate for UGT1A1, with an S_{50} value of less than 0.5 μM, which is far below the S_{50} value of other UGT1A1 probe substrates, such as etoposide ($S_{50} = 285$ μM in HLM) or NCHN ($S_{50} = 365$ μM in HLM) [12,26].

3.4. Detection of UGT1A1 activities in tissue preparations

To further explore the practicability of this newly developed LC-FD based assay for sensing UGT1A1 activities in real samples, this assay was applied for sensing UGT1A1 activities in real samples. As shown in Fig. 4A, the UGT1A1 activities in microsomes from HLM, HIM, HKM and HLuM were determined by the LC-FD, using NHPN as the probe substrate. In addition, the protein levels of UGT1A1 in the same tissue preparations were assayed using Western blotting. The results clearly demonstrated that UGT1A1 was abundant in the human liver and the small intestine, barely detected in the kidney, and was undetectable in lung microsomes (Fig. 4B). These findings were highly consistent with those of several previous reports regarding UGT1A1 expression in the human body [27] and with the protein levels of UGT1A1 listed in the protein atlas database (https://www.proteinatlas.org/). It is worth noting that the determined UGT1A1 activities in the different tissue preparations are in good agreement with the (native) UGT1A1 protein levels in these biological samples, suggesting that the LC-FD based assay for sensing UGT1A1 is reliable and can be used for sensing the real activities of this key enzyme in complex biological samples.

3.5. UGT1A1 inhibition assays

The newly developed LC-FD based method was also applied in screening and characterization of UGT1A1 inhibitors, which is very useful for assessing and preventing potential risks of drug/herb-drug interactions. In this study, we used the leukemia drug niloti-nib as a known UGT1A1 inhibitor to test the inhibitory effects of nilotinib on UGT1A1 mediated NHPN-*O*-glucuronidation in re-combinant hUGT1A1, pooled HLM and HeLa-UGT1A1 cells. As shown in Fig. 5, UGT1A1-mediated NHPN-*O*-glucuronidation in all the tested enzyme sources could be strongly inhibited by nilotinib in a dose-dependent manner. The IC_{50} values for nilotinib, however, varied between the enzyme sources and they were 29.2 nM, 53.1 nM and 1494.0 nM, for recombinant UGT1A1, HLM and HeLa-UGT1A1 cells, respectively (Table S3). The data showed that the inhibition potency of nilotinib against UGT1A1 in living cells is much weaker than in recombinant UGT1A1 and in the isolated microsomal fraction of liver cells. Notably, the much weaker inhibition of UGT1A1 by nilotinib in intact cells, as revealed by our results (Table S3) was in good agreement with the approval of nilotinib as drug and that hyperbilirubinemia was not its main side effect. In addition, the new inhibition results were consistent with those in the previous reports regarding UGT1A1 inhibition [19], and also suggested that the newly developed LC-FD based assay is suitable for characterization and screening UGT1A1 inhibitors in different enzyme sources.

3.6. UGT1A1 induction assays

The new LC-FD based assay was subsequently used to evaluate

the induction of the UGT1A1 gene by small molecules in living cells. In this study, Caco-2 cells were used as model cells, while real-time PCR and NHPN-based biochemical methods were used to measure the mRNA level and catalytic activities of UGT1A1, respectively [20]. As shown in Fig. 6, both the mRNA level and O-lucuronidation activities of UGT1A1 were significantly enhanced by the presence of chrysin in the incubation medium in a dose-dependent manner. Furthermore, the increase in UGT1A1 activities (determined by the new LC-FD assay with NHPN as the substrate) matched quite well the relative abundance of UGT1A1 mRNA levels (detected by real-time PCR). The only slight difference was the relatively high activities seen already at the control sample, which could be attributed to the fact that UGT1A1 had already been expressed before the start of the experiment. Taking all the results in Fig. 6 into account, the results clearly demonstrated that the newly developed UGT1A1 activities assay provided a practical assay for screening and characterization UGT1A1 inducers via monitoring the formation of NHPNG in living cells.

4. Conclusion

In summary, a reliable and easy-to-use LC-FD based assay has been developed and validated for ultra-sensitive UGT1A1 activities assays in various biological systems, using NHPN-O-glucuronidation as the probe reaction. The newly developed LC-FD based assay shows several important advantages over previously reported UGT1A1 activities assays, including high selectivity and sensitivity, reliable and ease of use, as well as strong anti-interference ability. The LOQ of the LC-FD based assay is much lower than that of previously reported UGT1A1 activities assays, making this assay more suitable for sensing UGT1A1 activities in real samples. Furthermore, the new assay system has been successfully applied to quantify UGT1A1 activities in human tissue preparations and even to screening the regulatory effects of small molecules on UGT1A1 in living cells. Collectively, this study provides a reliable and easy-to-use method for sensing UGT1A1 activities in biological systems, which will be very useful for exploring the relevance of this conjugative enzyme to human diseases, as well as for rapid screening and discovery of effective modulators, both inhibitors and inducers of this key enzyme.

Conflicts of interest

The authors declare that there are no conflicts of interest.

Acknowledgments

Appendix A. Supplementary data

Supplementary data to this article can be found online at https://doi.org/10.1016/j.jpha.2020.05.005.

References

[1] X.Y. Liu, X. Lv, P. Wang, et al., Inhibition of UGT1A1 by natural and synthetic flavonoids, Int. J. Biol. Macromol. 126 (2019) 653—661.
[2] Z. Shen, C. Lv, S. Zeng, Significance and challenges of stereoselectivity assessing methods in drug metabolism, J. Pharm. Anal. 6 (2016) 1—10.
[3] X. Lv, Y.L. Xia, M. Finel, et al., Recent progress and challenges in screening and characterization of UGT1A1 inhibitors, Acta Pharm. Sin. B 9 (2019) 258—278.
[4] A.F. McDonagh, Bilirubin toxicity to human erythrocytes: a more sanguine view, Pediatrics 120 (2007) 175—178.
[5] T.K. Kiang, M.H. Ensom, T.K. Chang, UDP-glucuronosyltransferases and clinical drug-drug interactions, Pharmacol. Ther. 106 (2005) 97—132.
[6] A. Kadakol, S.S. Ghosh, B.S. Sappal, et al., Genetic lesions of bilirubin uridine-diphosphoglucuronate glucuronosyltransferase (UGT1A1) causing Crigler-Najjar and Gilbert syndromes: correlation of genotype to phenotype, Hum. Mutat. 16 (2000) 297—306.
[7] J.J. Wang, J.J. Guo, J. Zhan, et al., An in-vitro cocktail assay for assessing compound-mediated inhibition of six major cytochrome P450 enzymes, J. Pharm. Anal. 4 (2014) 270—278.
[8] Database from Us Food and Drug Administration, Guidance for industry: drug interaction studies—study design, data analysis, implications for dosing and labeling recommendations; Draft guidance, 2012. http://www.fda.gov/downloads/Drugs/GuidanceComplianceRegulatoryInformation/Guidances/UCM292362.pdf.
[9] G. Ma, J. Lin, W. Cai, et al., Simultaneous determination of bilirubin and its glucuronides in liver microsomes and recombinant UGT1A1 enzyme incubation systems by HPLC method and its application to bilirubin glucuronidation studies, J. Pharmaceut. Biomed. Anal. 92 (2014) 149—159.
[10] J.K. Fallon, H. Neubert, T.C. Goosen, et al., Targeted precise quantification of 12 human recombinant uridine-diphosphate glucuronosyl transferase 1A and 2B isoforms using nano-ultra-high-performance liquid chromatography/tandem mass spectrometry with selected reaction monitoring, Drug Metab. Dispos. 41 (2013) 2076—2080.
[11] H. Harada, T. Endo, Y. Momose, et al., A liquid chromatography/tandem mass spectrometry method for detecting UGT-mediated bioactivation of drugs as their N-acetylcysteine adducts in human liver microsomes, Rapid Commun. Mass Spectrom. 23 (2009) 564—570.
[12] X. Lv, G.B. Ge, L. Feng, et al., An optimized ratiometric fluorescent probe for sensing human UDP-glucuronosyltransferase 1A1 and its biological applications, Biosens. Bioelectron. 72 (2015) 261—267.
[13] X. Lv, L. Feng, C.Z. Ai, et al., A practical and high-affinity fluorescent probe for uridine diphosphate glucuronosyltransferase 1A1: a good surrogate for bilirubin, J. Med. Chem. 60 (2017) 9664—9675.
[14] X. Lv, J.B. Zhang, J. Hou, et al., Chemical probes for human UDP-glucuronosyltransferases: a comprehensive review, Biotechnol. J. 14 (2019), e1800002.
[15] E. Quan, H. Wang, D. Dong, et al., Characterization of chrysin glucuronidation in UGT1A1-overexpressing HeLa cells: elucidating the transporters responsible for efflux of glucuronide, Drug Metab. Dispos. 43 (2015) 433—443.
[16] X. Zhang, D. Dong, H. Wang, et al., Stable knock-down of efflux transporters leads to reduced glucuronidation in UGT1A1-overexpressing HeLa cells: the evidence for glucuronidation-transport interplay, Mol. Pharm. 12 (2015) 1268—1278.
[17] B. Zhang, J. Yang, Z. Qin, et al., Mechanism of the efflux transport of demethoxycurcumin-O-glucuronides in HeLa cells stably transfected with UDP-glucuronosyltransferase 1A1, PloS One 14 (2019) 1—20.
[18] K. Fujita, M. Sugiyama, Y. Akiyama, et al., The small-molecule tyrosine kinase inhibitor nilotinib is a potent noncompetitive inhibitor of the SN-38 glucuronidation by human UGT1A1, Canc. Chemother. Pharmacol. 67 (2011) 237—241.
[19] L. Ai, L. Zhu, L. Yang, et al., Selectivity for inhibition of nilotinib on the catalytic activity of human UDP-glucuronosyltransferases, Xenobiotica 44 (2014) 320—325.
[20] C.M. Smith, R.A. Graham, W.L. Krol, et al., Differential UGT1A1 induction by chrysin in primary human hepatocytes and HepG2 Cells, J. Pharmacol. Exp. Therapeut. 315 (2005) 1256—1264.
[21] T. Walle, Y. Otake, A. Galijatovic, et al., Induction of UDP-glucuronosyltransferase UGT1A1 by the flavonoid chrysin in the human hepatoma cell line hep G2, Drug Metab. Dispos. 28 (2000) 1077—1082.
[22] N. Li, D. Wang, Z. Sui, et al., Development of an improved three-dimensional in vitro intestinal mucosa model for drug absorption evaluation, Tissue Eng. C Methods 19 (2013) 708—719.
[23] H. Bothe, C. Gotz, N. Stobbe-Maicherski, et al., Luteolin enhances the

bioavailability of benzo(a)pyrene in human colon carcinoma cells, Arch. Biochem. Biophys. 498 (2010) 111—118.

[24] Y. Chen, L. Zeng, Y. Wang, et al., The expression, induction and pharmacological activity of CYP1A2 are post-transcriptionally regulated by microRNA hsa-miR-132-5p, Biochem. Pharmacol. 145 (2017) 178—191.

[25] J. Zhou, T.S. Tracy, R.P. Remmel, Bilirubin glucuronidation revisited: proper assay conditions to estimate enzyme kinetics with recombinant UGT1A1, Drug Metab. Dispos. 38 (2010) 1907—1911.

[26] Z.M. Wen, M.N. Tallman, S.Y. Ali, et al., UDP-glucuronosyltransferase 1A1 is the principal enzyme responsible for etoposide glucuronidation in human liver and intestinal microsomes: structural characterization of phenolic and alcoholic glucuronides of etoposide and estimation of enzyme kinetics, Drug Metab. Dispos. 35 (2007) 371—380.

[27] N. Blumberg, J.M. Cholette, A.E. Schmidt, et al., Management of platelet disorders and platelet transfusions in ICU patients, Transfus. Med. Rev. 31 (2017) 252—257.

Short communication

Screening of the whole human cytochrome P450 complement (CYPome) with enzyme bag cocktails

Sangeeta Shrestha Sharma, Shishir Sharma, Matthias Bureik[*]

School of Pharmaceutical Science and Technology, Health Sciences Platform, Tianjin University, Tianjin, 300072, China

ARTICLE INFO

ABSTRACT

We have previously introduced the use of permeabilized fission yeast cells (enzyme bags) that recombinantly express full-length CYPs for drug metabolism studies. Such enzyme bags are cells with pores that function as enzymes in situ. They can easily be prepared without a need for ultracentrifugation and may be used in similar protocols as microsomes. In this study we report the preparation of enzyme bag cocktails that permit the testing of multiple CYPs in a single enzyme bag reaction. Moreover, we established a convenient testing scheme that permits a rapid screen of all human CYPs for activity towards any given candidate substrate. An important aspect of this approach is the reduction of individual CYP test assays. If a cocktail containing many CYPs tests negative, it follows that all CYPs included in that cocktail need not be tested individually, thus saving time and resources. The new protocol was validated using two probe substrates.

1. Introduction

The majority of drugs used in human patients are substrates of drug metabolizing enzymes [1], which are classified into the two groups of Phase I and Phase II enzymes depending on the type of reaction they catalyze: Phase I is characterized by functionalization reactions (such as redox reactions), while in Phase II conjugation reactions occur (such as glucuronidation). The most important enzymes in Phase I metabolism are the cytochrome P450 enzymes (CYPs or P450s), which belong to a large superfamily of monooxygenases present in all biological kingdoms [2]. The 57 human CYPs are all membrane bound proteins that are primarily found either on the cytoplasmic side of the endoplasmic reticulum or on the matrix side of the inner mitochondrial membrane. CYPs need to be reduced in order to catalyze redox reactions and therefore depend on electron transfer proteins. In mitochondria, there is a short electron transfer chain encompassing adrenodoxin (Adx) and adrenodoxin reductase (AdR), while in the endoplasmic reticulum, there is a single electron transfer partner, cytochrome P450 reductase (CPR or POR) [3]. Human CYPs metabolize a large variety of compounds belonging to many different chemical classes and typically catalyze aliphatic or aromatic hydroxylations; however, in principle they can also perform many other reaction types [4,5]. In analogy to the genome or the proteome, the total complement of human CYPs can be referred to as the human CYPome [6].

In the field of drug metabolism, many so-called cocktail approaches were described in the past. These include protocols that use cocktails of drug or candidate drug molecules, those that employ mixtures of recombinantly expressed and purified human CYPs, and even double cocktails where a compound mixture is given to an enzyme mixture [7]. Such techniques are used for the study of the metabolism of candidate drug compounds, for CYP inhibition assays, and for investigations of drug-drug interactions [8].

While such approaches have efficiency advantages of parallel incubation and parallel LC/MS/MS analysis of multiple probes, they suffer from the significant mutagenesis (such as removal of parts that serve as membrane anchors) needed to allow for recombinant high-level expression in bacteria; thus, the resulting proteins can hardly be considered as 'wild-type'. A solution to these issues is the recombinant expression of unmodified full-length enzymes in eukaryotic hosts such as yeast, insect, or mammalian cells, where the membrane localization of the enzymes is retained. Such recombinant eukaryotic cells have typically been used for drug metabolism studies either in whole-cell biotransformations or for the preparation of microsomes.

Whole-cell biotransformations are easy to perform and

---

convenient because the cofactor NADPH is directly produced inside the living cells. But substrates and products need to pass several biological barriers (such as plasma membrane and cell wall), which is a severe problem for compounds that display very low membrane permeability. An alternative is the use of microsomes prepared from recombinant eukaryotic cells, but this method has its own issues (tedious long-term ultracentrifugation and lack of scalability). Thus, there is no perfect P450 assay as all methods have their respective advantages and disadvantages. We have recently introduced the use of permeabilized fission yeast cells (enzyme bags) that recombinantly express full-length CYPs [9] or UDP-glucuronosyltransferases (UGTs) [10] for drug metabolism studies. Such enzyme bags are cells with pores that function as enzymes *in situ*. They can easily be prepared without a need for ultracentrifugation and may be used in similar protocols as microsomes.

It was the aim of this study to create a new procedure that allows for the testing of multiple CYPs in a single enzyme bag reaction. Moreover, we wanted to establish a convenient testing scheme that permits a rapid screen of all human CYPs for activity towards any given candidate substrate.

2. Materials and methods

2.1. Chemicals and reagents

Ammonium chloride, Na_2HPO_4, glucose, KH_2PO_4, and potassium hydrogen phthalate were from Chemart Chemical (Tianjin, China). Agar, biotin, $CaCl_2 \cdot H_2O$, citric acid, $CuSO_4 \cdot 5H_2O$, $FeCl_3 \cdot 6H_2O$, H_3BO_3, inositol, KCl, KI, $MnSO_4$, $MgCl_2 \cdot 6H_2O$, $MoO_4 \cdot 2H_2O$, Na_2SO_4, nicotinic acid, sodium pantothenate, thiamine, and $ZnSO_4 \cdot 7H_2O$ were from Kermel Chemical (Tianjin, China). Luciferin-BE, Luciferin-H, Luciferin-ME, and the NADPH regeneration system were from Promega (Madison, USA); Triton-X100 was from Leagene (Beijing, China); Tris-HCl was from AKZ-Biotech (Tianjin, China); glycerol was from Dingguo (Tianjin, China); white 96-well microtiter plates were from Nunc (Thermofisher scientific, Lagenselbold, Germany). All other chemicals and reagents used were of the highest grade available.

2.2. Fission yeast strains, media and general techniques

All strains used in this study have been described previously [11]. In these strains, expression of human CPR and all human CYPs is regulated by the strong thiamine-repressible *nmt1* promoter of fission yeast [12]. Preparation of media and basic manipulation methods of *S. pombe* were carried out as described [13]. Briefly, strains were generally cultivated at 30 °C in Edinburgh Minimal Medium (EMM) with supplements of 0.1 g/L final concentration as required. Liquid cultures were kept shaking at 230 rpm. Thiamine was used at a concentration of 5 μM throughout.

2.3. Preparation of enzyme bags and enzyme bag cocktails

Fission yeast strains were cultured on EMM plates with 5 μM thiamine at 30 °C for 3 days and then precultured in 10 mL EMM broth at 230 rpm and 30 °C for 24 h. Precultures were then used to inoculate 200 mL EMM broth in 500 mL Erlenmeyer flasks, which were then incubated under the same conditions for 24 h. For each assay 5×10^7 cells were transferred to 1.5 mL Eppendorf tubes, pelleted and incubated in 1 mL of 0.3 % Triton-X100 in Tris-KCl buffer (200 mM KCl, 100 mM Tris-HCl pH 7.8) at room temperature for 60 min at 230 rpm for permeabilization. The different sets of cocktails were prepared by mixing cells of different strains prior to permeabilization with a final cell density of 5×10^7 cells/cocktail/reaction, so that regardless of the number of CYPs included, each

cocktail contained the same number of cells. After three washing steps with cold 50 mM NH_4HCO_3 buffer, enzyme bags were gently resuspended in 100 μL PBS with 50 % glycerol, flash frozen in liquid nitrogen, and stored at −80 °C until use.

2.4. Biotransformation of proluciferins and bioluminescence detection

Enzyme bag preparations were thawed on ice, once washed with 100 μL 100 mM potassium phosphate buffer, pH 7.4, and then used for biotransformations as described previously [9]. Briefly, a concentrated CYP reaction mixture (containing fourfold concentrated substrate and potassium phosphate buffer) was added to the cell pellets in 1.5 mL Eppendorf tubes after permeabilization and washing. Substrates Luciferin-H and Luciferin-ME were both used at a final concentration of 100 μM while preliminary experiments with Luciferin-BE were done at a final substrate concentration of 50 μM. CYP reactions were started by adding the twofold concentrated NADPH regeneration system. Samples were incubated for 3 h at 37 °C and 1000 rpm. After centrifugation at 16,000 *g* for 1 min the supernatants were transferred to white microtiter plates and an equal amount of reconstituted luciferin detection reagent was added to each well. Plates were then incubated at room temperature for 20 min and luminescence was recorded on a Magellan infinite 200Pro microplate reader (Tecan; Männedorf, Switzerland). In all cases, reaction parameters (reaction times and enzyme concentrations) were within the linear range.

2.5. Statistical analysis

All data were calculated from experiments done at least twice in triplicates and are presented as mean ± SD. Statistical significance was determined using a two-tailed *t*-test. Differences were considered significant if $P < 0.05$. Statistical analysis was done using GraphPad Prism 5.01 (GraphPad Software Inc., La Jolla, CA; USA).

3. Results and discussion

3.1. Preparation of enzyme bag cocktails and testing strategy

In order to allow for the simultaneous testing of several CYPs in the same enzyme bag assay, we developed a new methodological approach. In this procedure, fission yeast strains are cultivated as previously described but after determination of cell densities and before cell permeabilization, equal numbers of cells from different strains were mixed. In this way, roughly comparable amounts of CYPs should be contained in every cocktail. For validation of this approach, preliminary experiments were performed using the test substrate Luciferin-BE and enzyme bag cocktails that only included up to four different CYPs. In addition, we also compared the activity of freshly prepared enzyme bag cocktails with those that underwent one freeze-thaw cycle and were retested after one day, five days, or one year, respectively. These experiments demonstrated that the combination of several CYPs into a single enzyme bag cocktail is possible, and they also showed a reasonable stability of results even after one year of storage (Fig. S1).

Next, we designed a testing tree that encompasses a hierarchy of cocktails (Fig. S2). On top of the tree is the Master cocktail (M) that contains enzyme bags made from all 57 individual strains. On the second level, there are four cocktails (A to D) that contain enzyme bags made from 14 or 15 individual strains as indicated. In selecting the individual enzymes contained in each cocktail we followed the official CYP nomenclature, which means that cocktail A contains CYP1A1 to CYP2F1, cocktail B contains CYP2J2 to CYP4F3, and so on. On the third level of the hierarchy, there are twelve cocktails (1—12)
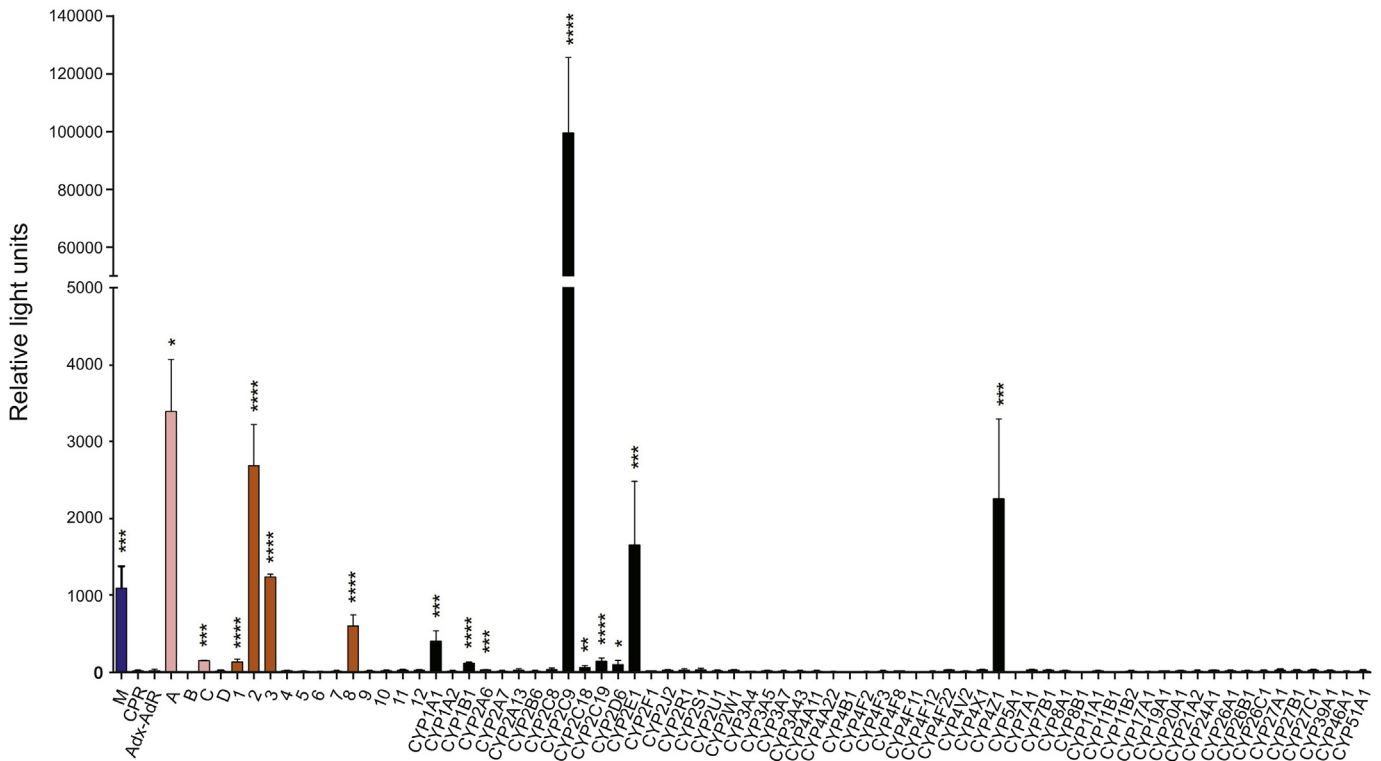
Fig. 1. Enzymatic activity of enzyme bag cocktails and enzyme bags containing single CYPs towards the substrate Luciferin-H. Cocktail M (containing all 57 CYPs) is shown in dark blue, cocktails A-D (containing 14 or 15 CYPs) are shown in pink, cocktails 1–12 (containing 4 or 5 CYPs) are shown in orange, and individual CYPs are shown in black. CPR: Control with enzyme bags containing only CPR. Adx-AdR: Control with enzyme bags containing only Adx and AdR. *$P < 0.05$, **$P < 0.01$, ***$P < 0.005$, ****$P < 0.001$.
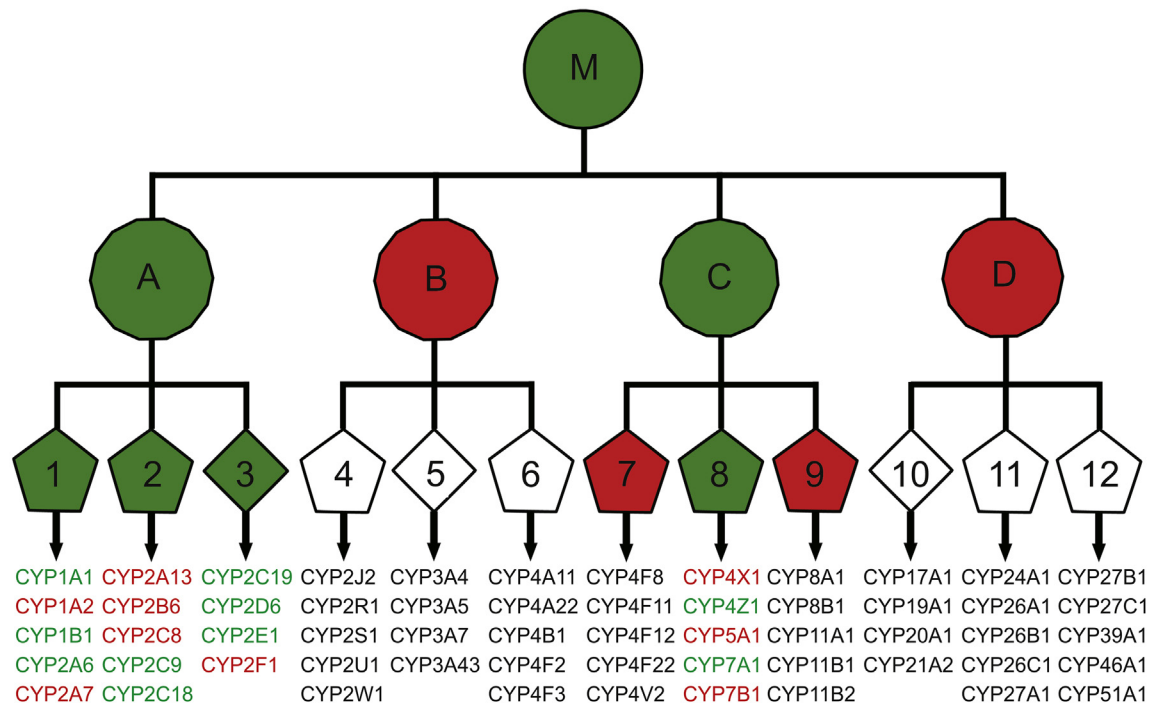
Fig. 2. Scheme of the cocktails testing tree showing an overview of the results obtained in the activity assays of enzyme bag cocktails and enzyme bags containing single CYPs towards the substrate Luciferin-H. Green: Cocktails or individual enzymes testing positive. Red: Cocktails or individual enzymes testing negative. Black: Cocktails or individual enzymes not tested.
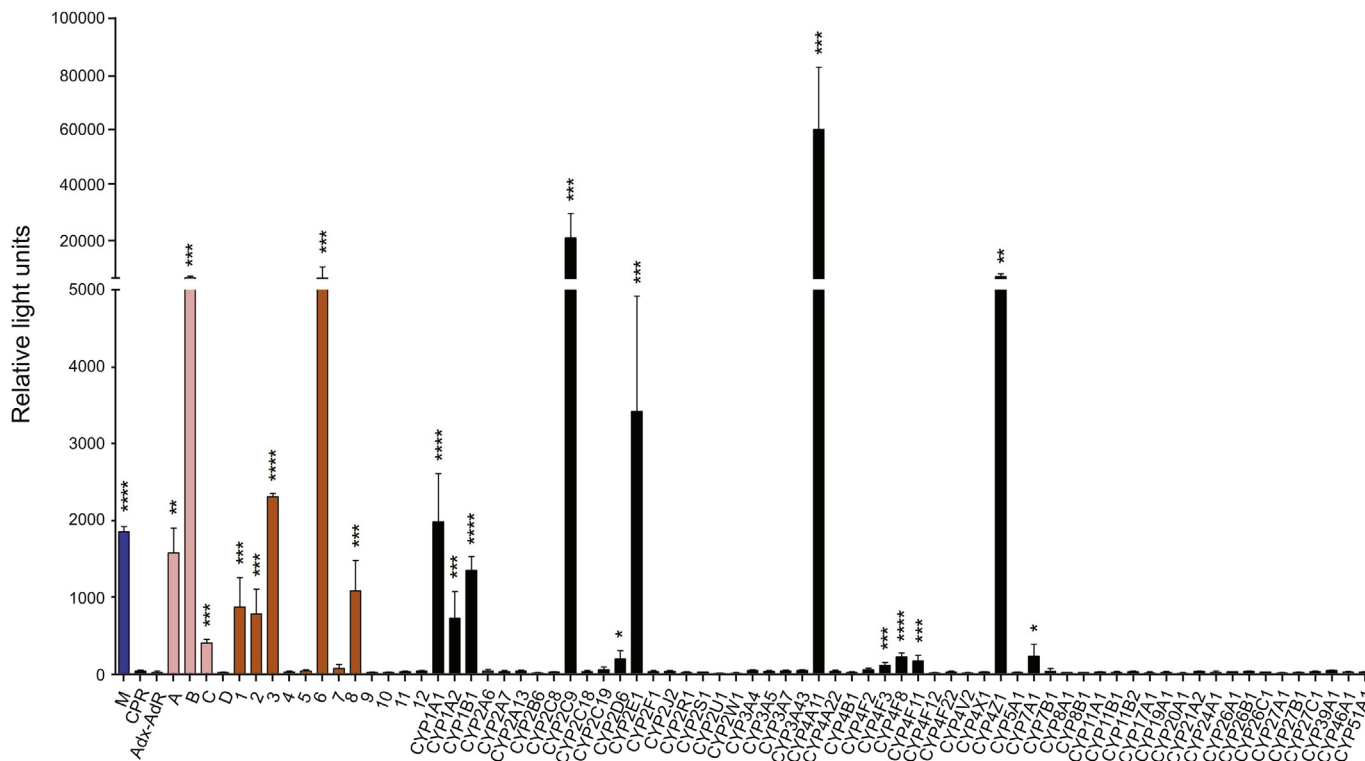
Fig. 3. Enzymatic activity of enzyme bag cocktails and enzyme bags containing single CYPs towards the substrate Luciferin-ME. Cocktail M (containing all 57 CYPs) is shown in dark blue, cocktails A–D (containing 14 or 15 CYPs) are shown in pink, cocktails 1–12 (containing 4 or 5 CYPs) are shown in orange, and individual CYPs are shown in black. CPR: Control with enzyme bags containing only CPR. Adx-AdR: Control with enzyme bags containing only Adx and AdR. *$P < 0.05$, **$P < 0.01$. ***$P < 0.005$, ****$P < 0.001$.
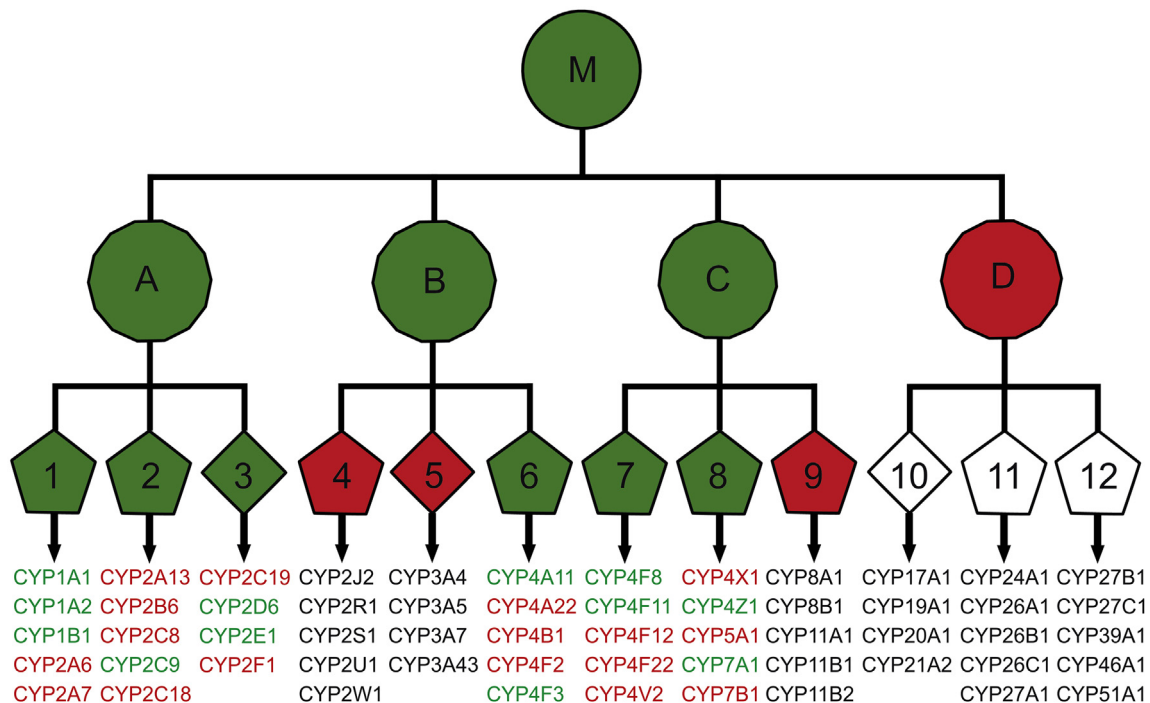
Fig. 4. Scheme of the cocktails testing tree showing an overview of the results obtained in the activity assays of enzyme bag cocktails and enzyme bags containing single CYPs towards the substrate Luciferin-ME. Green: Cocktails or individual enzymes testing positive. Red: Cocktails or individual enzymes testing negative. Black: Cocktails or individual enzymes not tested.

that contain enzyme bags made from four or five individual strains, again in the order of the nomenclature. The procedure we established makes an important distinction between qualitative and quantitative analysis: Experiments with enzyme bag cocktails are essentially only used for obtaining yes/no answers, whereas experiments with enzyme bags made from individual strains (i.e. containing only one human CYP) are intended to yield quantitative activity data (as in our previous publications). In order to account for small activities that might be observed in cocktails where only one CYP present can catalyze the reaction and/or that activity is low, we decided to consider any cocktail that gave a positive result once to be positive, which means that the corresponding cocktails on the next level of the hierarchy would be tested. By contrast, we only considered a cocktail to be negative for a certain reaction if a negative result was obtained in three individual assays. This would then result in the corresponding cocktails on the next level of the hierarchy not to be tested. The advantage of such an approach becomes apparent if we consider the situation where a candidate compound is only metabolized by a single CYP, for instance CYP2C9. Without the enzyme bag cocktail approach, all 57 human CYPs would have to be tested to verify this fact. By contrast, using our testing tree only eight cocktails and five individual enzymes need to be tested: Cocktail M would be positive, as would be cocktail A, but not B, C or D. Next, cocktails 1 to 3 (those corresponding to A) would be tested, with cocktail 2 testing positive and both 1 and 3 negative; finally, the five enzymes that make up cocktail 2 would be tested individually, revealing CYP2C9 to be positive and the other four negative. Thus, with only 13 assays the single CYP responsible for the observed activity could be identified. Having obtained that information, detailed enzymatic studies using the one CYP in question can then be performed with the aim of yielding quantifiable data.

3.2. CYP profiling of the luminogenic probe substrate Luciferin-H

In our previous study we have reported the functional expression of all human CYPs in fission yeast and reported their activity towards the two probe substrates Luciferin-H and Luciferin-ME [11]. Such proluciferins can be converted by CYPs to luciferin, which in turn produces light upon oxidation by luciferase [14]. Therefore, these two substrates are perfect candidates for the validation of the enzyme bag cocktail approach as activity data for all cocktails can be predicted. Firstly, we tested Luciferin-H, which is converted to luciferin by a CYP-dependent aryl hydroxylation reaction. In our previous study we found that CYP2C9, CYP2E1, and CYP4Z1 (in this order) displayed by far the highest activities towards this substrate [11]. When subjecting this substrate to the testing tree procedure, we observed significant activity with the Master cocktail M as could be expected (Fig. 1). On the second level of the hierarchy, cocktails A and C gave positive results while B and D did not. Cocktail A showed much higher activity than C as the former contains both CYP2C9 and CYP2E1 while the latter only contains CYP4Z1. The third level of the testing scheme gave positive results for cocktails 1 to 3 and 8, again as expected. The 19 enzymes contained in these four cocktails were then tested individually, with eleven giving positive results and the remaining eight being negative (Fig. 2). These results are in good agreement with our previous data. All enzymes that showed strong activity in the earlier study also did so in these experiments. There are some borderline cases where activities are quite low in comparison to controls and where statistical significance therefore may vary.

3.3. CYP profiling of the luminogenic probe substrate Luciferin-ME

The second part of the enzyme bag cocktail validation consisted of activity measurements for Luciferin-ME, which is converted to luciferin by a CYP-dependent aliphatic hydroxylation reaction followed by dissociation of the resulting hemiacetal [14]. For this substrate, CYP4A11, CYP2E1, CYP4Z1, and CYP2C9 (in this order) had previously shown the highest activities [11]. Again, cocktail M showed good activity as expected, and cocktails A to C (but not D) were also positive (Fig. 3). Of the former, cocktail B displayed the highest activity as it contains CYP4A11, with A (containing CYP2E1 and CYP2C9) and C (CYP4Z1) showing lower but still significant activity. On the third level of the testing scheme, positive results were obtained for cocktails 1 to 3 and 6 to 8, again as expected. Individual testing of the 29 enzymes contained in these six cocktails led to 12 positive and 17 negative results (Fig. 4). Again, results are in good agreement with previous data.

4. Conclusions

Experiments using HLMs (or microsomes from other tissues) are necessarily biased towards those CYPs that display high activity in the tissue of origin. Moreover, there is no human cell type that expresses all CYPs, so some enzymes will always be missed. With the availability of all human CYPs being recombinantly produced in the same host microbe we now have demonstrated the preparation of much more unbiased cocktails as equal amounts of the cells that produce the different CYPs were combined. Moreover, additional special cocktails can also be made, such as cocktails containing all CYPs known to be expressed in any given tissue, or cocktails containing all CYPs involved in the metabolism of certain chemical classes of compounds (e.g. steroids). Therefore, in this study we present a platform technology that has a huge variety of applications in the future.

The attribution of observed CYPs activities displayed by human microsomes is often done by blocking this activity using 'specific' inhibitors of the CYP enzyme in question. However, so far there is no published data where any such inhibitors were tested against all human CYPs; thus, there is always a risk that these compounds inadvertently coinhibit other CYPs for whom the inhibitory effect is not yet known. The enzyme bag cocktail approach presented in this study avoids this problem, as the different CYPs contained in any of the cocktails can always be individually tested. Thus, validation of the cocktail results at the level of the individual enzymes can always be performed.

Conflicts of interest

The authors declare that there are no conflicts of interest.

Appendix A. Supplementary data

Supplementary data to this article can be found online at https://doi.org/10.1016/j.jpha.2020.05.003.

References

[1] J.A. Williams, R. Hyland, B.C. Jones, et al., Drug-drug interactions for UDP-glucuronosyltransferase substrates: a pharmacokinetic explanation for typically observed low exposure (AUCi/AUC) ratios, Drug Metab. Dispos. 32 (2004) 1201–1208.
[2] R. Bernhardt, Cytochromes P-450, in: W. Lennarz, M. Lane, P. Modrich, J. Dixon, E. Carafoli, J. Exton, D. Cleveland (Eds.), Encyclopedia of Biological Chemistry, Academic Press, 2005, pp. 544-549.
[3] F. Hannemann, A. Bichet, K.M. Ewen, et al., Cytochrome P450 systems-biological variations of electron transport chains, Biochim. Biophys. Acta 1770 (2007) 330–344.
[4] R. Bernhardt, V.B. Urlacher, Cytochromes P450 as promising catalysts for biotechnological application: chances and limitations, Appl. Microbiol. Biotechnol. 98 (2014) 6185–6203.
[5] F.P. Guengerich, Common and uncommon cytochrome P450 reactions related

to metabolism and chemical toxicity, Chem. Res. Toxicol. 14 (2001) 611−650.

[6] D.C. Lamb, T. Skaug, H.L. Song, et al., The cytochrome P450 complement (CYPome) of Streptomyces coelicolor A3(2), J. Biol. Chem. 277 (2002) 24000−24005.

[7] L. Di, E.H. Kerns, Drug-Like Properties: Concepts, Structure Design and Methods from ADME to Toxicity Optimization, Academic Press, 2016.

[8] I. Johansson, M. Ingelman-Sundberg, Genetic polymorphism and toxicology-with emphasis on cytochrome P450, Toxicol. Sci. 120 (2011) 1−13.

[9] Q. Yan, D. Machalz, A. Zollner, et al., Efficient substrate screening and inhibitor testing of human CYP4Z1 using permeabilized recombinant fission yeast, Biochem. Pharmacol. 146 (2017) 174−187.

[10] F. Yang, D. Machalz, S. Wang, et al., A common polymorphic variant of UGT1A5 displays increased activity due to optimized cofactor binding, FEBS Lett. 592 (2018) 1837−1846.

[11] P. Durairaj, L. Fan, W. Du, et al., Functional expression and activity screening of all human cytochrome P450 enzymes in fission yeast, FEBS Lett. 593 (2019) 1372−1380.

[12] K. Maundrell, nmt1 of fission yeast. A highly transcribed gene completely repressed by thiamine, J. Biol. Chem. 265 (1990) 10857−10864.

[13] C. Alfa, P. Fantes, J. Hyams, et al., Experiments with Fission Yeast. A Laboratory Course Manual, Cold Spring Harbor Press, Cold Spring Harbor, NY, 1993.

[14] J.J. Cali, D. Ma, M. Sobol, et al., Luminogenic cytochrome P450 assays, Expet Opin. Drug Metabol. Toxicol. 2 (2006) 629−645.